Development of New Therapeutic Materials for Mitigation of Amyloid Neurotoxicity Associated with Alzheimer's Disease

A Dissertation Submitted for the Degree of

Doctor of Philosophy

By

Subrata Mondal

Roll No. 156122003

Department of Chemistry

Indian Institute of Technology Guwahati

November, 2020

Department of Chemistry
IIT Guwahati

PhD Thesis

Development of New Therapeutic Materials for Mitigation of Amyloid Neurotoxicity Associated with Alzheimer's Disease

By

Subrata Mondal

Supervisor

Prof. Parameswar Krishnan Iyer

November, 2020

भारतीय प्रौद्योगिकी संस्थान गुवाहाटी
Indian Institute of Technology Guwahati
Guwahati- 781039, Assam, India

Statement

The work contained in this thesis titled '**Development of New Therapeutic Materials for Mitigation of Amyloid Neurotoxicity Associated with Alzheimer's Disease'** has been carried out by me under the supervision of Prof. Parameswar Krishnan Iyer, Professor, Department of Chemistry, Indian Institute of Technology Guwahati. This work has not been submitted elsewhere for the award of any degree.

Subrata Mondal

Roll No. 156122003
Department of Chemistry
IIT Guwahati
Guwahati-781039
Assam, India

November, 2020

भारतीय प्रौद्योगिकी संस्थान गुवाहाटी
Indian Institute of Technology Guwahati
Guwahati- 781039, Assam, India

Certificate

It is certified that the work contained in the thesis titled '**Development of New Therapeutic Materials for Mitigation of Amyloid Neurotoxicity Associated with Alzheimer's Disease**' by Subrata Mondal, a student of Department of Chemistry, Indian Institute of Technology Guwahati, for the award of the degree of Doctor of Philosophy has been carried out under my supervision. This work has not been submitted elsewhere for any degree.

Parameswar Krishnan Iyer

Professor,
Department of Chemistry and
Centre for Nanotechnology
IIT Guwahati
Guwahati – 781039
Assam, India

November, 2020

Dedicated to My Parents

Acknowledgements

Completion of this doctoral thesis was not possible unless I had the support and encouragement of several people around me. Today, when I am standing at the end of this journey, I would like to thank all those people who made this thesis possible and an unforgettable experience for me.

To commence with, I feel a deep sense of gratitude to my parents and sisters who formed part of my vision and provide persistent inspiration in each and every situation in my life. Words may prove a meagre means to write down my feelings for my *Parents*. I dedicate this Ph.D. Thesis to my parents for their endless and unconditional love with moral values.

First of all, I would like to thank my thesis supervisor, Prof. Parameswar Krishnan Iyer for his guidance and motivation throughout the research work. This milestone would have been a dream for ever if I hadn't had the opprtunity to meet Prof. Iyer at a point in my life -full of struggles and difficulties. I earnestly thank him for having trust in me. I feel fortunate to having him as my mentor who always motivated me with his hard work, dedication and optimism.

Besides my supervisor, I am highly indebted to my doctoral committee members, Prof. Bhisma K Patel, Dr. Bhubaneswar Mandal and Dr. Sachin Kumar for their valuable suggestion. Their advices and crucial comments helped me to widen my research area improve my thesis.

The completion of this thesis became possible only with the help of my collaborators, who had provided strong support and guidance along with lab facilities. I sincerely thank my collaborators Dr. Manas Borthakur and Dr. Pankaj Kalita, Pub Kamrup College, Assam, India for their continuous help and support.

I convey my special thanks to Dr. Sayan Roy Chowdhury who helped at the early days of my PhD. He taught me all the basics, experiments and techniques that

were needed. I also like to thank my earnest junior Priyam, who deserve the best and utmost respect for his hard work, diligence and indispensable input into the overall research work. I especially thank Ashish Bhaiya and Anamika for sharing their enormously broad knowledge and showing endless patience.

I am thankful to my seniors Ekta di, Niranjan Bhaiya, Muthu Bhaiya, Sameer Bhaiya, Akhtar Bhaiya, Suresh Bhaiya, Radha Bhaiya, Bheem Bhaiya, Arvin Bhaiya, Gopi bbhaiya, Dip bhaiya, Priyanka di, Jupitara di for their valuable suggestions and guidance. I am fortunate to have collegues like Retwik, Rahul, Ramesh Bhaiya, Ritesh, Indrani, Nasima, Kavita, Anita, Nehal, Debika, Paromita, Rajdikshit, Soumalya, Dibash, Tamal, Rabindra, Ritesh, Biki, Anwesha and Muzaffer bhaiya who provided me a healthy and positive environment for the research.

I take this opportunity to express my sincere gratitude to some of my close friends- Milan, Tousif, Muninder, Gopal, Swapna, Angshuman, Aniruddha, Prasenjit, Saikat, Krishna, Shuvendu, Nirmalya, Souradeep, Parvej, Shantanu who apart from their active help in my thesis work, always encouraged me in my academic and non-academic endeavours.

I sincerely acknowledge the funding sources that made my PhD work possible, Department of Science and Technology (DST), I remain thankful to the Central Instruments Facility (CIF) and DST funded Organic Electronics Lab, IIT Guwahati.

Finally, I thank almighty God to bless me with a great life and strength to follow my dreams, and being with me in all my failure and success!

Subrata

Synopsis

Alzheimer's Disease (AD) is a progressive neurodegenerative disorder characterized by memory declination and cognitive disabilities.[1] Brain regions playing critical role in learning and memory exhibit atrophy but the underlying molecular mechanisms for neurodegeneration remains to be a point of debate. Substantial data extracted from biochemical experiments, genetics and animal modelling studies suggest that amyloid oligomers originating from self-aggregation of amyloid β (Aβ), a 40 amino acid peptide having cross-β sheeted conformation are the hallmark of this disease.[2] Aβ because of their unique structural features are prone to undergo self-aggregation to form low molecular weight (LMW) Aβ oligomers. These LMW oligomers formed during the early stage AD have recently proven to induce neuronal cell death even in picomolar concentration and are considered as the major pathogens in AD.[3] Hence, inhibit the aggregation, improve clearance and impede formation of Aβ oligomers has been established to be an efficient therapeutic strategy in the fight against AD. Hence, drug discovery approaches nowadays are being redirected to Aβ based strategies. During the decade (2002-2012), 48% of the clinical trials were targeted on Aβ.[4] In parallel to this, approaches targeting several enzymes (such as secretases) have shown promising results. The production of Aβ is usually controlled by a proteolytic enzyme α-secretase and their activation may suppress total Aβ content in brain. A wide range of small molecule based drugs including Etazolate, Selegiline, PRZ-03140 is known to activate α-secretase and subjected to clinical trials.[5] The Aβ production can also be suppressed by inhibition of γ- secretase. However, suppression of Aβ production can be vulnerable due to the fact that a minimum amount of Aβ is essential for neuroprotection activities in brain.[6] Hence, strategies focused on inhibiting Aβ aggregation could be the best one and universally appreciated. In recent years wide variety of materials have developed in order to target Aβ aggregation. Among them, nanoparticle-based inhibition would the most efficient, and has received maximum attention in AD therapeutics due to their plasmonic properties, size tunability and ease of surface functionalization.[7] Nanoparticles by virtue of their nano dimension can translocate through the blood brain barrier.[8] Consequently, if nanoparticles can regulate the oligomerisation and disaggregate mature amyloid fibrils, they can possibly be utilized as medications to control neurodegenerative amyloid diseases like Alzheimer's. However, the small sizes of the nanoparticles often lead to toxicity and limits their application in biological system. In parallel to this, polymer based materials are also getting high importance because of their high pH stability, enhanced cell viability and ease of multi-functionalization.[9] A wide range of small molecules also have been tested against their activity towards amyloid aggregation.

Tramisprosate is known to bind with Aβ and suppress its toxicity. Inspite of having its activity towards amyloid inhibition, it failed in phase III clinical trials because of unwanted side effects arising from poor selectivity towards Aβ. Curcumin, an active composition of turmeric has been recognized as one of the most efficient amyloid inhibitors. It is known for its BBB permeability and high binding affinity to Aβ.

However, as of now, none of these strategies have proved to be effective since most of these strategies are targeted towards single biophysical/biochemical events associated with AD. In this regard, this thesis collectively aims to develop multidirectional therapeutics that regulate amyloid oligomerisation as well as block multiple biochemical events that ultimate lead to neuronal damage involved in AD.

A brief detail of the thesis work has been summarized below,

Chapter 1: Details about the already existing developments and strategies to inhibit production, aggregation and clearance of Aβ along with other indirect strategies taken to fight against AD and a brief detail of the thesis.

Chapter 2: Nanoparticle assisted regulation of nucleation pathway of amyloid tetramer and inhibition of their fibrillation kinetics.

Chapter 3: Template mediated detoxification of low-molecular-weight amyloid oligomers and regulation of their nucleation pathway.

Chapter 4: Amyloid targeting 'artificial chaperone' impairs oligomer mediated neuronal damage and mitochondrial dysfunction associated with AD.

Chapter 5: An 'artificial fiber' attenuates amyloid fibrillation and mitigates of neuronal damage associated with AD.

Chapter 1: Introduction

A worldwide quest is under way to find new treatments to stop, slow or even prevent Alzheimer's disease. Because new drugs take years to produce from concept to market — and because drugs that seem promising in early-stage studies may not work as hoped in large-scale trials. To advance this effort this thesis focuses to develop new therapeutics against AD (Fig S1). In this chapter, a brief discussion regarding different types of protein misfolding diseases especially AD and biochemical events like oxidative stress, neuroinflammation and mitochondrial dysfunction leading to amyloid toxicity has been discussed in a nut shell. Along with diverse potential application of classical development strategies, their limitations and

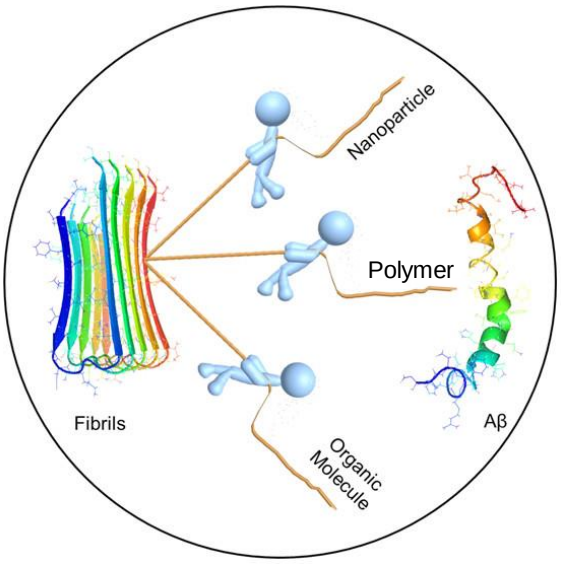

Fig S1: *Inhibition of amyloid aggregation by novel drug material*[10]

need of new development strategies and a concluding remark on the overall thesis work has also been highlighted in this part.

Chapter 2: Nanoparticle Assisted Regulation of Nucleation Pathway of Amyloid Tetramer and Inhibition of Their Fibrillation Kinetics

Low molecular weight (LMW) soluble amyloid oligomers have been established as primary neurotoxic species that play a key role in Alzheimer's disease aetiology. However, detection and separation of such energetically unfavoured, metastable species are extremely challenging due to their short lifetime and dynamic nature. In this chapter, the aggregation of Aβ has been precisely regulated to produce their tetramer. The chemistry and kinetics of such tetrameric species is extremely important since it is the most toxic species among the pool of LMW amyloid oligomer. Hence, the inhibition kinetics of tetramers could offer insights into developing early phase therapeutics for amyloidosis. The in-depth structural characterization as well as the regulation of these isolated tetramers has also been achieved for the first time in an *in vitro* model using nontoxic novel N-methyl D-aspartic acid (NMDA) functionalized gold nanoparticle (GNP-NMDA). GNP-NMDA interacts specifically through electrostatic interactions to form stable GNP-amyloid coaggregates and redirects the nucleation toward secondary nucleation pathway unlike in control experiment where nucleation proceeds mainly via primary nucleation pathway (Fig. S2). NMDA receptor modulators have been approved by the Food and Drug Administration (FDA) as an existing treatment for moderate to severe stage Alzheimer's Disease (AD); hence, GNP decorated with NMDA offers a promising strategy

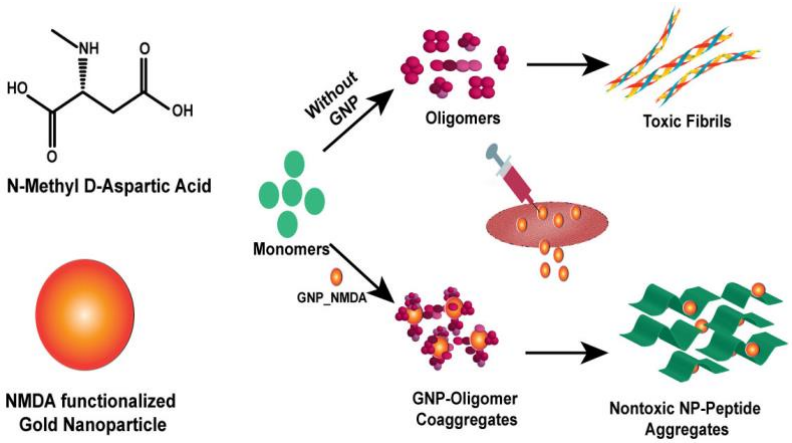

Fig. S2*: Structure of NMDA Functionalized Gold Nanoparticle (GNP-NMDA) and Modulation of Aβ Nucleation Pathway by GNP-NMDA.*[11]

toward AD. This remarkable strategy for the inhibition of the most neurotoxic LMW tetramer form of the soluble amyloid oligomers toward a nontoxic aggregation path by GNP-NMDA presents a rationale target for drug designing and to develop early stage therapeutics against several neurodegenerative diseases.

Chapter 3: Template Mediated Detoxification of Low Molecular Weight Amyloid Oligomers and Regulation of Their Nucleation Pathway

Multiple lines of evidences have established that amyloid tetramers are the major pathogen and plays key role in pathogenesis of AD. The building up of such toxic oligomeric aggregates in the brain plays host to a downstream of events, causing damage to axons, dendrites, synapses and finally premature apoptosis of neuro cells. Hence, their kinetic inhibition may be regarded as a potential therapeutic strategy against AD. In this chapter, inhibition of fibrillation of the amyloid tetramer has been achieved by using a template comprised of a conjugated polymer i.e. isatin functionalized polyfluorene (PFIS).

Isatin interacts with tetramers noncovalently to modulate its fibrillation by forming stable polymer–peptide coaggregates (Fig. S3). In parallel to this, hydrophobic PFIS forms spherical nanoparticle in water that provides an external surface, which functions to modulate nucleation pathway of the oligomers. The polymer–peptide coaggregates are nontoxic in nature. Hence, these observations offer a potential strategy to suppress neurotoxicity of a LMW oligomer by forming nontoxic coaggregates. In parallel to this, our methodology also provides a potential strategy to observe and regulate nucleation pathway of the oligomers as well.

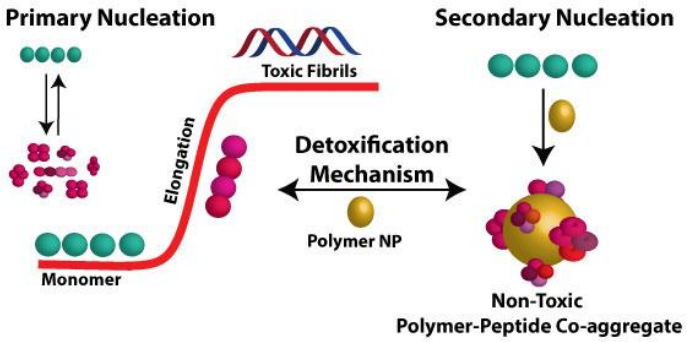

Fig. S3*: Regulation of nucleation pathway of amyloid tetramer by novel isatin functionalized polymer.*[12]

Chapter 4: Amyloid Targeting 'Artificial Chaperone' Impairs Oligomer Mediated Neuronal Damage and Mitochondrial Dysfunction Associated with Alzheimer Disease

In this chapter, a newly developed, conjugated polymer based artificial chaperone (PFBZ) has shown to exhibit multidimensional anti-amyloidogenic activity with exceptional selectivity towards amyloid mediated neuronal damage in a wild type (WT) mouse model. An accurate dose of this artificial chaperone PFBZ, results in successful attenuation of amyloid triggered internal hemorrhage and pyknosis in cerebral cortex of WT mouse. PFBZ efficiently prevents ROS generation and protects mitochondria from ROS mediated damage. The nano dimension of PFBZ chaperone ultimately helps it to translocate through the BBB under normal circulation and successfully recovers the amyloid mediated internal hemorrhage in a WT mice brain. The multidimensional activity of PFBZ was further evidenced in neuroblastoma cell line by caspase activation and mitochondrial membrane potential (MMP) biomarkers and was complemented by brain histology and electron microscopy data. It has been observed that PFBZ acts as a protective coating over Amyloid surface and resists it from interacting with cell membrane and prevent inducing toxicity (Fig. S4). This artificial chaperone PFBZ shows very special properties such as its multipotent and highly biocompatible nature and the first of its kind in targeting amyloid β and BBB permeability with a potential in eradicating amyloid triggered neurotoxicity implicated in numerous human disorders through a rare synergistic mechanism. Overall, these work has been achieved by performing spectroscopic, microscopic, biophysical and animal model experiments with great care to establish these unique multidimensional concepts of an artificial chaperone and provides a potential lead for the development of anti-amyloidogenic drugs which may find broad application in eradicating protein Misfolding diseases.

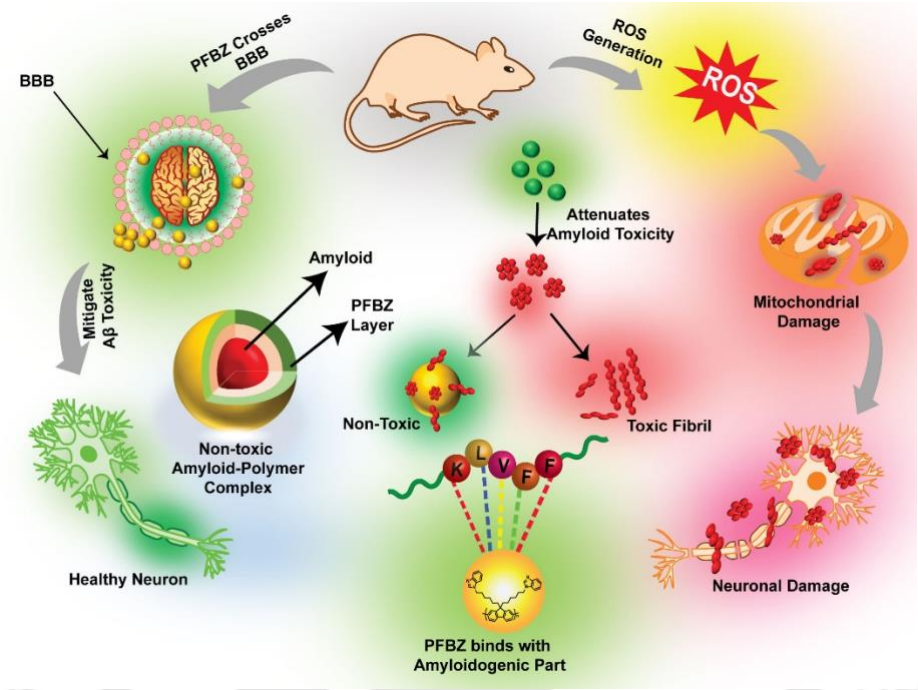

Fig. S4*: Manifestation of amyloid mediated neuronal damage and neuroprotection by PFBZ. Schematic presentation of binding of PFBZ with the 'Amyloidogenic Domain' in Aβ and possible mechanism associated with mitigation of amyloid triggered neurotoxicity.*

Chapter 5: An 'Artificial Fiber' Attenuates Amyloid Fibrillation and Provides Enhanced Neuroprotection from Amyloid Toxicity Associated with Alzheimer's Disease

Alzheimer's Disease (AD) is an irreversible memory disorder associated with bundles of neuropathological events including amyloid aggregation that triggers oxidative stress, mitochondrial dysfunction and results in premature apoptosis of neuro cells. Herein, a multi-targeted drug molecule, INHQ has been developed by integrating an imidazole ring and 8-hydroxyquinoline functionality with a hydrophobic naphthalimide core. The novel drug molecule undergoes self-aggregation to form nano fiber in physiological condition. The nano dimension of the 'Artificial Fiber' helps it to translocate through blood brain barrier under normal circulation. The presence of 8-hydroxyquinoline ring contributed to its efficient Cu(II) chelation and thereby inhibited metal dependent amyloid fibrillation. The presence of hydrophobic Naphthalimide core helps it to attain nano fibrillar morphology through π-interaction. NMR experiments and *in silico* studies reveal that INHQ offers excellent binding affinity towards Aβ predominantly through π-interactions mainly with Gly33 and Met35. It is

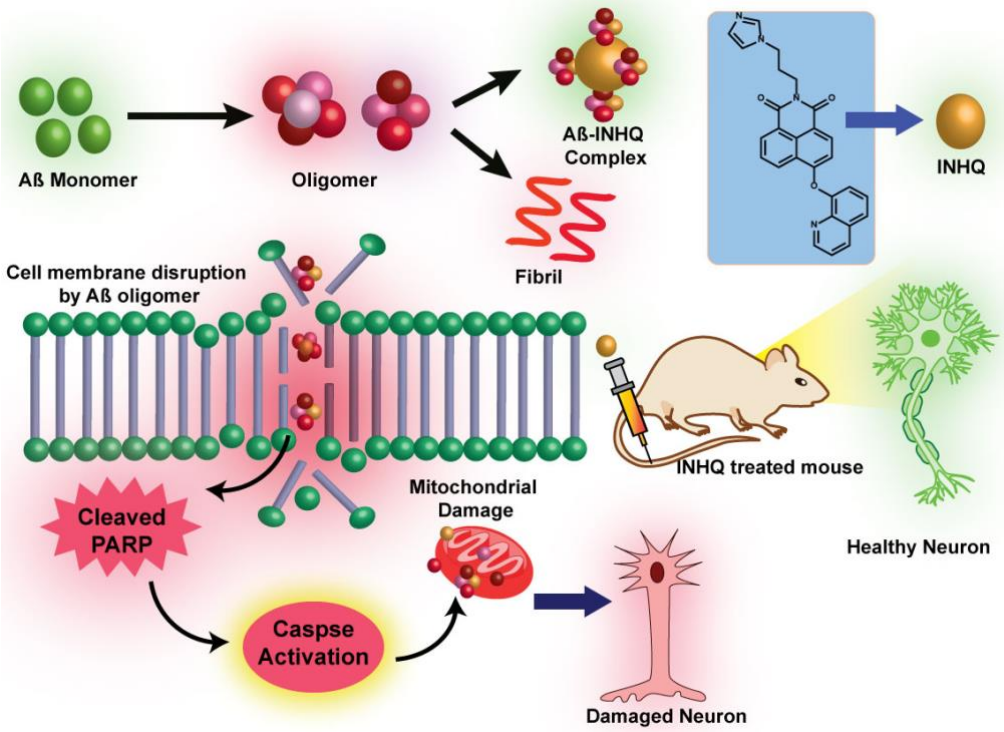

Fig. S5*: Schematic presentation of biochemical pathway associated with amyloid mediated neuronal damage and neuroprotection by INHQ.*

evident from *in vitro* cytotoxicity experiments that INHQ offers enhanced neuroprotection from amyloid toxicity. It has been observed that INHQ prevents caspase activation and PARP fragmentation and thereby rescues neuro cells from mitochondrial dysfunction (Fig. S5). This conjugated artificial fiber based nano drug showed exceptional properties such as its multipotent and highly biocompatible nature and stable in wide range of pH. The neuroprotection from amyloid toxicity was carefully validated in mouse model. It was observed that an accurate dose of INHQ fiber successfully attenuated amyloid triggered internal hemorrhage and pyknosis in cerebral cortex of WT mouse. These key anti-amyloidogenic activities makes INHQ a lead therapeutic candidate to attenuate Aβ toxicity associated with AD.

Future Aspects and Thesis Overview

Alzheimer's disease is one of the most prevalent form of dementia affecting 15 million people worldwide. In this chapter, a synoptic future perspective has summarised. In this thesis, I have elucidated fundamental biophysical and biochemical basis of amyloid neurotoxicity and putative therapeutic strategies to resolve them. A wide range of materials starting from nanoparticle to polymer and small molecule based drugs have been developed

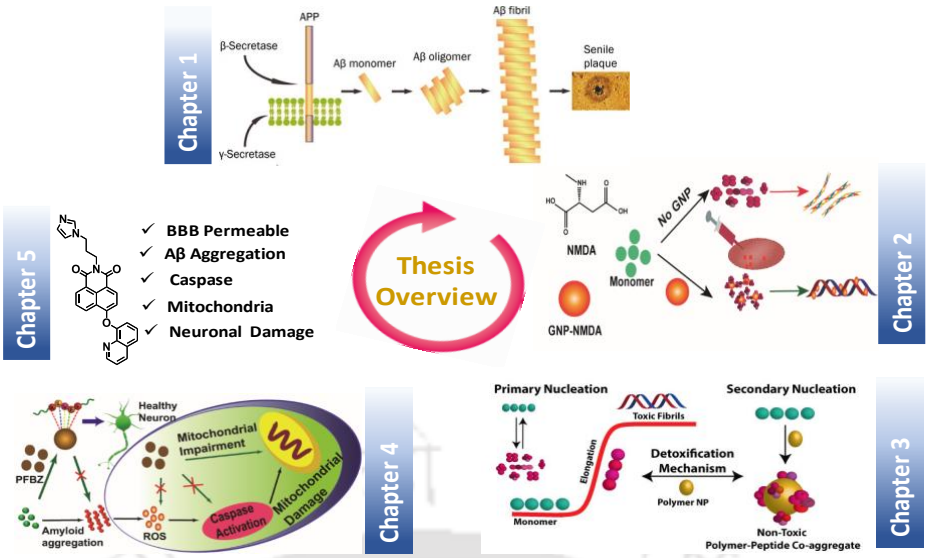

Fig. S5*: Thesis overview: Development of new therapeutic strategies to mitigate amyloid neurotoxicity associated with AD.*

and their therapeutic efficacy against AD has been evaluated. A brief overview of research output (Scheme S5) has also been summarised in this final chapter. Briefly, in chapter 2, amyloid tetramers, the most toxic form of amyloid oligomers have been isolated and their kinetics has been explored. It was observed that the tetramers undergo nucleation predominantly through primary pathway leading to amyloid neurotoxicity. However, a novel gold nanoparticle has been developed and shown to regulate the nucleation pathway in presence of that. Although, gold nanoparticle shows excellent stability during the experiment, in long run it suffers from stability issues. To overcome the issue, a novel polymer, PFIS has been developed in Chapter 3. PFIS forms nano particle in aqueous medium and regulates amyloid oligomerisation in vitro. It has been observed that PFIS suppress the amyloid neurotoxicity by regulating amyloid nucleation from primary to secondary pathway. In Chapter 4, benzimidazole functionalized multidirectional 'artificial chaperone' has been introduced. PFBZ sequesters amyloidogenic domain of Aβ, prevent aggregation and thereby blocks several biochemical pathways (such as generation of reactive oxygen species, caspase activation, mitochondrial dysfunction etc.) that leads to amyloid neurotoxicity. PFBZ by virtue of its nano dimension translocate through BBB and impair neuronal damage triggered by neurotoxic Aβ aggregates. In Chapter 4, a small molecule-based AD drug, INHQ has been developed. The interaction between INHQ and Aβ was explored by *in vitro* and *in silico* studies. INHQ targets multifactorial toxicity associated AD. The anti-amyloidogenic properties of INHQ was validated in WT mouse model and yields promising results against AD. The work presented in the thesis provides insight that could be used for designing novel and higher-efficacy derivatives of putative drugs which may prevent the onset and progression of AD and amyloid-related disorders.

Contents

Abbreviations

Alzheimer's Disease	AD
Amyloid β	Aβ
Amyloid β Oligomers	Aβ-O
Human Cerebrospinal Fluid	HCSF
Blood Brain Barrier	BBB
Low Molecular Weight	LMW
High Molecular Weight	HMW
Nanoparticle	NP
Gold Nanoparticle	GNP
N-Methyl D-Aspartic Acid	NMDA
Thioflavin T	ThT
Wild Type	WT
Mitochondrial Membrane Potential	MMP
mitochondrial permeability transition pore	mPTP
Nuclear magnetic resonance	NMR
Isatin	Is
Benzimidazole	BZ
Food and Drug Administration	FDA
Circular Dichroism	CD
Fourier-Transform Infrared Spectroscopy	FT-IR
Atomic Force microscopy	AFM
Transmission Electron Microscopy	TEM
Phosphate Buffered Saline	PBS
Dulbecco's Modified Eagle Medium	DMEM
Dimethyl Sulfoxide	DMSO
Hexafluoro-2-propanol	HFIP
Trifluoroacetic Acid	TFA
Isothermal titration calorimetry	ITC
Fluorescence Activated Cell Sorting	FACS
4′,6-diamidino-2-phenylindole	DAPI
Dentate Gyrus	DG
Kunitz Protease Inhibitor	KPI
Poly (ADP-ribose) polymerase	PARP
Red Blood Cell	RBC
Apoptosis Inducing Factor	AIF
Deoxyribonucleic Acid	DNA
Adenosine Triphosphate	ATP

1

Introduction

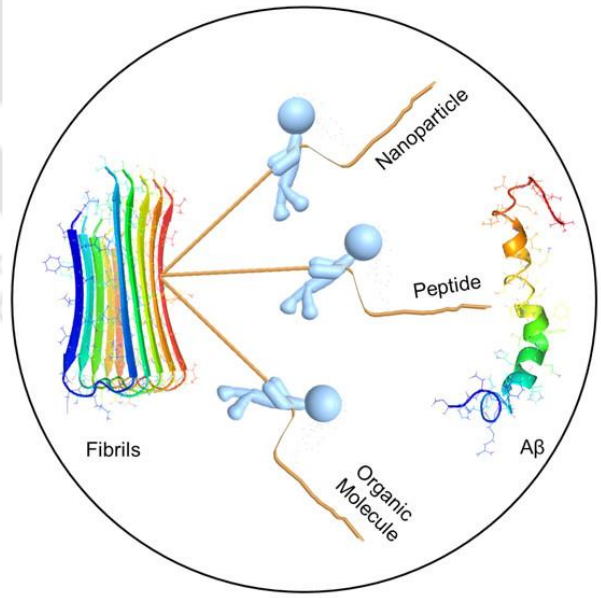

1

Introduction

1.1. The Amyloids

Proteins are the primary building blocks of life that control a variety of events (such as transportations of biomolecules, DNA replication, responding to stimuli, etc.) on which our life depends.[1] The properties of the proteins usually depend on the linear amino acid sequence and stable conformer associated with it. Energetically, a protein can adopt numerous conformations (Figure 1.1).[2] However, it is required to fold into a highly specific 3-dimensional structure to function appropriately. The physiological health depends on its success and disorder on failure. However, there is no well-established consensus on why and how proteins fold. Many physical and chemical parameters, including aging, translational issues, protein size, side-chain interaction, ionic strength, pH, and hydrophobicity, determine the rate and possibility of protein folding.[3] However, the energy criterion is the key determining factor in protein folding. The native state of the protein must be energetically favored, i.e., be at a minimum in the protein folding energy landscape.[4] Thus, the folding process can be described by a funneled energy landscape where the protein folds energetically downhill.[5] This folding

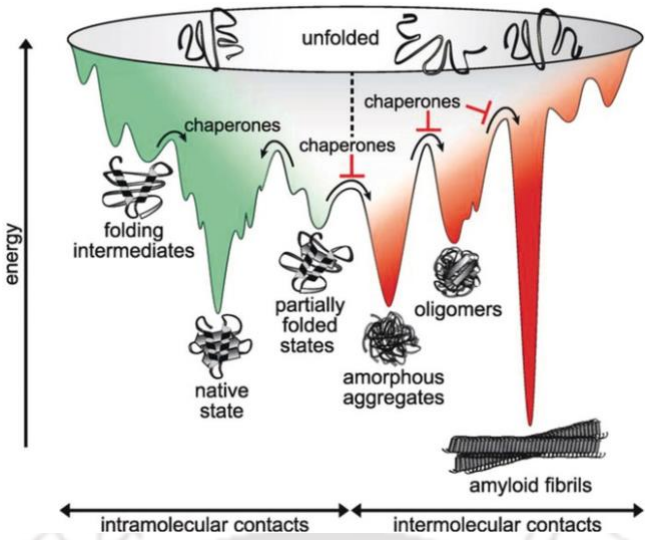

Figure 1.1: The energy landscape of protein folding (green) and aggregation (red). During folding from the unfolded state (unfolded polypeptide chains) toward the natively folded state, protein folding and aggregation are competing reactions. Polypeptide molecules sample various conformations driven by intramolecular interactions while traveling downhill on a potential free-energy surface (green part) toward the thermodynamically favorable native state. Kinetically trapped on- or off-pathway intermediates (folding intermediates and partially folded states) occupy low-energy states. The kinetically trapped off-pathway intermediates are prone to establish intermolecular interactions (red part), thereby resulting in the assembly of various forms of aggregates such as amorphous aggregates, β-sheet-rich oligomers, and amyloid fibrils, with the latter having been previously postulated as the thermodynamic ground state. Molecular chaperones provide folding assistance by lowering free-energy barriers and by inhibiting intermolecular interactions, therefore promoting folding into the native conformation.[4]

pathway embraces several transition states with energy barriers that have to be overcome. The native folded state can be described as a dynamic equilibrium with (partially) unfolded states, and these dynamics are believed to be responsible for protein folding.[4]

A wide range of human diseases is associated with protein misfolding.[6] The misfolded proteins attain a pathological state where regulation in the folding efficiency of a specific protein results in the reduction in the amount of protein available to operate its usual function. Usually, most of the misfolding diseases arise due to the conversion of a specific protein or peptide from it's native functional state to a high molecular weight fibrillar aggregates. The highly ordered structures are known as 'Amyloid Fibrils' or plaques. The 'Amyloids' can be classically defined as a class of proteins that occurs in tissue deposits and stains with congo red to emit (fluorescence) green and exhibit yellow or orange birefringes under polarised light.[7] Amyloid was discovered as early as a few centuries ago.[8] Initially, it was thought to be

comprised of carbohydrate as it stains with iodine. However, the connection that the structure adopted by the amyloids in the fibrillar form is very similar to the structure associated with neurodegenerative diseases was made much later. In last two decade, numerous amyloid proteins have been characterized throughout the human body, in distinct locations, operating important roles in some cases.[9] Although they differ in their primary sequence, origin, and physiological functions, they share the common property to form stable aggregates enriched in β-sheet. A recent study reveals that protein misfolding and aggregation not only lead to the loss of functions but also gains in toxicity, which triggers many amyloid diseases.[10] At least thirty human diseases have been identified that are associated with protein aggregation and misfolding.[7] A list of most common amyloid triggered diseases have been tabulated in Table 1.1. These neurological disorders involve fibrillary aggregates of particular proteins. The fibrillary aggregates are structurally similar across all the amyloid induced disorders.[11-12] They are known to involve common molecular and cellular mechanisms, including nucleation of the proteins followed by oligomerization and fibril formation.[13] Fibrillar and oligomeric amyloid aggregates are the potential source of neurotoxicity that ultimately leads to neurodegenerative disorders depending on the protein involved.

1.2. Alzheimer's Disease:

Alzheimer's disease (AD), an irreversible brain disorder first diagnosed more than 100 years ago, still remains a curse to society, victimizing one in ten individuals above 65 years' age due to lack of efficient therapeutic strategy.[14] According to a survey by King's College London, presently 46.8 million people are living with AD, and the figure is predicted to triple by 2050. AD is the most common form of dementia that results in memory loss and inabilities in learning, thinking, and decision making. It is a progressive memory disorder where symptoms gradually worsen over time. In the early stage, memory loss is mild. However, in the later stage, the patient loses the ability to perform basic activities. AD is the only disease in the top 10 causes of death in the united states for which no disease-modifying strategy or preventive measures exist.[15] The difficulties include the incomplete understanding of disease pathogenesis, difficulties in the animal model, and translating of potential *in vitro* drugs into *in vivo* activities. Disease-modifying strategies strictly rely on targeting an entity related to the disease. However, the complex interplay of the molecular mechanism associated with AD is not completely understood. Based on this limited understanding, it is relatively difficult to characterize if a pathological observation is playing a causative role or not. Many biomedical strategies have been targeted, with some of the potential candidates reaching several clinical trials.[16-17] Among these, strategies targeting Amyloid β (Aβ) have shown to play a key role in AD pathogenesis.

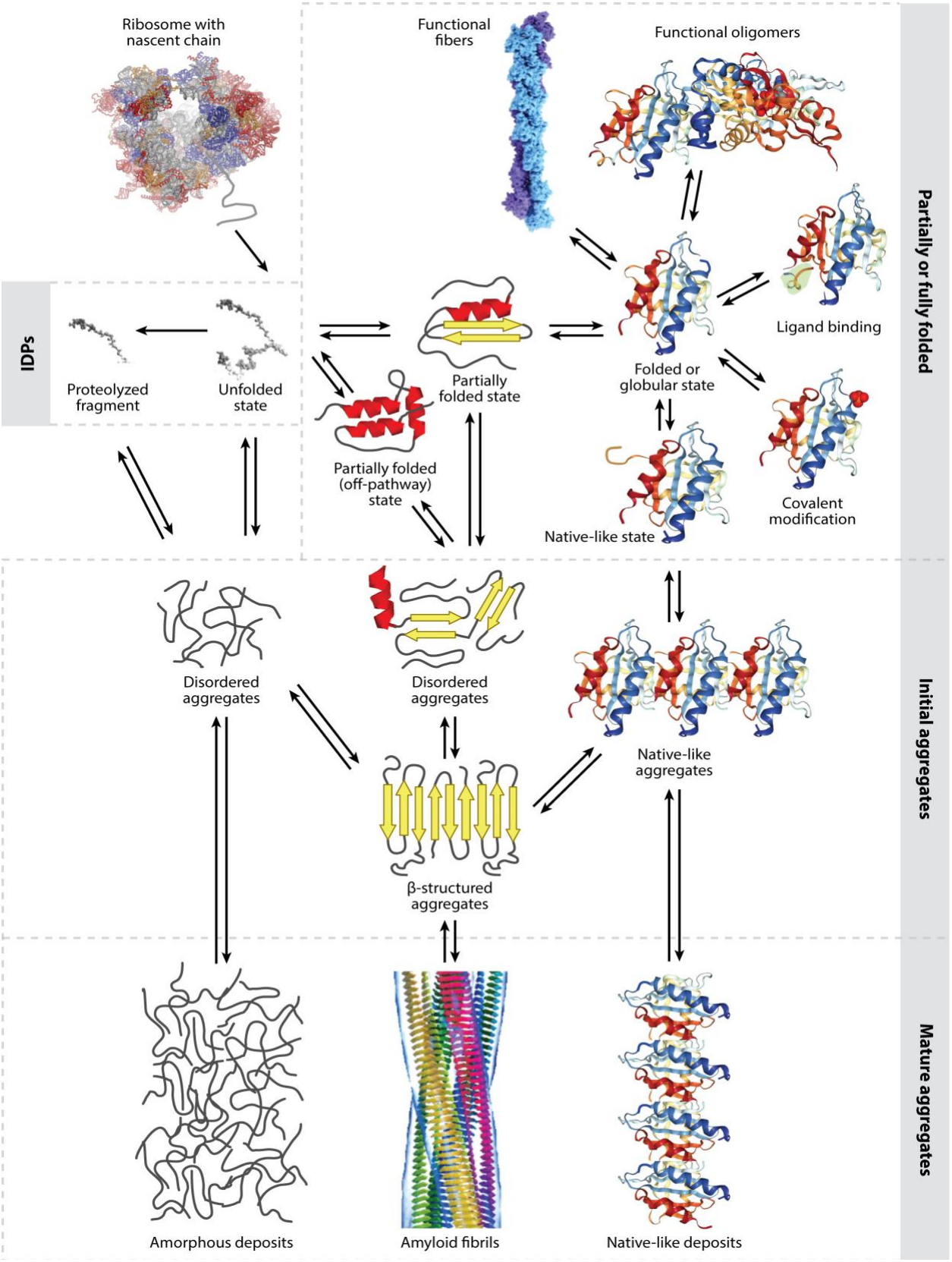

Figure 1.1. *Multiple conformational states of amyloids. IDPs: Intrinsically disordered proteins.* [2]

***Table 1.1**: Protein misfolding diseases associated with proteins and peptides.*

Pathological condition	Protein associated with the diseases
Alzheimer's disease	Aβ peptides (plaques); tau protein (tangles)
Type II diabetes	Amylin (aa 1-37)
Parkinson's disease	α-Synuclein (aa 1-100)
Huntington's disease	Huntingtin (intact or poly(Q) rich fragments)
Fronto-temporal dementias	Tau (wild type or mutant)
Senile systemic amyloidosis	Transthyretin (full length or fragments)
Hemodialysis-related amyloidosis	β2-Microglobulin
Familial amyloid polyneuropathy III	Apolipoprotein A1 (fragments)
Hereditary non-neuropathic systemic amyloidosis	Lysozyme (mutants)
Hereditary renal amyloidosis	Fibrinogen
Injection localized amyloidosis	Insulin
Medullary carcinoma of the thyroid	Calcitonin

1.3. Amyloid β (Aβ)

Amyloid β (Aβ) is a 4.3 kDa fibrillogenic polypeptide, exists in multiple isoforms and prone to undergo self-aggregation.[18] The aggregated Aβ is the major constituent of amyloid fibrils, the pathological hallmark of AD. The peptide originates through proteolytic cleavage of amyloid precursor protein by β and γ secretase.[19] α secretase functions to follow a non-amyloidogenic pathway. In contrast, β and γ secretase functions in the amyloidogenic pathway where β secretase contributes to the N-terminus and γ secretase regulates the length of the peptide. The resulting product varies from 38-43 residues. However, most amyloidogenic residues are Aβ40 and Aβ42. In human cerebrospinal fluid (HCSF), Aβ40 is the most abundant, but Aβ42 is more amyloidogenic in nature.[18] Thus, the relative ratio of Aβ40: Aβ42 in HCSF is used to differentiate AD from other forms of neurological disorder.[20] Although, Aβ has been strongly implicated in the pathogenesis of AD, it seems to have profound physiological functions in healthy conditions as it exists in physiological fluids and non-neuronal cells.[21-22] A recent report reveals that Aβ in picomolar concentration actually induces synaptic plasticity, indicating a concentration-dependent dual role of Aβ.[23] In addition, the appropriate concentration of Aβ in brain fluid has also been reported to help the recovery from acute brain injury, suggesting a physiological role of Aβ in a healthy individual.[23]

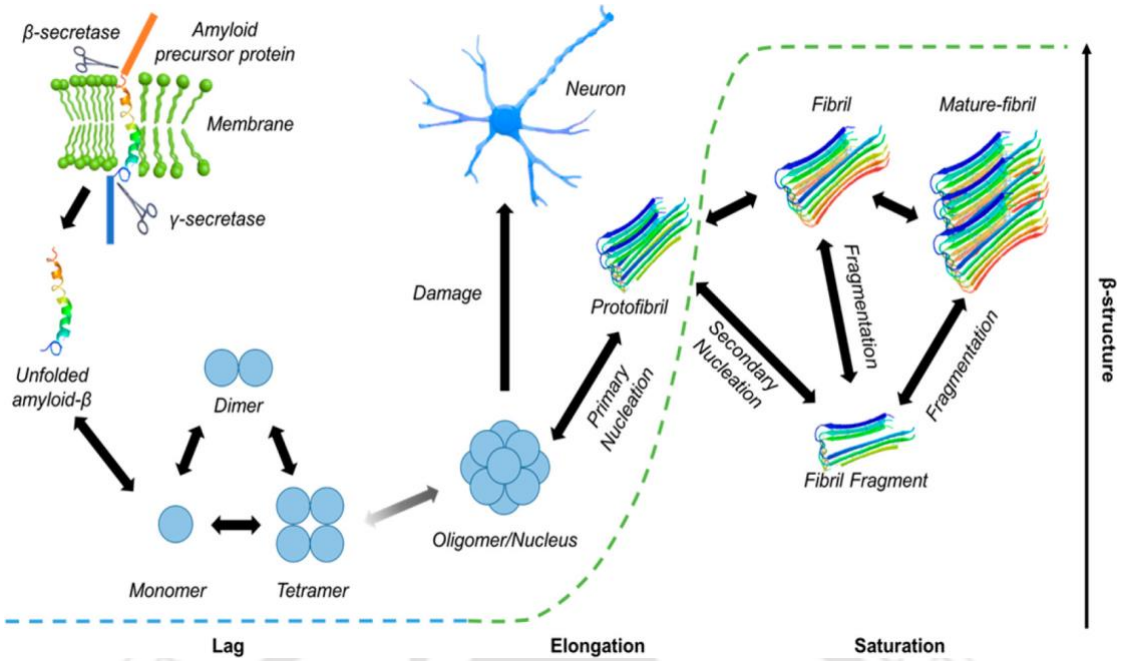

Figure 1.2: *Formation of Aβ fibrils. Aβ is produced from amyloid precursor protein (APP) after sequential proteolytic cleavage by β- and γ-secretases. Fibrils are formed via a variety of pathways by nucleation-dependent kinetics, which can be mainly categorized as lag, elongation, and saturation phase. There also exists fragmentation to catalyze the preformed fibrils to form new fibrils. The Aβ oligomers are believed to cause damage to neuron cells.*[24]

1.4. Amyloid Aggregation and Amyloid Oligomers

Both Aβ40 and Aβ42 are highly prone to undergo self-aggregation. The aggregation propensity can be attributed to the C-terminal hydrophobic residues and KLVFF residues at mid-region.[25] The detailed *in vitro* study of the Aβ aggregation pathway reveals that it is a nucleation dependent pathway comprised of a lag phase, elongation phase, and saturation phase (Figure 1.2). The lag phase includes the formation of nuclei at a critical concentration below which aggregation reaction is not likely to occur. Once the nuclei are formed, it undergo further proliferation into mature fibrillar aggregates through seeding. The fibrillation process is believed to proceed through multiple intermediates, known as oligomers. The soluble oligomeric Aβ aggregates can exist in different forms with a molecular weight ranging from 8 kDa dimers to >100 kDa protofibrils. The small aggregates are spherical in nature, while protofibrils possess an elongated threadlike morphology.[26] The low molecular weight soluble oligomers formed during the early stage of fibril formation have recently proven to induce neuronal cell death even in picomolar concentration and are considered as the major

pathogens in AD.[27-28] A study on amyloid precursor protein (APP) transgenic mice revealed that low molecular weight (LMW) amyloid oligomers not only cause synaptic loss but also affect other parameters related to AD pathology, including enhanced ROS (reactive oxygen species) production, abnormal tau phosphorylation, neuronal loss, and microglial activation.[29] Consequently, stable LMW oligomers and protofibrillar species generated from oligomers

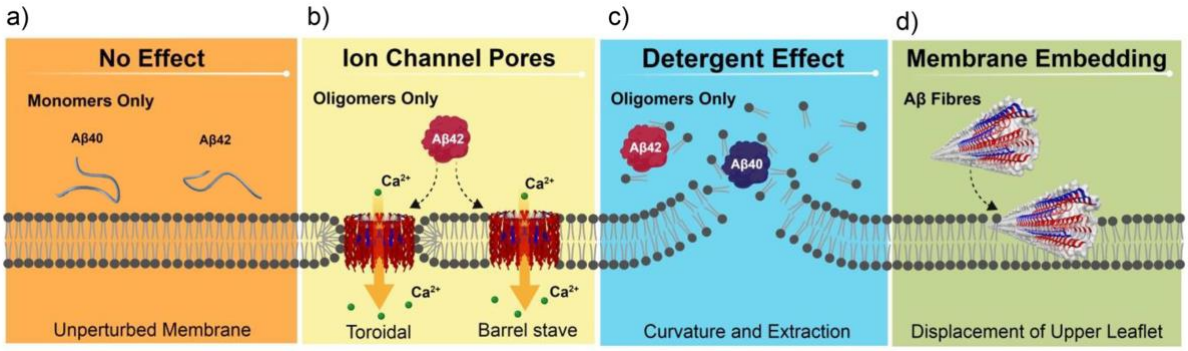

Figure 1.3: *The mechanisms of Aβ mediated membrane disruption depend on Aβ structure. Aβ monomers, oligomers, and fibers have distinct impacts on membrane integrity. a) Aβ monomers have little impact on membrane structure. b) only oligomeric Aβ42 has the ability to form ion channel pores in cellular membranes. c) oligomers of both Aβ42 and Aβ40 have a widespread detergent effect causing lipid extraction, curvature, and rupture of the membrane bilayer. d) the ability of A to form ion channels or have a deterrent effect is lost on assembly into amyloid fibers; instead, fibers can laterally embed into the membrane and displace the upper leaflet of the bilayer*

become 50-times more neurotoxic than the fibrils.[30] It has been shown that Aβ oligomers possess profound detergent-like properties and disrupt cell membranes of neuronal cells to exert neurotoxicity, unlike monomers or fibrillary aggregates (Figure 1.3).[31]

Hence, in recent years, research attention is being focused on the separation and characterization of LMW oligomeric species and their unique biological activity rather than traditional amyloid fibrils as the target.[31]

1.5. Therapeutic Approaches

Considering the key role of Aβ in AD, many drug discovery strategies have concentrated on the development of Aβ-based therapeutics. During the decade (2002-2012), 48% of the clinical trials were targeted towards Aβ.[43] Efforts were focused on reducing Aβ production (targeting secretases), increasing clearance (activating degrading enzymes), and regulating aggregation (small molecules and chaperones).[44-45] Approaches to suppress the

Table 1.2: Different types of oligomers and their features

Name	Properties	Reference
Dimers – tetramers	8-20 kDa, LTP-inhibiting, present in human brain and CSF	27, 28, 32
ADDLs	~10-20mer, >40 kDa, spherical, present in CSF and the human brain, triggers tau phosphorylation	33-35
Oligomers	15-20mer, >40 kDa, neurotoxic, spherical, present in the human brain	36-37
Globulomers	~60 kDa, globular, present in the human brain	38
Protofibrils	>20mer, >100 kDa, linear with beaded appearance, neurotoxic, present in tg-mouse and cell culture media, brain and human AD brain, associated with memory deficits in tg-mice	39-41
Annular aggregates	Synthetic, 150-250 kDa, 7-10 nm in diameter	42

production of Aβ by inhibiting γ-secretase have been restricted because of its essential proteolytic activities.[45] Moreover, strategies aimed at inhibiting Aβ production or increasing Aβ clearance have been found to be vulnerable by conceptual setbacks, as reports have indicated that a minimum amount of Aβ is essential for neuroprotection in the healthy brain.[46] Inhibition of β secretase may not lead to unwanted toxicity of a similar kind. However, the

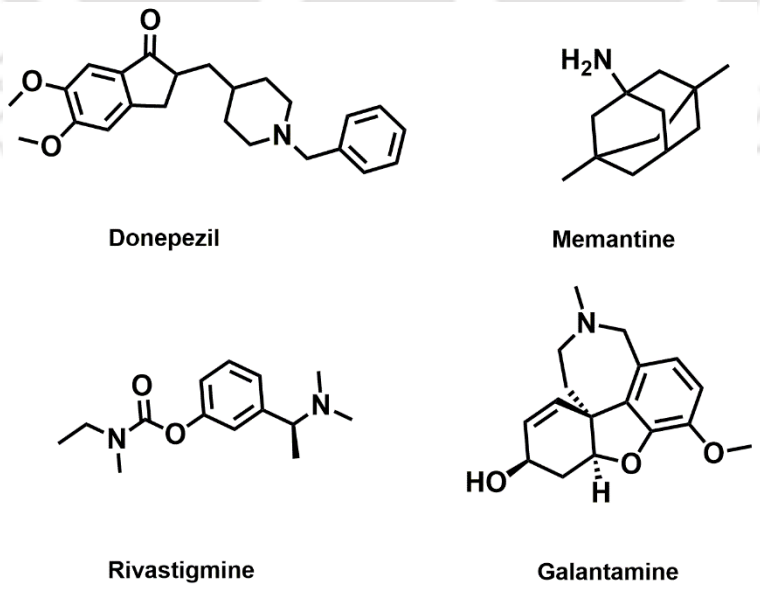

***Figure 1.4**: Currently recommended drugs for AD*

development of β secretase inhibitors is highly challenging because of their larger pocket that requires larger molecules with poor BBB permeability.[47] Hence, approaches to inhibit the aggregation process of Aβ have been globally appreciated, as it would only target the toxic species without affecting the functional Aβ levels. Chemical structures of a few potential AD drugs have been shown in figure 1.4.

1.5.1. Inhibition of Amyloid Aggregation

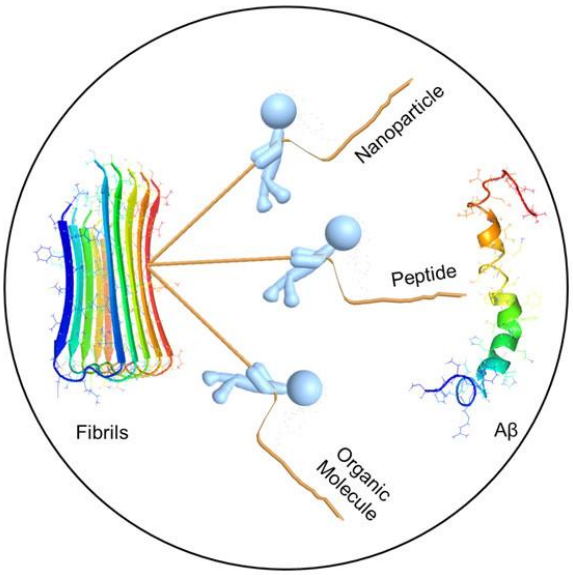

Figure 1.5: *Schematic presentation of nanoparticles, peptides, and organic molecules showing anti-amyloid properties.*

In recent years, an immense effort has been dedicated to develope therapeutic approaches to inhibit Aβ aggregation. These include binding monomeric peptides, electrostatic interactions, blocking oligomeric intermediates, stabilizing native folded state, etc. Many materials, including small molecules, nanomaterial, polymers, peptides, antibodies, have been employed to achieve efficient inhibition (Figure 1.5). Yet every material has its own advantages and limitations.

Nanoparticles: Recently, nanoparticle (NP) based therapeutics have received immense interest. These are particles of 1-100 nm in diameter with suitable surface functionality. Similar to the amyloidogenic proteins, most of the NPs possess a tendency to undergo self-aggregation, indicating a significant impact on amyloid diseases.[48] The NPs often show excellent selectivity towards target proteins because of suitable surface functionalization.[24] However, other physical parameters, including size, shape, and charge, play a vital role in

determining their physicochemical effect on the target protein. A recent study showed that smaller nanoparticles are more efficient in inhibiting amyloid fibrillation.[48]

Polymers: In recent years, polymer-based therapeutic materials have received great attention because of their high stability in physiological systems, cell viability, tunable molecular weight, and ease of multi-functionalization. It has also been demonstrated recently that the molecular weight of the polymers plays a vital role in determining the degree of anti-amyloid activities of the polymers.[49]

8-hydroxyquinoline functionalized polyfluorene (PFHQ) have also been developed to mitigate amyloid induced cell damage *in vitro*.[50] The amyloid-like surface of PFHQ provides extra room to interact with mature amyloid fibril and their clearance. A novel isatin functionalized polyfluorene (PFIS), reported by a similar group, is known to regulate the nucleation pathway of Aβ. PFIS has been shown to modulate the nucleation to a secondary pathway from the primary nucleation pathway and thereby suppress the neurotoxicity of Aβ.[51] A reactive amphiphilic polymer to inhibit amyloid oligomerization has also been reported.[52]

Small Molecules: A wide range of small molecule amyloid inhibitors have been developed in search of anti-amyloid therapeutics.[53] Some general characteristics of small molecule-based inhibitors have been explored. These include pieces of evidence that most of the small molecule inhibitors modulate the self-aggregation pathway rather than inhibiting it.[54] Various independent remodeling pathways are possible, and notably, relatively small changes in

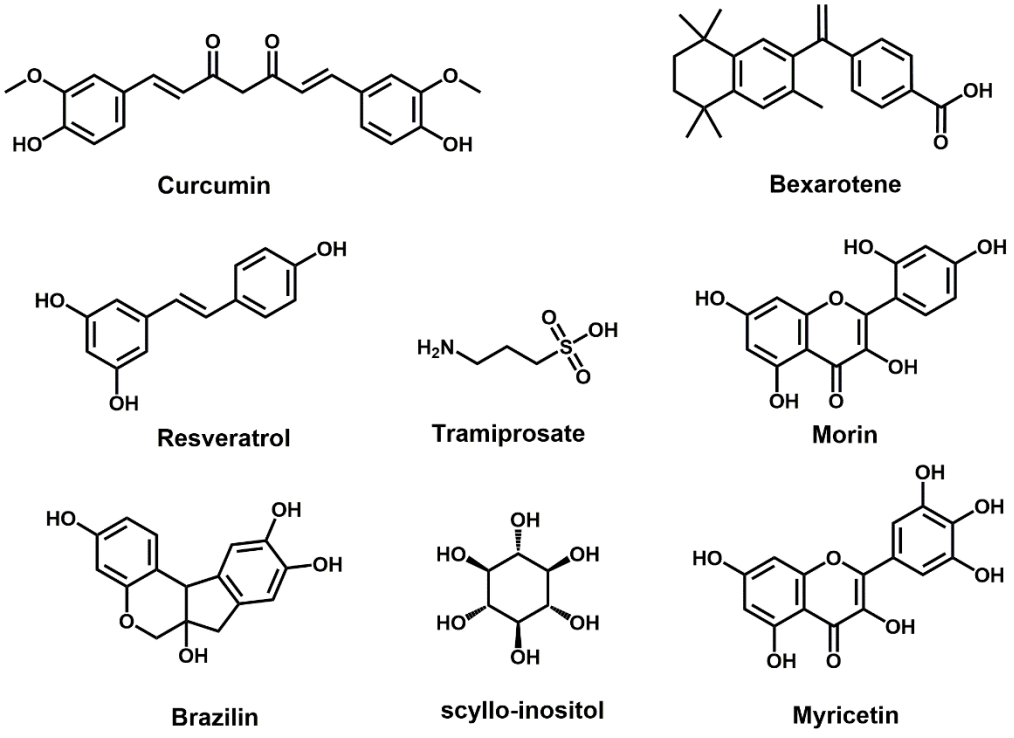

***Figure 1.6**: Small molecule inhibitors for amyloid aggregation*

compound structure can bring dramatic changes in the mechanism of how compounds operate to perturb the amyloid aggregation process.[54-56] This highlights the significance of compound screening and explore a structure-activity relationship (SAR) to identify active pharmacophores and lead future drug discovery mission. A brief discussion of key inhibitors has been presented above (Figure 1.6).

Curcumin is an active ingredient found in turmeric and has been recognized as one of the most efficient amyloid inhibitors.[57] Numerous theoretical and experimental studies reveal that it binds with both Aβ oligomers and fibrils, thereby inhibiting oligomerization, enhancing clearance of preformed Aβ fibrils, and suppressing their neurotoxicity.[57-58] Bexarotene was identified as a multipotent potent AD therapeutic through recognition of its ability to promote Aβ degradation by means of increasing ApoE production and Aβ aggregation modulation. Several kinetic details reveal that it blocks the primary nucleation of Aβ and thereby mitigating the neurotoxicity associated with Aβ aggregates.[59] Resveratrol is known for its neuroprotective effects in AD models. The compound inhibits Aβ aggregation as well as disintegrates matured Aβ fibrils.[60] Tramisprosate is a Non-Steroidal Anti Inflammatory Drug (NSAID) that is known to bind with Aβ and suppress its toxicity.[61] Although this compound shows appreciable anti-AD properties; it failed in phase III clinical trial because of its poor selectivity.[62] In parallel to this, several small molecule-based inhibitors, including morin, brazilin, scyllo-inositol, myricetin have also shown promising anti-AD properties.[63-65]

Peptides: Peptides usually denote linear molecules consisting of at least two amino acid residues. This biological material or artificially manufactured substance is an outstanding alternative to pharmaceuticals, because of its essential role in regulating biological functions. However, the difficulty arising with rapid degradation implies problems for administration and delivery.[66] In 1996, a study revealed that the hydrophobic sequence, Aβ16–21 (KLVFFA), perturbs interactions leading to oligomerization, whereby typical antiparallel β-sheet motif was formed as a result of their interaction with full-length Aβ40 and Aβ42. Later, a wide variety of Aβ sequences with LVFFA and KLVFF motifs were also developed to be effective in modulating Aβ fibrillation in vitro.[67] In addition to this, a proline residue, is known to be a β-sheet breaker, was also incorporated to develop a proline based central hydrophobic sequence in order to perturb Aβ fibrillation.[68] The main reason behind this is the involvement of the nitrogen in proline lacking a proton, which helps to prevent hydrogen bond formation essential in the fibrillation process. Likewise, methylation in amide groups is also an excellent strategy to design new inhibitors. The N-methyl group actually improves the solubility in aqueous media and, in turn, suppresses the Aβ aggregation.[69] A peptide-based inhibitor, named Aspan, belongs to this category has even been in the Phase II clinical trial.[70] A list of potential peptide-based amyloid inhibitors has been enlisted in table 1.3.[24]

Table 1.3: Peptide-based inhibitors of amyloid aggregation.

Name	Sequence	Function	Reference
None	KLVFF	Lay a good foundation to discover the KLVFF bearing inhibitor	25
H_2	G-QKLVFFAEDVGGaKKKKKK	Solvent effect on the toxicity inhibition in a cellular model.	70
DDX	hydrophilic moiety-KLVFF	Toxicity inhibition induced by the aid of hydrophilic moiety.	71
D3	D-RPRTRLHTHRNR	It established the groundwork for D3 and its derivative to accomplish preclinical study.	72
None	VVIA	Oligomerization inhibition induced by the C-terminal peptides	73
iAβ5	LPFFD-PEG	Phase I and II clinical trials.	68
None	IGLMVG	The cellular model shows toxicity inhibition by one of a C-terminal peptide.	74

1.5.2. Regulation of Secretase Activities

α-secretase is a proteolytic enzyme that cleaves amyloid precursor protein (APP) in its transmembrane region to produce Aβ.[75] Such activation reduces production of Aβ which in turn lowers Aβ content.[76] Increasing the activity of α-secretases via the activation of associated signaling cascades has been considered as one of the best therapeutic approaches to design drugs against AD.[77] A wide range of small molecule-based drugs, including Etazolate, Selegiline, PRZ-03140 are known to activate α-secretase and subjected to clinical trials.[78-79] BACE1 is a

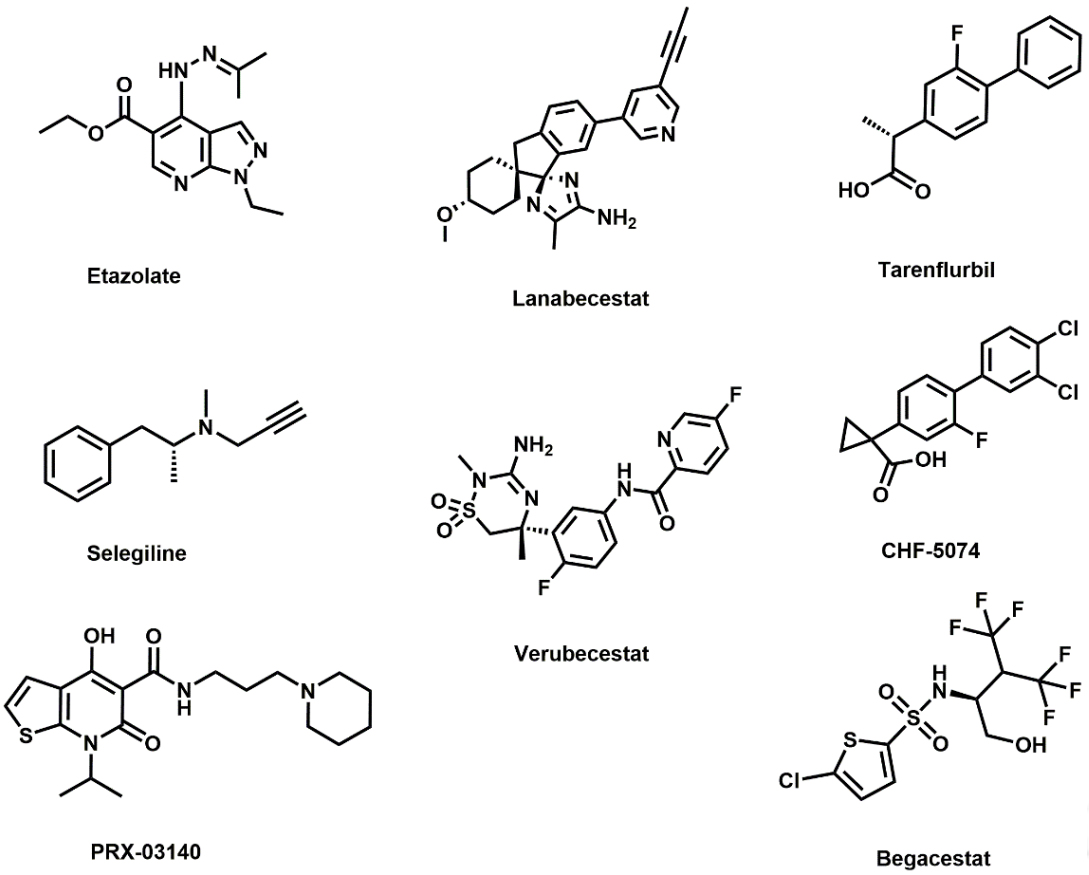

***Figure 1.7**: Chemical structures of a few potential secretase inhibitors.*

sequence-specific β site APP cleaving enzyme that is considered as a potential candidate for β-secretase.[80] Although it is not always causative in AD, it functions to produce more Aβ by favoring β-secretase cleavage. Some of the successful BACE1 inhibitors like Lanabecestat, Verubecestat have resulted in reduced levels of Aβ.[80-82] However, due to the large active site of BACE1, most of the BACE1 inhibitors show poor BBB permeability. γ secretase cleaves the C terminal domain of APP and releases its cytoplasmic domain. It is also influenced by presenilin 1 and 2 (PS-1 and PS-2), which seemed to determine where at the C-terminal, cleavage of Aβ occurs by γ-secretase. These γ secretase inhibitors are capable of lowering the Aβ levels without disturbing the production of non-pathogenic isoforms of Aβ. The most important secretase inhibitors have been shown in Figure 1.7.

1.5.4. Metal Ion Chelation

In parallel to the aggregated Aβ, a high level of neurotoxic metal ions like iron, copper, aluminum, zinc in the AD brain clearly indicates the involvement of such metals in the disease.[83-84] The central nervous system (CNS) is very susceptible to oxidative damage. These

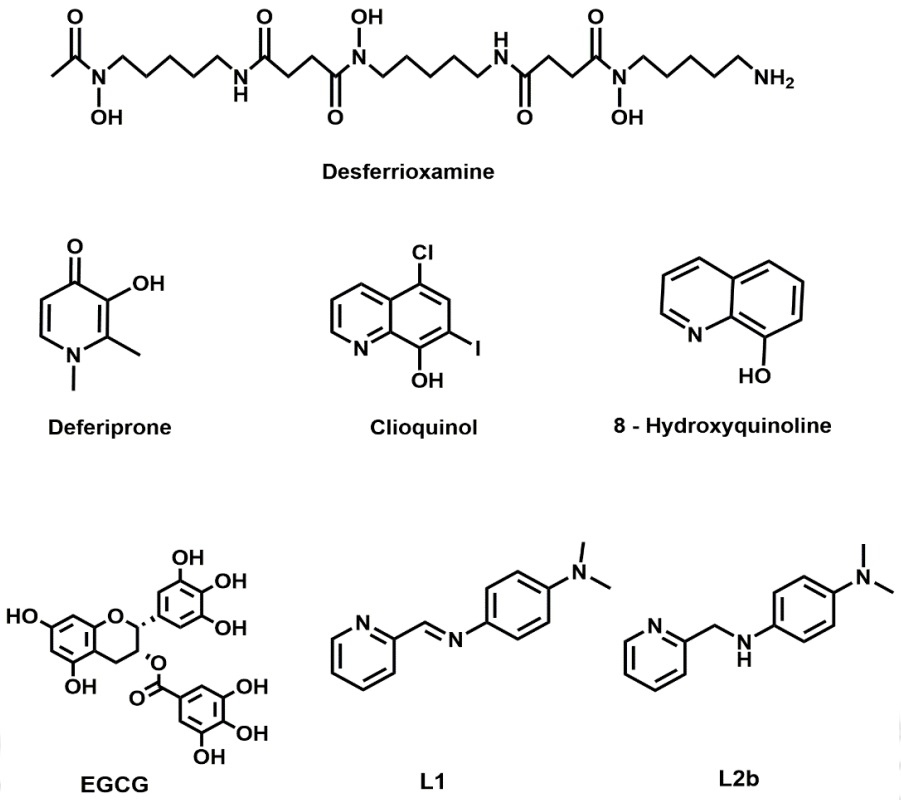

Figure 1.8: *Chemical structures of some potential metal ion chelators implicated in AD.*

transition metal ions, especially copper and iron, catalyzes Fenton type redox reactions to produce reactive oxygen species (ROS) that finally result in oxidative damage in the brain.[85]

Hence, sequestering such toxic metals may be regarded as a therapeutic approach against AD (Figure 1.8). However, the application of metal ion chelation in AD therapy first came into the picture after the discovery of metal chelator, Desferrioxamine (DFO), that eliminates excess aluminum and iron from the body. It is the only metal chelator drug approved by the FDA, used for clearance of excessive iron. DFO exhibited promising results in slowing down the progress of AD in the clinical trial.[86] Although the study was based on Aluminium chelation, DFO strongly binds with iron, copper, and zinc as well. However, the poor BBB permeability and low absorption in the gastrointestinal tract limits its clinical application. Deferiprone is also a chelator of iron and aluminum approved in Europe only but not in the United States.[87] Although it shows high oral activity and BBB permeability, it produces serious side effects in CNS.[88] Thus, the application of most of the iron chelators are restricted due to their serious toxicity or low BBB permeability. Clioquinol is a derivative of 8-hydroxyquinoline that shows BBB permeability and therapeutic benefits related to AD. It chelates with copper and zinc with a higher affinity than for calcium and manganese. Clioquinol therapy has shown to slow down cognitive decline in AD patients.[89] Also, some of the polyphenols are known to show metal chelation abilities. Epigallocatechin gallate, a

polyphenol present in green tea extract, is known as an iron chelator and able to remove excess iron from the brain. It has been demonstrated to attenuate iron toxicity and oxidative stress-induced neuronal damage in neuroblastoma cells.[90] A small molecule-based metal ion chelator, L1, has been developed for the removal of excess copper and zinc ions from the AD brain. However, the low stability of L1 in an aqueous medium limits its application. The modified structure L2b shows appreciable metal chelation and Aβ binding abilities. The molecule translocates through BBB as it possesses molecular weight less than 450 (Lipinski's rule) and is relatively lipophilic (clogP<5). However, no strong clinical evidence for the beneficial effect of such chelators in AD has been found, which further demands the development of new therapeutic materials.

1.5.5. Oxidative Stress

Oxidative damage is one of the major pathological hallmarks in AD. It is usually induced by ROS that damage lipids, proteins and nucleic acids to impair cellular functions and disrupt membrane properties, including membrane integrity, fluidity, ion transport, enzyme activities, and protein crosslinking.[91] High level of ROS results in cell death.[91] Also, soluble oligomeric aggregates are known to enhance the ROS level. The occurrence of an increased amount of lipid peroxidation product including 2-propenal and 4-hydroxynonenal in HCSF and plasma of AD patients strongly implicates the involvement of oxidative stress in AD.[92]

Aging: Age is an important risk factor in AD. The accumulation of oxidative damaged DNA, proteins, and lipids have been found to increase with age.[92] Numerous pieces of evidence of an increase in oxidative stress with the aging process can be partly correlated with neurodegeneration.[92]

Lipid Peroxidation and Protein Oxidation: The cell membranes are composed of phospholipids, the primary target of ROS. Hydroxyl, peroxy, and alkoxy radicals are mainly involved in lipid peroxidation.[92] The interactions of ROS with membrane increase free calcium ion transport through the membrane that eventually leads to neuronal apoptosis.[93] On interaction with the protein, ROS results in the formation of protein-carbonyl derivative, a biomarker of protein oxidation.[94] α-enolase has been characterized as an enzyme and as a target of protein oxidation that contributes to AD pathogenesis.[95]

DNA Oxidation: ROS causes oxidative damage to mitochondrial DNA. It results in the breakage of DNA strand, DNA cross-linking, oxidation to deoxyribose, etc. Oxidation to mitochondrial DNA results in dysregulated aging and other biochemical factors associated with neurodegeneration.[96]

Oxidation to Met^{35}: The oxidation state of Met^{35} in Aβ regulates the rate of fibril formation. Oxidation to Met^{35} enhances the rate of fibril formation compared to non-oxidized Aβ.[97]

1.5.6. Neuroinflammation

In parallel to oxidative stress, Aβ oligomers can trigger inflammatory responses via pattern recognition receptors (PRR) such as Toll-like, NOD-like (nucleotide-binding oligomerization domain) receptors, receptor for the advanced glycation end product (RAGE), formyl peptide, and scavenger receptors on glial cells and neurons that contribute to AD pathology.[98] The amyloidogenic folding of α-synuclein also induces neuroinflammation by activating similar types of receptors like NOD-like receptors pyrin domain and Toll-like receptor 2.[99] In both Alzheimer's and Parkinson's disease, the activation of astroglial and microglial cells brings about major inflammatory responses. Based on the staining for microglial activation and post-mortem analysis of PD affected brains, it is postulated that the dopaminergic neurodegeneration occurring early in the disease process is accompanied by the widespread activation of microglial cells.[100-101] It has also been reported that the release of α-Synuclein aggregates or its pathological mutant A53T by neuronal cells activates proinflammatory cytokines from glial cells in vitro.[102] The αS oligomers released from the neuro cells are usually internalized by the astrocytes triggering proinflammatory cytokines and chemokines. This inflammatory response is because of the transmission of αS aggregates from neurons to glial cells, associated with the extent of glial accumulation of αS aggregates and changes in glial gene expression profiles to an inflammatory response.[103]

1.5.7. Mitochondrial Dysfunction

Mitochondria are easy targets of such ROS, and their enhanced level usually leads to mitochondrial dysfunction.[104] In addition, the interaction of toxic Aβ aggregates with several mitochondrial proteins and enzymes such as alcohol dehydrogenase, ATP synthase, and cyclophilin-D play a crucial role in mitochondrial dysfunction.[105-107] Moreover, Aβ oligomers, while interacting with such biological entities, activates caspase-3 and triggers mitochondria induced neuronal apoptosis. Recent research reveals that mitochondrial dysfunction is one of the most important signatures of AD in early-stage.[108] Aβ oligomers are also known to activate caspase-3 and cleave Poly (ADP-ribose) polymerase (PARP). The cleaved PARP is known as an endogenous mitochondrial toxin that depolarises mitochondrial membrane potential (MMP) and disrupts membrane integrity.[109] The fluorometric imaging of MMP can be performed using JC-1 dye, a dual-color probe that targets live mitochondria in a membrane potential-dependent manner. When excited, the dye undergoes J-aggregation to emit intense

red fluorescence upon entering inside live mitochondria with high membrane potential. However, it does not undergo any aggregation and emits green emission in dying mitochondria with low MMP. The Aβ oligomers usually interact with the cyclophilin-D and help to open mitochondrial permeability transition pore (mPTP).[105] The opening of mPTP allows uncontrolled transportation of cytosolic solute that, in turn, damages the mitochondrial structure. The damage results in mitochondrial dysfunction, including impaired energy production and initiation of neuronal apoptosis.[105] Hence, impairment of mitochondrial dysfunction can also be a lead strategy in combating AD. A new class of drug molecule that targets TSPO, one of the lead composition of the mPTP and shown to restore mitochondrial dysfunction from Aβ induced neurotoxicity was also developed recently.[110] Several synthetic materials designed to combat mitochondrial damage has also been reported.[111-112] Further, a novel drug molecule by simple chemical modification in natural product Berberine, with the potential to attenuate multifaceted toxicity associated with AD, have also been reported. The multitargetted drug molecule can combat Aβ oligomerization, metal-induced oxidative stress, and mitochondrial dysfunction related to AD.[113]

1.5.8. Blood-Brain Barrier

In order to target CNS disorders, including AD, BBB permeability is one of the essential criteria that any potential drug molecule must satisfy. The BBB is a highly efficient and selective barrier composed of endothelial cells glued together with the help of a chaperon and protects the brain from unwanted molecules and pathogens. It is the authority that controls the transportation of drug molecules, ions, proteins, and other molecules inside the brain. The lack of therapeutic against AD and other brain disorders is due to the poor BBB permeability of most of the drug molecules. There is no universal rule that predicts the real BBB permeability of a newly developed drug. There are multiple routes to translocate through BBB: (1) transcellular and paracellular routes, (2) lipophilic pathways (influx/efflux), (3) receptor-induced transcytosis, and (4) absorptive triggered transcytosis.

1.5.9. Animal Models

The APP/PS1 mouse model expresses two transgenes: human APP with Swedish mutant and human PS1 along with L166p mutant.[114-115] The Swedish APP mutant produces Aβ 6-8 fold because of a different cellular position of β-secretase APP cleavage.[116] The mutant, L166P PS1 is quite aggressive, with AD symptoms beginning in patients as early as 24 years of age.[116] The APPS1 mutant produces plaques characteristic to real human AD patients. In addition, the plaques form at a relatively faster rate. Likewise, these mice develop cognitive

decline: by eight months' age, they face more difficulties in learning a maze task than their wild type congener.[114] Hence, these AD mouse models are ideal for investigating plaque formation with respect to time. Such plaques exhibit a similar molecular structure and demonstrate some neuronal and cognitive deficits of AD that sorts it an ideal model in which to investigate plaque development.

In this thesis, Aβ toxicity has been investigated and impaired in a wild type mouse model. Although WT mice are unable to develop Aβ plaques on their own, the nervous system is susceptible to Aβ neurotoxicity resulting in neuronal damage. Although WT mice lack advanced cognitive ability as possessed by APP mutants, they may serve as a robust, economical, and high-throughput alternative to complement transgenic mouse models.

1.6. Thesis Synopsis:

Motivated by the unmet need to develop an efficient therapeutic strategy to combat AD, the aim of this thesis is to design various therapeutic materials to inhibit the oligomerization of Aβ and block several neurochemical pathways that lead to neurotoxicity associated with AD. The main research outputs are presented in five chapters of this thesis, the contents of which are outlined below-

Chapter 1 includes a brief discussion about AD and the existing therapeutic strategies such as regulation of Aβ production, inhibition of Aβ aggregation, and other strategies like metal ion chelation, oxidative stress, mitochondrial dysfunction, etc. In addition, Aβ neurotoxicity and their validation in cell lines and animal models also have been included.

Chapter 2 aims to isolate the tetrameric form of Aβ, the most toxic oligomers associated with Aβ neurotoxicity. The aggregation of monomeric Aβ was tuned to produce a toxic oligomeric form, and tetrameric species were isolated through native PAGE electrophoresis, and toxicity was assessed in the neuroblastoma cell line. Finally, a novel gold nanoparticle functionalized with N-methyl D-aspartic (NMDA) acid was developed and demonstrated to mitigate the neurotoxicity of the tetramer by blocking the oligomerization of Aβ through electrostatic interaction.

Chapter 3 deals with the development of an Isatin functionalized polymeric template in order to regulate the nucleation pathway of Aβ and mitigate its toxicity. Isatin core is highly biologically important. However, its poor solubility in any solvent limits its application in medicinal chemistry. Incorporation of Isatin functionality in polyfluorene backbone highly improves its solubility. Furthermore, on interaction with Aβ, it regulates the nucleation to a

secondary pathway through the formation of a polymer-peptide co-aggregate. As a result, the toxicity of Aβ was significantly suppressed.

Chapter 4 describes the development of a novel 'artificial chaperon' that can sequester toxic amyloid beta (Aβ) by binding at their 'amyloidogenic domain' and impair amyloid mediated neuronal damage in a high throughput wild type (WT) mouse model. Most importantly, an optimal dose of PFBZ successfully recovered amyloid triggered internal hemorrhage in the cerebral cortex of the WT mouse. This was evidenced by elevation in reactive oxygen species (ROS) level, caspase activation, and mitochondrial dysfunction biomarkers and was complemented by brain histology and electron microscopy data. The multipotent and highly biocompatible polymer nano-drug may find broad applications in eradicating amyloid triggered neurotoxicity implicated in numerous human disorders.

Chapter 5 includes the development strategy of a small molecule drug that inhibits Aβ aggregation and disrupts mature amyloid fibrils through multiple π interactions. The probe functions to block a chain of biochemical events, including PARP cleavage, caspase activation, and mitochondrial dysfunction that leads to neuronal loss in AD. The results were further verified using a wild type mouse model where an appropriate dose of INHQ was able to attenuate amyloid mediated internal hemorrhage.

Chapter 6 consists of the epilogue of the thesis. This chapter concludes the thesis with a summary of my research outputs.

1.7. References

1. Marth, J. D. A unified vision of the building blocks of life. *Nat. Cell Biol.* **2008,** *10,* 1015-1015.

2. Chiti, F.; Dobson, C. M. Protein misfolding, amyloid formation, and human disease: a summary of progress over the last decade. *Annu. Rev. Biochem.* **2017,** *86,* 27-68.

3. Herczenik, E.; Gebbink, M. F. B. G. Molecular and cellular aspects of protein misfolding and disease. *FASEB J.* **2008,** *22,* 2115-2133.

4. Adamcik, J.; Mezzenga, R. Protein folding and misfolding: mechanism and principles. *Angew. Chem. Int. Ed.* **2018,** *57,* 8370-8382.

5. Englander, S. W.; Mayne, L. The nature of protein folding pathways. *Proc. Natl. Acad. Sci. U. S. A.* **2014,** *111*, 15873-15881.

6. Chiti, F.; Dobson, C. M. Protein misfolding, functional amyloid, and human disease. *Annu. Rev. Biochem.* **2006,** *75*, 333-366.

7. Sipe, J. D.; Benson, M. D.; Buxbaum, J. N.; Ikeda, S.-i.; Merlini, G.; Saraiva, M. J. M.; Westermark, P. Nomenclature 2014: amyloid fibril proteins and clinical classification of the amyloidosis. *Amyloid* **2014,** *21*, 221-224.

8. Sipe, J. D.; Cohen, A. S. Review: history of the amyloid fibril. *J. Struct. Biol.* **2000,** *130*, 88-98.

9. Fowler, D. M.; Koulov, A. V.; Alory-Jost, C.; Marks, M. S.; Balch, W. E.; Kelly, J. W. Functional amyloid formation within mammalian tissue. *PLoS Biol.* **2005,** *4*, e6.

10. Stefani, M.; Dobson, C. M. Protein aggregation and aggregate toxicity: new insights into protein folding, misfolding diseases and biological evolution. *J. Mol. Med.* **2003,** *81*, 678-699.

11. Dobson, C. M. Protein folding and misfolding. *Nature* **2003,** *426*, 884-890.

12. Baker, D. A surprising simplicity to protein folding. *Nature* **2000,** *405*, 39-42.

13. Ross, C. A.; Poirier, M. A. Protein aggregation and neurodegenerative disease. *Nat. Med.* **2004,** *10*, S10-S17.

14. Mount, C.; Downton, C. Alzheimer disease: Progress or profit? *Nat. Med.* **2006,** *12*, 780-784.

15. Alzheimer's Association. 2017 Alzheimer's disease facts and figures. *Alzheimer's & Dementia* **2017,** *13*, 325-373.

16. Parsons, C. G.; Rammes, G. Preclinical to phase II amyloid beta (Aβ) peptide modulators under investigation for Alzheimer's disease. *Expert Opin. Invest. Drugs* **2017,** *26*, 579-592.

17. Doig, A. J.; del Castillo-Frias, M. P.; Berthoumieu, O.; Tarus, B.; Nasica-Labouze, J.; Sterpone, F.; Nguyen, P. H.; Hooper, N. M.; Faller, P.; Derreumaux, P. Why is research on amyloid-β failing to give new drugs for Alzheimer's disease? *ACS Chem. Neuro.* **2017,** *8*, 1435-1437.

18. Hamley, I. W. The Amyloid beta peptide: A chemist's perspective. role in Alzheimer's and fibrillization. *Chem. Rev.* **2012,** *112*, 5147-5192.

19. Querfurth, H. W.; LaFerla, F. M. Alzheimer's disease. *N. Engl. J. Med.* **2010,** *362*, 329-344.

20. Lewczuk, P.; Kornhuber, J.; Toledo, J. B.; Trojanowski, J. Q.; Knapik-Czajka, M.; Peters, O.; Wiltfang, J.; Shaw, L. M. Validation of the erlangen score algorithm for the prediction of the development of dementia due to Alzheimer's disease in pre-dementia subjects. *J. Alzheimer's Dis.* **2015,** *48*, 433-441.

21. Seubert, P.; Vigo-Pelfrey, C.; Esch, F.; Lee, M.; Dovey, H.; Davis, D.; Sinha, S.; Schiossmacher, M.; Whaley, J.; Swindlehurst, C.; McCormack, R.; Wolfert, R.; Selkoe, D.; Lieberburg, I.; Schenk, D. Isolation and quantification of soluble Alzheimer's β-peptide from biological fluids. *Nature* **1992,** *359*, 325-327.

22. Shoji, M.; Golde, T. E.; Ghiso, J.; Cheung, T. T.; Estus, S.; Shaffer, L. M.; Cai, X. D.; McKay, D. M.; Tintner, R.; Frangione, B.; et, a. Production of the Alzheimer amyloid beta protein by normal proteolytic processing. *Science* **1992,** *258*, 126.

23. Puzzo, D.; Privitera, L.; Leznik, E.; Fa, M.; Staniszewski, A.; Palmeri, A.; Arancio, O. Picomolar amyloid-beta positively modulates synaptic plasticity and memory in hippocampus. *J. Neurosci.* **2008,** *28*, 14537-14545.

24. Han, X.; He, G. Toward a rational design to regulate β-amyloid fibrillation for Alzheimer's disease treatment. *ACS Chem. Neuro.* **2018,** *9*, 198-210.

25. Tjernberg, L. O.; Näslund, J.; Lindqvist, F.; Johansson, J.; Karlström, A. R.; Thyberg, J.; Terenius, L.; Nordstedt, C. Arrest of -amyloid fibril formation by a pentapeptide ligand. *J. Biol. Chem.* **1996,** *271*, 8545-8548.

26. Serpell, L. C. Alzheimer's amyloid fibrils: Structure and assembly. *Biochim. Biophys. Acta Mol. Basis Dis.* **2000,** *1502*, 16-30.

27. Cleary, J. P.; Walsh, D. M.; Hofmeister, J. J.; Shankar, G. M.; Kuskowski, M. A.; Selkoe, D. J.; Ashe, K. H. Natural oligomers of the amyloid-β protein specifically disrupt cognitive function. *Nat. Neurosci.* **2005,** *8*, 79-84.

28. Walsh, D. M.; Klyubin, I.; Fadeeva, J. V.; Cullen, W. K.; Anwyl, R.; Wolfe, M. S.; Rowan, M. J.; Selkoe, D. J. Naturally secreted oligomers of amyloid β protein potently inhibit hippocampal long-term potentiation in vivo. *Nature* **2002,** *416*, 535-539.

29. Tomiyama, T.; Matsuyama, S.; Iso, H.; Umeda, T.; Takuma, H.; Ohnishi, K.; Ishibashi, K.; Teraoka, R.; Sakama, N.; Yamashita, T.; Nishitsuji, K.; Ito, K.; Shimada, H.; Lambert, M. P.; Klein, W. L.; Mori, H. A Mouse model of amyloid β oligomers: Their contribution to synaptic alteration, abnormal tau phosphorylation, glial activation, and neuronal loss in vivo. *J. Neurosci.* **2010,** *30*, 4845-4856.

30. Jana, M. K.; Cappai, R.; Pham, C. L. L.; Ciccotosto, G. D. Membrane-bound tetramer and trimer Aβ oligomeric species correlate with toxicity towards cultured neurons. *J. Neurochem.* **2016,** *136*, 594-608.

31. Bode, D. C.; Freeley, M.; Nield, J.; Palma, M.; Viles, J. H. Amyloid-β oligomers have a profound detergent-like effect on lipid membrane bilayers, imaged by atomic force and electron microscopy. *J. Biol. Chem.* **2019**, *19*, 7566-7572.

32. Shankar, G. M.; Li, S.; Mehta, T. H.; Garcia-Munoz, A.; Shepardson, N. E.; Smith, I.; Brett, F. M.; Farrell, M. A.; Rowan, M. J.; Lemere, C. A.; Regan, C. M.; Walsh, D. M.; Sabatini, B. L.; Selkoe, D. J. Amyloid-β protein dimers isolated directly from Alzheimer's brains impair synaptic plasticity and memory. *Nat. Med.* **2008,** *14*, 837-842.

33. Lambert, M. P.; Barlow, A. K.; Chromy, B. A.; Edwards, C.; Freed, R.; Liosatos, M.; Morgan, T. E.; Rozovsky, I.; Trommer, B.; Viola, K. L.; Wals, P.; Zhang, C.; Finch, C. E.; Krafft, G. A.; Klein, W. L. Diffusible, nonfibrillar ligands derived from Abeta1-42 are potent central nervous system neurotoxins. *Proc. Natl. Acad. Sci. U. S. A.* **1998,** *95*, 6448-6453.

34. Gong, Y.; Chang, L.; Viola, K. L.; Lacor, P. N.; Lambert, M. P.; Finch, C. E.; Krafft, G. A.; Klein, W. L. Alzheimer's disease-affected brain: presence of oligomeric A beta ligands (ADDLs) suggests a molecular basis for reversible memory loss. *Proc. Natl. Acad. Sci. U. S. A.* **2003,** *100*, 10417-10422.

35. Wang, H.-W.; Pasternak, J. F.; Kuo, H.; Ristic, H.; Lambert, M. P.; Chromy, B.; Viola, K. L.; Klein, W. L.; Stine, W. B.; Krafft, G. A.; Trommer, B. L. Soluble oligomers of β amyloid (1-42) inhibit long-term potentiation but not long-term depression in rat dentate gyrus. *Brain Res.* **2002,** *924*, 133-140.

36. Kayed, R.; Head, E.; Thompson, J. L.; McIntire, T. M.; Milton, S. C.; Cotman, C. W.; Glabe, C. G. Common structure of soluble amyloid oligomers implies common mechanism of pathogenesis. *Science* **2003,** *300*, 486.

37. Deshpande, A.; Mina, E.; Glabe, C.; Busciglio, J. Different conformations of amyloid beta induce neurotoxicity by distinct mechanisms in human cortical neurons. *J. Neurosci.* **2006,** *26*, 6011-6018.

38. Barghorn, S.; Nimmrich, V.; Striebinger, A.; Krantz, C.; Keller, P.; Janson, B.; Bahr, M.; Schmidt, M.; Bitner, R. S.; Harlan, J.; Barlow, E.; Ebert, U.; Hillen, H. Globular amyloid β-peptide1-42 oligomer - a homogenous and stable neuropathological protein in Alzheimer's disease. *J. Neurochem.* **2005,** *95*, 834-847.

39. Walsh, D. M.; Lomakin, A.; Benedek, G. B.; Condron, M. M.; Teplow, D. B. Amyloid β-Protein Fibrillogenesis: detection of a protofibrillar intermediate. *J. Biol. Chem.* **1997,** *272*, 22364-22372.

40. Johansson, A.-S.; Garlind, A.; Berglind-Dehlin, F.; Karlsson, G.; Edwards, K.; Gellerfors, P.; Ekholm-Pettersson, F.; Palmblad, J.; Lannfelt, L. Docosahexaenoic acid stabilizes soluble amyloid-β protofibrils and sustains amyloid-β-induced neurotoxicity in vitro. *FEBS J.* **2007,** *274*, 990-1000.

41. Walsh, D. M.; Hartley, D. M.; Kusumoto, Y.; Fezoui, Y.; Condron, M. M.; Lomakin, A.; Benedek, G. B.; Selkoe, D. J.; Teplow, D. B. Amyloid β-Protein Fibrillogenesis:

structure and biological activity of protofibrillar intermediates. *J. Biol. Chem.* **1999,** *274*, 25945-25952.

42. Lashuel, H. A.; Hartley, D.; Petre, B. M.; Walz, T.; Lansbury, P. T. Amyloid pores from pathogenic mutations. *Nature* **2002,** *418*, 291-291.

43. Cummings, J. L.; Morstorf, T.; Zhong, K. Alzheimer's disease drug-development pipeline: few candidates, frequent failures. *Alz. Res. Ther.* **2014,** *6*, 37-43.

44. Wolfe, M. S. Therapeutic strategies for Alzheimer's disease. *Nat. Rev. Drug Discovery* **2002,** *1*, 859-866.

45. Citron, M. Alzheimer's disease: Strategies for disease modification. *Nat. Rev. Drug Discovery* **2010,** *9*, 387-398.

46. Giuffrida, M. L.; Caraci, F.; Pignataro, B.; Cataldo, S.; De Bona, P.; Bruno, V.; Molinaro, G.; Pappalardo, G.; Messina, A.; Palmigiano, A.; Garozzo, D.; Nicoletti, F.; Rizzarelli, E.; Copani, A. Beta-amyloid monomers are neuroprotective. *J. Neurosci.* **2009,** *29*, 10582-10587.

47. Citron, M. Strategies for disease modification in Alzheimer's disease. *Nat. Rev. Neurosci.* **2004,** *5*, 677-685.

48. Xia, Y. Nanomaterials at work in biomedical research. *Nat. Mater.* **2008,** *7*, 758-760.

49. Song, Y.; Moore, E. G.; Guo, Y.; Moore, J. S. Polymer–peptide conjugates disassemble amyloid β fibrils in a molecular weight dependent manner. *J. Am. Chem. Soc.* **2017,** *139*, 4298-4301.

50. Chowdhury, S. R.; Agarwal, M.; Meher, N.; Muthuraj, B.; Iyer, P. K. Modulation of amyloid aggregates into nontoxic coaggregates by hydroxyquinoline appended polyfluorene. *ACS Appl. Mater. Interfaces* **2016,** *8*, 13309-13319.

51. Mondal, S.; Kumar, V.; Roy Chowdhury, S.; Shah, M.; Gaur, A.; Kumar, S.; Iyer, P. K. Template-mediated detoxification of low-molecular-weight amyloid oligomers and regulation of their nucleation pathway. *ACS Appl. Bio Mater.* **2019,** *2*, 5306-5312.

52. Sun, H.; Liu, J.; Li, S.; Zhou, L.; Wang, J.; Liu, L.; Lv, F.; Gu, Q.; Hu, B.; Ma, Y.; Wang, S. Reactive amphiphilic conjugated polymers for inhibiting amyloid β assembly. *Angew. Chem. Int. Ed.* **2019,** *58*, 5988-5993.

53. Schreiber, S. L. Small molecules: The missing link in the central dogma. *Nat. Chem. Biol.* **2005,** *1*, 64-66.

54. Ladiwala, A. R. A.; Dordick, J. S.; Tessier, P. M. Aromatic small molecules remodel toxic soluble oligomers of amyloid β through three independent pathways. *J. Biol. Chem.* **2011,** *286*, 3209-3218.

55. Kodali, R.; Wetzel, R. Polymorphism in the intermediates and products of amyloid assembly. *Curr. Opin. Struct. Biol.* **2007,** *17*, 48-57.

56. Necula, M.; Kayed, R.; Milton, S.; Glabe, C. G. Small molecule inhibitors of aggregation indicate that amyloid β oligomerization and fibrillization pathways are independent and distinct. *J. Biol. Chem.* **2007,** *282*, 10311-10324.

57. Yang, F.; Lim, G. P.; Begum, A. N.; Ubeda, O. J.; Simmons, M. R.; Ambegaokar, S. S.; Chen, P. P.; Kayed, R.; Glabe, C. G.; Frautschy, S. A.; Cole, G. M. Curcumin inhibits formation of amyloid β oligomers and fibrils, binds plaques, and reduces amyloid in vivo. *J. Biol. Chem.* **2005,** *280*, 5892-5901.

58. Yanagisawa, D.; Taguchi, H.; Yamamoto, A.; Shirai, N.; Hirao, K.; Tooyama, I. Curcuminoid binds to amyloid-β 1-42 oligomer and fibril. *J. Alzheimer's Dis.* **2011,** *24*, 33-42.

59. Cramer, P. E.; Cirrito, J. R.; Wesson, D. W.; Lee, C. Y.; Karlo, J. C.; Zinn, A. E.; Casali, B. T.; Restivo, J. L.; Goebel, W. D.; James, M. J.; Brunden, K. R.; Wilson, D. A.; Landreth, G. E. ApoE-directed therapeutics rapidly clear beta-amyloid and reverse deficits in AD mouse models. *Science* **2012,** *335*, 1503-1506.

60. Ladiwala, A. R. A.; Lin, J. C.; Bale, S. S.; Marcelino-Cruz, A. M.; Bhattacharya, M.; Dordick, J. S.; Tessier, P. M. Resveratrol selectively remodels soluble oligomers and fibrils of amyloid aβ into off-pathway conformers. *J. Biol. Chem.* **2010,** *285*, 24228-24237.

61. Gervais, F.; Paquette, J.; Morissette, C.; Krzywkowski, P.; Yu, M.; Azzi, M.; Lacombe, D.; Kong, X.; Aman, A.; Laurin, J.; Szarek, W. A.; Tremblay, P. Targeting soluble aβ peptide with tramiprosate for the treatment of brain amyloidosis. *Neurobiol. Aging* **2007,** *28*, 537-547.

62. Karran, E.; Hardy, J. A critique of the drug discovery and phase 3 clinical programs targeting the amyloid hypothesis for Alzheimer disease. *Ann. Neurol.* **2014,** *76*, 185-205.

63. Lemkul, J. A.; Bevan, D. R. Morin inhibits the early stages of amyloid β-peptide aggregation by altering tertiary and quaternary interactions to produce "off-pathway" structures. *Biochemistry* **2012,** *51*, 5990-6009.

64. Porat, Y.; Abramowitz, A.; Gazit, E. Inhibition of amyloid fibril formation by polyphenols: structural similarity and aromatic interactions as a common inhibition mechanism. *Chem. Biol. Drug Des.* **2006,** *67*, 27-37.

65. Du, W.-J.; Guo, J.-J.; Gao, M.-T.; Hu, S.-Q.; Dong, X.-Y.; Han, Y.-F.; Liu, F.-F.; Jiang, S.; Sun, Y. Brazilin inhibits amyloid β-protein fibrillogenesis, remodels amyloid fibrils and reduces amyloid cytotoxicity. *Sci. Rep.* **2015,** *5*, 7992-8002.

66. Schubert, U.; Antón, L. C.; Gibbs, J.; Norbury, C. C.; Yewdell, J. W.; Bennink, J. R. Rapid degradation of a large fraction of newly synthesized proteins by proteasomes. *Nature* **2000,** *404*, 770-774.

67. Matsunaga, Y.; Fujii, A.; Awasthi, A.; Yokotani, J.; Takakura, T.; Yamada, T. Eight-residue Aβ peptides inhibit the aggregation and enzymatic activity of Aβ42. *Regul. Pept.* **2004,** *120*, 227-236.

68. Rocha, S.; Cardoso, I.; Börner, H.; Pereira, M. C.; Saraiva, M. J.; Coelho, M. Design and biological activity of β-sheet breaker peptide conjugates. *Biochem. Biophys. Res. Commun.* **2009,** *380*, 397-401.

69. Pratim Bose, P.; Chatterjee, U.; Nerelius, C.; Govender, T.; Norström, T.; Gogoll, A.; Sandegren, A.; Göthelid, E.; Johansson, J.; Arvidsson, P. I. Poly-N-methylated amyloid

β-peptide (aβ) c-terminal fragments reduce aβ toxicity in vitro and in drosophila melanogaster. *J. Med. Chem.* **2009,** *52*, 8002-8009.

70. Ghanta, J.; Shen, C.-L.; Kiessling, L. L.; Murphy, R. M. A Strategy for designing inhibitors of β-amyloid toxicity. *J. Biol. Chem.* **1996,** *271*, 29525-29528.

71. Akikusa, S.; Watanabe, K. I.; Horikawa, E.; Nakamura, K.; Kodaka, M.; Okuno, H.; Konakahara, T. Practical assay and molecular mechanism of aggregation inhibitors of β-amyloid. *J. Pep. Res.* **2003,** *61*, 1-6.

72. Wiesehan, K.; Buder, K.; Linke, R. P.; Patt, S.; Stoldt, M.; Unger, E.; Schmitt, B.; Bucci, E.; Willbold, D. Selection of d-amino-acid peptides that bind to Alzheimer's disease amyloid peptide aβ1–42 by mirror image phage display. *ChemBioChem* **2003,** *4*, 748-753.

73. Fradinger, E. A.; Monien, B. H.; Urbanc, B.; Lomakin, A.; Tan, M.; Li, H.; Spring, S. M.; Condron, M. M.; Cruz, L.; Xie, C.-W.; Benedek, G. B.; Bitan, G. C-terminal peptides coassemble into Aβ42 oligomers and protect neurons against Aβ42-induced neurotoxicity. *Proc. Nat. Acad. Sci. U. S. A.* **2008,** *105*, 14175-14180.

74. Bansal, S.; Maurya, I. K.; Yadav, N.; Thota, C. K.; Kumar, V.; Tikoo, K.; Chauhan, V. S.; Jain, R. C-Terminal Fragment, Aβ32–37, Analogues protect against aβ aggregation-induced toxicity. *ACS Chem. Neuro.* **2016,** *7*, 615-623.

75. Kuhn, P.-H.; Wang, H.; Dislich, B.; Colombo, A.; Zeitschel, U.; Ellwart, J. W.; Kremmer, E.; Roßner, S.; Lichtenthaler, S. F. ADAM10 is the physiologically relevant, constitutive α-secretase of the amyloid precursor protein in primary neurons. *EMBO J.* **2010,** *29*, 3020-3032.

76. Lichtenthaler, S. F. Alpha-secretase in Alzheimer's disease: molecular identity, regulation and therapeutic potential. *J. Neurochem.* **2011,** *116*, 10-21.

77. Hong-Qi, Y.; Zhi-Kun, S.; Sheng-Di, C. Current advances in the treatment of Alzheimer's disease: focused on considerations targeting Aβ and tau. *Transl. Neurodegen.* **2012,** *1*, 21.

78. Youdim, M. B. H. Multi target neuroprotective and neurorestorative anti-parkinson and anti-alzheimer drugs ladostigil and m30 derived from rasagiline. *Exp. Neurobiol.* **2013,** *22*, 1-10.

79. Lahiri, D. K.; Maloney, B. Beyond the signaling effect role of amyloid-β42 on the processing of APP, and its clinical implications. *Exp. Neurol.* **2010,** *225*, 51-54.

80. Das, B.; Yan, R. A close look at bace1 inhibitors for Alzheimer's disease treatment. *CNS Drugs* **2019,** *33*, 251-263.

81. Moussa-Pacha, N. M.; Abdin, S. M.; Omar, H. A.; Alniss, H.; Al-Tel, T. H. BACE1 inhibitors: Current status and future directions in treating Alzheimer's disease. *Med. Res. Rev.* **2020,** *40*, 339-384.

82. Coimbra, J. R. M.; Marques, D. F. F.; Baptista, S. J.; Pereira, C. M. F.; Moreira, P. I.; Dinis, T. C. P.; Santos, A. E.; Salvador, J. A. R. Highlights in BACE1 inhibitors for Alzheimer's disease treatment. *Front. Chem.* **2018,** *6*, 178-188.

83. Scott, L. E.; Orvig, C. Medicinal inorganic chemistry approaches to passivation and removal of aberrant metal ions in disease. *Chem. Rev.* **2009,** *109*, 4885-4910.

84. Gaggelli, E.; Kozlowski, H.; Valensin, D.; Valensin, G. Copper homeostasis and neurodegenerative disorders (Alzheimer's, prion, and Parkinson's diseases and amyotrophic lateral sclerosis). *Chem. Rev.* **2006,** *106*, 1995-2044.

85. Olanow, C. W. An introduction to the free radical hypothesis in Parkinson's disease. *Ann. Neurol.* **1992,** *32*, S2-S9.

86. McLachlan, D. R.; Kruck, T. P.; Lukiw, W. J.; Krishnan, S. S. Would decreased aluminum ingestion reduce the incidence of Alzheimer's disease? *Can. Med. Assoc. J.* **1991,** *145*, 793-829.

87. Kontoghiorghes, G. J. New concepts of iron and aluminium chelation therapy with oral L1 (deferiprone) and other chelators. A review. *Analyst* **1995,** *120*, 845-851.

88. Richardson, D. R. The therapeutic potential of iron chelators. *Expert Opin. Invest. Drugs* **1999,** *8*, 2141-2158.

89. Ritchie, C. W.; Bush, A. I.; Mackinnon, A.; Macfarlane, S.; Mastwyk, M.; MacGregor, L.; Kiers, L.; Cherny, R.; Li, Q.-X.; Tammer, A.; Carrington, D.; Mavros, C.; Volitakis, I.; Xilinas, M.; Ames, D.; Davis, S.; Beyreuther, K.; Tanzi, R. E.; Masters, C. L. Metal-protein attenuation with iodochlorhydroxyquin (clioquinol) targeting aβ amyloid deposition and toxicity in Alzheimer disease: A pilot phase 2 clinical trial. *Arch. Neurol.* **2003,** *60*, 1685-1691.

90. Zhao, J.; Xu, L.; Liang, Q.; Sun, Q.; Chen, C.; Zhang, Y.; Ding, Y.; Zhou, P. Metal chelator EGCG attenuates Fe(III)-induced conformational transition of α-synuclein and protects AS-PC12 cells against Fe(III)-induced death. *J. Neurochem.* **2017,** *143*, 136-146.

91. Taqi, A. K.; Iftekhar, H.; Ausaf, A.; Asma, P.; Shazia, A.; Saima, Q.; Ibrahim, M. A.; Ghulam, M. A.; Gjumrakch, A. Recent updates on the dynamic association between oxidative stress and neurodegenerative disorders. *CNS Neuro. Disord. Drug Targets* **2016**, *15*, 310-320.

92. Uttara, B.; Singh, A. V.; Zamboni, P.; Mahajan, R. T. Oxidative stress and neurodegenerative diseases: a review of upstream and downstream antioxidant therapeutic options. *Curr. Neuropharmacol.* **2009,** *7*, 65-74.

93. Kirkitadze, M. D.; Kowalska, A. Molecular mechanisms initiating amyloid beta-fibril formation in Alzheimer's disease. *Acta Biochim. Pol.* **2005,** *52*, 417-423.

94. Stadtman, E. R.; Berlett, B. S. Reactive oxygen-mediated protein oxidation in aging and disease. *Chem. Res. Toxicol.* **1997,** *10*, 485-494.

95. Korolainen, M. A.; Goldsteins, G.; Alafuzoff, I.; Koistinaho, J.; Pirttila, T. Proteomic analysis of protein oxidation in Alzheimer's disease brain. *Electrophoresis* **2002,** *23*, 3428-3433.

96. Wiseman, H.; Halliwell, B. Damage to DNA by reactive oxygen and nitrogen species: role in inflammatory disease and progression to cancer. *Biochem. J.* **1996,** *313*, 17-29.

97. Snyder, S. W.; Ladror, U. S.; Wade, W. S.; Wang, G. T.; Barrett, L. W.; Matayoshi, E. D.; Huffaker, H. J.; Krafft, G. A.; Holzman, T. F. Amyloid-beta aggregation: selective inhibition of aggregation in mixtures of amyloid with different chain lengths. *Biophys. J.* **1994,** *67*, 1216-1228.

98. Salminen, A.; Ojala, J.; Kauppinen, A.; Kaarniranta, K.; Suuronen, T. Inflammation in Alzheimer's disease: amyloid-β oligomers trigger innate immunity defence via pattern recognition receptors. *Prog. Neurobiol.* **2009,** *87*, 181-194.

99. Gustot, A.; Gallea, José I.; Sarroukh, R.; Celej, María S.; Ruysschaert, J.-M.; Raussens, V. Amyloid fibrils are the molecular trigger of inflammation in Parkinson's disease. *Biochem. J.* **2015,** *471*, 323-333.

100. McGeer, P. L.; Itagaki, S.; Boyes, B. E.; McGeer, E. G. Reactive microglia are positive for hla-dr in the substantia nigra of Parkinson's and Alzheimer's disease brains. *Neurology* **1988,** *38*, 1285-1291.

101. Gerhard, A.; Pavese, N.; Hotton, G.; Turkheimer, F.; Es, M.; Hammers, A.; Eggert, K.; Oertel, W.; Banati, R. B.; Brooks, D. J. In vivo imaging of microglial activation with [11C](R)-PK11195 PET in idiopathic Parkinson's disease. *Neurobiol. Dis.* **2006,** *21*, 404-412.

102. Alvarez-Erviti, L.; Couch, Y.; Richardson, J.; Cooper, J. M.; Wood, M. J. A. Alpha-synuclein release by neurons activates the inflammatory response in a microglial cell line. *Neurosci. Res.* **2011,** *69*, 337-342.

103. Lee, T.-P.; Matteliano, M. L.; Middleton, E. Effect of quercetin on human polymorphonuclear leukocyte lysosomal enzyme release and phospholipid metabolism. *Life Sci.* **1982,** *31*, 2765-2774.

104. Lin, M. T.; Beal, M. F. Mitochondrial dysfunction and oxidative stress in neurodegenerative diseases. *Nature* **2006,** *443*, 787-795.

105. Du, H.; Guo, L.; Fang, F.; Chen, D.; A Sosunov, A.; M McKhann, G.; Yan, Y.; Wang, C.; Zhang, H.; Molkentin, J. D.; Gunn-Moore, F. J.; Vonsattel, J. P.; Arancio, O.; Chen, J. X.; Yan, S. D. Cyclophilin-D deficiency attenuates mitochondrial and neuronal

perturbation and ameliorates learning and memory in Alzheimer's disease. *Nat. Med.* **2008,** *14*, 1097-1105.

106. Schmidt, C.; Lepsverdize, E.; Chi, S. L.; Das, A. M.; Pizzo, S. V.; Dityatev, A.; Schachner, M. Amyloid precursor protein and amyloid-β peptide bind to ATP synthase and regulate its activity at the surface of neural cells. *Mol. Psychiatry* **2008,** *13*, 953-969.

107. Lustbader, J. W.; Cirilli, M.; Lin, C.; Xu, H. W.; Takuma, K.; Wang, N.; Caspersen, C.; Chen, X.; Pollak, S.; Chaney, M.; Trinchese, F.; Liu, S.; Gunn-Moore, F.; Lue, L.-F.; Walker, D. G.; Kuppusamy, P.; Zewier, Z. L.; Arancio, O.; Stern, D.; Yan, S. S.; Wu, H. ABAD directly links aß to mitochondrial toxicity in Alzheimer's disease. *Science* **2004,** *304*, 448-452.

108. Ankarcrona, M.; Mangialasche, F.; Winblad, B. Rethinking alzheimer's disease therapy: are mitochondria the key? *J. Alzheimer's Dis.* **2010,** *20*, S579-S590.

109. Baek, S. H.; Bae, O. N.; Kim, E. K.; Yu, S. W. Induction of mitochondrial dysfunction by poly(ADP-ribose) polymer: implication for neuronal cell death. *Mol. Cells* **2013,** *36*, 258-266.

110. Kim, T.; Yang, H. Y.; Park, B. G.; Jung, S. Y.; Park, J.-H.; Park, K. D.; Min, S.-J.; Tae, J.; Yang, H.; Cho, S.; Cho, S. J.; Song, H.; Mook-Jung, I.; Lee, J.; Pae, A. N. Discovery of benzimidazole derivatives as modulators of mitochondrial function: A potential treatment for Alzheimer's disease. *Eur. J. Med. Chem.* **2017,** *125*, 1172-1192.

111. Samanta, S.; Rajasekhar, K.; Babagond, V.; Govindaraju, T. Small molecule inhibits metal-dependent and independent multifaceted toxicity of Alzheimer's disease. *ACS Chem. Neuro.* **2019,** *10*, 3611-3621.

112. Rajasekhar, K.; Mehta, K.; Govindaraju, T. Hybrid multifunctional modulators inhibit multifaceted Aβ toxicity and prevent mitochondrial damage. *ACS Chem. Neuro.* **2018,** *9*, 1432-1440.

113. Rajasekhar, K.; Samanta, S.; Bagoband, V.; Murugan, N. A.; Govindaraju, T. Antioxidant berberine derivative inhibits multifaceted amyloid toxicity. *iScience* **2020,** *23*, 101005.

114. Radde, R.; Bolmont, T.; Kaeser, S. A.; Coomaraswamy, J.; Lindau, D.; Stoltze, L.; Calhoun, M. E.; Jäggi, F.; Wolburg, H.; Gengler, S.; Haass, C.; Ghetti, B.; Czech, C.; Hölscher, C.; Mathews, P. M.; Jucker, M. Aβ42-driven cerebral amyloidosis in transgenic mice reveals early and robust pathology. *EMBO Rep.* **2006,** *7*, 940-946.

115. Mullan, M.; Crawford, F.; Axelman, K.; Houlden, H.; Lilius, L.; Winblad, B.; Lannfelt, L. A pathogenic mutation for probable Alzheimer's disease in the APP gene at the N terminus of β amyloid. *Nat. Genet.* **1992,** *1*, 345-347.

116. Citron, M.; Oltersdorf, T.; Haass, C.; McConlogue, L.; Hung, A. Y.; Seubert, P.; Vigo-Pelfrey, C.; Lieberburg, I.; Selkoe, D. J. Mutation of the β-amyloid precursor protein in familial Alzheimer's disease increases β-protein production. *Nature* **1992,** *360*, 672-674.

2

Nanoparticle Assisted Regulation of Nucleation Pathway of Amyloid Tetramer and Inhibition of Their Fibrillation Kinetics

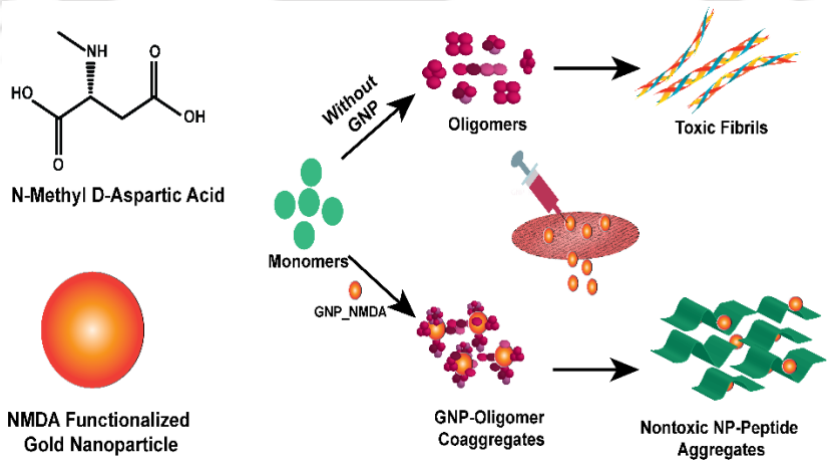

1. Mondal, S.; Chowdhury, S. R.; Shah, M.; Kumar, V.; Kumar, S.; **Iyer, P. K.*** Nano particle assisted regulation of nucleation pathway of amyloid tetramer and inhibition of their fibrillation kinetics. *ACS Appl. Bio Mater.*, **2019**, *2*, 2137-2142.

2

Nanoparticle Assisted Regulation of Nucleation Pathway of Amyloid Tetramer and Inhibition of Their Fibrillation Kinetics

Abstract:

Low molecular weight (LMW) soluble amyloid oligomers have been established as primary neurotoxic species that play a key role in Alzheimer's disease etiology. However, detection and separation of such energetically unfavored, metastable species are extremely challenging due to their short lifetime and dynamic nature. In this work, the aggregation of amyloid beta has been precisely regulated to produce their tetramer, the most toxic species among the pool of LMW amyloid oligomer since this tetramer is of key scientific importance and its inhibition could offer insights into developing early phase therapeutics for amyloidosis. The in-depth structural characterization as well as the regulation of these isolated tetramers has also been achieved for the first time in an in vitro model using nontoxic novel N-methyl d-aspartic acid (NMDA) functionalized gold nanoparticle (GNP-NMDA) that interacts specifically through electrostatic interactions to form stable GNP-amyloid coaggregates and directing the nucleation toward secondary nucleation pathway rapidly unlike in control experiment where nucleation proceeds mainly via primary nucleation pathway. NMDA receptor modulators are approved by the Food and Drug

Administration (FDA) as an existing treatment for moderate to severe stage Alzheimer's Disease (AD); hence, GNP decorated with NMDA offers a promising strategy toward AD. This remarkable strategy for the inhibition of the most neurotoxic LMW tetramer form of the soluble amyloid oligomers toward a nontoxic aggregation path by GNP-NMDA presents a rationale target for drug designing and to develop early stage therapeutics against several neurodegenerative diseases.

2.1. Introduction:

Alzheimer's disease (AD), an irreversible brain disorder, first diagnosed more than 100 years ago, still remains a curse to the society, affecting 30 million people worldwide, victimizing one in ten individuals above 65 years' age, due to lack of efficient therapeutic strategy.[1] This neurodegenerative disorder results in neuronal and synaptic loss in subcortical region including cerebral cortex in the human brain.[2] Intense research activity suggests that amyloid fibrils originating from self-aggregation of amyloid β peptide having cross-β sheeted conformation are the hallmark of this disease.[3] However, metastable, low molecular weight soluble oligomers formed during the early stage of fibril formation have recently proven to induce neuronal cell death even in Pico molar concentration and are considered as the major pathogens in AD.[4–6] A study on amyloid precursor protein (APP) transgenic mice reveals that low molecular weight (LMW) amyloid oligomers not only cause synaptic loss, but also affect other parameters related to AD pathology including enhanced ROS (reactive oxygen species) production, abnormal tau phosphorylation, neuronal loss, and microglial activation.[7] Consequently, stable LMW oligomers and protofibrillar species generated from oligomers become 50-times more neurotoxic than the fibrils.[8] Hence, in recent years, research attention is being diverted toward separation and characterization of LMW oligomeric species and their unique biological activity rather than traditional amyloid fibrils as target. However, owing to their unstructured, dynamic, and metastable nature, the oligomeric state still remains a labyrinth to the scientific community. A wide range of LMW oligomeric species including dimers, trimers, tetramers, dodecamers, etc. are known, and their cellular neurotoxicity is believed to depend on their molecular weight (numbers of monomer aggregated).[7–9] Recently, tetramers have been characterized as the most toxic species among the pool of LMW amyloid oligomers.[9] Consequently, unveiling the chemistry of amyloid tetramer is fundamentally very significant and of extraordinary scientific interest, but since they are noncrystalline

very little information on their structural features is known. Further, their inhibition toward a nontoxic aggregation path can offer a platform to develop early stage therapeutics against several neurodegenerative diseases. Although, a pool of materials including polymer, small molecules, peptide, nanoparticle have been developed to target amyloid aggregation, a negatively charged, functionalized nanoparticle is very uncommon and are under development.[10–16] Herein, for the first time, a nanoparticle based nontoxic inhibitor for amyloid tetramer (LMW oligomer) has been developed, and its ability to interact with GNP-NMDA has been unveiled. We have successfully regulated the amyloid aggregation selectively to obtain its tetramer (LMW oligomer) and studied its inhibition judiciously to acquire valuable insight into developing early phase therapeutics for amyloidosis. This 17 kDa tetramer was well characterized through biophysical and biochemical techniques such as SDS-PAGE, circular dichroism (CD), Fourier-transform infrared spectroscopy (FT-IR), and atomic force microscopy (AFM), providing valuable insights into the LMW tetramer. In addition, a nontoxic GNP functionalized with N-methyl D-aspartic acid was also synthesized that possessed remarkable ability to inhibit the fibrillation kinetics of this toxic amyloid tetramer and modulating it to a secondary nucleation pathway thereby forming an electrical double layer with GNP-NMDA and suppressing its neurotoxicity (Scheme 2.1).

2.2 Experiments

2.2.1 Preparation of LMW Oligomers (Tetramer) & Fibrils

LMW amyloid oligomers (tetramers-17 kDa) were prepared by modifying a previously reported protocol.[17,18] Briefly, 0.1 mg of synthetic Aβ40 was dissolved in 20 µL of hexafluoro-2-propanol (HFIP), evaporated to dryness under argon atmosphere, 10 µL of DMSO was added, followed by addition of 10 mM phosphate buffered saline (PBS, pH 7.4) containing 10 mM NaCl and 0.02% sodium azide. The mixture was sonicated for 1 min and allowed to incubate for 0.5 h at 37 °C. The final mixture was centrifuged at 10,000 rpm for 1 h at 4 °C, and the supernatant was collected. Presence of tetramer was confirmed from native PAGE analysis. The tetrameric species was cut and dissolved in a mixture containing 150 mM NaCl, 0.1 mM EDTA, 50 mM Tris HCl at pH 7.4. The presence of sole tetramer was

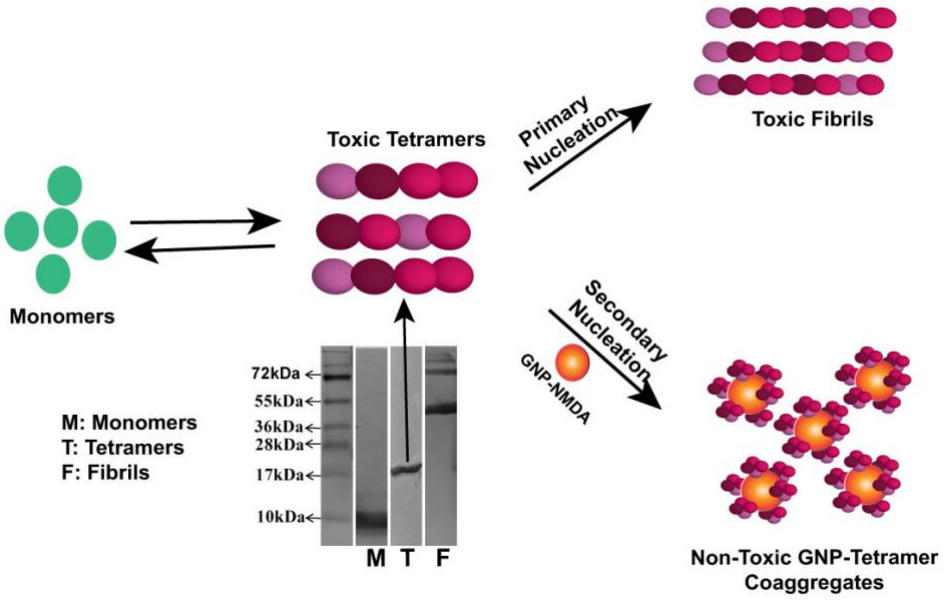

Scheme 2.1. *Modulation of Aβ Nucleation Pathway by NMDA Functionalized Gold Nanoparticle (GNP-NMDA)*

further confirmed using native PAGE analysis. HMW oligomers and fibrils were prepared by incubating for 48 h. The existence of LMW, HMW oligomers, and fibrils was confirmed from electrophoresis and AFM (Figure 2.1A). Final concentration was determined by UV–vis spectroscopy using Beer–Lambert law.

2.2.2 Characterization of Tetramers & Fibrils

To confirm the presence of oligomers and their size, native gel electrophoresis experiment was performed. The sample incubated for 1 h showed a clear defined band corresponding to 17 kDa, which confirmed the presence of tetramer in the solution. Similarly, the sample incubated for 48 h showed a group of band mostly corresponding to 56 kDa, 72 kDa, etc., representing the presence of HMW oligomers and fibrils in the solution (Figure 2.1A). The morphology of the amyloid tetramers was further studied by AFM (Figure 2.1B). The amyloid tetramers possess a dimension of ~50 nm (Figure 2.1B).

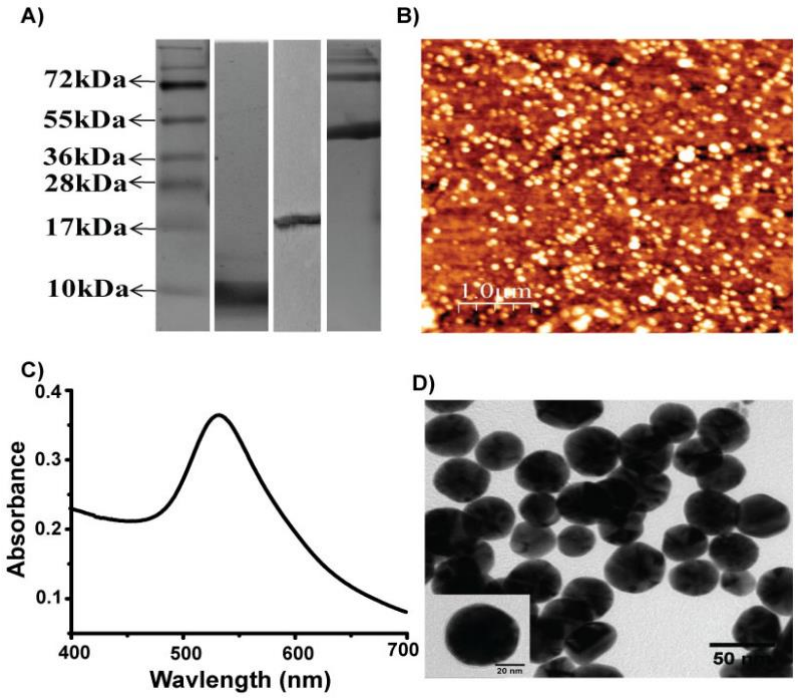

Figure 2.1. *(A) Characterization of amyloid tetramer by electrophoresis experiment: ladder, mixture of monomer and dimer of amyloid beta40, amyloid tetramer, mixture of HMW oligomer, and fibrils, respectively, from left. (B) AFM morphology of amyloid tetramer. (C) UV–vis absorption spectra of GNP in water. (D) TEM images of GNP, TEM image of a single particle (inset).*

2.2.3 Synthesis of GNP-NMDA

NMDA conjugated GNP was synthesized using modified Turkevich method.[19] Briefly, 50 mL of aqueous solution of 10^{-3} (M) Gold(III) chloride trihydrate was taken in a three neck round-bottom flask and was heated to 150 °C for 30 min with continuous stirring (1100 rpm). Then 1.5 mL of aqueous solution of 10^{-3} (M) NMDA was added to it to observe a color change to red–maroon immediately. The heating was stopped and stirring continued until the solution cooled to room temperature. Excess Gold(III) chloride was removed by centrifugation and characterized by UV–vis spectroscopy, zeta potential, FT-IR spectroscopy, and electron microscopy. Newly formed GNP-NMDA showed characteristic SPR band at 540 nm (Figure 2.1C). Transmission electron microscopy (TEM) revealed that the GNP-NMDAs were spherical with an average diameter of 40 nm (Figure 2.1D). To confirm the NMDA conjugation on gold surface, FT-IR spectroscopy was performed (Figure A-1). The FT-IR signal includes a band at 1639 and 2857 cm^{-1}, a

characteristic band for C═O and N-Me group present in NMDA. Furthermore, surface charge on gold was measured using zeta potential and found to be −10.9 mV (Figure A-2). The NMDA functionalized GNP-NMDAs were highly stable under physiological conditions (37 °C, PBS buffer, pH 7.4).

2.2.4 Thiflavin T Assay

ThT fluorescence assay was performed to investigate inhibition kinetics of Aβ40 LMW oligomer (tetramer). Ten micromolar Aβ40 LMW oligomer sample was incubated both in the presence as well as in the absence of 1 nM GNP-NMDA in 2.5 mM PBS buffer at 37 °C for 54 h, and aliquots were collected at required time intervals starting from 0 to 54 h. Twenty micromolar ThT was added to each sample, excited at 440 nm, emission was recorded at 484 nm, and finally emission intensity was plotted with respect to time.

2.2.5 MTT Assay

To investigate the cytotoxicity of the material SH-SY- 5Y with density 10^5 cells/well (per 100 µL) cells were seeded in 96- well tissue culture plates. The cells were incubated for 16 h in DMEM/F12 in a 5% CO_2 incubator at 37 °C. After discarding the media, each well was cleaned with PBS. Then GNP-NMDA solution was added to each well having different concentration and allowed to incubate for 24 h. Ten microliters of 5 mg/mL MTT in PBS solution was added and incubated for 4 h. After removal of the media, 100 µL of DMSO was poured in each well and absorbance recorded at 570 nm. All experiments were repeated thrice, and the relative percentage of cell viability was presented as a relative percentage with respect to the untreated cells (Figure 2.4A). MTT assay indicated that at even higher concentration (1.25 nM) of GNP-NMDA, only 28% cell death occurred. In the presence of only 1 nM (working concentration) GNP-NMDA, the occurrence of cell death was even lower.

2.3 Results and Discussion

The study of tetramer kinetics is very challenging since they are energetically unfavored and metastable species due to their shorter lifetime and dynamic nature, yet it remains a priority area to be explored. Considering these challenges, the aggregation

kinetics of Aβ40 LMW oligomer was studied using ThT assay incubating Aβ40 (10 μM) for 54 h at 37 °C in 2.5 mM PBS (pH 7.2) in presence as well as in the absence of 1 nM GNP-NMDA (Figure 2.2A). Tetramers do not bind with the ThT like monomeric Aβ40 and produce a sigmoidal behavior in ThT experiment time dependently. The GNP equipped with NMDA on its surface likely interacts with amyloid tetramer via electrostatic interaction and thereby stabilizes the metastable species producing almost a straight line in ThT experiment. The inhibition effect was monitored using three different concentrations of GNP-NMDA and a gradual enhancement in inhibitory effect was observed with the increase in GNP-NMDA concentration. Hence, GNP-NMDA functions dose dependently to inhibit the amyloid fibrillation. When 1 nM free NMDA was incubated with Aβ40 tetramer, it showed very negligible tendency toward inhibition. Hence, it was evident that NMDA molecules show inhibition property only when they are conjugated with GNP. The inhibition tendency of nanoparticles is often controlled by their surface charge.

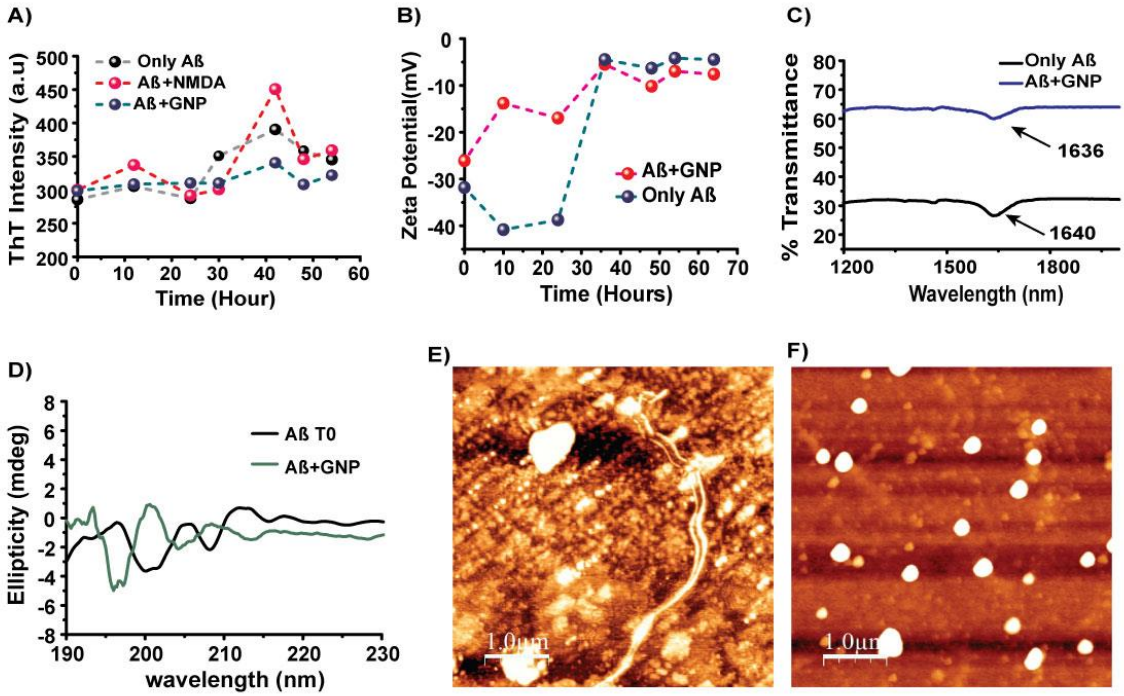

Figure 2.2: *A) Fibrillation kinetics of 20 μM Aβ40(AB) in presence as well as in the absence of 1 nM, 0.5 nM GNP-NMDA and 1 nM NMDA in 2.5 mM PBS buffer (pH 7.4), 37 °C. B) Change in zeta potential of 20 μM Aβ40 and in presence of 1 nM GNP-NMDA. C) FT-IR spectra of Aβ40 after incubating for 54 h in presence and in absence of GNP-NMDA. D) CD spectra of Aβ40 at T=0 h in absence of GNP-NMDA and in presence of GNP-NMDA after 54 h E) AFM image of amyloid fibril found after 54 h incubation F) Amyloid-GNP-NMDA coaggregates formed on incubation with GNP-NMDA for 54 h.*

In general, positively charged GNP-NMDA induce fibrillation and negatively charged GNP-NMDA resist amyloid fibrillation.[20] NMDA functionalized GNP-NMDA also showed a negative zeta potential due to the presence of carboxylate in (Figure 2.2B). In FT-IR spectroscopy, Aβ40 tetramer, after 54 h incubation, showed a peak at 1640 cm^{-1}, which is a signature of β sheet conformation.[22] Interestingly, the peak shifted to 1636 cm^{-1} in the presence of GNP-NMDA after 54 h incubation, which indicated an alteration in β structure (Figure 2.2C). Detail conformational insight was obtained from CD spectroscopy, where Aβ40 tetramer showed a positive peak at 196 nm, 206 nm, 212 nm and a negative peak at 201 and 212 nm (Figures 2.2D and Figure A-3). On incubating them with GNP-NMDA for 54 h, significant shifts in all peaks were observed. A positive peak at 196 nm shifts to 193 nm, and the negative peak at 201 nm shifts to 197 nm with appearance of a new positive peak at 201 nm. Also the positive peak at 212 nm was shifted to 208 nm. The data suggested that GNP-NMDA favors the formation of unordered structure rather than β structure. Morphological studies carried out using AFM (Table 2.1) revealed that Aβ40 tetramers were

Table 2.1: *Summary of morphological study, amyloid beta and HCSF in presence as well as in absence of 1 nM GNP-NMDA over aging.*

Aggregates	Time (h)	Description	size	Aggregates	Time (h)	Description	size
amyloid tetramer	0	disordered spherical	50 ± 21 nm	amyloid fibrils	54	thread-like fibrils	100 nm width, 10 µm
amyloid oligomer in HCSF	54	disordered spherical	50 ± 35 nm	amyloid tetramer + GNP-NMDA	54	disordered spherical	225 ± 12 nm
amyloid fibrils in HCSF	54	thread like fibrils	200 nm width, 10 µm long	HCSF + GNP-NMDA	54	semi-spherical coaggregate	135 ± 10 nm width

small and spherical initially (Figure A-4). After 54 h incubation, Aβ40 tetramer produced a thread like fibrillar morphology as expected (Figures 2.2E and Figure A-5) but no such morphology was obtained in the presence of GNP-NMDA. Rather peptide-GNP coaggregates having a larger spherical morphology (Figure 2.2F and Figure A-6). was found. Thus, GNP-NMDA interacts with amyloid tetramer mainly via electrostatic interactions to form stable GNPamyloid coaggregates that have larger dimensions than the tetramer. Human cerebrospinal fluid (HCSF) is the natural warehouse of Aβ40. The formation of the Aβ-GNP coaggregates was also studied in HCSF samples (Figure 2.3A–D).

In ThT assay, the control HCSF samples showed lag phase at 36 h, followed by an elongation phase, but in the presence of GNP-NMDA (1 nM), no such elongation phase was observed (Figure 2.3A) due to the probable stabilization of early aggregates found in HCSF. On incubation for 54 h, HCSF samples yielded a band at 1634 cm^{-1} due to the presence of β sheet in FT-IR spectra, which was shifted to 1638 cm^{-1} (Figure 2.3B), suggesting that GNP-NMDA probably favors PBS buffer. When GNP-NMDA was added to the Aβ40 tetramer solution, abrupt decrease in negative charge was observed unlike in the control experiment (Figure 2.2B). As the aggregation proceeds toward fibrillation, monomer depletion occurred, which resulted in lesser monomer–monomer repulsion and an obvious decrease in surface charge resulted. Abrupt decrease in the presence of GNP-NMDA can be attributed to the electrostatic stabilization of amyloid tetramer by forming electrical double layer directed by entropy factor.[21] The inhibitory effect of GNP-NMDA on Aβ40 secondary structure was also explored using FT-IR (Figure 2.2C) and CD (Figure 2.2D). In FT-IR spectroscopy, Aβ40 tetramer, after 54 h incubation, showed a peak at 1640 cm^{-1}, which is a signature of β sheet conformation.[22] Interestingly, the peak shifted to 1636 cm^{-1} in the presence of GNP-NMDA after 54 h incubation, which indicated an alteration in β structure. Detail conformational was obtained from CD spectroscopy, where Aβ40 tetramer showed a positive peak at 196 nm, 206 nm, 212 nm and a negative peak at 201 and 212 nm (Figures 2.2D). On incubating them with GNP-NMDA for 54 h, significant shifts in all peaks were observed. A positive peak at 196 nm shifts to 193 nm, and the negative peak at 201 nm shifts to 197 nm with appearance of a new positive peak at 201 nm. Also the positive peak at 212 nm was shifted to 208 nm. The data suggested that GNP-NMDA favors the formation of unordered structure rather than β structure.

Morphological studies carried out using AFM (Table 2.1) revealed that Aβ40 tetramers were small and spherical initially. After 54 h incubation, Aβ40 tetramer produced a thread like fibrillar morphology as expected (Figures 2.2E), but no such morphology was obtained in the presence of GNP-NMDA. Rather peptide-NP coaggregates having a larger spherical morphology (Figure 2.2F) was found. Thus, GNP-NMDA interacts with amyloid tetramer mainly via electrostatic interactions to form stable GNPamyloid coaggregates that have larger dimensions than the tetramer.

Human cerebrospinal fluid (HCSF) is the natural warehouse of Aβ40. The formation of amyloid-GNP-NMDA coaggregates was also studied in HCSF samples (Figure 2.3A–D). In ThT assay, the control HCSF samples showed lag phase at 36 h, followed by an elongation phase, but in the presence of GNP-NMDA (1 nM), no such elongation phase was observed (Figure 2.3A) due to the probable stabilization of early aggregates found in HCSF.

On incubation for 54 h, HCSF samples yielded a band at 1634 cm^{-1} due to the presence of β sheet in FT-IR spectra, which was shifted to 1638 cm^{-1} (Figure 2.3B), suggesting that GNP-NMDA probably favors the formation of more unordered structure. In CD spectra, HCSF solution showed a negative peak at 193 nm and a positive peak at 200 nm (Figure 2.3C and Figure A-7). After incubating for 54 h, the negative peak shifted to 196 nm with a positive peak at 200 nm. However, when incubated in the presence of GNP-NMDA, a negative peak at 199 nm and a distinct peak at 203 nm was observed. The morphological changes occurring in the presence of GNP-NMDA, were monitored by AFM. In HCSF sample, oligomeric aggregates were clearly visible and acquired 35 nm height and 50 ± 35 nm width (Figures 2.3D and A-8). After 54 h incubation, mature thread like amyloid fibrils were found, while in the presence of GNP-NMDA, larger spherical morphology was formed (Figures 2.3E-F and Figure A-9).

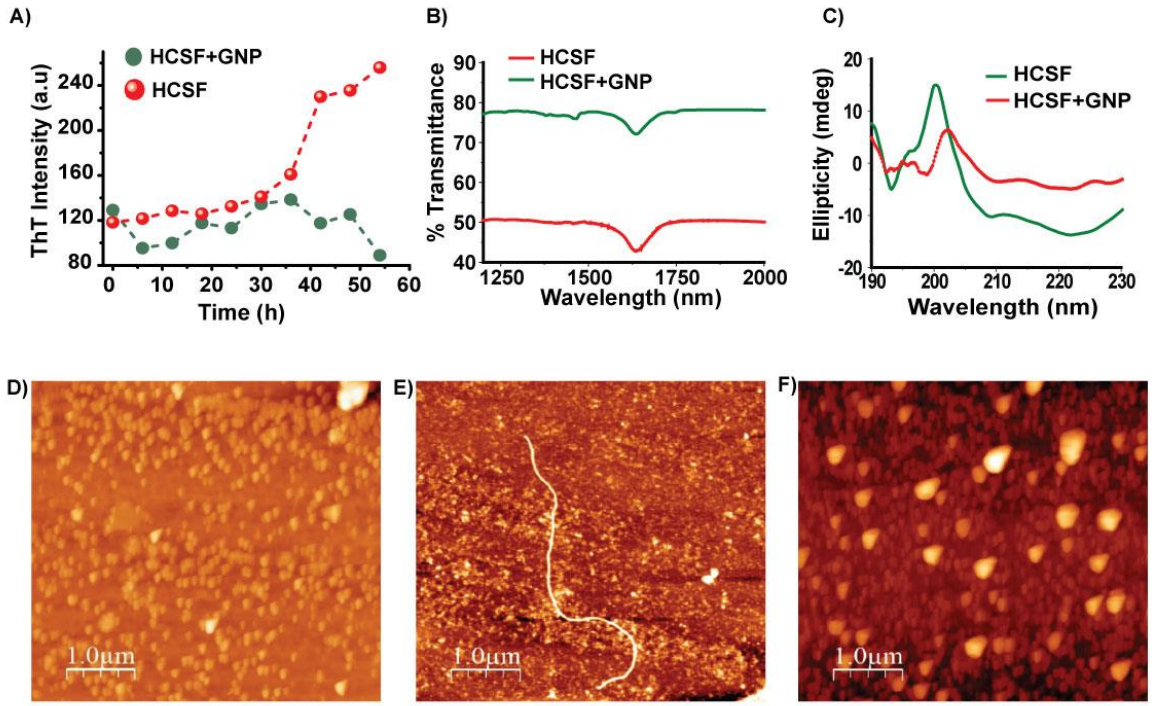

***Figure 2.3**: A) Fibrillation kinetics of 20 μM Aβ40(AB) in HCSF sample in presence and absence of 1 nM GNP-NMDA in 2.5 mM PBS buffer (pH 7.4), 37 °C, B) FT-IR spectra of HCSF samples after incubating 54 h in presence and absence of 1 nM GNP. C) CD spectra of Aβ40 at T=0 H in absence and presence of 1 nM GNP-NMDA after 54 h D) AFM image of amyloid early aggregates in HCSF samples E) AFM image of Amyloid fibril found in HCSF sample F) Amyloid-GNP co-aggregates found in HCSF on in-cubation with GNP-NMDA for 54 h.*

2.3.1 Discussion

In recent studies, it has been revealed that higher cytotoxicity of LMW amyloid oligomers is of greater concern than that for the amyloid fibrils, due to which research on these oligomers is gaining prominence. However, obtaining structural information on these oligomers has remained challenging due to their noncrystalline nature and their metastable behavior. Their isolation and characterization are also unreported, and their kinetic studies have never been performed previously. Herein, the toxic LMW amyloid oligomer (tetramer) has been detected and isolated by controlling the amyloid aggregation with high degree of reproducibility for the first time. The formed amyloid tetramer has been characterized by electrophoresis and spectroscopic techniques. The separation of tetramers is of high clinical importance as they are 50-times more neurotoxic than the fibrillar species.[8] The formation of amyloid aggregate is a multistep process, among which nucleation is the obligatory step. Usually, in a bulk solution, primary nucleation predominates where no foreign surface is present. Anything like lipid vesicles, air–water interface, or some other protein can function like a surface and direct the nucleation toward secondary nucleation pathway.[23] Primary nucleation involves "head-on" aggregation of the monomers. Secondary nucleation corresponds to the nucleation of new fibrils from monomer that is facilitated by the presence of existing fibrils, e.g., through surface-catalysis. Evidence that secondary nucleation might play a role in fibril amplification in vivo comes from in vitro experiments, in which secondary nucleation rates can be very high even under completely quiescent conditions. Nevertheless, secondary nucleation involves random aggregation on some

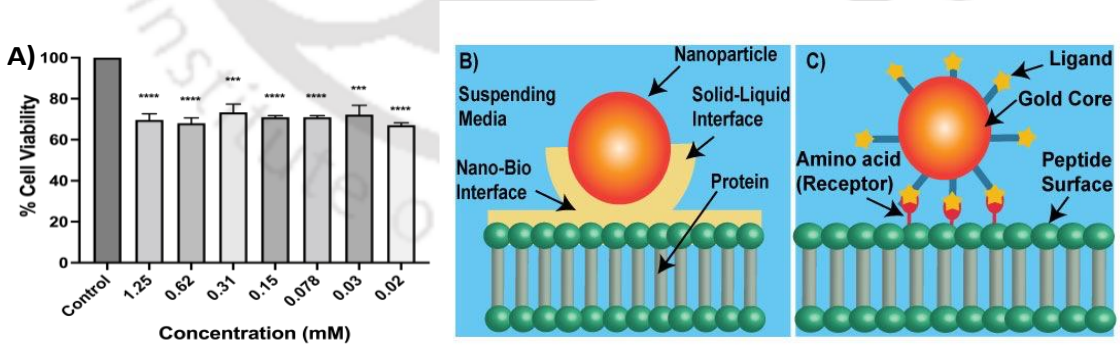

***Figure 2.4**: A) Cell Viability Assay of GNP. (The data represent the mean ± SD of n=3 individual experiments. t-test. ***P <0.001, ****P< 0.0001.) B) Representation of interface in between nanoparticle and biomolecules C) Representation of mechanism of GNP interacting with the amino acid residue of the peptide.*

external surface. The nature of nucleation pathway can be accurately determined from the kinetic data.[23] GNP-NMDA functions as an inhibitor of secondary nucleation process providing an external surface unlike in control experiment where primary nucleation is involved. In the presence of GNP-NMDA, a reduced slope in growth phase was observed and the effect was saturated with increasing GNP-NMDA concentration, which is a kinetic signature of secondary nucleation inhibitors.[23] Such kind of inhibition is mainly guided by electrostatic interaction at the nanobio interface (Figure 2.4B) among amyloid beta and NMDA via hydrogen bonding and electrostatic interactions (Figure 2.4C). The electrostatic interactions are governed by the charges present on the GNP-NMDA surface and can be monitored by zeta potential measurement. A minimum fluctuation in zeta potential throughout the kinetic pathway was observed in the presence of GNP-NMDA unlike in control experiment where an abrupt decrease in zeta potential was observed. Hence, we can assume that such phenomenon happened due to the occurrence of an electrostatic interaction mediated by GNP-NMDA that stabilizes Aβ tetramer and locks the conformation from fibrillation. When a charged surface of GNP-NMDA was added to the biological medium, an electrical double layer consisting of two oppositely charged layers was formed.[24] The first layer composed of directly absorbed Aβ40 on GNP-NMDA surface, mainly through electrostatic force and hydrogen bonding, while the second layer is composed of free ions originating mainly from buffers bound to the surface by electrostatic force. To have more mechanistic insight into peptide–nanoparticle interaction, it was assumed that mainly carboxyl group and methylated amine group play a dramatic role mainly via hydrogen bonding and electrostatic interaction.[25] The "entropy effect" is another concept that governs many physicochemical phenomena. Each protein has its own "comfort zone" where its entropy is minimum and stability is maximum. GNP–amyloid interaction is accompanied by a supply of extra energy to the system to shift it from its "comfort zone". This transition is possible if the entropy of the "second state" (where GNP-amyloid coaggregation occurs) is higher than that in "native state". When a GNP-NMDA with hydrophilic surface approaches the Aβ, hydrophilic part of the peptide is exposed, and interaction can take place directly through hydrogen bonding. In this case, mainly, the carboxylate group present on the NMDA in GNP surface plays the lead role in forming hydrogen bonding with Aβ40. The mechanism is in good accordance with our observation of inhibition of the neurotoxic tetramer. The toxicity study with GNP-NMDA revealed that the material is highly biocompatible and nontoxic toward SH-SY-5Y cell line. At 1.25 nM, the cell survival was 72%, which supports the fact that GNPNMDA can be used in an in vivo model and paves the way for further investigation.

2.4. Conclusion

Oligomers being the primary toxic species involved in amyloid fibrillation are crucial in early stage diagnostics for Alzheimer disease and have been at the center of research attention. In this work, we have successfully regulated the Aβ40 oligomerization process and selectively grown 17 kDa amyloid tetramer, the most neurotoxic species among the LMW oligomers that play a key role toward neuronal cell death. Obtaining structural information on amyloid oligomer has been extremely difficult due to their noncrystalline and unstable nature. The tetramers isolated herein have been characterized elaborately using electrophoresis, FT-IR, CD, and AFM experiments and provide key information on their structural features. Since NMDA receptor modulators are approved by FDA for treating Alzheimer's disease (AD), we utilized GNP decorated with NMDA as a promising strategy for the first time and demonstrated the kinetic inhibition of these highly neurotoxic tetramers. This novel nontoxic GNPNMDA combination altered the nucleation pathway of the tetramer successfully. From the kinetic data, it was evident that GNP-NMDA redirected the nucleation toward secondary nucleation pathway by forming stable GNP-amyloid coaggregates mainly through electrostatic interactions unlike in control experiment where probably primary nucleation pathways are involved. These studies along with kinetic experiments provided clarity on the amyloid oligomer aggregation pathway and afforded a key strategy in developing a rationale target for drug designing and early stage therapeutics for AD.

2.5. Materials & Methods

2.5.1 Materials

All chemicals and reagents were obtained from Sigma Aldrich and used without further purification. HPLC grade solvents and Milli-Q water was used in all the experiments. Amyloid β-protein fragment 1–40 (Aβ40) was purchased from G.L Biochem Ltd., Shanghai, China. Microscopy study were performed using a new glass slides. The Human Cerebrospinal Fluid (HCSF) samples were provided by Guwahati Neurological Research Centre and Hospital (GNRC), Guwahati, India. These samples were obtained from patients as part of routine treatments. Nonetheless, information about the purpose of this experiment was explained at the time of sample collection following the bioethics policy of the hospital.

2.5.2 Instrumentation

UV–visible absorption and fluorescence spectral studies were performed using a Perkin Elmer Lambda-25 spectrometer and BioTek SynergyMx microplate reader respectively. Fouriertransform infrared (FT-IR) spectra were recorded on a Perkin Elmer spectrometer with samples prepared as KBr pellets. The hydrodynamic sizes and zeta potentials measurements were performed using Zetasizer Nano series Nano-ZS90 instrument. TEM images were clicked by JEOL 2100 transmission electron microscope. Atomic force microscopy (AFM) was performed on Bruker Innova SPM model, with the tapping mode.

2.5.3. Preparation GNP-NMDA stock solution

GNP-NMDA stock solution was prepared at the concentration of 100 X 10^{-9} mL^{-1} in 1 mL water. This stock solution was further diluted using 10 mM PBS buffer to desire concentration for each experiment. All the optical experiments such as UV-Visible, FT-IR and fluorescence titrations were performed in 10 mM PBS buffer and pH maintained at 7.4.

2.5.4. Sample Preparation for Aβ40 Monomer

First of all, Aβ (1–40) was treated with trifluoroacetic acid/1,1,1,3,3,3-hexafluuor-2-propanol (TFA/HFIP) by an established method to remove preexisting aggregates. 0.1 mg of Aβ (1–40) was taken in a 2.5 mL plastic tube and dissolved in TFA to obtain a homogeneous aggregates free solution. TFA was evaporated in argon environment. Any left-over TFA was further removed by adding HFIP followed by evaporation under argon gas flow to obtain a film like material. The process was repeated thrice. To the plastic vial, 2.5 mL of PBS buffer (10 mM, pH 7.4) was added followed by sonication to obtain a final concentration of 1.6 X 10^{-4} M. This was used as stock solution and diluted using PBS buffer as per requirement.

2.5.5. Sample Preparation for Aβ40 fibrils

The monomeric Aβ (1–40) was prepared following method given in 2.5.4. To make fibrillary aggregates of Aβ, 10 μM monomeric sample was incubated for 96 hours at 37 °C with steady agitation. The fibrils were characterised using Fluorescence, CD and AFM techniques.

2.5.6. Selection of HCSF samples

The existence of Aβ aggregates in HCSF samples was confirmed by adding 50 µL HCSF (1 µM) solution into ThT (20 µM) solution (10 mM PBS, pH 7.4). A similar fluorescence enhancement in ThT spectrum in presence of Aβ1-40 at 482 nm was observed in presence of amyloid aggregates in HCSF. Further, aggregation of Aβ1–40 amyloid fibrils in HCSF was monitored both in the presence and absence of modulators with different time treatment by monitoring ThT (20 µM) fluorescence enhancement peak at λ_{em} 482 nm (λ_{ex} 440 nm) using a microplate reader.

2.5.7. Thioflavin T Assay

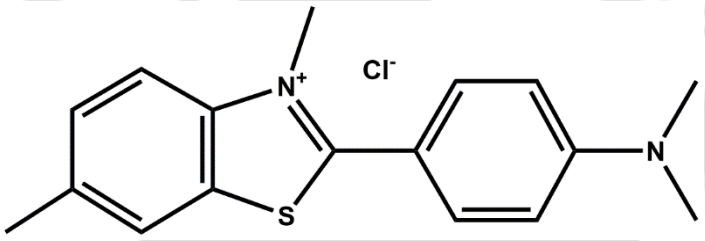

Figure 2.5: *Chemical structure of Thioflavin T*

Thioflavin T (Figure 2.5) is a cationic, benzothiazole salt, widely used to visualize and quantify the presence of misfolded amyloid aggregates both *in vitro* and *in vivo*. When it binds to beta sheet-rich misfolded protein/peptide structures, like amyloid aggregates, the dye offers a marked enhancement in fluorescence intensity and a characteristic red shift of its emission spectrum. Another studies reveals that, fluorescence changes as result of the interaction with double stranded DNA. The mechanism of fluorescence enhancement upon binding to amyloid aggregates is mainly due to the rotational restriction of the central C–C bond connecting the benzothiazole and aniline rings. Thus Thioflavin T (ThT) is usually used for the detection and measurement of amyloid fibrils and in addition for the investigation of fibrillization kinetics of Aβ utilizing fluorescence spectroscopy. The observed emission at ~484 nm is corresponding to the amount of amyloid fibrils present, and in this manner, the extent of fibrillation can be monitored by measuring the time-dependent enhancement in fluorescence. Then again, a decrease in the ThT fluorescence is frequently taken as a sign of restraint of the macromolecular amyloid self-assembly processes.

2.5.8. MTT Assay:

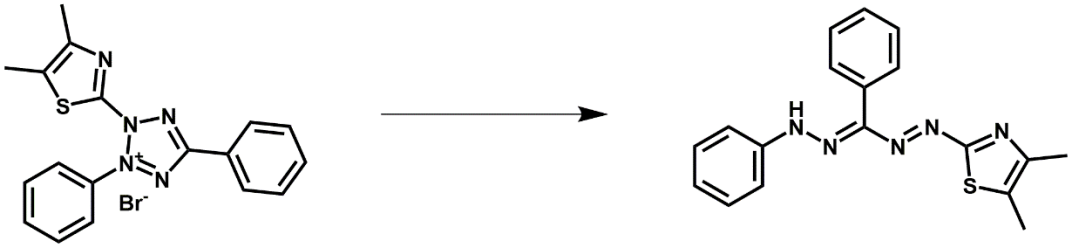

Figure 2.6: *Chemical Reaction involved in MTT Assay*

The MTT assay is a colorimetric assay for assessing cytotoxic activities of a medicinal compound. NAD(P)H-dependent cellular oxidoreductase enzymes usually reflect the number of viable cells present under defined conditions. Such enzymes reduce the tetrazolium dye MTT 3-(4,5-dimethylthiazol-2-yl)-2,5-diphenyltetrazolium bromide (Figure 2.6) to its insoluble formazan, which has a purple color.

3-(4,5-dimethylthiazol-2-yl)-2,5-diphenyl tetrazolium bromide (MTT) is a yellow dye, is reduced to purple formazan in live cells. A solubilization solution (usually either dimethyl sulfoxide, an acidified ethanol solution, or a solution of the detergent sodium dodecyl sulfate in diluted hydrochloric acid) is added to dissolve the insoluble purple formazan product into a red coloured solution. The absorbance of this colored solution can be quantified by measuring at a certain wavelength (usually 570 nm) by a UV-Vis spectrophotometer. The degree of light absorption is dependent on the degree of formazan concentration accumulated inside the cell and on the cell surface. In our experiment, we performed MMT experiment using following protocol.

Cell culture: SH-SY-5Y cells is a neuroblastoma cell line derived from human bone marrow. SH-SY-5Y cells were cultured in complete growth media, Dulbecco's Modified Eagle Medium (DMEM, HiMedia) with 10% fetal bovine serum (Gibco) and antibiotics (Anti-Anti, Gibco) at 37 °C in 5% CO2 incubator. Cell line used in this study were gifted by National centre for cell science (NCCS), Pune.

SH-SY-5Y cells were seeded into 96-well plates at an initial seeding density of 1,00,000 cells/well in 100 µl medium. The cells were cultured for 24 h at 37 °C in 5% CO2. Then, cells of each well were treated with variable concentration of GNP-NMDA ranging from 0-1.25 nM in a concentration range 0-50 µM in 100 µl serum free media. After incubation for 24 h, the 3-(4, 5-dimethylthiazol-2yl)-2, 5-diphenyltetrazolium bromide (MTT) solution (10 µl, 5 mg/mL in PBS) was added to each well. Plate is further incubated

for 3 hours at 37 °C in 5% CO_2, wrapped in aluminum foil. After incubation, MTT-containing medium was replaced by 100 µl Dimethyl Sulfoxide (DMSO) to solubilize MTT-formazan crystals. After incubation for 5 min at 37 °C, absorbance was measured at 570 nm and reference reading at 690 nm was recorded in ELISA microplate reader (Infinite 200 PRO, TECAN). Each of the samples was repeated with 3 replicates. The results were normalized by setting the cell viability of SH-SY-5Y cells in PBS buffer control to be 100%.

2.5.9. Sample Preparation for CD Spectroscopy

We have performed CD spectroscopy to investigate the effect of GNP on secondary structure of tetrameric Aβ40. 10 µM tetrameric Aβ40, 20 µM prefibrillar Aβ40 and 100 µL HCSF sample was incubated both in the presence as well as in absence of 1 nM GNP in 2.5 mM PBS buffer at 37 °C for 54 hours, aliquots were collected at required time interval starting from 0 to 54 hours. CD spectroscopy was performed using 100 nm/sec sacn rate in the wavelength 190 nm – 260 nm range.

2.5.10. Sample Preparation for Zeta potential

10 µM tetrameric Aβ40, 20 µM prefibrillar Aβ40 and 100 µL HCSF sample was incubated both in the presence as well as in absence of 1 nM GNP in 2.5 mM PBS buffer at 37 °C for 54 hours, aliquots were collected at required time interval starting from 0 to 54 hours. Zeta potential study was carried out in Malvern zeta sizer instrument using quartz cuvette.

2.5.11. Sample Preparation for Zeta potential

For AFM study samples collected for CD spectroscopy was used. 50 µL of the sample was diluted in 500 µL. 50 µL of the resulting diluted sample was drop casted on a clean glass substrate and allowed to dry for overnight. For Particle Size Distribution of AFM images, we made three AFM samples from the same samples used for ThT Assay followed by required dilution. As in 10µM×10µM area number of particles are too low for statistical analysis we merged four AFM images in a single image and continues statistical analysis using image J software.

2.5.12. Sample Preparation for AFM Analysis

For AFM study samples collected for CD spectroscopy was used. 50 µL of the sample was diluted in 500 µL. 50 µL of the resulting diluted sample was drop casted on a clean glass substrate and allowed to dry for overnight. For Particle Size Distribution of AFM images, we made three AFM samples from the same samples used for ThT Assay followed by required dilution. As in 10µM×10µM area number of particles are too low for statistical analysis we merged four AFM images in a single image and continues statistical analysis using image J software.

2.6 References

(1) Mount, C.; Downton, C. Alzheimer disease: Progress or profit? *Nat. Med.* **2006**, *12*, 780– 784.

(2) Holtzman, D. M.; Morris, J. C.; Goate, A. M. Alzheimer's disease: The challenge of the second century. *Sci. Transl. Med.* **2011**, *3*, 77.

(3) Chiti, F.; Dobson, C. M. Protein misfolding, amyloid formation, and human disease: A summary of progress over the last decade. *Annu. Rev. Biochem.* **2017**, *86*, 27-68.

(4) Cleary, J. P.; Walsh, D. M.; Hofmeister, J. J.; Shankar, G. M.; Kuskowski, M. A.; Selkoe, D. J.; Ashe, K. H. Natural oligomers of the amyloid-beta protein specifically disrupt cognitive function. *Nat. Neurosci.* **2005**, *8*, 79-84.

(5) Walsh, D. M.; Klyubin, I.; Fadeeva, J. V.; Cullen, W. K.; Anwyl, R.; Wolfe, M. S.; Rowan, M. J.; Selkoe, D. J. Naturally secreted oligomers of amyloid beta protein potently inhibit hippocampal long-term potentiation in vivo. *Nature,* **2002**, *416*, 535- 539.

(6) Narayan, P.; Holmstrom, K. M.; Kim, D. H.; Whitcomb, D. J.; Wilson, M. R.; George-Hyslop, P. S.; Wood, N. W.; Dobson, C. M.; Cho, K.; Abramov, A. Y.;

Klenerman, D. Rare individual amyloid-β oligomers act on astrocytes to initiate neuronal damage. *Biochemistry,* **2014**, *53*, 2442-2453.

(7) Tomiyama, T.; Matsuyama, S.; Iso, H.; Umeda, T.; Takuma, K.; Ishibashi, K.; Teraoka, R.; Sakama, N.; Yamashita, T.; Nishitsuji, K.; Ito, K.; Shimada, H.; Lambert, M. P.; Klein, W. L.; Mori, H. J. A mouse model of amyloid beta oligomers: Their contribution to synaptic alteration, abnormal tau phosphorylation, glial activation, and neuronal loss in vivo. *J. Neurosci.* **2010**, *30*, 4845-4856.

(8) Sandberg, A.; Luheshi, L. M.; Sollvander, S.; Pereira de Barros, T.; Macao, B.; Knowles, T. P.; Biverstal, H.; Lendel, C.; EkholmPetterson, F.; Dubnovitsky, A.; Lannfelt, L.; Dobson, C. M.; Hard, T. Stabilization of neurotoxic Alzheimer amyloid-β oligomers by protein engineering. *Proc. Natl. Acad. Sci. U. S. A.* **2010**, *107*, 15595-15600.

(9) Jana, M. K.; Cappai, R.; Pham, C. L. L.; Ciccotosto, G. D. J. Membrane-bound tetramer and trimer Aβ oligomeric species correlate with toxicity towards cultured neurons. *J. Neurochem.* **2016**, *136*, 594-608.

(10) Dao, P.; Ye, F. F.; Liu, Y.; Du, Z. Y.; Zhang, K.; Dong, C. Z.; Meunier, B.; Chen, H. X. Development of phenothiazine-based theranostic compounds that act both as inhibitors of β-amyloid aggregation and as imaging probes for amyloid plaques in Alzheimer's disease. *ACS Chem. Neurosci.* **2017**, *8*, 798-806.

(11) Muthuraj, B.; Chowdhury, S. R.; Iyer, P. K. Modulation of amyloid-β fibrils into mature microrod-shaped structure by histidine functionalized water-soluble perylene diimide. *ACS Appl. Mater. Interfaces* **2015**, *7*, 21226-21234.

(12) Hong, Y. N.; Meng, L. M.; Chen, S. J.; Leung, C. W. T.; Da, L. T.; Faisal, M.; Silva, D. A.; Liu, J. Z.; Lam, J. W. Y.; Huang, X. H.; Tang, B. Z. Monitoring and inhibition of insulin fibrillation by a small organic fluorogen with aggregation-induced emission characteristics. *J. Am. Chem. Soc.* **2012**, *134*, 1680-1689

(13) Chowdhury, S. R.; Agarwal, M.; Meher, N.; Muthuraj, B.; Iyer, P. K. Modulation of amyloid aggregates into nontoxic coaggregates by hydroxyquinoline appended polyfluorene. *ACS Appl. Mater. Interfaces* **2016**, *8*, 13309-13319.

(14) Margalith, I.; Suter, C.; Ballmer, B.; Schwarz, P.; Tiberi, C.; Sonati, T.; Falsig, J.; Nystrom, S.; Hammarstrom, P.; Aslund, A.; Nilsson, K. P. R.; Yam, A.; Whitters, E.; Hornemann, S.; Aguzzi, A. Polythiophenes inhibit prion propagation by stabilizing prion protein (PRP) aggregates. *J. Biol. Chem*. **2012**, *287*, 18872-18887.

(15) Beck, M. W.; Derrick, J. S.; Kerr, R. A.; Oh, S. B.; Cho, W. J.; Lee, S. J.; Ji, Y.; Han, J.; Tehrani, Z. A.; Suh, N.; Kim, S.; Larsen, S. D.; Kim, K. S.; Lee, J. Y.; Ruotolo, B. T.; Lim, M. H. Structure mechanism based engineering of chemical regulators targeting distinct pathological factors in Alzheimer's disease. *Nat. Commun*. **2016**, *7,* 13115.

(16) Gao, G.; Zhang, M.; Gong, D.; Chen, R.; Hu, X.; Sun, T. The size-effect of gold nanoparticles and nanoclusters in the inhibition of amyloid-β fibrillation. *Nanoscale* **2017**, *9*, 4107-4113.

(17) Wu, J. W.; Breydo, L.; Isas, J. M.; Lee, J.; Kuznetsov, Y. G.; Langen, R.; Glabe, C. Fibrillar oligomers nucleate the oligomerization of monomeric amyloid β but do not seed fibril formation. *J. Biol. Chem*. **2010**, *285*, 6071-6079.

(18) Kayed, R.; Head, E.; Thompson, J. L.; McIntire, T. M.; Milton, S. C.; Cotman, C. W.; Glabe, C. G. Common structure of soluble amyloid oligomers implies common mechanism of pathogenesis. *Science* **2003**, *300*, 486-489.

(19) Kimling, J.; Maier, M.; Okenve, B.; Kotaidis, V.; Ballot, H.; Plech, A. Turkevich method for gold nanoparticle synthesis revisited. *J. Phys. Chem. B* **2006**, *110*, 15700-15707.

(20) Liao, Y. H.; Chang, Y. J.; Yoshiike, Y.; Chang, Y. C.; Chen, Y. R. Negatively charged gold nanoparticles inhibit Alzheimer's amyloid- β fibrillization, induce fibril dissociation, and mitigate neurotoxicity. *Small* **2012**, *8*, 3631-3639.

(21) Nel, A. E.; Madler, L.; Velegol, D.; Xia, T.; Hoek, E. M.; Somasundaran, P.; Klaessig, F.; Castranova, V.; Thompson, M. Understanding biophysicochemical interactions at the nano-bio interface. *Nat. Mater.* **2009**, *8*, 543-557.

(22) Zandomeneghi, G.; Krebs, M. R. H.; Mccammon, M. G.; Fandrich, M. FTIR reveals structural differences between native betasheet proteins and amyloid fibrils. *Protein Sci.* **2004**, *13*, 3314-3321.

(23) Tornquist, M.; Michaels, T. C. T.; Sanagavarapu, K.; Yang, X.; Meisl, G.; Cohen, S. I. A.; Knowles, T. P. J.; Linse, S. Secondary nucleation in amyloid formation. *Chem. Commun.* **2018**, *54*, 8667- 8684.

(24) Rijkers, D. T. S.; Hoppener, J. W. M.; Posthuma, G.; Lips, C. J. M.; Liskamp, R. M. J. Inhibition of amyloid fibril formation of human amylin by n-alkylated amino acid and -hydroxy acid residue containing peptides. *Chem. Eur. J.* **2002**, *8*, 4285-4291.

(25) Sousa, A. A.; Hassan, S. A.; Knittel, L. L.; Balbo, A.; Aronova, M. A.; Brown, P. H.; Schuck, P.; Leapman, R. D. Biointeractions of ultrasmall glutathione-coated gold nanoparticles: Effect of small size variations. *Nanoscale* **2016**, *8*, 6577-6588.

2.6. Appendix A: Additional Figures for Chapter 2

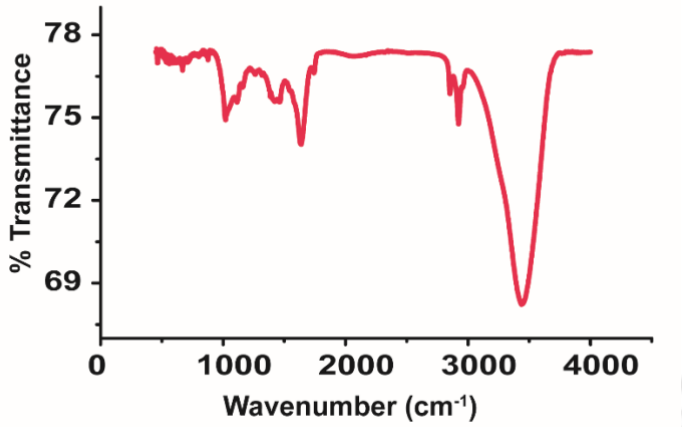

Figure A-1*: FT-IR spectrum of GNP-NMDA.*

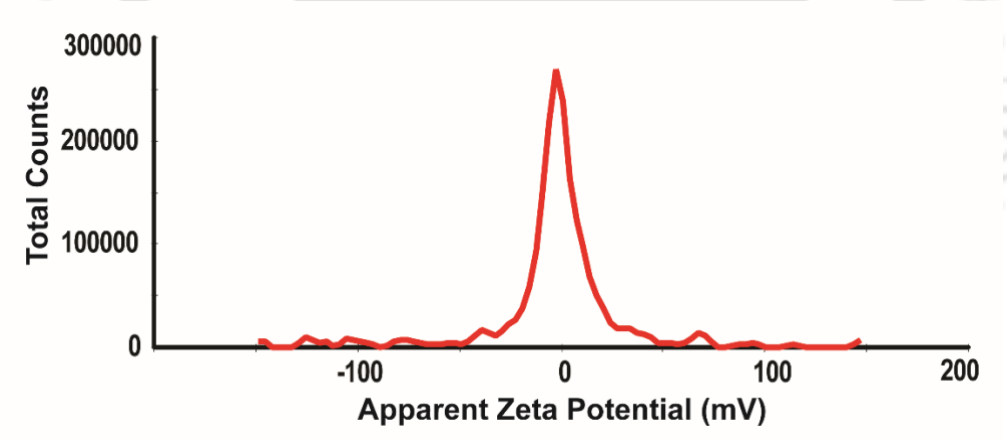

Figure A-2: *Zeta potential of GNP-NMDA.*

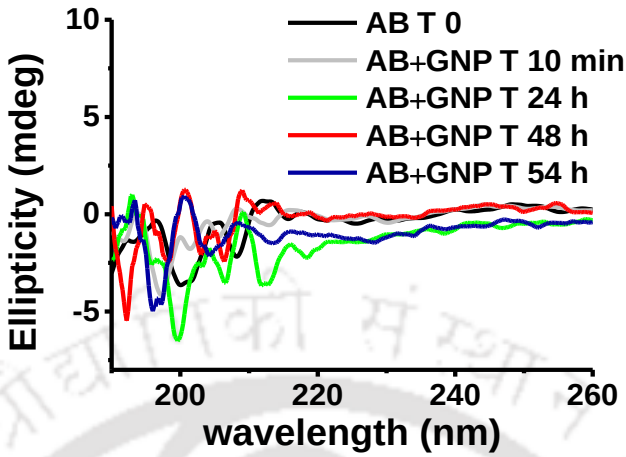

Figure A-3: *CD spectra of Aβ (AB) tetramer in absence and in presence of GNP with respect to time.*

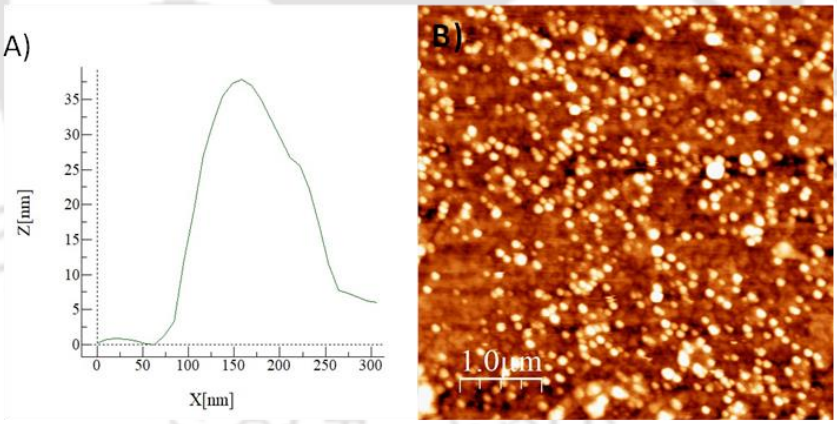

Figure A-4: A) Height profile amyloid beta40 tetramers. B) AFM image of amyloid beta40 tetramers.

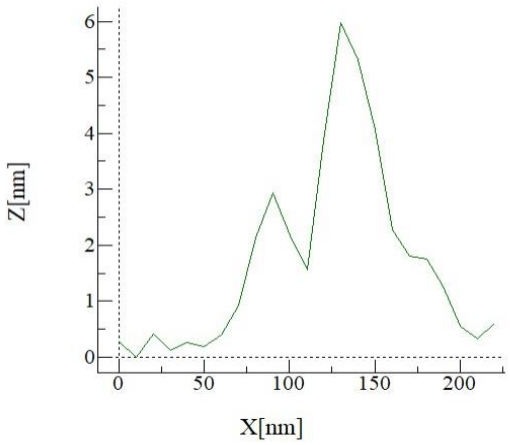

Fig. A-5*: Height profile of Amyloid beta40 fibrils.*

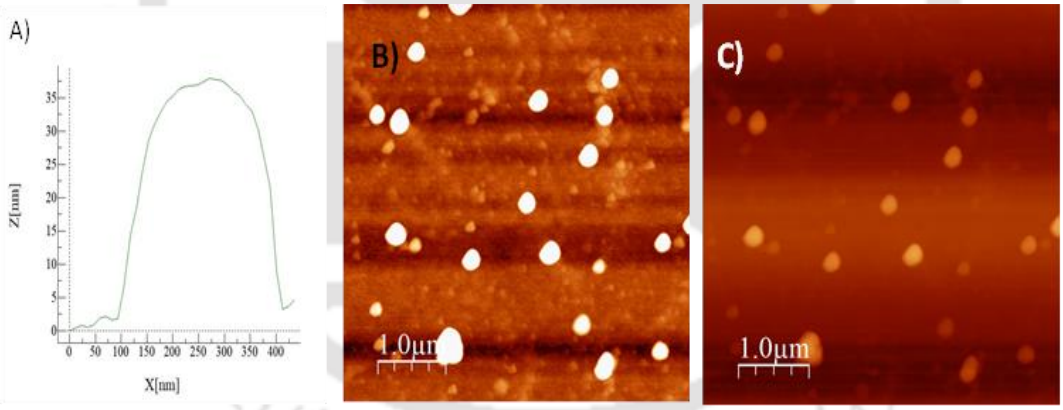

Fig. A-6*: A) Height profile of Amyloid-GNP co-aggregates. (B-C) AFM image of Amyloid-GNP co-aggregates.*

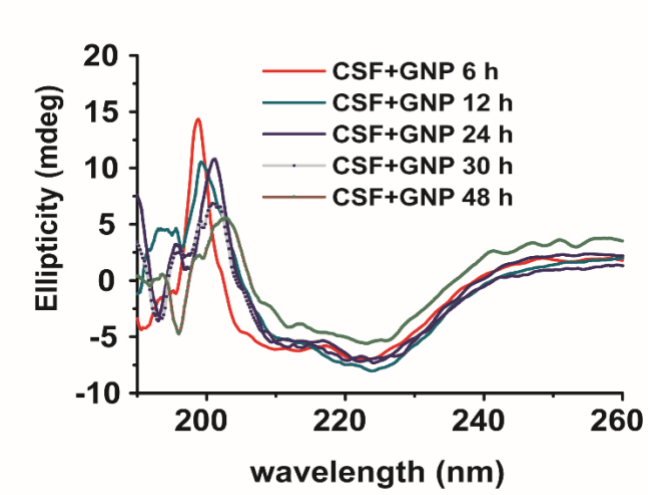

Fig. A-7. *CD spectra of Human Cerebrospinal Fluid in absence and in presence of GNP with respect to time.*

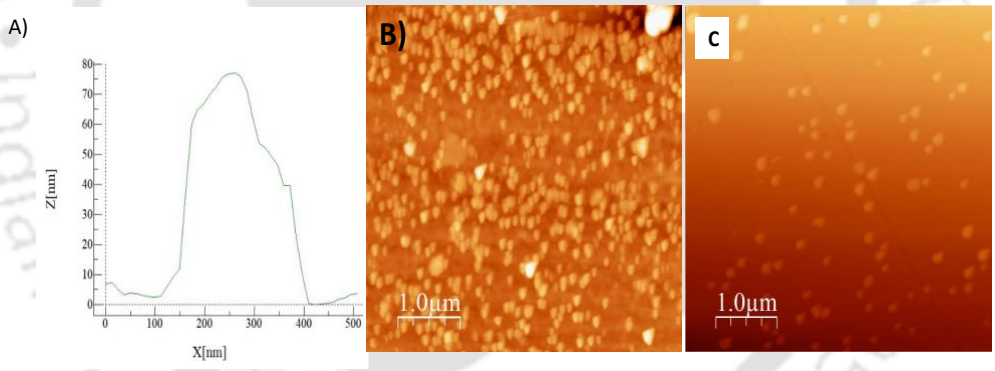

Fig. A-8*: A) Height profile of early aggregates in HCSF samples (B-C) AFM image of early aggregates in HCSF samples.*

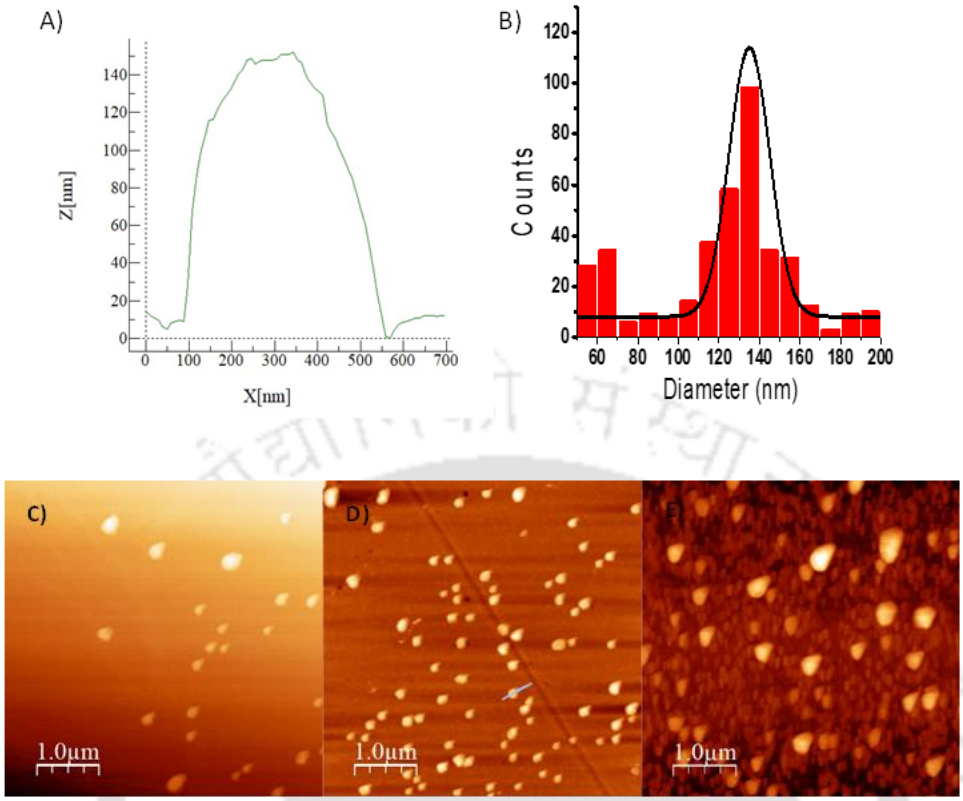

Fig. A-9: *A) Height profile of GNP-Amyloid coaggregates in HCSF samples. B) Average particle size distribution of Amyloid-GNP co-aggregates in HCSF, (C-E) AFM morphology of GNP-Amyloid coaggregates in HCSF samples.*

3

Template-Mediated Detoxification of Low-Molecular-Weight Amyloid Oligomers and Regulation of Their Nucleation Pathway

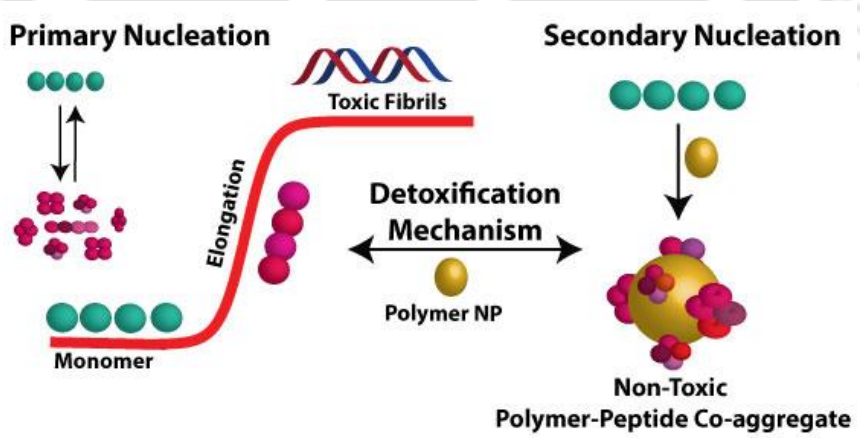

1. **Mondal, S.**; Kumar, V.; Chowdhury, S. R.; Shah, M.; Gaur, A.; Kumar, S.; Iyer, P. K.* Template mediated detoxification of low-molecular-weight amyloid oligomers and regulation of their nucleation pathway. *ACS Appl. Bio Mater.,* **2019**, *2*, 5306-5312.

3

Template Mediated detoxification of Low Molecular Weight Amyloid Oligomers and Regulation of Their Nucleation Pathway

Abstract

Amyloid tetramer, the most toxic low-molecular-weight (LMW) amyloid oligomer, leads to synaptic dysfunction and plays a vital role in pathophysiology of Alzheimer's disease (AD). Hence, their kinetic inhibition may be regarded as a potential therapeutic strategy against AD. However, because of their dynamic, metastable nature, not much information has been gathered about them. Herein, amyloid tetramers have been isolated from a mixture pool of low- and high-molecular-weight amyloid oligomers. Kinetics of such tetrameric species has been studied in an in vitro model and inhibition of the fibrillation of the species has been achieved by means of a novel isatin functionalized polyfluorene derivative (PFIS). Isatin interacts with tetramers noncovalently to modulate its fibrillation by forming stable polymer–peptide coaggregates. In parallel to this, hydrophobic PFIS forms spherical nanoparticle in water that provides an external surface, which functions to modulate nucleation pathway of the oligomers. The polymer–peptide coaggregates are nontoxic in nature. Hence, these observations offer a potential strategy to suppress neurotoxicity of a LMW oligomer by forming nontoxic coaggregates. In parallel to this, our

methodology also provides a potential strategy to observe and regulate nucleation pathway of the oligomers as well.

3.1. Introduction:

Alzheimer Disease (AD), a fatal neurodegenerative disease leading to synaptic dysfunction and behavioural changes is characterised by deposition of Amyloid Fibrils (amyloid aggregates) in subcortical region and cerebral cortex of the human brain.[1-3] However, recent research activity reveals that soluble oligomeric intermediates are the most neurotoxic species and contribute as key factors in neuronal cell death associated with AD.[4-7] An *in vivo* experiment with transgenic mice revealed that deposition of insoluble Aβ fibrils led to minimal neuronal loss.[8] In humans also, the abundance of a large amount of amyloid plaques in cognitically normal aged individual proved that minimal relation exists among Aβ fibrils and synaptic dysfunction.[9-11] On the other hand, oligomeric intermediates have been found to trigger enhanced neurotoxicity along with other clinical factors associated with AD like microglial activation, increased ROS productions and hyper-phosphorylation of tau protein.[12] Hence, all these evidences lead to a single conclusion that soluble oligomeric Aβ plays a central role in AD rather than insoluble fibrillary species. Hence, molecular mechanism associated with oligomerisation may help us explore the key event by which a benign protein transforms to a neurotoxic form. However, due to their heterogeneous, metastable and dynamic identity, studies involving oligomeric state have remained a great challenge. Oligomerisation is a multistep process in which nucleation is the obligatory step.[13-14] According to the classical theory of nucleation, it is the fundamental step towards formation of a new thermodynamic step having lower free energy formed via self-aggregation.[15] Upto now, two types of nucleation pathway are known, viz. primary nucleation and secondary nucleation.[16-17] Primary nucleation usually occurs in bulk solution, 'Head on' aggregation with a rate solely dependent on monomer concentration leading to linear or chain like fibril. On the other hand, secondary nucleation pathway involves formation of fibril with rate proportional to concentration of both monomers and preformed fibrils.[16] Therefore, presence of little amount of preformed fibrils catalyses the rate of fibril formation through secondary nucleation pathway.[16] Surprisingly, fibril formed through different nucleation pathway differs in extent of toxicity.[18] A cell viability study on human neuroblastoma cells reveals that fibril formed in primary nucleation pathway exhibits enhanced neurotoxicity over the fibrils formed via secondary nucleation pathway.[18]

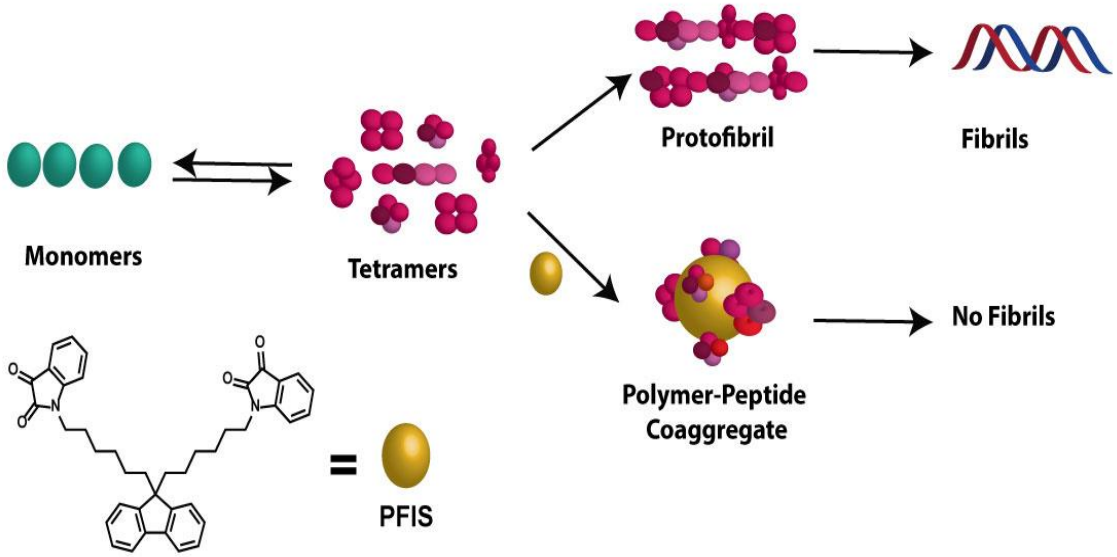

Scheme 3.1*. Regulation of Nucleation Pathway of Amyloid Tetramer by Novel Isatin Functionalized Polymer.*

Therefore, regulation of nucleation pathway of oligomers may lead to an efficient therapeutic strategy against cognitive dysfunction.

However, among the low molecular weight amyloid oligomers tetramers are found to be at least fifty times more neurotoxic than the other species.[19] Herein, amyloid tetramers have been judiciously isolated from the mixtures of LMW oligomers and fibrils and their kinetic property has been studied. An isatin functionalized conjugated polymer (PFIS) has been developed that specifically interacts with the isolated tetramer to form stable nontoxic polymer-peptide coaggregates and resist it from further proliferation (Scheme 3.1). Isatin can be found in nature in plant named *isatis tinctoria*. The derivatives natural compound known to have various biological activity including antioxidant, antibancterial, anti-anxiety, anti-malarial, anti-HIV and anti-fungal properties.[20-22] However, its activity towards AD has not been reported. Newly synthesized isatin functionalized polyflurene (PFIS) forms a nanoparticle in water and provides an external surface that directs nucleation pathways of the tetramer to secondary pathway (Scheme 3.1). Detoxification of toxic tetramer through complexation and regulation of nucleation pathway reported in this work is of prime clinical importance in developing early phase therapeutics for AD.

3.1. Experimental Section

3.1.1. Synthesis of PFIS

Isatin-functionalized polyfluorene was synthesized according to the synthetic route shown in Figure B-1 by modifying an established protocol.[23] Briefly, alkylation of fluorene was performed using 1,6 dibromohexane in the presence of 50% aqueous sodium hydroxide and the separated organic part was purified by column chromatography. The product was subjected to oxidative polymerization in nitrobenzene solvent using ferric chloride ($FeCl_3$) under inert atmosphere followed by precipitation in methanol and drying under vacuum. The molecular weight (Mw) of the polymer was found to be 6670 g mol^{-1} with a polydispersity index (PDI) of 2.3 (THF, Polystyrene as internal standard). Finally, Isatin was attached by replacing the terminal bromine in alkyl chain in DMF solvent in the presence of potassium carbonate. Desired polymer (PFIS) was again precipitated in methanol and characterized by ^{13}C and ^{1}H NMR using DMSO-d_6 as solvent (Figures B2–B4).

3.1.2. Preparation of LMW Aβ40 Oligomer (Tetramer)

LMW Aβ40 oligomer (tetramer) was prepared following an established protocol reported earlier.[24] Briefly, 0.1 mg of commercial Aβ40 was added in 20 µL of HFIP (hexafluoro-2-propanol). The excess HFIP was vaporized under an argon atmosphere and 10 µL of DMSO was added to the solution. To the resulting solution was added 10 mM phosphate buffered saline (PBS, pH 7.2) along with 10 mM NaCl and 0.02% sodium azide and it incubated for 1 h at 37 °C. The resulting mixture was centrifuged at 10 000 rpm for 1 h and supernatant was collected. Existence of tetramer was confirmed using native PAGE analysis. It showed a clear band at approximately 17 kDa. Respective band (17 kDa) for tetrameric species was cut and dissolved in 50 mM tris HCl (pH 7.4), 0.1 mM EDTA, and 150 mM NaCl. Isolated tetramer was again confirmed using native PAGE analysis (Figure B-5). Figure B-5 clearly shows bands for ladder (L), amyloid tetramer (T), a mixture of monomer and dimer of Aβ40 (M), and a mixture of HMW oligomer and fibrils (F), respectively. Tetramers were also characterized by atomic force microscopy (AFM) and circular dichroism spectroscopy (Figures B-6).

3.1.3. HCSF Sample as Natural Store House of Aβ40

Human cerebrospinal fluid (CSF) contains Aβ40. The presence of Aβ40 can be confirmed by ThT intensity measurements. 50 μL HCSF sample was added to 20 μM ThT and fluorescence spectra (Excitation 440 nm) was recorded before and after addition of HCSF. ThT emission intensity was found to be enhanced in the presence of HCSF samples. Similar enhancement was observed in the presence of only Aβ40, which clearly indicated the presence of Aβ40 in HCSF samples.

3.2. Results

Investigation of fibrillation kinetics involving LMW amyloid oligomers are extremely difficult because of their unstructured and dynamic nature. In this work, LMW amyloid oligomer (tetramer) was isolated and purified from aggregated amyloid mixture with good yield. The oligomer was incubated solely as well as in the presence of the conjugated polymer (PFIS) under physiological condition (10 mM PBS buffer, pH 7.4, 37 °C) for 120 h and the interaction between the two was thoroughly explored.

The kinetics of inhibition was monitored by ThT assay. Briefly, Aβ40 tetramer (5 μM) was incubated for 96 h in the presence as well as in absence of PFIS (1 μM) in physiological condition, i.e., 10 mM PBS buffer (pH 7.2) at 37 °C. Sample specimens were collected at every 6 h interval from 0 to 120 h, 20 μM ThT was added, and emission was recorded at 480 nm (excitation 440 nm). The LMW amyloid oligomers, which lacks in β content, shows least affinity toward ThT. On incubation for 24 h, an abrupt enhancement in ThT intensity was observed, confirming the formation of β-enriched fibrillar species. The enhancement was saturated after 30 h producing a sigmoidal behavior in ThT assay. However, when 1 μM PFIS was added to the 5 μM Aβ solution, complete inhibition in fibrillation process was observed due to the formation of comparatively stable peptide–polymer coaggregates which does not change with time producing a straight-line type behavior in fibrillation kinetics (Figure 3.1A). Variable concentration of PFIS was made to interact with tetramers and dose-dependent inhibition was observed (Figure 3.1A).

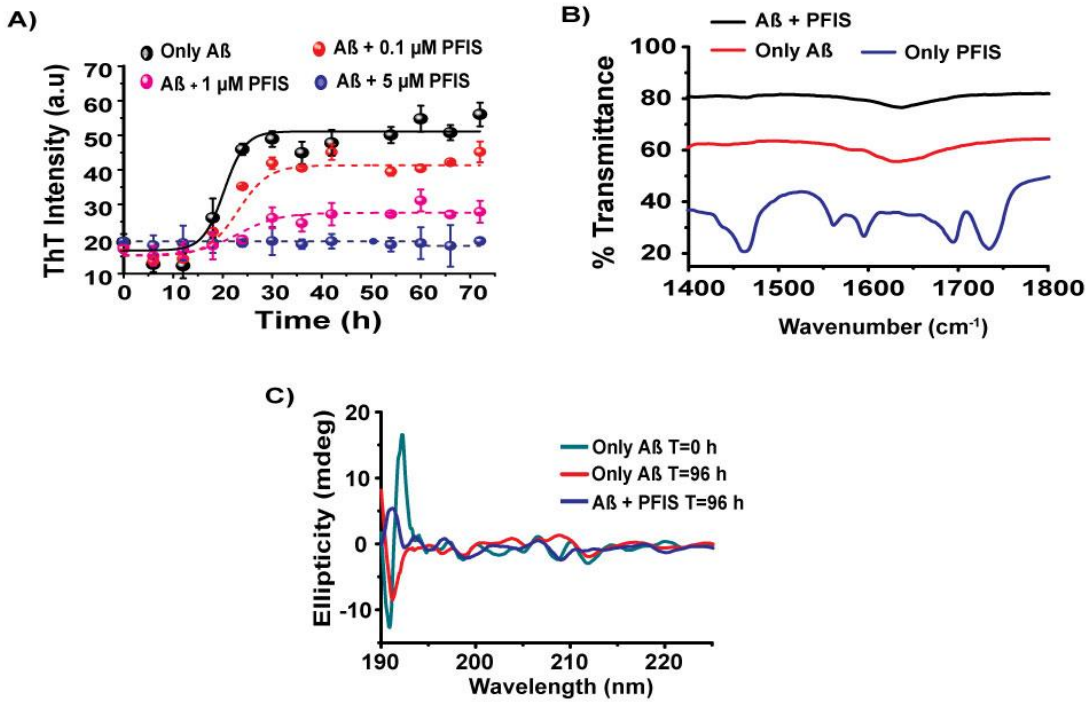

Figure 3.1. *(A) Fibrillation kinetics of Aβ40 (5 µM) in the presence and absence of 5, 1, and 0.1 µM PFIS in 10 mM PBS buffer (pH 7.4), 37 °C. The line indicates sigmoidal fit. The data represent the mean ± SEM of n=3 individual experiments. (B) FT-IR spectra of Aβ40 in the presence and absence of 1 µM PFIS. (C) CD spectra of Aβ40 in the presence and in absence of PFIS.*

To have an insight into secondary structure of Aβ, FT-IR was performed (Figure 3.1B). FT-IR spectra of Native PFIS shows multiple peaks at 1460, 1560, 1595, 1694, and 1736 cm^{-1} because of –OH bending (arises from enol form of isatin), aromatic C=C, C=C (isatin), C=O (amide), and C=O (ketone) stretching, respectively. On incubation for 72 h, LMW Aβ oligomer showed a peak at 1630 cm^{-1} indicating the presence of antiparallel β-sheet (red line).[25] On the other hand, on incubation with PFIS, the polymeric HFIS nano particle affects the β-sheet pattern and shifts the peak to 1638 cm^{-1} (blue line). However, to study the detail effect of PFIS in secondary structure, the analysis was performed using circular dichroism (CD) spectroscopy (Figure 3.1C). In CD spectroscopy, the oligomeric Aβ tetramer appears with a negative peak at 208 nm and a weak band near 222 nm (green line). All the three bands indicate the presence of a helical conformation in the system.[26] The band at 222 nm rises due to n–π* transition of the peptide group while the π–π* transition produces bands at 208 nm mainly through exciton splitting (parallel exciton).[27–30] The tetrameric spectra also possess a negative band at 217 nm and a positive band at 195 nm arising due to n–π* and π–π* transition of β sheet conformer.[31] Hence, it is evident that the spectrum of tetrameric species actually consists of a mixture of α and β

conformers. On incubating the solution in physiological condition for 96 h, the bands representing α helix completely disappeared, and bands responsible for β sheet conformer (only negative bands at 217 nm) only survived. Interestingly, on incubation with PFIS polymer, positive bands at 193 nm along with negative bands at 222 nm (responsible for α helix) reappeared along with positive bands at 195 nm, and negative bands at 219 nm (responsible for β sheets). Hence, from CD analysis, it can be concluded that the polymer PFIS assists the tetramer to retain its nontoxic helical conformation and resists its inherent folding tendency. Dynamic light scattering (DLS) technique reveals the presence of micrometer size particles in the solution. Initially, tetrameric amyloid beta showed a hydrodynamic diameter of 2.8 μM on incubation for 24 h, which increased up to 4.3 μM and finally reached 13.91 μM after 96 h of incubation. On the other hand, in the presence of PFIS, the primary species shows a diameter of 0.5 μM, which finally reached 3.6 μM after 96 h of incubation, providing ample evidence that the amyloid tetramer sare strictly prevented from forming large fibrillar species. Although amyloid oligomers usually show sizes in the nanometer region, it is quite unusual for micrometer-sized particles to be observed in DLS. However, the DLS technique determines the hydrodynamic radius of the particle obtained from the diffusional properties of the particle in solution that represents mainly particle size with hydration shell and shape effects. To get rid of such interferences and more in-depth atomic level understanding, we performed AFM studies.

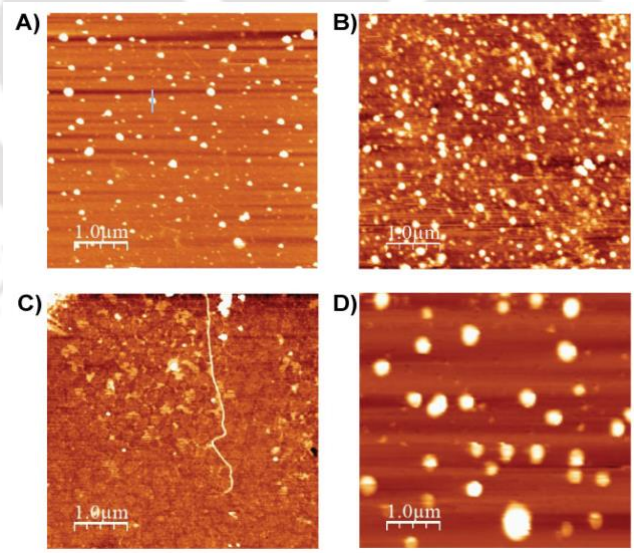

Figure 3.2. *(A) AFM morphology of PFIS nanoparticle in water, (B) AFM morphology of amyloid tetramer, (C) AFM morphology of amyloid fibrils formed in absence of PFIS, (D) AFM morphology of the amyloid-polymer co-aggregates.*

3.2.1. Morphological Studies:

The morphological studies carried out using AFM experiments revealed that PFIS forms spherical nanoparticle in water having diameter ~300 nm (Figure 3.2A and Figure B-7). Such kind of nanoparticle actually acts like a template by providing a surface that favors the formation of peptide–polymer coaggregates. Amyloid tetramers are spherical in nature with dimension 50 ± 21 nm (Figure 3.2B and Figure B-6). However, on incubation for 96 h, the initial spherical oligomer was finally converted to 4 μM long fibrillar morphology (Figure 3.2C and Figure B-7). However, on incubation with PFIS, no such fibrillar morphology was found; instead, spherical and comparatively larger peptide–polymer coaggregates (0.5 μM) were obtained (Figure 3.2D and B-9). Thus, isatin-functionalized polyfluorene modulates the fibrillation kinetics of the amyloid tetramer by forming a stable nontoxic amyloid–polymer coaggregate.

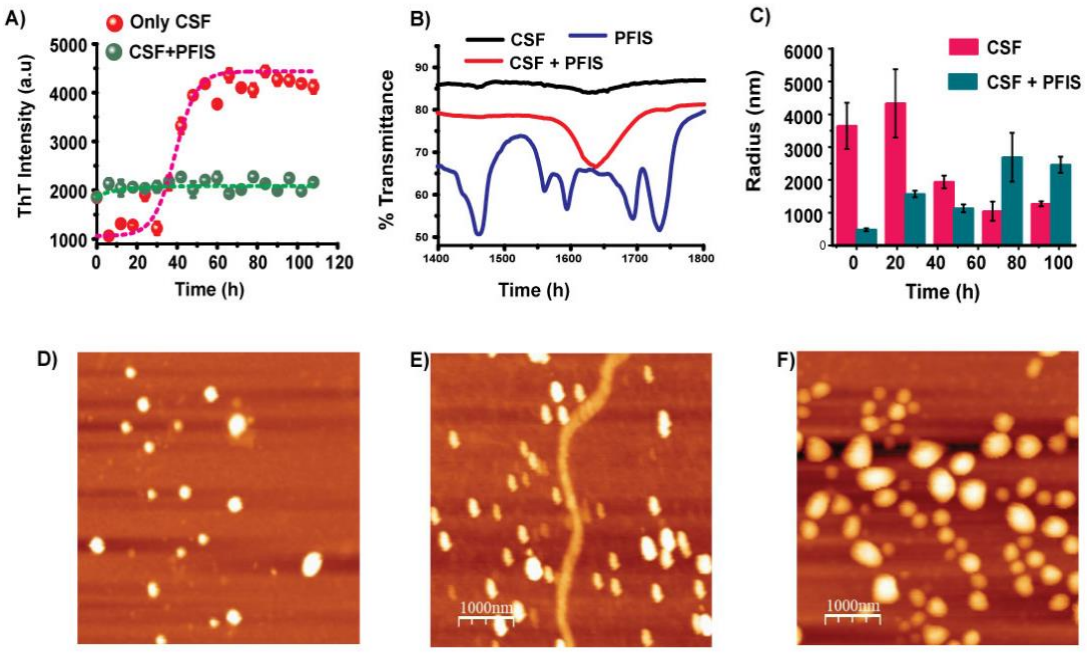

Figure 3.3. *(A) Fibrillation kinetics of 100 μL HCSF in the presence and absence of 1 μM PFIS in 10 mM PBS buffer (pH 7.4, 37 °C). (B) FT-IR spectra of Aβ40 present in HCSF in the presence and absence of PFIS. (C) DLS measurement of Aβ40 present in HCSF in the presence and absence of PFIS. AFM image of (D) CSF oligomer, (E) CSF fibril, and (F) CSF-polymer co-aggregate.*

3.2.2. Studies with HCSF

Human cerebrospinal fluid (HCSF) plays a vital role in AD diagnosis and therapeutics, as it contains amyloid beta and hence is believed to be a prime biomarker for AD.[32-33] HCSF samples were collected from GNRC hospital and their aggregation was studied using ThT assay, FT-IR, and AFM experiments. Collected HCSF samples showed a lag phase up to 36 h followed by a growth phase and a saturated phase following ideal amyloid kinetics (Figure 3.3A). However, in the presence of the polymer PFIS, the ThT intensity was found to be almost unchanged throughout the experiment, producing a straight line type behavior that indicated complete inhibition of the amyloid fibrillation. Such inhibition activity can be correlated with exactly the same found with commercial amyloid beta samples as shown in Figure 3.1A. In FT-IR spectroscopy, HCSF samples, on incubation for 96 h showed a peak at 1627 cm^{-1} indicating the presence of β-sheet structure (Figure 3.3B).[25] However, on incubation in the presence of PFIS, the peak was shifted to 1637 cm^{-1}, indicating a modulation in β-sheet pattern. The inhibition activity can be tracked using DLS techniques as well. The CSF-polymer coaggregates initially show a size of 480 nm, after which it increases to 1570 nm and then it remains almost constant throughout the experiment (Figure 3.3C). In AFM experiment, native CSF aggregates show particles having 150 nm diameter (Figure 3.3D). On incubation for 96 h in physiological conditions, it was transformed to fibrillar morphology (Figure 3.3E and B-10). However, when incubated in the presence of 1 μM PFIS, no fibrillar morphology was found; instead, rather larger spherical morphology appeared (Figure 3.3F and B-11).

3.2.3. MTT Assay:

Cytotoxicity of the polymer PFIS was studied using MTT assay on SH-SY-5Y cell lines having density 10^5 cells/well (per 100 μL). The cells were taken in a 96 well tissue culture plates and incubated for 16 h in DMEM/F12 within a 5% CO2 incubator at 37 °C. After that the media was discarded and the well was washed with PBS buffer. The PFIS solution with different concentration (0.097 mM to 100 mM) was poured to the wells and incubated for 24 h. It was further incubated for 4 h after addition of 10 μL of 5 mg/mL MTT in PBS solution. The media was then removed and 100 μL of DMSO was added and absorbance recorded at 570 nm. The experiment was repeated thrice and the percentage of cell viability was presented and compared with untreated cells. The result of the MTT assay reveals that desired conjugated polymer PFIS shows no significant toxicity in the concentration range 97 μm to 100 mM (Figure 3.4A).

3.3. Discussion

In our previous work, we reported hydroxyquinoline functionalized polyfluorene for modulation of amyloid monomers.[23] However, recent research reveals that oligomers are much more neurotoxic than the fibrillary aggregates and hence contribute to AD to maximum extent.[34] However, because of their metastable nature is very difficult to isolate them. Herein, neurotoxic amyloid tetramers have been isolated and their inhibition in fibrillation kinetics has been achieved by isatin functionalized polyfluorene. In parallel to this, nucleation pathway of the oligomers also has been regulated by this novel polymer. Isatin and its derivative represent an essential class of heterocyclic compounds that have immense activity in biological systems and hence they can be used as an essential precursor for drug development. Recently, isatin has received immense scientific attention because of its excellent anticancer activity. Isatin derivatives (such as sunitinib V and toceranib

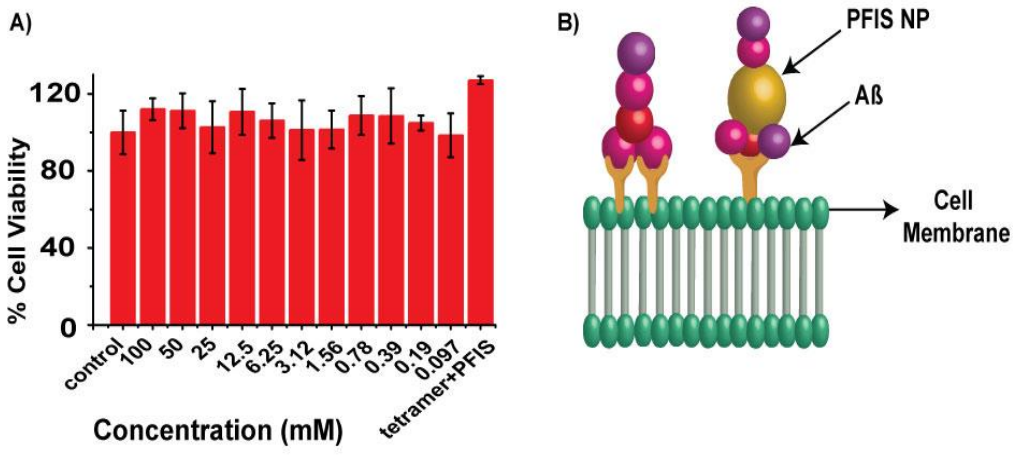

Figure 3.4. *(A) Cell viability assay of PFIS. The error bar indicates the values of mean ± SD of three experiments. (B) Schematic representation of interaction between polymer nanoparticle, amyloid tetramer, and cell membrane.*

phosphate) are known as clinically approved anticancer drugs. In addition, some of the isatin derivatives are known to show antioxidant, antifungal, antibacterial, antidiabetic, anti-inflammatory, antimalarial, anti-HIV and antianxiety activity.[20–22] These special class of compounds are also known to have numerous inhibition activity toward carbonic anhydrase, tyrosine kinase and tubulin. However, its antiamyloidogenic activity is still unknown. Hence, isatin attached to polyfluorene backbone can be an excellent choice for studying inhibition activity toward amyloid fibrillation. The native polymer PFIS, having a hydrophobic backbone undergoes self-aggregation to form spherical nanoparticle when dispersed in water (Figure 3.2A). The polymer nanoparticle indeed functions as an efficient

template that actually provides an external surface where the aggregation kinetics takes place which results in regulation of fibrillation pathway of the oligomers. However, isatin assists the amyloid tetramers to bring them closer to the nanoparticle through noncovalent interactions. Usually it is believed that carboxyl groups of the isatin plays a vital role by forming hydrogen bond with the peptide.

Nucleation pathways of the LMW oligomers are of great clinical importance, as they are the obligatory step toward fibril formation. Generally, in the absence of any external surface, primary nucleation predominates. It is the most dominant nucleation pathway involving "head-on" aggregation of the monomers (Figure 3.4B). On the other hand, secondary nucleation involves random aggregation of the monomers on some external surface (Figure 3.4B). Nature of the nucleation pathway happening in the solution can be elucidated from the kinetic data.[34] In the presence of PFIS, a reduction in slope during growth phase was observed in fibrillation kinetics and the effect seemed to be saturated with the increase in concentration of the PFIS (Figure 3.2A). The reduction in slope is the kinetic signature of the secondary nucleation.[35] The polymer shows no significant toxicity in a wide concentration range (97 μm to 100 mM). In addition to this, polymer-oligomer coaggregates also does not exhibit any toxicity. Native amyloid oligomers are highly toxic in nature and plays a vital role in onset of AD. Hence, newly synthesized conjugate polymer empowers us to suppress toxicity of the amyloid oliogomers by forming polymer-oligomer coaggregates.

3.4. Conclusion

Low-molecular-weight amyloid oligomers are extremely important in pathophysiology of the AD. Amyloid tetramers has been isolated from a pool of fibrillar and oligomeric mixtures. Their kinetic inhibition has been achieved by a novel Isatin functionalized polymer. The mechanistic detail of the inhibition also has been explored. PFIS having a hydrophobic backbone forms spherical nanoparticle in water which provides a surface where nucleation of the oligomers takes place. Isatin, being a biologically active natural compound interacts noncovalently with the oligomers and regulates the nucleation of the oligomers toward secondary nucleation pathway. The PFIS also decreases the neurotoxicity of the amyloid oligomers by forming polymer–peptide coaggregates. Hence, isatin-functionalized novel conjugated polymer, PFIS empowers us to regulate nucleation pathways of the amyloid oligomers as well as reduces neurotoxicity of the oligomers, which may have further application in drug development against AD.

3.5. Materials and Method

3.5.1. Materials

1,1,1,3,3,3-Hexafluoro 2 propanol (HFIP), Fluorene, potassium carbonate, 1,6-Dibromohexane, Ferric chloride, Phosphate buffered saline (PBS), DMEM, Trifluoroacetic acid (TFA), Isatin were purchased from Merck, Sigma Aldrich and were used without further purification. Human Amyloid β 1-40 was obtained from G L Biochem Ltd., Shanghai, China. During experiments HPLC grade solvents and Milli-Q water was used in all cases. The Human Cerebrospinal Fluid (HCSF) samples were collected from Guwahati Neurological Research Centre and Hospital (GNRC), Guwahati, India.

3.5.2. Instrumentation

Fluorescence and UV-Vis spectral acquisition was performed using Horiba Scientific Fluoromax-4 Spectrofluorometer and Perkin Elmer Lambda-25 spectrometer respectively. During fluorescence spectral acquisition 10 mm x 10 mm quartz cuvette was used and emission was recorded at 90° with respect to the excitation beam. Measurements for ThT fluorescence assay was performed using Tecan microplate reader in a Corning 96 Well Black Polystyrene Microplate (Cat. No. 3631). Dynamic Light Scattering (DLS) study were performed using Malvern Zetasizer Nano series Nano-ZS90. Circular Dichroism (CD) were performed in a quartz cuvette (1 mm path length) using JASCO J-1500-150 Spectrometer. NMR spectra were recorded using $CDCl_3$ as a solvent in a Bruker AscendTM 600 MHz spectrometer. Morphological characterization was performed using Bruker Innova Atomic Force Microscope in non-contact mode.

3.5.3. Stock Solution Preparation

10 mM PFIS was prepared in DMF by dissolving required amount of solid PFIS and further diluted as required. The resulting solution was filtered by 0.22 μM syringe filter.

3.5.4. HFIP/TFA treatments of Aβ

Pre-existing aggregates of Aβ (1–40) was removed using trifluoroacetic acid/1, 1, 1, 3, 3, 3-hexafluuor-2-propanol (TFA/HFIP) by an established method. 0.1 mg of Aβ (1–40) was added to a 2.5 mL plastic vial and dissolved in TFA to obtain aggregates free homogeneous solution. TFA was then evaporated in argon environment. Any left-over TFA

was further removed by adding HFIP followed by evaporation using argon gas flow to obtain a film like material. This process was repeated thrice. To the plastic vial, 2.5 mL of PBS (10 mM, pH 7.4) was added followed by sonication and vortexing to obtain a final concentration of 1.6 X 10^{-4} M. Fibril formation was monitored using a ThT binding assay.

3.5.6. Isolation of LMW amyloid oligomers (tetramers)

LMW Aβ40 oligomer (tetramer) was prepared following an established protocol reported earlier by Iyer et al (10.1021/acsabm.9b00128). Briefly, 0.1 mg commercial Aβ40 was added in 20 µl HFIP (hexafluoro-2-propanol), excess HFIP was vaporized under argon and 10 µl DMSO was added to the solution. To the resulting solution 10 mM Phosphate buffered saline (pH 7.2) along with 0.02% sodium azide and 10 mM NaCl was added and incubated for one hour in 37 °C. It was centrifuged at 10,000 rpm for one hour and supernatant was collected. Presence of tetramer was confirmed using native PAGE analysis. It showed a clear band nearly at 17 kDa. Respective band (17 kDa) for tetrameric species was cutted and dissolved in a solution containing 50 mM TRIS.HCl (pH 7.4), 0.1 mM EDTA, and 150 mM NaCl. Isolated tetramer was again confirmed using native PAGE analysis and characterized by circular dichroism spectroscopy and atomic force microscopy.

3.5.7. Selection of HCSF samples

The presence of Aβ fibrils in HCSF was confirmed by adding 50 µL HCSF (1 µM) solution into ThT (40 µM) solution (10 mM PBS, pH 7.4). A similar fluorescence enhancement in ThT spectrum in presence of Aβ1-40 at 482 nm was observed upon binding with amyloid aggregates in HCSF. Further, aggregation of Aβ1–40 amyloid fibrils in HCSF was monitored both in the presence and absence of modulators with different time incubations by monitoring ThT (20 µM) fluorescence enhancement peak at λem 482 nm (λex 440 nm) using a microplate reader.

3.5.8. Synthesis of PFIS

9, 9-Bis-(6-bromohexyl)-9H-fluorene: Fluorene (2 g, 12.032mmol), 50% aq. NaOH and a catalytic amount of tetra-butyl ammonium Iodide (TBAI) (0.888 g, 2.406 mmol) were added to a 100 mL round bottom flask and then degassed 3 times by applying freeze-thaw cycles. 1,6- dibromohexane (20.632 g, 84.227 mmol) was added through a syringe

(degassed) and the mixture was stirred continuously for 6 hours at 70 °C. The reaction mixture was cooled to room temperature and extracted with chloroform. The organic layer was washed with water and dried over anhydrous sodium sulphate. The solvent was removed under vacuum and excess 1, 6-dibromohexane was removed through shortpath distillation and the crude was purified using Column Chromatography over a pad of silica gel using hexane as an eluent to get the desired doubly alkylated product as yellow oil.

Poly 9, 9-Bis-(6-bromohexyl)-9H-fluorene (PF-Br): Anhydrous ferric chloride ($FeCl_3$) (1.30g, 8.12 mmol) and 9, 9-Bis-(6-bromohexyl)-9H-fluorene (2.0 g, 4.06 mmol) were dissolved in 15 mL nitrobenzene in a 100 mL three-necked round-bottom flask equipped with a nitrogen inlet. The reaction mixture was stirred at room temperature for 36 hours, followed by precipitation from methanol. The resulting polymer, poly 9, 9-Bis-(6-bromohexyl)-9H-fluorene was precipitated in methanol again and again to remove excess 9, 9-Bis-(6-bromohexyl)-9H-fluorene. Solvent was evaporated in rotary evaporator and dried under reduced vacuum to obtain 1.3 g (65%) Poly 9, 9-Bis-(6-bromohexyl)-9H-fluorene (PF-Br) as dark brown powder. The polymer was characterised using ^{1}H NMR spectroscopy.

^{1}H NMR (600 MHz, CDCl3), δ (ppm): 7.86 (bp), 7.7 (bp), 7.3 (bp), 3.30 (bp), 2.1 (bp), 2.08 (bp), 1.6 (bp), 1.27 (bp), 0.83 (bp). Bp: broad peak

PF-IS: To synthesize PFIS, PF-Br (0.1 g, 0.203 mmol), Isatin (0.14 g, 1.01 mmol) and K_2CO_3 (0.28 g, 2.03mmol) were dissolved in 20 mL dry DMF and refluxed for 48 hours in a 50 mL round bottom flask. Organic layer was extracted in chloroform and washed with water to remove potassium carbonate. Then the solvent was removed through a rotavapor and dried under a high vacuum and then precipitated from methanol to remove excess isatin and obtain the final polymer (57 mg,~60%).

^{1}H NMR (600 MHz, CDCl3), δ (ppm): 0.8-0.9 (-CH2), 1.17-1.28 (-CH2), 1.52-1.6 (CH2), 2.0-2.1 (-CH2), 3.5 (-CH2-N), 6.7 (ArH), 7.0(ArH), 7.5 (ArH) 7.65 (ArH), 7.82(ArH).

^{13}C NMR (150 MHz, CDCl3), δ (ppm): 183.7, 158.0, 151.1, 138.5, 125.5, 124.1, 117.4, 110.3, 76.7, 40.4, 29.7, 27.0, 27.6. ArH: Aromatic Hydrogen

3.5.9. Toxicity Assay:

The MTT assay is a colorimetric assay for assessing cytotoxic activities of a medicinal compound. NAD(P)H-dependent cellular oxidoreductase enzymes usually reflect the number of viable cells present under defined conditions. Such enzymes reduce the tetrazolium dye MTT 3-(4,5-dimethylthiazol-2-yl)-2,5-diphenyltetrazolium bromide to its insoluble formazan, which has a purple color.

3-(4,5-dimethylthiazol-2-yl)-2,5-diphenyl tetrazolium bromide (MTT) is a yellow dye, is reduced to purple formazan in live cells. A solubilization solution (usually either dimethyl sulfoxide, an acidified ethanol solution, or a solution of the detergent sodium dodecyl sulfate in diluted hydrochloric acid) is added to dissolve the insoluble purple formazan product into a colored solution. The absorbance of this colored solution can be quantified by measuring at a certain wavelength (usually 570 nm) by a UV-Vis spectrophotometer. The degree of light absorption is dependent on the degree of formazan concentration accumulated inside the cell and on the cell surface. In our experiment, we performed MMT experiment using following protocol.

Cell culture: SH-SY-5Y cells is a neuroblastoma cell line derived from human bone marrow. SH-SY-5Y cells were cultured in complete growth media, Dulbecco's Modified Eagle Medium (DMEM, HiMedia) with 10% fetal bovine serum (Gibco) and antibiotics (Anti-Anti, Gibco) at 37 °C in 5% CO_2 incubator. Cell line used in this study were gifted by National centre for cell science (NCCS), Pune.

SH-SY-5Y cells were seeded into 96-well plates at an initial seeding density of 1,00,000 cells/well in 100 µl medium. The cells were cultured for 24 h at 37 °C in 5% CO_2. Then, cells of each well were treated with variable concentration of GNP-NMDA ranging from 0-1.25 nM in a concentration range 0-50 µM in 100 µl serum free media. After incubation for 24 h, the 3-(4, 5-dimethylthiazol-2yl)-2, 5-diphenyltetrazolium bromide (MTT) solution (10 µl, 5 mg/mL in PBS) was added to each well. Plate is further incubated for 3 hours at 37 °C in 5% CO_2, wrapped in aluminum foil. After incubation, MTT-containing medium was replaced by 100 µl Dimethyl Sulfoxide (DMSO) to solubilize MTT-formazan crystals. After incubation for 5 min at 37 °C, absorbance was measured at 570 nm and reference reading at 690 nm was recorded in ELISA microplate reader (Infinite 200 PRO, TECAN). Each of the samples was repeated with 3 replicates. The results were normalized by setting the cell viability of SH-SY-5Y cells in PBS buffer control to be 100%.

3.6. Reference:

(1) Taylor, J. P.; Hardy, J.; Fischbeck, K. H. Biomedicine - toxic proteins in neurodegenerative disease. *Science* **2002**, *296*, 1991-1995.

(2) Sacchettini, J. C.; Kelly, J. W. Therapeutic strategies for human amyloid diseases. *Nat. Rev. Drug Discov.* **2002**, *1*, 267-275.

(3) Holtzman, D. M.; Morris, J. C.; Goate, A. M. Alzheimer's disease: The challenge of the second century. *Sci Transl Med* **2011**, *3*.

(4) Lesne, S.; Koh, M. T.; Kotilinek, L.; Kayed, R.; Glabe, C. G.; Yang, A.; Gallagher, M.; Ashe, K. H. A specific amyloid-beta protein assembly in the brain impairs memory. *Nature* **2006**, *440*, 352-357.

(5) Bucciantini, M.; Giannoni, E.; Chiti, F.; Baroni, F.; Formigli, L.; Zurdo, J. S.; Taddei, N.; Ramponi, G.; Dobson, C. M.; Stefani, M. Inherent toxicity of aggregates implies a common mechanism for protein misfolding diseases. *Nature* **2002**, *416*, 507-511.

(6) Kayed, R.; Head, E.; Thompson, J. L.; McIntire, T. M.; Milton, S. C.; Cotman, C. W.; Glabe, C. G. Common structure of soluble amyloid oligomers implies common mechanism of pathogenesis. *Science* **2003**, *300*, 486-489.

(7) Walsh, D. M.; Klyubin, I.; Fadeeva, J. V.; Cullen, W. K.; Anwyl, R.; Wolfe, M. S.; Rowan, M. J.; Selkoe, D. J. Naturally secreted oligomers of amyloid beta protein potently inhibit hippocampal long-term potentiation in vivo. *Nature* **2002**, *416*, 535-539.

(8) Lorenzo, A.; Yankner, B. A. Beta-amyloid neurotoxicity requires fibril formation and is inhibited by congo red. *Proc. Natl. Acad. Sci. U. S. A.* **1994**, *91*, 12243-12247.

(9) Terry, R. D.; Masliah, E.; Salmon, D. P.; Butters, N.; Deteresa, R.; Hill, R.; Hansen, L. A.; Katzman, R. Physical basis of cognitive alterations in Alzheimer's disease synapse loss is the major correlate of cognitive impairment. *Ann. Neurol.* **1991**, *30*, 572-580.

(10) Dickson, D. W.; Crystal, H. A.; Bevona, C.; Honer, W.; Vincent, I.; Davies, P. Correlations of synaptic and pathological markers with cognition of the elderly. *neurobiol. Aging*. **1995**, *16*, 285-298.

(11) Delaere, P.; Duyckaerts, C.; Masters, C.; Beyreuther, K.; Piette, F.; Hauw, J. J. Large amounts of neocortical beta-a4 deposits without neuritic plaques nor tangles in a psychometrically assessed, nondemented person. *Neurosci. Lett.* **1990**, *116*, 87-93.

(12) Tomiyama, T.; Matsuyama, S.; Iso, H.; Umeda, T.; Takuma, H.; Ohnishi, K.; Ishibashi, K.; Teraoka, R.; Sakama, N.; Yamashita, T.; Nishitsuji, K.; Ito, K.; Shimada, H.; Lambert, M. P.; Klein, W. L.; Mori, H. A mouse model of amyloid beta oligomers: Their contribution to synaptic alteration, abnormal tau phosphorylation, glial activation, and neuronal loss in vivo. *J. Neurosci.* **2010**, *30*, 4845-4856.

(13) Knowles, T. P. J.; Waudby, C. A.; Devlin, G. L.; Cohen, S. I. A.; Aguzzi, A.; Vendruscolo, M.; Terentjev, E. M.; Welland, M. E.; Dobson, C. M. An analytical solution to the kinetics of breakable filament assembly. *Science* **2009**, *326*, 1533-1537.

(14) Cremades, N.; Cohen, S. I. A.; Deas, E.; Abramov, A. Y.; Chen, A. Y.; Orte, A.; Sandal, M.; Clarke, R. W.; Dunne, P.; Aprile, F. A.; Bertoncini, C. W.; Wood, N. W.; Knowles, T. P. J.; Dobson, C. M.; Klenerman, D. Direct observation of the interconversion of normal and toxic forms of alpha-synuclein. *Cell* **2012**, *149*, 1048-1059.

(15) Sear, R. P. Nucleation: theory and applications to protein solutions and colloidal suspensions. *J Phys. Condens. Mat.* **2007**, *19*, 033131.

(16) Tornquist, M.; Michaels, T. C. T.; Sanagavarapu, K.; Yang, X.; Meisl, G.; Cohen, S. I. A.; Knowles, T. P. J.; Linse, S. Secondary nucleation in amyloid formation. *Chem. Commun.* **2018**, *54*, 8667-8684.

(17) Cohen, S. I. A.; Cukalevski, R.; Michaels, T. C. T.; Saric, A.; Tornquist, M.; Vendruscolo, M.; Dobson, C. M.; Buell, A. K.; Knowles, T. P. J.; Linse, S. Distinct thermodynamic signatures of oligomer generation in the aggregation of the amyloid-beta peptide. *Nat. Chem.* **2018**, *10*, 523-531.

(18) Cohen, S. I. A.; Linse, S.; Luheshi, L. M.; Hellstrand, E.; White, D. A.; Rajah, L.; Otzen, D. E.; Vendruscolo, M.; Dobson, C. M.; Knowles, T. P. J. Proliferation of amyloid-beta 42 aggregates occurs through a secondary nucleation mechanism. *Proc. Natl. Acad. Sci. U. S. A.* **2013**, *110*, 9758-9763.

(19) Jana, M. K.; Cappai, R.; Pham, C. L. L.; Ciccotosto, G. D. Membrane bound tetramer and trimer A beta oligomeric species correlate with toxicity towards cultured neurons. *J. Neurochem.* **2016**, *136*, 594-608.

(20) Andreani, A.; Burnelli, S.; Granaiola, M.; Leoni, A.; Locatelli, A.; Morigi, R.; Rambaldi, M.; Varoli, L.; Cremonini, M. A.; Placucci, G.; Cervellati, R.; Greco, E. New isatin derivatives with antioxidant activity. *Eur. J. Med. Chem.* **2010**, *45*, 1374-1378.

(21) Clarkson, C.; Smith, P. J.; Lehman, J.; Gut, J.; Rosenthal, P. J.; Chibale, K. Design, synthesis and anti-plasmodial evaluation in vitro of new 4-aminoquinoline isatin derivatives. *Bioorg. Med. Chem.* **2005**, *13*, 3249-3261.

(22) Varun; S.; Kakkar, R. Isatin and its derivatives: a survey of recent syntheses, reactions, and applications. *Med. chem. commun.* **2019**, *10*, 351-368.

(23) Chowdhury, S. R.; Agarwal, M.; Meher, N.; Muthuraj, B.; Iyer, P. K. Modulation of amyloid aggregates into nontoxic coaggregates by hydroxyquinoline appended polyfluorene. *ACS Appl. Mater. Interfaces* **2016**, *8*, 13309-13319.

(24) Mondal, S.; Chowdhury, S. R.; Shah, M.; Kumar, V.; Kumar, S.; Iyer, P. K. Nanoparticle assisted regulation of nucleation pathway of amyloid tetramer and inhibition of their fibrillation kinetics. *ACS Appl. Bio Mater.* **2019**. *2*, 2137-2142.

(25) Zandomeneghi, G.; Krebs, M. R. H.; Mccammon, M. G.; Fandrich, M. FT-IR reveals structural differences between native beta-sheet proteins and amyloid fibrils. *Protein Sci.* **2004**, *13*, 3314-3321.

(26) Holzwarth, G.; Doty, P. The Ultraviolet circular dichroism of polypeptides. *J. Am. Chem. Soc.* **1665**, *87*, 218-228.

(27) Schellman, J. A.; Oriel, P. Origin of the cotton effect of helical polypeptides. *J. Chem. Phys.* **1962**, *37*, 2114-2124.

(28) Woody, R. W. Optical rotation of oriented helices: Calculation of the rotatory dispersion and circular dichroism of the alpha helix. *J. Chem. Phys.* **1967**, *46*, 4927-4945.

(29) Moffitt, W. Optical rotatory dispersion of helical polymers. *J. Chem. Phys.* **1956**, *25*, 467-478.

(30) Tinoco, I. J.; Woody, R. W. Absorption and rotation of light by helical polymers: the effect of chain length. *J. Chem. Phys.* **1963**, *38*, 1317-1325.

(31) Li, L. K.; Spector, A. Circular dichroism of beta-poly-l-lysine. *J. Am. Chem. Soc.* **1969**, *91*, 220-222.

(32) Nakamura, T.; Shoji, M.; Harigaya, Y.; Watanabe, M.; Hosoda, K.; Cheung, T. T.; Shaffer, L. M.; Golde, T. E.; Younkin, L. H.; Younkin, S. G.; Hirai, S. Amyloid beta protein levels in cerebrospinal fluid are elevated in early onset Alzheimers disease. *Ann. Neurol.* **1994**, *36*, 903-911.

(33) Maruyama, M.; Arai, H.; Tanji, H.; Higuchi, M.; Okamura, N.; Matsui, T.; Sasaki, H.; Sugita, M.; Yoshida, H.; Matsushita, S.; Higuchi, S. Cerebrospinal fluid amyloid beta (1-42) levels in the mild cognitive impairment stage of Alzheimer's disease. *Neurobiol. Aging*. **2002**, *23*, S379-S380.

(34) Tornquist, M.; Michaels, T. C. T.; Sanagavarapu, K.; Yang, X. T.; Meisl, G.; Cohen, S. I. A.; Knowles, T. P. J.; Linse, S. Secondary nucleation in amyloid formation. *Chem. Commun*. **2018**, *54*, 8667-8684.

Appendix B: Additional Data for Chapter 3

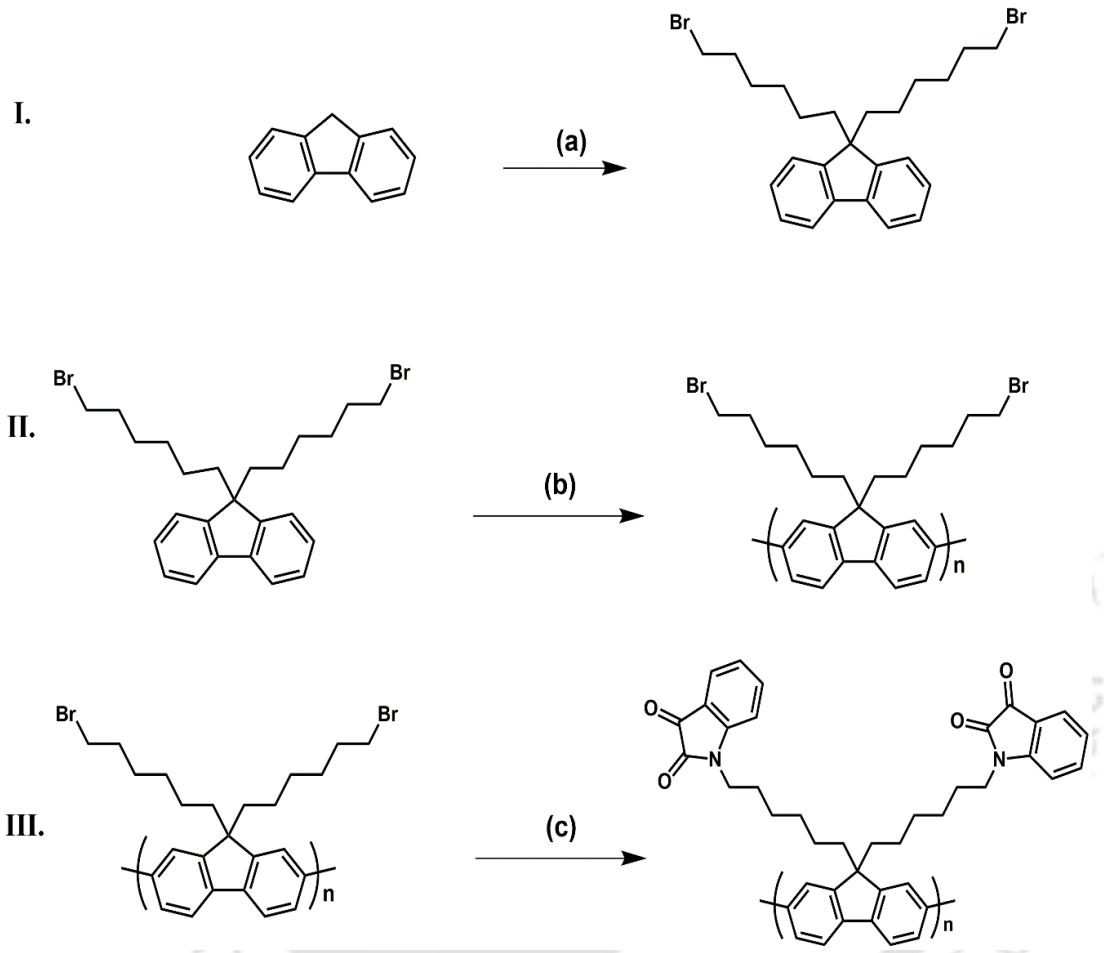

***Figure B-1**: Synthetic scheme of PFIS.*

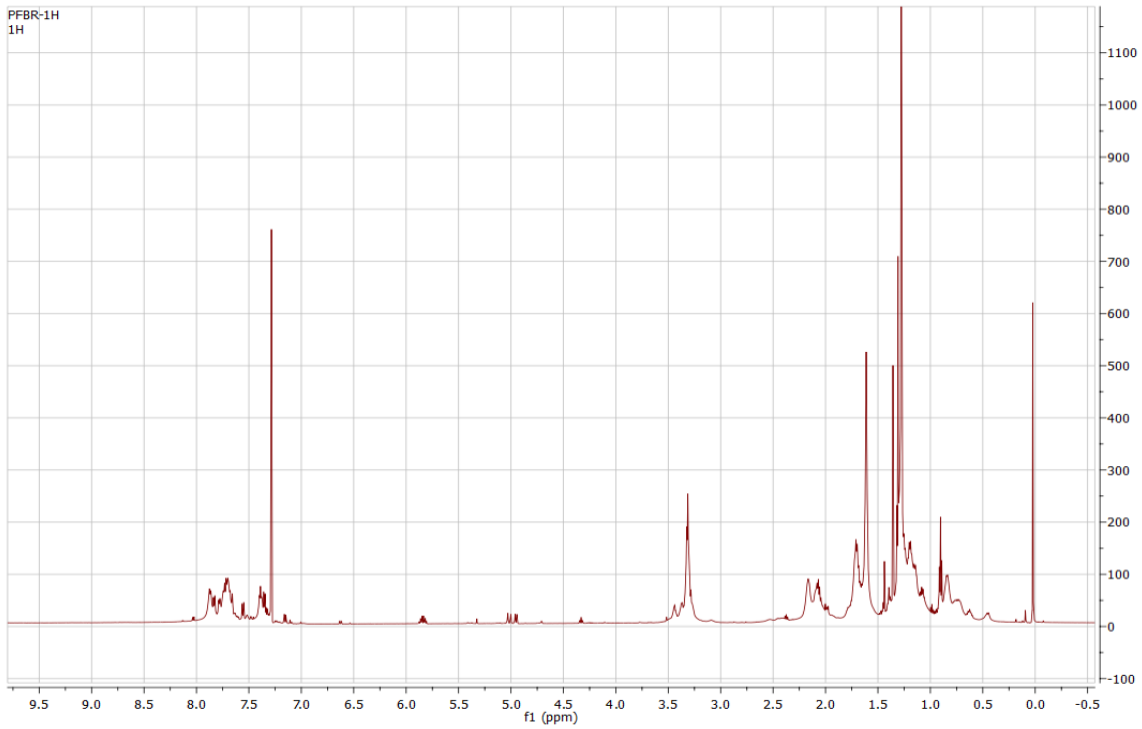

***Figure B-2**: ¹H NMR spectra of PF-Br.*

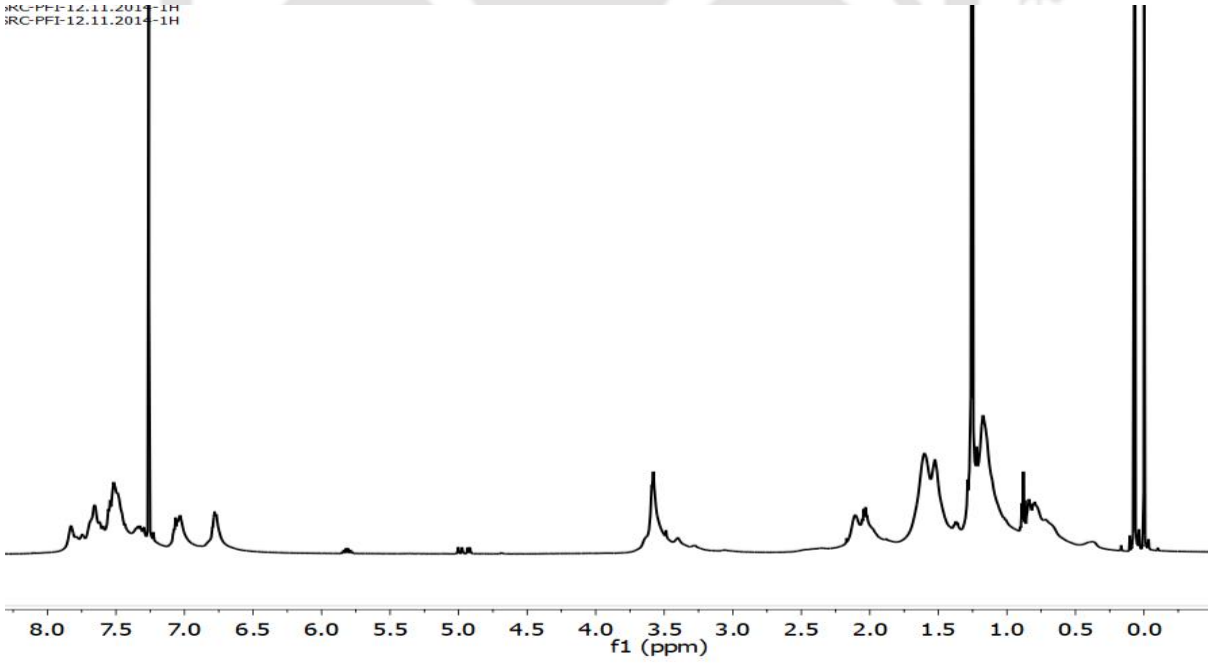

***Figure B-3**: ¹H NMR of PFIS.*

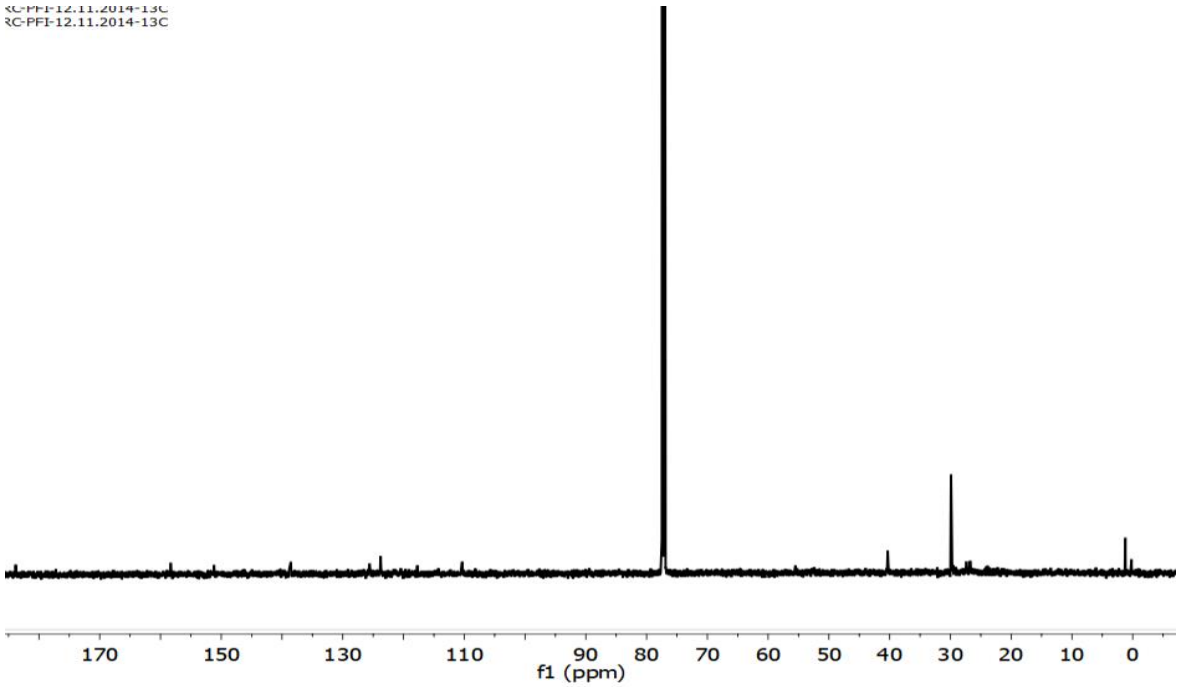

***Figure B-4**: [13]C NMR of PFIS.*

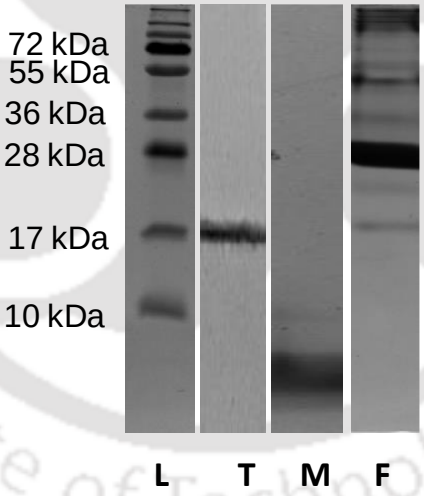

***Figure B-5**: A) Characterization of amyloid tetramer by electrophoresis experiment: ladder (L), amyloid tetramer (T), mixture of monomer and dimer of amyloid beta40 (M), mixture of HMW oligomer and fibrils (F) respectively from left.*

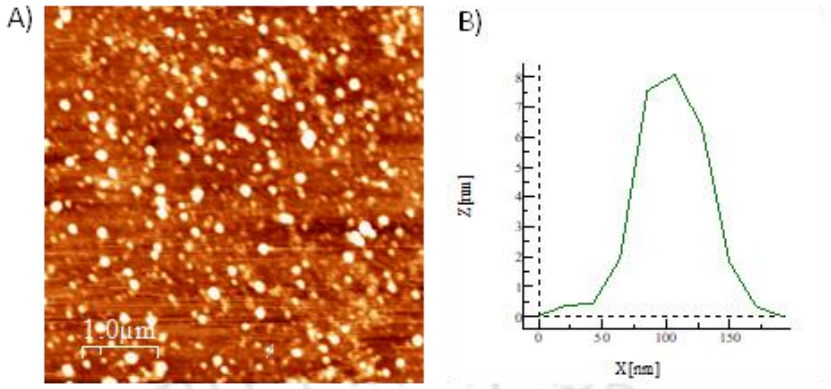

***Figure B-6**: A) AFM image of amyloid tetramer, B) Height profile of Amyloid tetramer.*

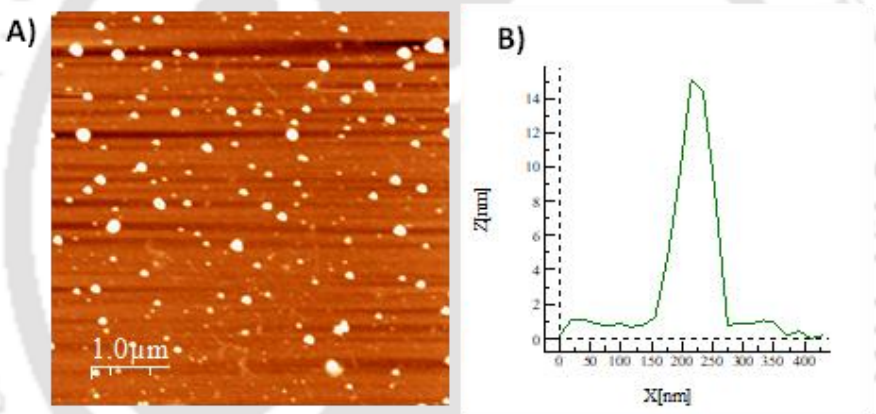

***Figure B-7:** A) AFM image of PFIS nanoparticle in water B) Height profile of PFIS nanoparticle.*

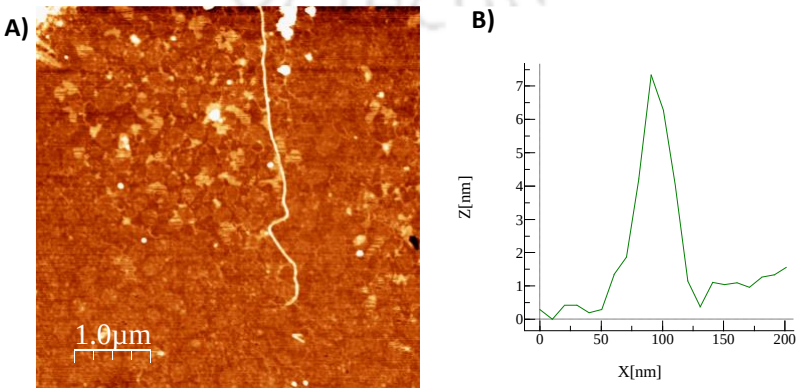

Figure B-8: A) AFM image of Amyloid fibrils, B) height profile of amyloid fibrils.

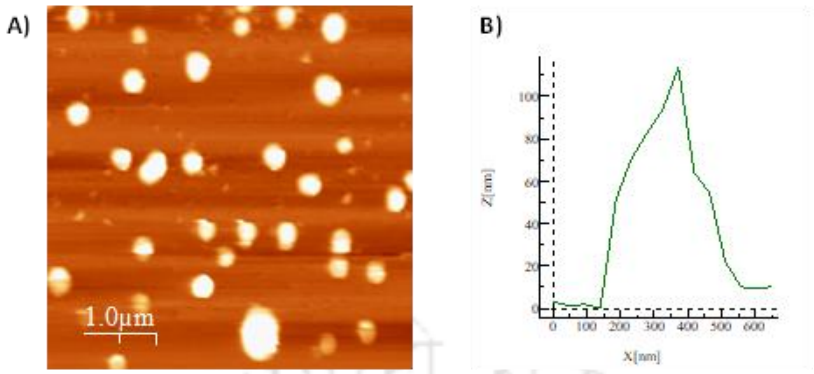

***Figure B-9**: A) AFM image of Amyloid-polymer co-aggregate B) height profile of amyloid-polymer co-aggregate.*

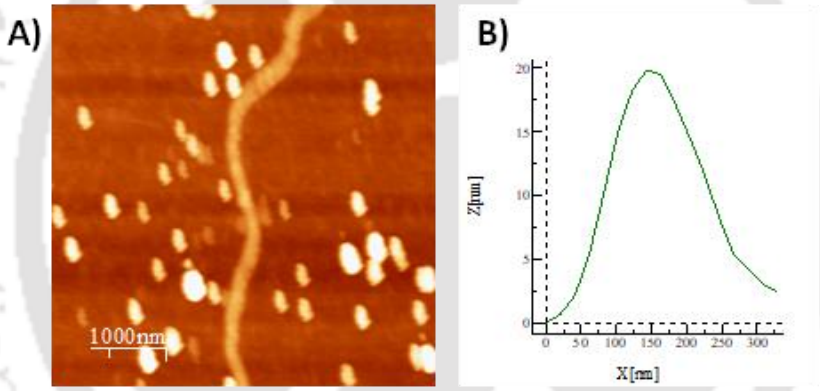

***Figure B-10**: AFM image of CSF fibrils B) Height profile of CSF fibril.*

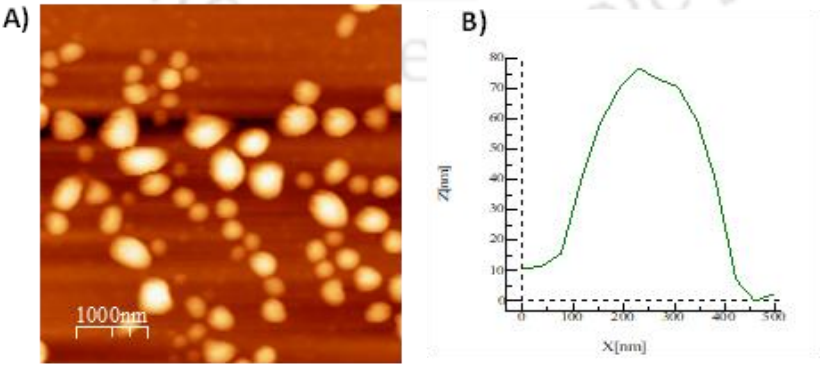

***Figure B-11**: A) AFM image of CSF-polymer co-aggregates B) Height profile of CSF-polymer co-aggregates.*

4

Amyloid Targeting 'Artificial Chaperone' Impairs Oligomer Mediated Neuronal Damage and Mitochondrial Dysfunction Associated with Alzheimer Disease

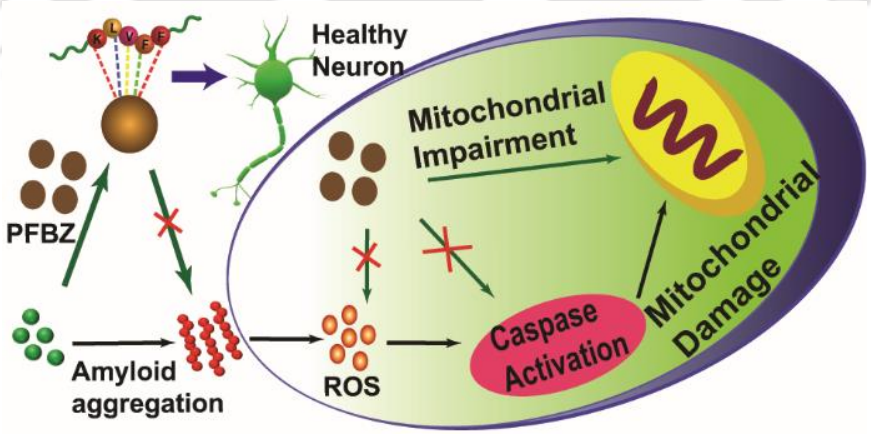

1. **Mondal, S**.; Vashi, Y.; Ghosh, P.; Borthakur, M.; Kumar, S.; Iyer, P. K.* Amyloid targeting "artificial chaperone" impairs oligomer mediated neuronal damage and mitochondrial dysfunction associated with Alzheimer's disease**.** *ACS Chem. Neurosci.* **2020**, *11*, 3277–3287.

4

Amyloid Targeting 'Artificial Chaperone' Impairs Oligomer Mediated Neuronal Damage and Mitochondrial Dysfunction Associated with Alzheimer Disease

Abstract:

Alzheimer's Disease (AD) is an irreversible memory disorder associated with bundles of neuropathological events including amyloid aggregation that triggers oxidative stress and mitochondrial dysfunction in humans. Herein, a new artificial chaperone PFBZ is reported to efficiently sequester toxic amyloid beta (Aβ) by binding at their 'Amyloidogenic do-main (Aβ16-21)' with unprecedented selectivity and impair amyloid mediated neuronal damage in a high throughput wild type (WT) mouse model. An accurate dose of PFBZ chaperone successfully attenuated amyloid triggered internal hemorrhage and pyknosis in cerebral cortex of WT mouse. The structural advantage of the polymer results in efficient Cu(II) chelation arresting a redox cycle to prevent ROS generation and protect mitochondria from ROS mediated damage. This was further evidenced by caspase activation and mitochondrial membrane potential (MMP) biomarkers and was complemented by brain histology and electron microscopy data which revealed that PFBZ chaperone gave a protective coating over amyloid surface and resists it from interacting with cell membrane and prevent inducing toxicity. This conjugated polymer artificial

chaperone based nano drug showed exceptional properties such as its multipotent and highly biocompatible nature, first of its kind specific amyloid (Aβ16-21) targeting behavior, bioimaging and BBB permeability with a potential to suppress amyloid triggered neurotoxicity implicated in numerous human disorders through a rare synergistic mechanism.

4.1. Introduction:

A wide range of human diseases develop due to failure of a specific peptide or protein to adopt or remain in its native conformational state. The pathological disorders are broadly referred to as Protein Misfolding Diseases.[1] Among them, Alzheimer's Disease (AD) is the most prevalent form of dementia which results in neuronal damage, synaptic dysfunction and progressive memory decline in humans.[2-3] Substantial data extracted from biochemical experiments, genetics and animal model studies indicate that extracellular fibrillary aggregates originating from self-aggregation of a peptide, namely amyloid beta (Aβ) plays a pivotal role in AD.[4-5] According to amyloid cascade hypothesis, dysregulation of amyloid homeostasis in AD brain results in enhanced amount of Aβ aggregates which initiates a series of events that finally leads to neuronal damage manifesting clinical dementia.[6-9] Although, precise biochemical mechanism leading to amyloid triggered neurotoxicity is poorly understood, the role of re-active oxygen species (ROS) and reactive nitrogen species (RNS) has been strongly implicated. Usually, Aβ oligomers in presence of redox active metals (like Cu^{2+}), undergo Fenton type reaction to produce ROS which results in oxidative damage in neuro cells.[10-14] Mitochondria are the easy targets of such ROS and their enhanced level usually leads to mitochondrial dysfunction.[15] In addition, interaction of toxic Aβ aggregates with several mitochondrial proteins and enzymes like alcohol dehydrogenase, ATP synthase and cyclophilin-D play a crucial role in mitochondrial dysfunction.[16-18] Aβ oligomer while interacting with such biological entities activates caspase-3 and triggers mitochondria induced neuronal apoptosis. Recent research reveals that mitochondrial dysfunction is one of the most important signatures of AD in early stage.[19] Therefore, due to the multiple factors being involved in AD aetiology, a specific multi-targeted therapeutic strategy has to be adopted that can inhibit Aβ oligomerisation, mitigate neuronal damage caused by multiple factors including mitochondrial dysfunctions, ROS production, caspase-3 activation, and many more. In the past few decades, therapeutic materials targeting solely Aβ have been developed.[20-24]

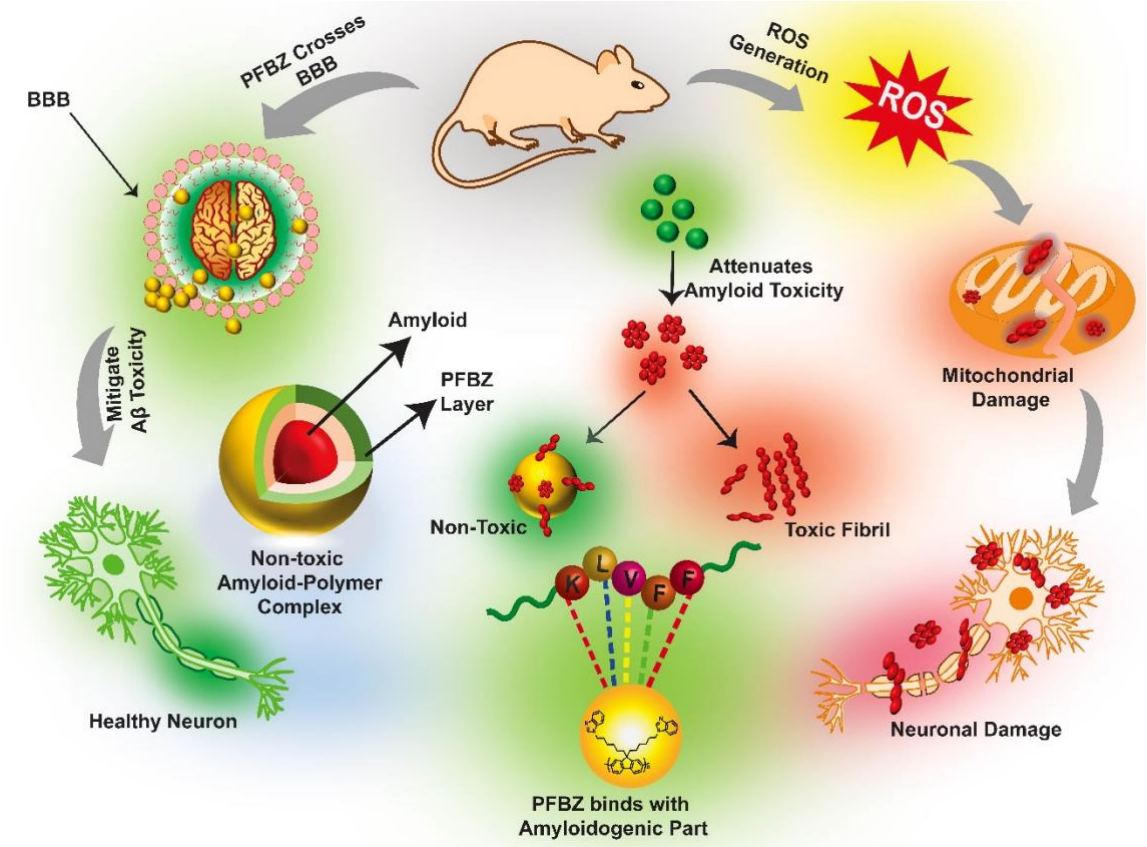

Scheme 4.1: *Manifestation of Amyloid mediated neuronal damage and neuroprotection by PFBZ. Schematic presentation of Binding of PFBZ with the 'Amyloidogenic Domain' in Aβ and possible mechanism associated with mitigation of amyloid triggered neurotoxicity.*

However, most of those single targeted drugs have proven to be inadequate and failed during different stages of clinical trials suggesting a multi-targeted drug approach to address multifactorial toxicity involved in AD to be the best option.[25-26] These limitations in single targeted drugs prompted us to systematically investigate the various biochemical events triggered by Aβ40 oligomers leading ultimately to mitochondrial dysfunction and neuronal damage in wild type (WT) mice. We also report for the first time the specific design of an amyloid targeting polymeric chaperone (PFBZ) that can mitigate Aβ triggered neurotoxicity through regulation of ROS production, caspase activation, and mitochondrial dysfunction (Scheme 4.1). Comprehensive studies in a WT mouse model revealed that Aβ oligomer is responsible for neuronal damages including internal haemorrhage in cerebral cortex of WT mice. However, on application of accurate dose of chaperone PFBZ, the damages were successfully recovered, which is a clinically vital observation. These studies reveal that PFBZ alleviates the progress of AD through a synergistic mechanism and possesses multipotent anti-AD drug characteristics. Thus, PFBZ chaperone offers a new

design strategy for fulfilling the elusive multitargeted approach for the development of anti-AD drugs.

4.2 Results

Aβ16–21 is the central fibril forming core and is known as the "amyloidogenic domain" of Aβ40.[30–33] Hence, it is required to safeguard such segments in order to avoid unwanted amyloid aggregation. With this vital knowledge, a new artificial chaperone PFBZ was strategically designed that selectively targets the 'amyloidogenic domain' (Aβ16–21) of Aβ and thereby blocks the aggregation process (Figure 4.1a-b). Detailed quantification of the chaperone-like activity reveals that Aβ16–21 binds with PFBZ in 4:1 ratio with maximum binding constant (K) 2.72 × 105 M^{-1}, enthalpy change (ΔH) is -4.321×10^4 cal/mol, and Gibbs free energy change (ΔG) is −8940 J (Figure 4.1c). At physiological conditions (pH 7.4, 37 °C), PFBZ exhibits a positive zeta potential (+2.94 mV), which on interaction with negatively charged Aβ16–21(−2.61 mV) and Aβ40 (−3.82 mV) markedly elevated up to −0.314 mV, indicating adsorption of anionic Aβ on to the surface of PFBZ (Figure 4.1d). As a result, the high affinity of PFBZ for Aβ can be attributed mainly to the electrostatic interaction among them. Furthermore, the ITC experiment involving Aβ40 (100 μM and PFBZ (10 μM) was performed to explore the interaction between them. The Kd values are almost similar in both the cases. In case of PFBZ + Aβ40 binding, $K_d = 4.39 \times 10^4$ M^{-1} (Figure C1), while in case of PFBZ + Aβ16–21, Kd = 2.72 × 105 M^{-1}. The stoichiometry of PFBZ + Aβ40 binding is 3:1 which is distinct from PFBZ + Aβ16–21 binding (stoichiometry: 4:1). Further, interaction of Aβ with PFBZ was monitored through time-dependent emission of PFBZ, which on incubation gradually increased up to 1.5-fold up to 24 h and reduced thereafter (Figure 4.1e and Figure C2). The variation in PFBZ fluorescence intensity can be attributed to the time-dependent alteration of zeta potential of the amyloid oligomers. In our previous work, it has been reported that on incubation with amyloid oligomers, the probe intensity increases gradually up to 24 h.[32] In another report, the zeta potential of amyloid oligomers variation during the course of fibrillation reaction was shown.[20] It has been observed that the zeta potential of the oligomers shows a negative zeta potential, which decreases up to 24 h and attains a maximum negative value at 24 h. Hence, the interaction between PFBZ (+2.94 mV) and amyloid oligomers also increases with time up to 24 h. Consequently, the emission intensity of the PFBZ also increases and attains a maximum value at 24 h and decreases thereafter. The hydrodynamic diameter of the Aβ monomers increased gradually from 5.6 to 5560 nm, indicating the formation of micrometer long fibrillar

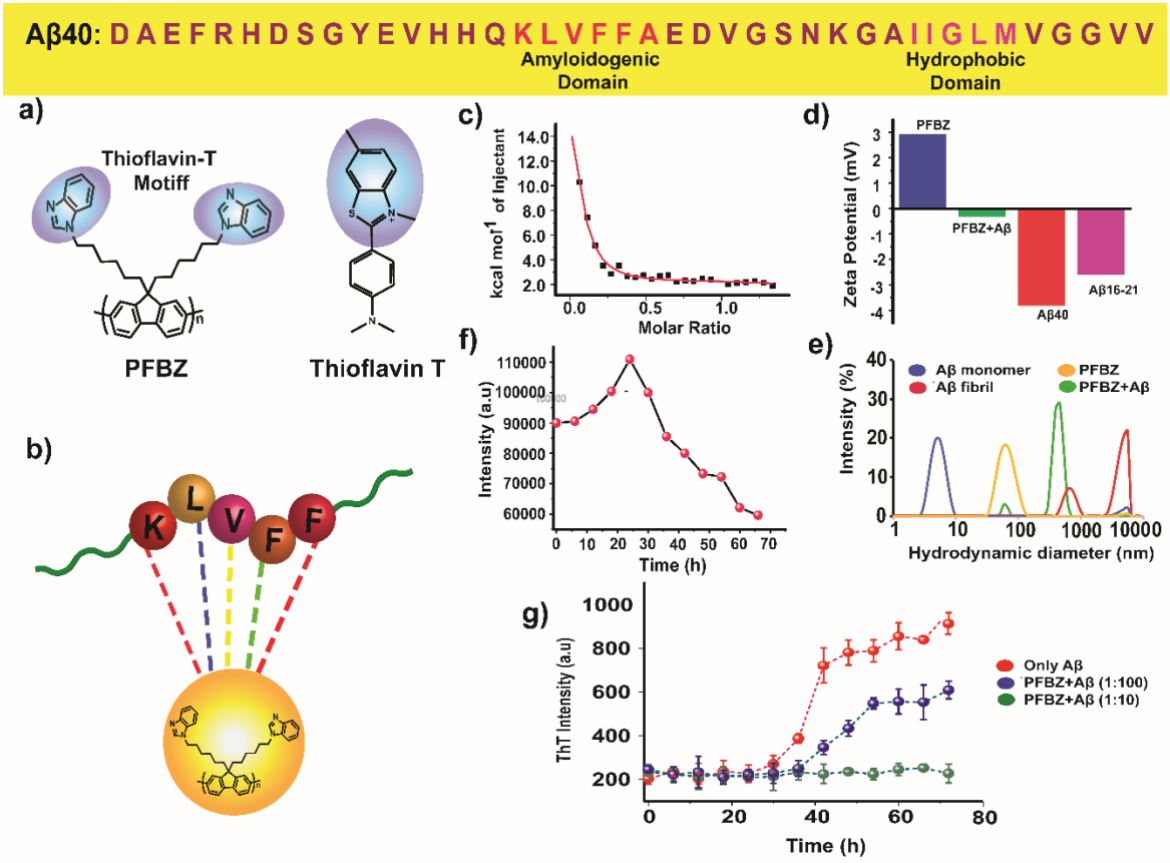

Figure 4.1: *a) chemical structure of artificial chaperon PFBZ and Thioflavin-T. b) schematic representation of PFBZ binding with amyloidogenic domain of Aβ40. c) ITC fitting data for the titration of Aβ16-21(100 μM) with PFBZ (10 μM). d) Zeta potential of PFBZ, PFBZ- Aβ40 co-aggregate, Aβ and Aβ16-21 at pH 7.0 (10 mM PBS buffer). e) Time dependent Fluorescence spectra of PFBZ (10 μM) incubated with Aβ40 (10 μM, wavelength: 360 nm). f) DLS measurement: Hydrodynamic diameter of Aβ40 before and after fibrillation in presence and in absence of PFBZ. Aβ40 fibril and Aβ40+PFBZ co-aggregate was made by incubating for 96 hours. g) Fibrillation kinetics of Aβ40 (10 μM) in presence and in absence of PFBZ in 10 mM phosphate buffered saline for 96 hours in 37 °C. The fibrillation kinetics of Aβ40 was measured by ThT binding assay. Data are presented as mean ± S D, n=3.*

.

Aβ (Figure 4.1f). However, the PFBZ chaperone inhibited the fibrillation by forming stable coaggregates with hydrodynamic diameter 450 nm. The effect of the artificial chaperone on Aβ fibrillation was further monitored through a Thioflavin-T assay (Figure 4.1g). Aβ (10 μM, pH 7.0, 37 °C, 96h) fibrillation kinetics follows a typical nucleation growth model consisting of three distinct phase: lag phase, elongation phase, and saturation phase. The saturation in ThT intensity after 42 h indicates a maximum formation of amyloid fibrils.

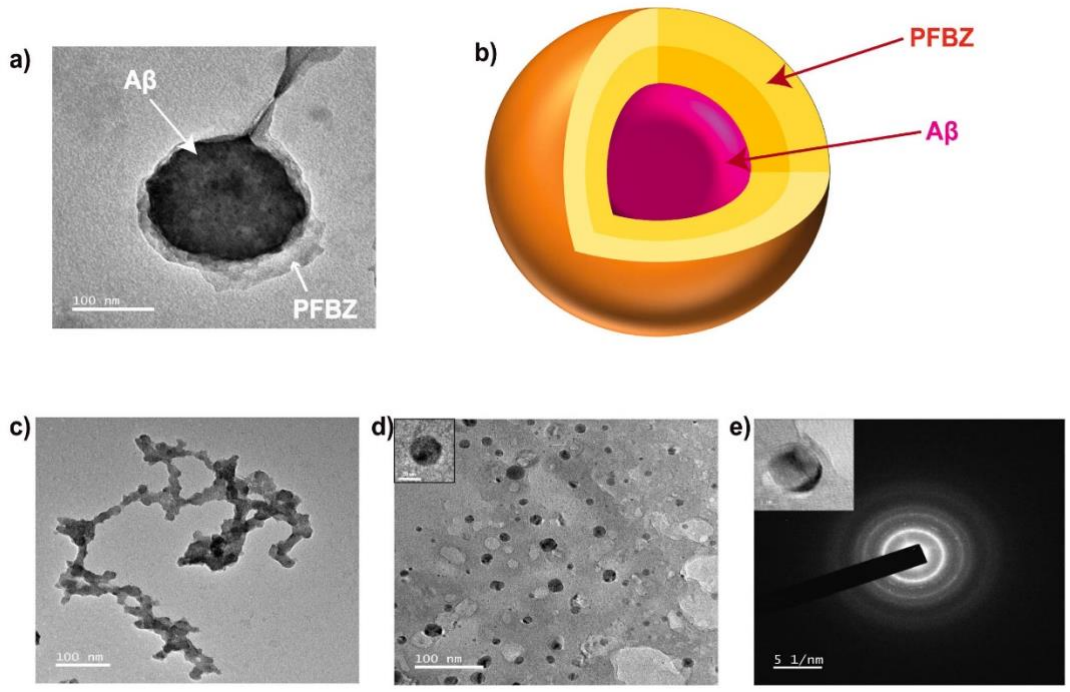

Figure 4.2: *a) TEM images of Aβ40-PFBZ co-aggregate. 10 μM Aβ40 was incubated with 1 μM PFBZ chaperone for 96 hours in 10 mM phosphate buffered saline in 37 ºC. b) schematic representation of Aβ-PFBZ co-aggregate. PFBZ corona has been shown on Aβ layer. c) TEM image of Aβ40 fibrils. d) TEM images of artificial chaperon PFBZ (inset image shows one single PFBZ nano dot). e) SAED pattern of Aβ40-PFBZ co-aggregate. TEM image Scale bar is 100 nm.*

However, in the presence of even a substoichiometric concentration (1:0.01) of the molecular chaperone PFBZ, aggregation propensity was markedly suppressed. On increasing PFBZ concentration (1:0.1), no enhancement in ThT signal was detected, indicating complete inhibition of Aβ fibrillation. The dose-dependent inhibition is mainly due to the high electrostatic interaction which leads to the formation of a stable Aβ-PFBZ cluster that was observed clearly under transmission electron microscopy (TEM) (Figure 4.2a). A core–shell particle-type morphology was observed where the PFBZ chaperone lies above the Aβ layer. As confirmed from ITC, PFBZ interacts with Aβ40 by binding at the Aβ16–21 fragment irrespective of its conformation. The mentioned experiments also indicate that the binding is instantaneous. Hence, PFBZ binds with Aβ40 monomers immediately when PFBZ is mixed with it, and consequently, Aβ40 does not get enough time to convert into an oligomeric form. However, in the of PFBZ chaperone, Aβ monomers (size ~5 nm; Figure C3a) undergo self-aggregation to form micrometer long mature fibrils (Figure 4.2c).

The PFBZ chaperone forms nanodots (size 9.04 ± 1.58 nm) in aqueous media mainly through hydrophobic interaction (Figure 4.2d) which, on incubation with Aβ for

96h, forms larger coaggregates (Figure 4.2a). Intriguingly, the relative crystallinity of coaggregates observed using a SAED pattern was further used to identify the position of Aβ and PFBZ layers in the cluster. Surprisingly, the PFBZ-amyloid coaggregates attain a higher crystallinity than the monomeric and fibrillar amyloids (Figure 4.2e and Figure C3b-c). Since none of the amyloid monomers or fibers are crystalline, the crystallinity of PFBZ-amyloid coaggregates can only arise if the PFBZ layer resides above the amyloid layer. Furthermore, the preformed mature Aβ fibril was prepared by incubating monomeric Aβ (10 μM, pH 7.0, 37 °C, 7 days) in physiological conditions (Figure C3d). When the PFBZ chaperone (1 μM, pH 7.0, 37 °C) was allowed to interact for 10 days at 37 °C with mature Aβ fibrils, PFBZ was able to disintegrate long mature amyloid fibrils (known to disrupt cell membranes and exert neurotoxicity) into shorter fibrils (Figure C3e-f).[34] However, the control experiment, that is, incubation (pH 7.0, 37 °C) of preformed mature amyloid fibrils (10 μM) for 10 days, yielded no major visible change in fibril morphology and size (Figure C3g). The effect of PFBZ on seeded proliferation of Aβ aggregation was explored by ThT assay. An Aβ (10 μM, pH 7.0, 37 °C, 96 h) monomer in the presence of a catalytic amount of preformed oligomer (seed) was incubated for 96 h. A similar experiment consisting of an Aβ (10 μM, pH 7.0, 37 °C) monomer in the presence of preformed oligomer and 10 μM PFBZ was performed to explore the inhibition tendency of PFBZ toward seeded aggregation (Figure C4). It was observed that a lag phase appeared very fast (<6 h). However, no enhancement in ThT intensity in the presence of PFBZ was observed. It is evident that PFBZ could successfully suppress seeded aggregation. The biophysical experiments reveal that the artificial chaperone PFBZ disintegrates mature amyloid fibrils and wraps around the Aβ, inhibiting these Aβ40 aggregates from interacting with cell membranes, thereby reducing their cytotoxicity. Utilizing this artificial chaperone PFBZ, we observed for the first time the detoxification of Aβ oligomer via a unique process of protective coating of artificial chaperone over it. We envision this unconventional approach to have a great significance in eradicating amyloid neurotoxicity in the future. The in vitro cytotoxicity of PFBZ chaperone and Aβ40 aggregates was explored via MTT assay. Cell viability of native PFBZ chaperone in variable concentrations (0.19–100 μM) was evaluated in both human neuroblastoma (SH-SY-5Y) and fibroblast (BHK) cell lines (Figure 4.3a and Figure C5) to observe very negligible toxicity. Mature Aβ40 aggregates (10 and 100 μM) show very low (56% and 40% respectively) cell viability (Figure 4.3b). However, a significant improvement in cell viability (90% and 79% respectively) has been achieved in the presence of 10 μM and 100 μM PFBZ (Figure 4.3b). The toxicity in the presence of Cu(II) was also monitored by MTT assay (Figure 4.3C). Amyloid toxicity was found to be enhanced in the presence of Cu(II). The Aβ toxicity was also visualized using calcein stain (Calcein AM,

Molecular Probes, catalog number: C3099) (Figure 4.3d). Usually, neuronal loss in AD is mainly due to the high level of oxidative stress caused by ROS produced from dysregulated redox metals like Cu(II) through a Fenton-type mechanism.[35] Moreover, a recent report has proven that oligomeric Aβ can directly induce ROS generation through a metal-independent pathway and interacts with cell membranes to trigger membrane disruption.[36] In our case, ROS production was quantified using CellRox green fluorescence (CellRox Green Reagent, Molecular Probes, catalog number: C10444) (Figure 4.3e). The cells incubated with Aβ in the presence of Cu(II) exhibited high levels of ROS (Figure 4.3e, marked by red) that usually attacks mitochondrial membranes finally leading to neuronal damage. Hence, chelation of redox active metals like Cu(II) is very crucial to reduce ROS-mediated neuronal damage. PFBZ chaperone as a Cu(II) chelator (Figure C2) blocks the redox cycle that leads to ROS production and thereby reduces the ROS in cells (Figure 4.3e, marked in green). Enhanced amounts of ROS produced by the Aβ + Cu(II) inclusion complex result in caspase-3 activation which is a signature of early apoptosis.[37] Aβ-induced caspase-3 activation was monitored using the colorimetric caspase-3 activity assay (Image-iT LIVE GreenCaspase-3 and -7 Detection Kit, Molecular Probes, catalog number: I35106). Caspase-3 was found to be activated in the case of Aβ treated cells only (caspase activity is visible in the green channel and dead cells were visible in the red channel, Figure 4.3f). However, the caspase activity was successfully attenuated in the presence of PFBZ. ROS produced by the Aβ + Cu(II) inclusion complex also affects mitochondrial membranes, which are recently reported to be early targets for Aβ-mediated neurotoxicity.[38-39] An effect of such ROS on mitochondria was further monitored via the mitochondrial membrane potential (MMP) using JC-1 dye (Molecular Probes, catalog number: T3168) that undergoes reversible change in fluorescence emission from green to red as the MMP increases (Figure 4.3g). On treatment with Aβ in the presence of Cu(II), a dramatic reduction in MMP (dominant green color) was observed, which, however, remains nearly unchanged (with respect to control) when Aβ + Cu(II) was treated in the presence of a PFBZ chaperone. MMP is the indicator of the mitochondrial health and its reduction indicates the disruption of a mitochondrial membrane which is believed to be a unique signature of early stage apoptosis: the caspase activation and apoptosis of the neurons.[40] These results strongly suggest that apoptosis in the cultured cells was mediated by mitochondrial dysfunction and caspase-3 activation. Thus, the PFBZ chaperone can suppress such toxic events and can be used as an efficient neuroprotecting agent. Another persistent challenge is the blood–brain barrier (BBB) permeability, a prerequisite for drugs targeting neurological disorder.

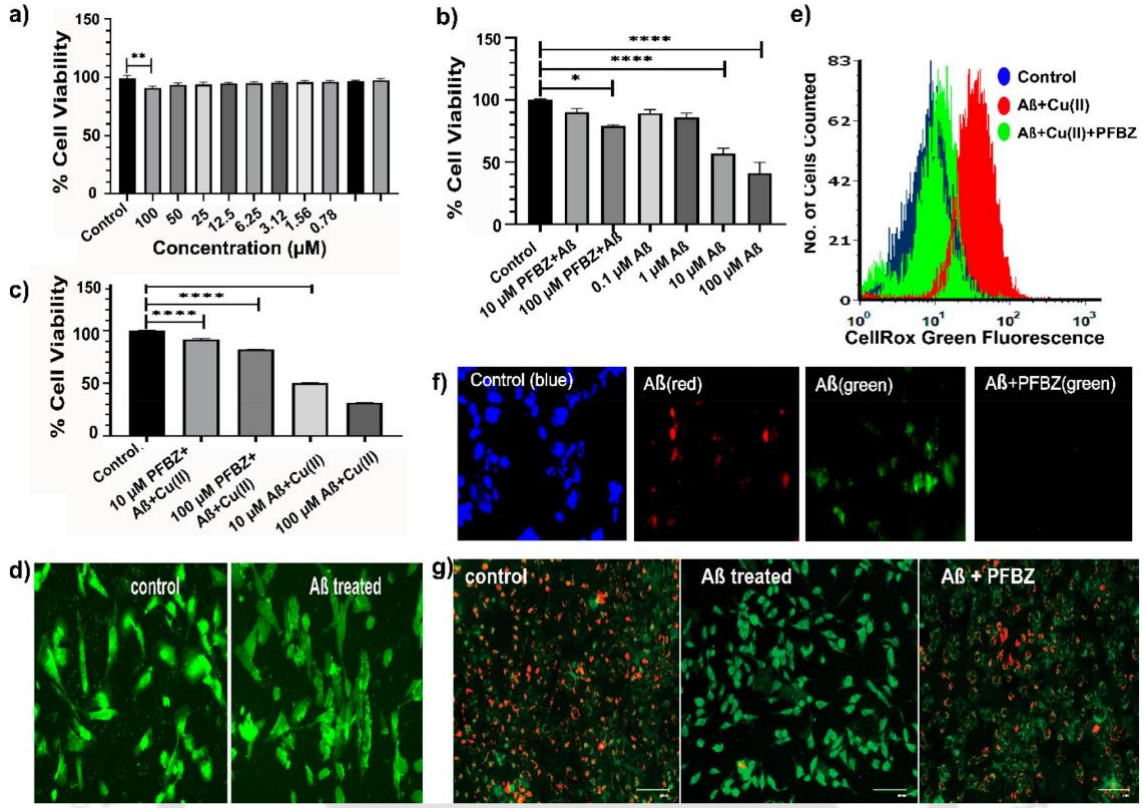

Figure 4.3: *(a) Cell viability of PFBZ chaperone in the SH-SY-5Y cell line using a MTT assay. (b) Reduction in Aβ40 (10 μM) neurotoxicity in the presence of PFBZ chaperone (1 μM). (c) Metal-dependent toxicity of Aβ40 aggregates in the presence of Cu(II). Cell viability was measured by MTT assay, and the data are shown as the mean ± SD of replicate groups. (d) Imaging Aβ treated cells using Calcein stain. (e) Production of ROS using CellRox green fluorescence. (f) Colorimetric evaluation of caspase-3 activation. (g) Monitoring of mitochondrial membrane potential using JC-1 dye.*

The PFBZ chaperone by virtue of its nano dimension (size 9.04 ± 1.58 nm) permeates through the BBB through interstitial spaces. To study the in vivo BBB permeability of PFBZ, 8 month-old lab-grade WT albino mice were used. The solution of artificial chaperone PFBZ nanodots was injected through the tail vein with a dosage of 20 mg/kg. These chaperone nanodots were allowed to distribute throughout the body for 30 min after which the mouse was sacrificed, each part was isolated, and relative fluorescence activity in homogenate of the respective organs was recorded to determine biodistribution of the maximum amount of PFBZ chaperone accumulated in the liver. A bright yellow fluorescence of PFBZ was observed in brain slices indicating translocation of the PFBZ chaperone through the BBB (Figure 4.4b) in normal circulation. However, no trace of the PFBZ chaperone was observed in control brain slices as expected. The neuroprotection activity of artificial chaperone PFBZ was evaluated by comparing neuronal damage caused by

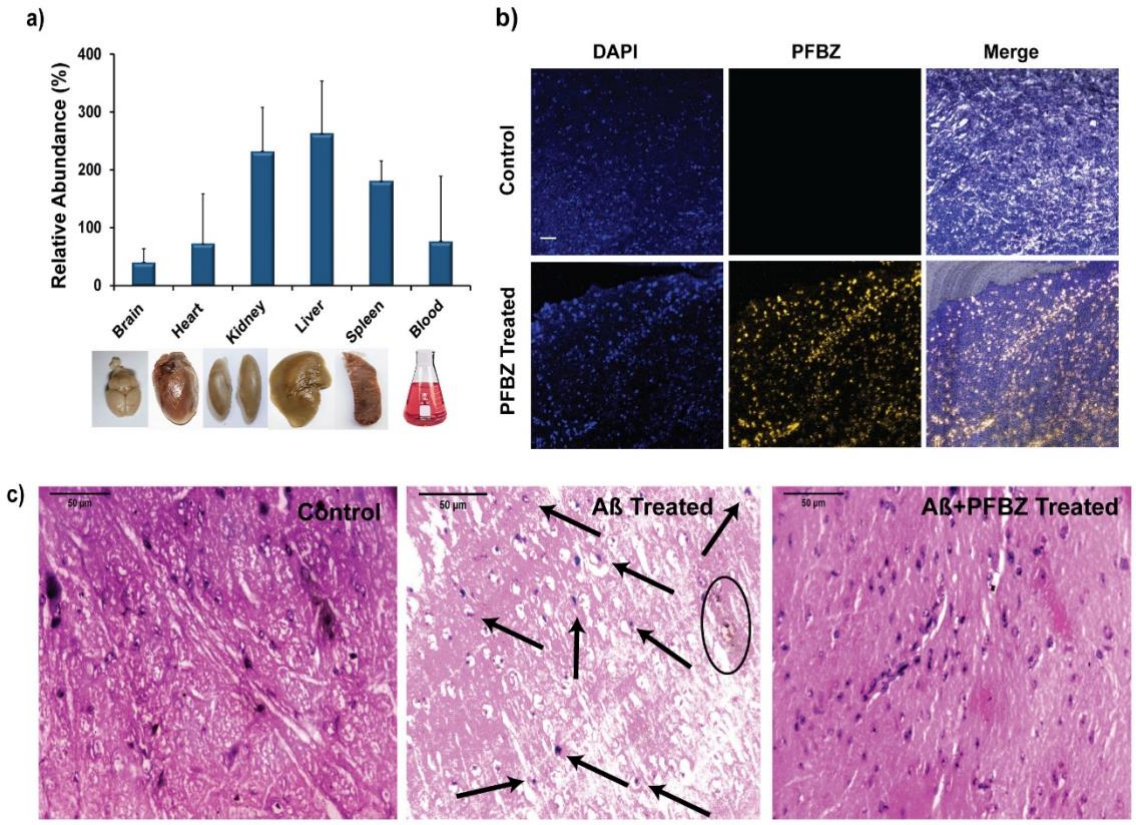

Figure 4.4: *a) Bio-distribution of PFBZ in brain, heart, kidney, liver, spleen and blood, (represented as the relative fluorescence intensity per mg of tissue using spectrofluorometry). b) BBB permeability: Co-localization of PFBZ in WT mouse hippocampus, Images were captured at 20× magnification using confocal microscope. Scale bar: 50 microns. c) Treatment effect of PFBZ for mitigation of the neurotoxicity associated with the Aβ aggregation in WT mice model. Histological observation of the brain tissues after different treatments. Brain tissues were collected from the WT mice and assessed by hematoxylin and eosin (HE), Scale bar, 50 μm.*

Aβ aggregates and Aβ-PFBZ coaggregates. The hippocampal neuronal morphology in the brain was observed after different treatments. In order to observe neuronal damage triggered by Aβ40 oligomers, the mice were administered with PBS (control), Aβ oligomers, and Aβ-PFBZ coaggregates through intracerebroventricular injection (3 mice per group; dose: 20 μg PBS/mice, 21 μg Aβ/mice, 2.8 μg Aβ-PFBZ/mice, respectively) for 7 days. Brain tissues were sectioned and stained with hematoxylin and eosin (H&E) dye for immunohistochemical analysis (Figure 4.4c). In the Aβ40 oligomer treated section, the number of cells was found to be extremely less compared to the control and Aβ40 + PFBZ treated sections. Moreover, signs of internal hemorrhage (marked in black circle) and pyknosis with standard apoptotic features including hyperchromatic nuclei (marked in arrow) were also observed. In contrast, negligible

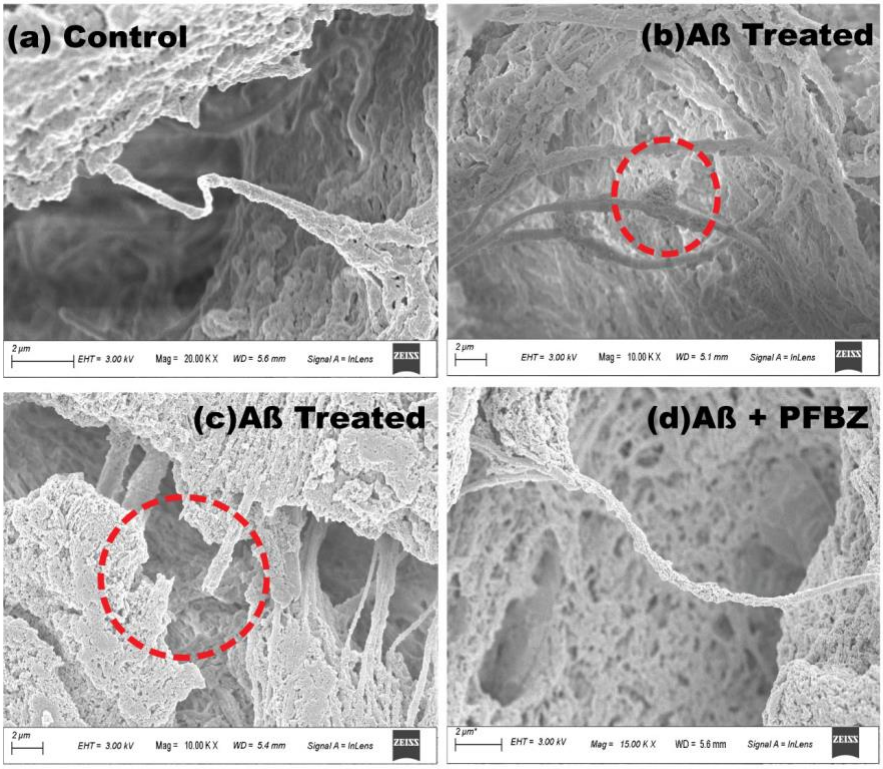

Figure 4.5: *Brain tissue sections (hippocampus region) were imaged using field enhanced scanning electron microscopy (FESEM): (a) Brain tissue sections of controlled mice. (b and c) Brain tissue sections of Aβ treated mice. (d) Brain tissue sections mice treated with Aβ+PFBZ. scale bar: 2 µm.*

pyknosis and internal hemorrhage were observed in the case of mice treated with Aβ- PFBZ, suggesting PFBZ chaperone nanodots had effectively mitigated the neuronal damages triggered by the Aβ oligomers. Furthermore, the effect of Aβ toxicity on the morphology of hippocampal neuron mainly in the dentate gyrus (DG) sub-region was carefully assessed using electron microscopy (Figure 4.5a–d). In case of sections treated with Aβ oligomers, a set of deformation and damage (marked in red circle) in hippocampal neurons was detected (Figure 4.5b-c). However, such deformation was not observed in the case of PFBZ + Aβ treated samples (Figure 4.5d). This is the first report where nanoscale deformation by Aβ oligomers in hippocampal neurons was directly visualized through an electron microscopy technique.

Recent reports reveal that Aβ40 oligomers exhibit a detergent-like effect on membranes by binding to the lipid bilayer and disrupting the membrane integrity that are central to the AD pathology.[34-41] As the neuronal membrane consists of lipid bilayers, the Aβ40 oligomer can cause deformation and membrane disruption in neuronal cells. However, the polymeric chaperone PFBZ wraps around the Aβ40 oligomer (Figure 4.2e) with a protective layer that resists the Aβ40 oligomer from interacting with neuronal

membranes and protects it from deformation. The deformation and neuronal loss can also occur through metal-dependent pathways (in the presence of Cu^{2+}). To ascertain the role of Cu(II), Aβ cytotoxicity was performed in the presence of Cu(II). It is evident from MTT experiments that 100 μM and 10 μM Aβ oligomers show 40% and 56% cell viability, respectively. The lower cell viability can be attributed to the higher cytotoxicity of Aβ oligomers. However, the cell viability even decreased to 31% and 50%, respectively, in the presence of 1 equiv of Cu(II). The toxicity data were further supported by a metal-dependent amyloid aggregation assay (Figure C6). It has been observed that the extent of amyloid aggregation has been increased in the presence of Cu(II). It is the lag phase which was greatly affected by the presence of the metal. Consequently, such enhancement results in a significant elevation in neurotoxicity in the presence of Cu(II) (Figure 4.3c). However, PFBZ, as a Cu(II) chelator, inhibits the metal-dependent amyloid aggregation by sequestering Cu(II) from Aβ solution. Previously, a fluorescein-based Cu(II) chelator that inhibited metal-dependent Aβ aggregation by sequestering Cu(II) present in human cerebrospinal fluid has been reported.[42] The elevation in Aβ cytotoxicity in the presence of redox active metals (such as Cu^{2+}) was also reported earlier.[43−46] Aβ is known to sequester Cu(II) through the histidine end with a high-binding constant to form the Aβ–Cu complex with linear geometry.[47] Formation of such Aβ–Cu complex has strongly been implicated in the progression of AD by enhancing neurotoxicity of Aβ oligomers.[48] It has been well established that the Aβ–Cu complex exerts enhanced neurotoxicity by initiating a chain of neurochemical events associated with ROS involved in neuronal cell death. The Aβ–Cu complex in the presence of oxygen undergoes a Fenton type of reaction to produce ROS in endogeneous conditions.[49-50] Such ROS easily target mitochondria and disrupt the mitochondrial membrane to result in mitochondrial dysfunction.[51] The condition of mitochondria could be tracked by measuring MMP. Hence, because of the elevation in amyloid fibrillation tendency and formation of high amounts of ROS, a sharp enhancement in cell viability in the presence of Cu(II) was observed.

Although, the effect of toxic Aβ40 on memory deficits has been well explored, the physiological effect still remains unexplored. The deposition of such species in blood vessels of the brain can lead to an internal brain hemorrhage.[52] Recent research reveals that a domain known as the Kunitz protease inhibitor (KPI) domain, present in Aβ, inactivates proteins in the blood causing clotting and results in microhemorrhages in brain and such links between inactivation by Aβ and internal hemorrhage have also been explored recently.[53-55] However, transgenic mice designed to make enhanced amounts of the amyloid precursor protein to Aβ peptide were largely affected by hemorrhages than WT mice.[55] In another study with Aβ isoform devoid of KPI domain, substantially smaller amounts of

hemorrhages are reported.[53] These two studies conclude that the deposition of Aβ in brain blood vessels may trigger chances of hemorrhage by blocking local coagulation.[52] Moreover, deposition of Aβ in blood vessels significantly disturbs their normal functions and leads to microhemorrhages. In the present work, amyloid toxicity has been demonstrated in a WT mouse model. Herein, the mice were administered with Aβ through the tail vein, hence Aβ can be deposited in blood vessels in the brain and triggers hemorrhage through aforementioned mechanisms. Although memory deficits triggered by amyloid aggregates were well explored, there is no mention about internal hemorrhages likely because of low concentrations and lower sizes of the oligomers used.[56] For oligomerization, Aβ was incubated for 1 h only to produce smaller (low molecular weight) oligomers (oligomer ≤ tetramer). Because of the smaller size of oligomers, the probability of vascular deposition is low.

Transgenic animals have the advantage of forming Aβ within their body. However, to monitor the neurotoxic effects, an Aβ oligomer solution was injected through intracerebroventricular injections. Previous studies have reported the effect of amyloid toxicity on both Swiss albino mice and C57BL/6 mice to observe similar learning, memory impairment, and synaptic loss evaluated from the water maze task in both rodents.[57] However, Swiss albino mice present a higher alteration in brain antioxidant parameter than C57BL/6 mice, which should be taken into account while selecting an appropriate model for AD. Recently, amyloid triggered memory deficits were shown in Swiss albino mice through behavioral studies (Y maze test, water maze test) and several in vivo studies including lipid peroxidation, protein oxidation, and caspase activation associated with AD.[58] In addition, it has been also observed that an adequate dose of Aβ can modulate activities of several enzymes including choline esterase, β secretase, and monoamine oxidase and produce neuronal damage as evident from histopathological analysis performed in the same model. Similar studies in the albino mouse model made by other groups also observed cognitive deficits on treatment with Aβ oligomers.[59] Hence, from the aforementioned literature, it is clearly evident that albino mice could be a good choice to validate the cascade of neurological events associated with AD. However, we agree that transgenic mouse models are a better option for validating a novel drug against AD. Although WT albino mice lack an advanced cognitive capacity as possessed by their transgenic littermates, they can serve as a robust and economic alternative to complement transgenic mouse models that are no longer deemed sufficient.

4.3 Discussion

Traditionally, drugs were designed with an aim to target single biological factors (usually proteins or enzyme) with a very high selectivity to negate any unwanted effects from mistargeting other physiological entities. With this perception, multi-target drugs were flagged as undesirable, as they were believed to produce adverse effects. However, the complexity of some diseases, such as AD, has clearly proven such single targeted drugs are inadequate to produce desired therapeutic effects.[60-61] Hence, to develop multi-target-directed therapeutics, polymers are an excellent choice due to their high cell viability, pH stability, nano dimension, and advantage of multiple functionalization. The polymeric chaperone PFBZ was designed in a strategic manner such that the pendant benzimidazole group resembles a part of ThT, a well-known sequester of amyloids (Figure 4.1a). The polyfluorene backbone provides sufficient hydrophobicity that leads the PFBZ chaperone to form nanodots in aqueous media with a bright yellow emission, a vital prerequisite for imaging studies. The nano dimensions of the PFBZ chaperone ultimately help it to translocate through BBB (Figure 4.4b). Hence, a polyfluorene backbone with a pendant benzimidazole group with bright yellow emission makes an excellent combined choice for use in AD therapeutics. The biophysical experiments suggest that the PFBZ chaperone is able to inhibit Aβ aggregation even in a very low substoichiometric molar ratio. The mechanism of inhibition is based on the chaperone-like activity of PFBZ. It targets Aβ40 through selective binding at the amyloidogenic domain primarily through electrostatic interaction. The opposite zeta potential of PFBZ (+2.94 mV) and Aβ40 (−3.82 mV) is the main reason behind the strong electrostatic interaction (Figure 4.1d). Aβ16−21 (zeta potential: −2.61 mV) is the central fibril forming core and known as the “amyloidogenic domain” of Aβ40. Hence, it is important to block such a core using some drug material in order to avoid unwanted amyloid aggregation. However, the selective interaction of an artificial chaperone toward Aβ16−21 is rare and unprecedented in existing literature. As a consequence of binding, the fibrillation tendency of Aβ40 was markedly diminished in the presence of the PFBZ chaperone. Electron microscopy data reveal that PFBZ wraps around Aβ aggregates, thereby preventing them from interacting with cell membranes and exerting toxic effects (Figure 4.2e). The Aβ triggered neuronal damage was evaluated in an in vivo WT mouse model using electron microscopy. An intracerebroventricular injection containing the PFBZ nanodot drug successfully mitigated the neuronal deformation, revealing for the first time its relationship with Aβ toxicity and was evidenced by in vitro assays of ThT, TEM, and cell viability studies. Furthermore, the PFBZ chaperone does not induce any harmful effects on healthy neuro cells owing to their high biocompatibility.

Thus, the complexity associated with AD necessitates a multi-targeted drug activity-based approach to mitigate the effect of neurotoxicity. The structural features of the PFBZ artificial chaperone allowed it be utilized as a potential amyloid inhibitor, metal chelation, ROS-mediated mitochondria damage prevention, bioimaging, BBB permeability, and lipid membrane protection. Thus, preventive nanomedicine against AD pathology based on the PFBZ chaperone offers a very unique approach and a new concept that can be further optimized into a multi-targeted drug for complex neurological disorders.

4.4. Conclusion

An artificial chaperone PFBZ, possessing a benzimidazole motif strapped to polyfluorene, offers a very unique set of anti-amyloidogenic properties such as high binding affinity toward Aβ16-21, metal chelation and alleviates the Aβ toxicity associated with AD. It is evident from a variety of biophysical studies that PFBZ binds with the major fibril forming core of Aβ and blocks the early events that leads to oligomerization. As a result of such amyloid sequestration, there was a marked elevation in the ROS level that ultimately blocks the biochemical cycle including caspase activation and mitochondrial dysfunction that finally leads to apoptosis in neuronal cells. The PFBZ structure allows efficient Cu(II) chelation, arrests a redox cycle to stop ROS generation, and protects the mitochondria from ROS-mediated damage. Further, this artificial chaperone crosses the BBB, despite being injected through the tail vein, as observed via the bright yellow fluorescence in brain slices indicating translocation of the PFBZ chaperone through BBB under normal circulation by virtue of its nano dimensions and successfully recovers the amyloid-mediated internal hemorrhage in a WT mice brain, a facet never witnessed previously with polymeric chaperones. This artificial chaperone PFBZ demonstrated multiple amyloid targeting properties, inhibiting amyloid fibrillation through both metal-dependent and -independent pathways and protecting neuronal cells from amyloid toxicity, confirming it to be a potential lead for the development of anti-amyloidogenic drugs as an immediate application.

4.5. Materials

All reagents were procured from Sigma Aldrich and utilized without purification. For experiments HPLC grade solvents and Milli-Q water were used. Amyloid-beta16-21(Aβ16-21) and Amyloid-beta 1-40 peptide fragment (Aβ40) was obtained from G.L Biochem Ltd., Shanghai, China. Borosil microscopy glass slides were used for microscopy

study including Atomic Force Microscopy (AFM) and confocal microscopy. Human Cerebrospinal Fluid was collected from Guwahati Neurological Research Centre and Hospital (GNRC), Guwahati, India following all the rules and regulation. A Brief Detail about the purpose of the experiment was described at the time of collection maintaining all the bioethics policy of the hospital. These samples were collected as a part of their routine medication.

4.6. Instrumentation

Fluorescence and UV-Vis spectra were recorded using BioTek SynergyMx microplate reader and Perkin Elmer Lambda-25 spectrometer respectively. Perkin Elmer spectrometer was used for FT-IR spectra acquisition. The zeta potentials and hydrodynamic sizes measurements were performed using Nano-ZS90 Zeta sizer Nano series instrument. TEM images were recorded by JEOL 2100 transmission electron microscope. Atomic force microscopy (AFM) was performed on Bruker Innova SPM model, with the tapping mode. Field Enhanced Scanning Electron Microscopy images were recorded in Zeiss SIGMA 300 instrument.

4.7. Synthesis of PFBZ:

4.7.1. Synthesis of 9, 9-Bis-(6-bromohexyl)-9H-fluorene:

In a 250 mL round bottom flask, Fluorene (1 g, 6.016 mmol), 50% aq. NaOH and a pinch (catalytic amount) of tetra-butyl ammonium Iodide (TBAI) (0.444 g, 2.1 mmol) were taken and then degassed 3 times with the application of freeze-thaw cycles. 1,6-dibromohexane (10.3 g, 42.11 mmol) was poured through a syringe, and the mixture was stirred continuously for 8 hours at 80 °C. The reaction mixture was allowed to cool to room temperature and extracted with chloroform. The organic layer was collected and washed with water and dried. The solvent was removed under vacuum and excess 1, 6-dibromohexane was removed through short path distillation, and the crude was purified using Column Chromatography.

4.7.2. Synthesis of Poly 9, 9-Bis-(6-bromohexyl)-9H-fluorene (PF-Br):

9, 9-Bis-(6-bromohexyl)-9H-fluorene was taken in a 100 mL round bottom flask and polymerization reaction was performed by anhydrous ferric chloride ($FeCl_3$) (1.30g, 8.12 mmol) dissolved in 15 mL nitrobenzene. The reaction mixture was stirred at room temperature for 40 hours, and resulting reaction mixture was precipitated from methanol. The resulting polymer, poly 9, 9-Bis-(6-bromohexyl)-9H-fluorene was dried under reduced vacuum to obtain 0.63 g (63%) as dark brown powder.

The molecular weight (Mw) of the polymer was found to be 6670 g mol^{-1} with a polydispersity index (PDI) of 2.3 (THF, Polystyrene as internal standard).[21]

^{1}H NMR (600 MHz, CDCl3), δ (ppm): 7.85 (bp), 7.68 (bp), 7.33 (bp), 3.2 (bp), 2.1 (bp), 2.05 (bp), 1.68 (bp), 1.26 (bp), 0.83 (bp), 0.6 (bp). Bp: broad peak

^{13}C NMR (600 MHz, CDCl3), δ (ppm): 151.5, 150.4, 141.3, 140.6, 127.29, 126.51, 122.9, 121.5, 120.3, 119.9, 55.5, 55.1, 45.3, 40.4, 34.18, 32.8, 32.23, 239.8, 29.2, 27.9, 26.6, 23.8, 22.7

4.7.3. Synthesis of PF-BZ:

To synthesize PFBZ, PF-Br (0.203 mmol), Benzimidazole (1.01 mmol) and K_2CO_3 (2.03 mmol) were taken in 15 mL DMF and refluxed for 48 hours in a 100 mL round bottom flask. After that solvent was removed through a rotavapor and precipitated from methanol to obtain the final yellow coloured desired polymer (~75%).

^{1}H NMR (600 MHz, $CDCl_3$), δ (ppm): 0.5-0.7 (-CH_2), 0.9-1.1 (-CH_2), 1.18, 1.4-1.6 (CH_2), 1.8-2.03 (-CH_2), 3.8 (-CH_2-N), 7.04-7.2 (ArH), 7.4-7.8 (ArH)

ArH: Aromatic Hydrogen

4.8. Sample Preparation:

4.8.1. Stock Solution Preparation:

10 mM PFBZ was prepared in DMF by dissolving the required amount of solid powdered PFBZ and further diluted as per requirement. The solution was filtered by 0.22 µM syringe filter.

4.8.2. Preparation of Aβ40 monomer:

Aβ40 monomers were prepared using protocol discussed in section 2.5.4.

4.8.3. Preparation of Aβ40 oligomer(tetramer):

Aβ40 monomers were prepared using protocol discussed in section 3.5.6.

4.8.4. Sample Preparation

Sample for CD, Zeta potential and AFM was prepared according to the section 2.5.9, 2.5.10. and 2.5.11 respectively.

4.8.5. Measurement of ROS Activity *in vitro*:

Cell culture: SH-SY-5Y cells is a neuroblastoma cell line derived from human bone marrow. SH-SY-5Y cells were cultured in complete growth media, Dulbecco's Modified Eagle Medium (DMEM, HiMedia) with 10% fetal bovine serum (Gibco) and antibiotics (Anti-Anti, Gibco) at 37 °C in 5% CO2 incubator. Cell line used in this study were gifted by National centre for cell science (NCCS), Pune.

SH-SY-5Y cells were seeded in 3 plates at an initial seeding density of 1,00,000 cells/well in 100 µl medium. The cells were treated with PBS (control), 50 µM toxic Aβ aggregates and 50 µM Aβ+PFBZ for 12 hours in 37 °C in 5% CO2. Then CellROX® Reagent at a final concentration of 5 µM was added to the cells and incubate for 30 minutes at 37°C. After that, medium was removed and cell were washed with PBS buffer for 3 times. Then, ROS activities was measured in flow cytometer.

4.8.6. Caspase Activation Experiment

Caspases (cysteine-aspartic proteases) belongs to a family of protease enzymes playing vital roles in programmed cell death. For caspase activation study human neuroblastoma cell (SH-SY-5Y) were cultured in DMEM media at at 37 °C in 5% CO2 incubator. The cells were seeded in six well plate and incubated for 12 hours. The cells were treated with PBS buffer (control), 50 µM Aβ aggregates and 50 µM PFBZ+ Aβ aggregates and incubated for 12 hours. The cells were treated with 1X FLICA reagent and incubated

for 1 h. Then the cells were washed twice with PBS and observe under fluorescence microscope.

4.8.7. JC-1 Assay

JC-1 is a novel cationic dye which accumulates in mitochondria. The dye exists as a monomer at low concentrations and exhibits green fluorescence, like fluorescein. At higher concentrations, the dye forms J-aggregates to exhibit a broad excitation spectrum and an emission maximum at ~590 nm. These characteristics make JC-1 a sensitive marker for mitochondrial membrane potential.

To monitor mitochondrial membrane potential (MMP), human neuroblastoma cell (SH-SY-5Y) were cultured in DMEM media at at 37 °C in 5% CO2 incubator. The cells were seeded in six well plate. The cell density was 10^6 cells/well containing 10% fetal bovine serum (FBS) in Dulbecco's Modified Eagle Medium (DMEM) and incubated at 37°C in 5% CO2. After 12 hours, media was discarded and each well was washed with phosphate-buffered saline (PBS) followed by addition of Aβ and Aβ+INHQ to each well at 50 µM concentrations. After 12 hours, 2 µM (final concentration) of JC-1 dye was added in each well and incubated at 37°C, 5% CO_2 for 15-30 min. Cells were then washed with PBS and observed under fluorescence microscope (FLoid Cell Imaging Station, Thermo Fischer Scientific) for progressive loss of red J-aggregate fluorescence and cytoplasmic diffusion of green monomer fluorescence.

4.8.8. *In vivo* Bio-distribution Study:

To determine the bio-distribution of PF-BZ in Brain especially in the cerebral cortex and other vital organs in the treated BALB/c mice, we collected all the required organs from the sacrificed BALB/c mice after completion of dosing regimens. All organ including brain samples were then washed with 10 mM PBS buffer, weighed, treated with 1 % HCl and held overnight at 4°C followed by gentle vortexing. Finally, these samples were crushed and centrifuged at 13,000 rpm. for 15 min at 4°C, and the supernatant was collected fluorescence activity was recorded in Horiba Fluoromax4 instrument using λex at 370 nm. The data are expressed as relative fluorescence units per gm tissue.

4.8.9. BBB Barrier Study:

Swiss albino mice (weight 25-30g) were used as the experimental animal model in the present study. The animal experiments were completed as per the approval of the IAEC, Gauhati University. The mice were caged at usual 12:12 hours light dark cycles with usual diet and water ad libitum. Daily handling of the animals was maintained to reduce the stress. Animals were divided into two groups (GROUP X and GROUP Y) along with one control group fed with normal saline. Each group contained five mice. Mice were administered at the dose 25 mg/kg per day for one week through teil vein. The drug was allowed to circulate through normal physiological flow. Then the animals were sacrificed and brain tissues were collected. Tissues were fixed in Carnoy's fixative. The fixed tissues were embedded in paraffin wax for histological study. Histological sections were prepared at 5 μm thickness using the laboratory rotary microtome. Sections were stained with DAPI using standard procedure and observed under confocal microscope.

4.8.10. FESEM Study of Brain Section:

Amyloid oligomer mediated neuronal damage in cerebral cortex and impairment of the same by the polymer in the treated mice was explored by FESEM. For studying neuronal damage triggered by amyloid oligomer, specimens were directly injected into the mouse brain through cranium. The behavior of the mouse was observed for an hour and allowed the sample circulate uniformly throughout the brain. After that, the mouse was sacrificed, and brain was isolated, washed with 10 mM PBS and plunged into Carnoy's Fixatip Solution. A thin section of the brain was cut and critically dried by SMDS solution. Images were recorded using Zeiss-Sigma Field Emission Scanning Electron Microscope (FESEM) instrument.

4.9. References:

(1) Chiti, F.; Dobson, C. M. Protein misfolding, functional amyloid, and human disease. *Ann. Rev. Biochem.* **2006**, *75*, 333-366.

(2) Kwon, H. J.; Cha, M.-Y.; Kim, D.; Kim, D. K.; Soh, M.; Shin, K.; Hyeon, T.; Mook-Jung, I. Mitochondria targeting ceria nanoparticles as antioxidants for Alzheimer's disease. *ACS Nano* **2016**, *10*, 2860-2870.

(3) Holtzman, D. M.; Morris, J. C.; Goate, A. M. Alzheimer's disease: The challenge of the second century. *Sci. Trans. Med.* **2011**, *3*, 77sr1.

(4) Chiti, F.; Dobson, C. M. Protein misfolding, amyloid formation, and human disease: A summary of progress over the last decade. *Ann. Rev. Biochem.* **2017**, *86*, 27-68.

(5) Nasica-Labouze, J.; Nguyen, P. H.; Sterpone, F.; Berthoumieu, O.; Buchete, N.-V.; Coté, S.; De Simone, A.; Doig, A. J.; Faller, P.; Garcia, A.; Laio, A.; Li, M. S.; Melchionna, S.; Mousseau, N.; Mu, Y.; Paravastu, A.; Pasquali, S.; Rosenman, D. J.; Strodel, B.; Tarus, B.; Viles, J. H.; Zhang, T.; Wang, C.; Derreumaux, P. Amyloid β protein and Alzheimer's disease: when computer simulations complement experimental studies. *Chem. Rev.* **2015**, *115*, 3518-3563.

(6) Ross, C. A.; Poirier, M. A. Protein aggregation and neurodegenerative disease. *Nat. Med.* **2004**, *10*, S10-S17.

(7) Morris, R. J.; Eden, K.; Yarwood, R.; Jourdain, L.; Allen, R. J.; MacPhee, C. E. Mechanistic and environmental control of the prevalence and lifetime of amyloid oligomers. *Nat. Comm.* **2013**, *4*, 1891.

(8) Karran, E.; Mercken, M.; Strooper, B. D. The amyloid cascade hypothesis for Alzheimer's disease: An appraisal for the development of therapeutics. *Nat. Rev. Drug Discov.* **2011**, *10*, 698-712.

(9) Hardy, J.; Selkoe, D. J. The amyloid hypothesis of alzheimer's disease: Progress and problems on the road to therapeutics. *Science* **2002**, *297*, 353-356.

(10) Gaggelli, E.; Kozlowski, H.; Valensin, D.; Valensin, G. Copper Homeostasis and Neurodegenerative Disorders (Alzheimer's, Prion, and Parkinson's Diseases and Amyotrophic Lateral Sclerosis). *Chem. Rev.* **2006**, *106*, 1995-2044.

(11) Hamley, I. W. The amyloid beta peptide: a chemist's perspective: Role in Alzheimer's and fibrillization. *Chem. Rev.* **2012**, *112*, 5147-5192.

(12) Sultana, R.; Butterfield, D. A. Role of oxidative stress in the progression of Alzheimer's disease. *J. Alz. Dis.* **2010**, *19*, 341-353.

(13) Zhang, J.; Perry, G.; Smith, M. A.; Robertson, D.; Olson, S. J.; Graham, D. G.; Montine, T. J. Parkinson's disease is associated with oxidative damage to cytoplasmic DNA and RNA in substantia nigra neurons. *Am. J. Pathol.* **1999**, *154*, 1423-1429.

(14) Dexter, D. T.; Carter, C. J.; Wells, F. R.; Javoy-Agid, F.; Agid, Y.; Lees, A.; Jenner, P.; Marsden, C. D. Basal lipid peroxidation in substantia nigra is increased in Parkinson's disease. *J. Neurochem.* **1989**, *52*, 381-389.

(15) Lin, M. T.; Beal, M. F. Mitochondrial dysfunction and oxidative stress in neurodegenerative diseases. *Nature* **2006**, *443*, 787-795.

(16) Du, H.; Guo, L.; Fang, F.; Chen, D.; A Sosunov, A.; M McKhann, G.; Yan, Y.; Wang, C.; Zhang, H.; Molkentin, J. D.; Gunn-Moore, F. J.; Vonsattel, J. P.; Arancio, O.; Chen, J. X.; Yan, S. D. Cyclophilin D deficiency attenuates mitochondrial and neuronal perturbation and ameliorates learning and memory in Alzheimer's disease. *Nat. Med.* **2008**, *14*, 1097-1105.

(17) Schmidt, C.; Lepsverdize, E.; Chi, S. L.; Das, A. M.; Pizzo, S. V.; Dityatev, A.; Schachner, M. Amyloid precursor protein and amyloid β-peptide bind to ATP synthase and regulate its activity at the surface of neural cells. *Mol. Psy.* **2008**, *13*, 953-969.

(18) Lustbader, J. W.; Cirilli, M.; Lin, C.; Xu, H. W.; Takuma, K.; Wang, N.; Caspersen, C.; Chen, X.; Pollak, S.; Chaney, M.; Trinchese, F.; Liu, S.; Gunn-Moore, F.; Lue, L.-F.; Walker, D. G.; Kuppusamy, P.; Zewier, Z. L.; Arancio, O.; Stern, D.; Yan, S. S.; Wu, H. ABAD directly links aß to mitochondrial toxicity in Alzheimer's disease. *Science* **2004**, *304*, 448-452.

(19) Ankarcrona, M.; Mangialasche, F.; Winblad, B. Rethinking Alzheimer's disease therapy: are mitochondria the key? *J. Alz. Dis.* **2010**, *20*, S579-S590.

(20) Mondal, S.; Chowdhury, S.R.; Shah, M.; Kumar, V.; Kumar, S.; Iyer, P. K. Nanoparticle assisted regulation of nucleation pathway of amyloid tetramer and inhibition of their fibrillation kinetics. *ACS Appl. Bio. Mater.* **2019**, *2*, 2137-2142.

(21) Mondal, S.; Kumar, V.; Roy Chowdhury, S.; Shah, M.; Gaur, A.; Kumar, S.; Iyer, P. K. Template-mediated detoxification of low-molecular-weight amyloid oligomers and regulation of their nucleation pathway. *ACS Appl. Bio. Mater.* **2019**, *2*, 5306-5312.

(22) Chowdhury, S. R.; Mondal, S.; Iyer, P. K. Blocking oligomeric insulin amyloid fibrillation via perylenebisimides containing dipeptide tentacles. *ACS Biomater. Sci. Eng.* **2018**, *4*, 4076-4083.

(23) Sun, H.; Lv, F.; Liu, L.; Wang, S. Reactive conjugated polymers for the modulation of islet amyloid polypeptide assembly. *ACS Appl. Mater. Interfaces* **2019**, *11*, 22973-22978.

(24) Sun, H.; Liu, J.; Li, S.; Zhou, L.; Wang, J.; Liu, L.; Lv, F.; Gu, Q.; Hu, B.; Ma, Y.; Wang, S. Reactive amphiphilic conjugated polymers for inhibiting amyloid β assembly. *Angew. Chem.* **2019**, *58*, 5988-5993.

(25) Salloway, S.; Sperling, R.; Fox, N. C.; Blennow, K.; Klunk, W.; Raskind, M.; Sabbagh, M.; Honig, L. S.; Porsteinsson, A. P.; Ferris, S.; Reichert, M.; Ketter, N.; Nejadnik, B.; Guenzler, V.; Miloslavsky, M.; Wang, D.; Lu, Y.; Lull, J.; Tudor, I. C.; Liu, E.; Grundman, M.; Yuen, E.; Black, R.; Brashear, H. R. Two phase 3 trials of bapineuzumab in mild-to-moderate Alzheimer's disease. *N. Engl. J. Med.* **2014**, *370*, 322-333.

(26) Doody, R. S.; Raman, R.; Farlow, M.; Iwatsubo, T.; Vel-las, B.; Joffe, S.; Kieburtz, K.; He, F.; Sun, X.; Thomas, R. G.; Aisen, P. S.; Siemers, E.; Sethuraman, G.; Mohs, R. A phase 3 trial of semagacestat for treatment of Alzheimer's disease. *N. Engl. J. Med.* **2013**, *369*, 341-350.

(27) Richardson, R. T.; Alekseev, O. M.; Grossman, G.; Widgren, E. E.; Thresher, R.; Wagner, E. J.; Sullivan, K. D.; Marzluff, W. F.; O'Rand, M. G. Nuclear autoantigenic sperm protein (NASP), a linker histone chaperone that is required for cell proliferation. *J. Biol. Chem.* **2006**, *281*, 21526-21534.

(28) Saibil, H. Chaperone machines for protein folding, unfolding and disaggregation. *Nat. Rev. Mol. Cell Biol.* **2013**, *14*, 630-642.

(29) Chowdhury, S. R.; Agarwal, M.; Meher, N.; Muthuraj, B.; Iyer, P. K. Modulation of amyloid aggregates into nontoxic coaggregates by hydroxyquinoline appended polyfluorene. *ACS Appl. Mater. Interfaces* **2016**, *8*, 13309-13319.

(30) Fändrich, M.; Fletcher, M. A.; Dobson, C. M. Amyloid fibrils from muscle myoglobin. *Nature* **2001**, *410*, 165-166.

(31) Sawaya, M. R.; Sambashivan, S.; Nelson, R.; Ivanova, M. I.; Sievers, S. A.; Apostol, M. I.; Thompson, M. J.; Balbirnie, M.; Wiltzius, J. J. W.; McFarlane, H. T.; Madsen, A.; Riekel, C.; Eisenberg, D. Atomic structures of amyloid cross-β spines reveal varied steric zippers. *Nature* **2007**, *447*, 453-457.

(32) Chowdhury, S. R.; Balaji, S. N.; Mondal, S.; Meher, N.; Trivedi, V.; Iyer, P. K. Modulating Early Stage Amyloid Aggregates by Dipeptide-Linked Perylenebisimides: Structure–Activity Relationship, Inhibition of Fibril Formation in Human CSF and Aβ1–40. *ACS Appl. Bio Mater.* **2018**, *1*, 403-413.

(33) Knowles, T. P. J.; Vendruscolo, M.; Dobson, C. M. The amyloid state and its association with protein misfolding diseases. *Nat. Mol. Cell. Biol.* **2014**, *15*, 384-396.

(34) Bode, D. C.; Freeley, M.; Nield, J.; Palma, M.; Viles, J. H. Amyloid-β oligomers have a profound detergent like effect on lipid membrane bilayers, imaged by atomic force and electron microscopy. *J. Biol. Chem.* **2019**, *294*, 7566-7572.

(35) Robert, A.; Liu, Y.; Nguyen, M.; Meunier, B. Regulation of copper and iron homeostasis by metal chelators: a possible chemotherapy for Alzheimer's disease. *Acc. Chem. Res.* **2015**, *48*, 1332-1339.

(36) Ke, P. C.; Sani, M.-A.; Ding, F.; Kakinen, A.; Javed, I.; Separovic, F.; Davis, T. P.; Mezzenga, R. Implications of peptide assemblies in amyloid diseases. *Chem. Soc. Rev.* **2017**, *46*, 6492-6531.

(37) Higuchi, M.; Honda, T.; Proske, R. J.; Yeh, E. T. H. Regulation of reactive oxygen species-induced apoptosis and necrosis by caspase 3-like proteases. *Oncogene* **1998**, *17*, 2753-2760.

(38) Mossmann, D.; Vögtle, F. N.; Taskin, Asli A.; Teixeira, Pedro F.; Ring, J.; Burkhart, Julia M.; Burger, N.; Pinho, Catari-na M.; Tadic, J.; Loreth, D.; Graff, C.; Metzger, F.; Sickmann, A.; Kretz, O.; Wiedemann, N.; Zahedi, René P.; Madeo, F.; Glaser, E.; Meisinger, C. Amyloid-β peptide induces mitochondrial dysfunction by inhibition of preprotein maturation. *Cell Metab.* **2014**, *20*, 662-669.

(39) Wang, X.; Su, B.; Siedlak, S. L.; Moreira, P. I.; Fujioka, H.; Wang, Y.; Casadesus, G.; Zhu, X. Amyloid-beta overproduction causes abnormal mitochondrial dynamics via

differential modulation of mitochondrial fission/fusion proteins. *Proc. Natl. Acad. Sci. U. S. A.* **2008**, *105*, 19318-19323.

(40) Liu, X.; Kim, C. N.; Yang, J.; Jemmerson, R.; Wang, X. In-duction of Apoptotic Program in Cell-Free Extracts: Requirement for dATP and Cytochrome C. *Cell* **1996**, *86*, 147-157.

(41) Williams, Thomas L.; Johnson, Benjamin R. G.; Urbanc, B.; Jenkins, A. Toby A.; Connell, Simon D. A.; Serpell, Louise C. Aβ42 oligomers, but not fibrils, simultaneously bind to and cause damage to ganglioside containing lipid membranes. *Biochem. J.* **2011**, *439*, 67-77.

(42) Muthuraj, B.; Layek, S.; Balaji, S. N.; Trivedi, V.; Iyer, P. K. Multiple function fluorescein probe performs metal chelation, disaggregation, and modulation of aggregated Aβ and aβ-Cu complex. *ACS Chem. Neuro.* **2015**, *6*, 1880-1891.

(43) Sowade, R. F.; Jahn, T. R. Seed-induced acceleration of amyloid-β mediated neurotoxicity in vivo. *Nat. Commun.* **2017**, *8*, 512.

(44) Samanta, S.; Rajasekhar, K.; Babagond, V.; Govindaraju, T. Small molecule inhibits metal-dependent and -independent multifaceted toxicity of Alzheimer's disease. *ACS Chem. Neuro.* **2019**, *10*, 3611-3621.

(45) Rajasekhar, K.; Mehta, K.; Govindaraju, T. Hybrid multifunctional modulators inhibit multifaceted aβ toxicity and prevent mitochondrial damage. *ACS Chem. Neuro.* **2018**, *9*, 1432-1440.

(46) Caballero, A. B.; Terol-Ordaz, L.; Espargaró, A.; Vázquez, G.; Nicolás, E.; Sabaté, R.; Gamez, P. Histidine rich oligopeptides to lessen copper mediated amyloid β toxicity. *Chem. Euro. J.* **2016**, *22*, 7268-7280.

(47) Girvan, P.; Teng, X.; Brooks, N. J.; Baldwin, G. S.; Ying, L. Redox kinetics of the amyloid-β-Cu complex and its biological implications. *Biochemistry* **2018**, *57*, 6228-6233.

(48) Cherny, R. A.; Atwood, C. S.; Xilinas, M. E.; Gray, D. N.; Jones, W. D.; McLean, C. A.; Barnham, K. J.; Volitakis, I.; Fraser, F. W.; Kim, Y.-S.; Huang, X.; Goldstein, L. E.; Moir, R. D.; Lim, J. T.; Beyreuther, K.; Zheng, H.; Tanzi, R. E.; Masters, C. L.; Bush, A. I. Treatment with a copper-zinc chelator markedly and rapidly inhibits β-amyloid accumulation in Alzheimer's disease transgenic mice. *Neuron* **2001**, *30*, 665-676.

(49) Hamley, I. W. The amyloid beta peptide: a chemist's perspective. role in Alzheimer's and fibrillization. *Chem. Rev.* **2012**, *112*, 5147-5192.

(50) Schubert, D.; Chevion, M. The role of iron in beta amyloid toxicity. *Biochem. Biophys. Res. Commun.* **1995**, *216*, 702-707.

(51) Lin, M. T.; Beal, M. F. Mitochondrial dysfunction and oxidative stress in neurodegenerative diseases. *Nature* **2006**, *443*, 787-795.

(52) del Zoppo, G. J. Bleeding in the brain: Amyloid-β may keep clots away. *Nat. Med.* 2009, 15, 1132-1133.

(53) Xu, F.; Previti, M. L.; Nieman, M. T.; Davis, J.; Schmaier, A. H.; Van Nostrand, W. E. AβPP/APLP2 family of kunitz serine proteinase inhibitors regulate cerebral thrombosis. *J. Neurosci.* **2009**, *29*, 5666-5670.

(54) Smith, R. P.; Higuchi, D. A.; Broze, G. J. Platelet coagulation factor xia-inhibitor, a form of Alzheimer amyloid precursor protein. Science **1990**, *248*, 1126-1128.

(55) Xu, F.; Previti Mary, L.; Van Nostrand William, E. Increased severity of hemorrhage in transgenic mice expressing cerebral protease nexin-2/amyloid β-protein precursor. *Stroke* **2007**, *38*, 2598-2601.

(56) Brouillette, J.; Caillierez, R.; Zommer, N.; Alves-Pires, C.; Benilova, I.; Blum, D.; Strooper, D. B.; Buée, L. Neurotoxicity and memory deficits induced by soluble low-molecular-weight amyloid-β1–42 oligomers are revealed in vivo by using a novel animal model. *J. Neurosci.* **2012**, *32*, 7852-7861.

(57) Prediger, R. D. S.; Franco, J. L.; Pandolfo, P.; Medeiros, R.; Duarte, F. S.; Di Giunta, G.; Figueiredo, C. P.; Farina, M.; Calixto, J. B.; Takahashi, R. N.; Dafre, A. L. Differential susceptibility following β-amyloid peptide-(1–40) administration in C57BL/6 and Swiss albino mice: Evidence for a dissociation between cognitive deficits and the glutathione system response. *Behav. Brain Res.* **2007**, *177*, 205-213.

(58) Nisha, S. A.; Devi, K. P. Gelidiella acerosa protects against Aβ 25–35-induced toxicity and memory impairment in Swiss Albino mice: an in vivo report. *Pharm. Biol.* **2017**, *55*, 1423-1435.

(59) Halawany, A. M. E.; Sayed, N. S. E. L.; Abdallah, H. M.; Dine, R. S. E. Protective effects of gingerol on streptozotocin-induced sporadic Alzheimer's disease: emphasis on inhibition of β-amyloid, COX-2, alpha-, beta - secretases and APH1a. *Scientific Reports* **2017,** *7*, 2902

(60) Bolognesi, M. L.; Cavalli, A. Multitarget drug discovery and polypharmacology. *ChemMedChem*. **2016**, *11*, 1190-1192.

(61) Bolognesi, M. L. Polypharmacology in a single drug: multitarget drugs. *Curr. Med. Chem*. **2013**, *20*, 1639-1645.

4.10. Appendix C: Additional Figures for Chapter-4

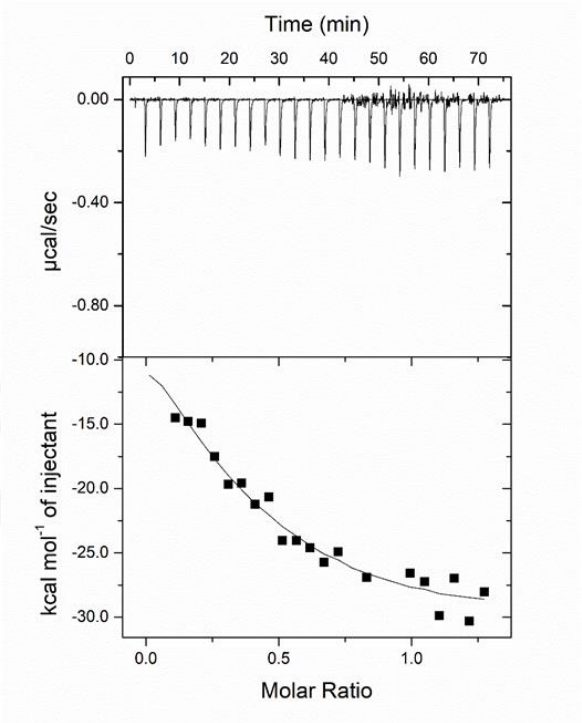

Figure C-1: *ITC fitting data for the titration of Aβ16-21(100 µM) with PFBZ (10 µM).*

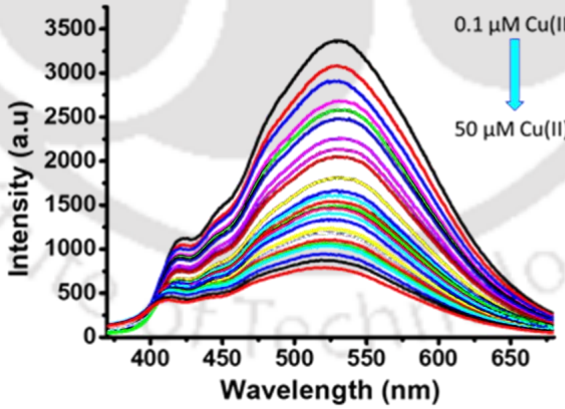

Figure C-2: *Fluorescence titration of Cu(II) with 10 µM PFBZ in 10 mM phosphate buffer.*

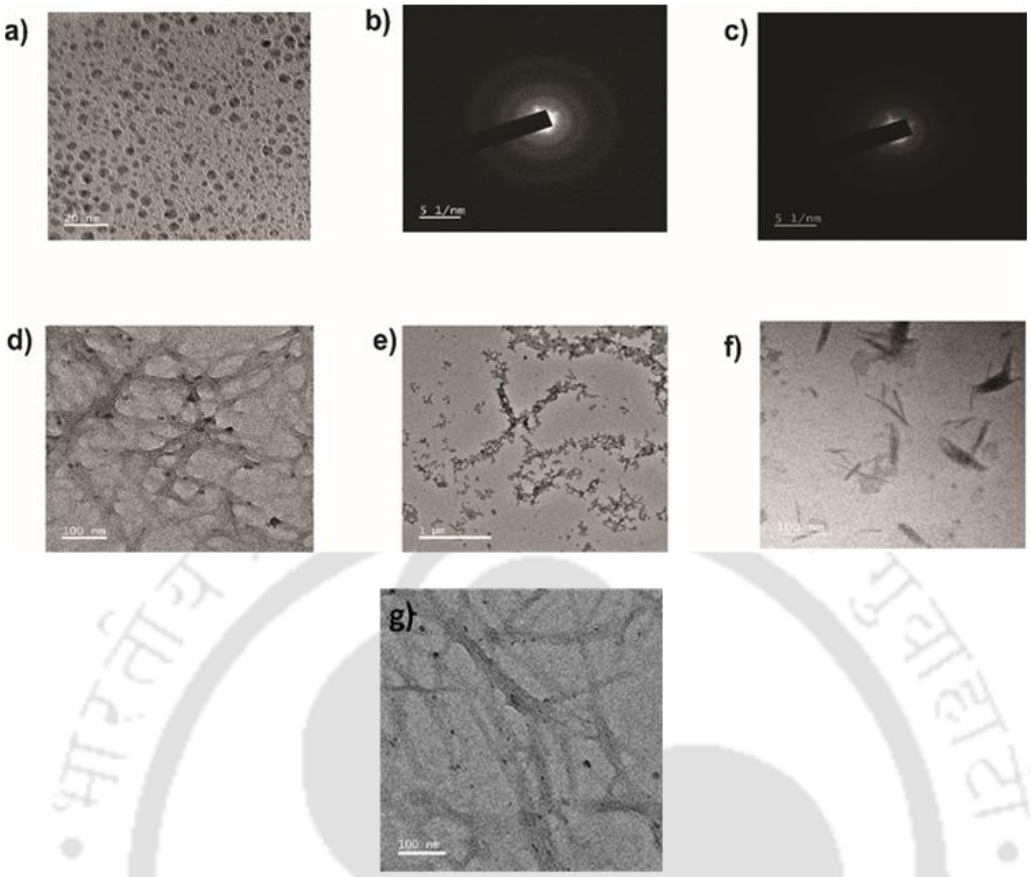

Figure C-3: *(a) TEM images of Aβ40 monomers. (b) SAED pattern of Aβ40 fibrils. (c) SAED pattern of Aβ40 monomers. (d) TEM image of preformed mature Aβ40 fibrils. (e) Interaction of PFBZ with mature Aβ40 fibrils evidenced through TEM. (f) Disintegration of mature Aβ40 fibrils by PFBZ nanodots. (g) Control Study: Incubation (pH 7.0, 37 °C) of preformed mature amyloid fibrils (10 μM) for 10 days.*

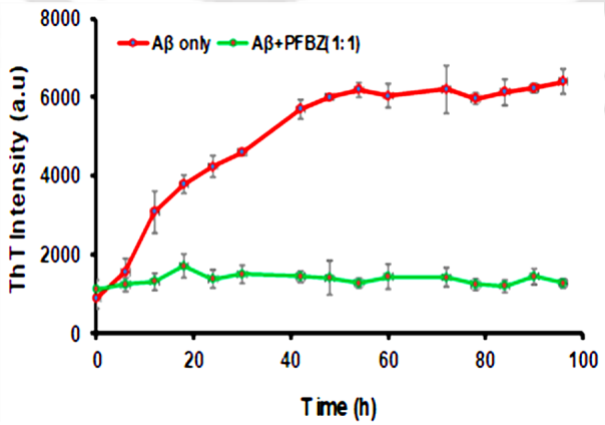

Figure C-4: *Fibrillation kinetics of Aβ40 (10 μM) in presence of catalytic amount of preformed oligomer (seed) and in absence of PFBZ in 10 mM phosphate buffered saline for 96 hours in 37 °C. The fibrillation kinetics was measured by ThT binding assay. Data are presented as mean ± S D, n=3.*

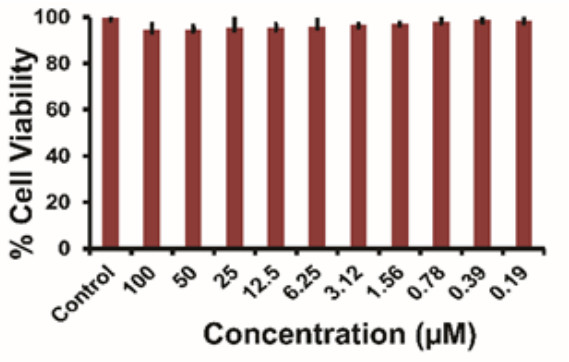

Figure C-5: *Cell viability of PFBZ chaperone in BHK cell line using MTT assay.*

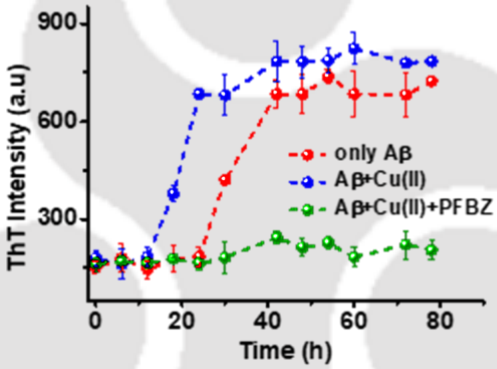

Figure C-6: *Fibrillation kinetics of preformed Aβ40 (10 μM) in with Cu(II) and in absence of PFBZ in 10 mM phosphate buffered saline for 96 hours in 37 °C. The fibrillation kinetics of Aβ40 was measured by ThT binding assay. Data are presented as mean ± S D, n=3.*

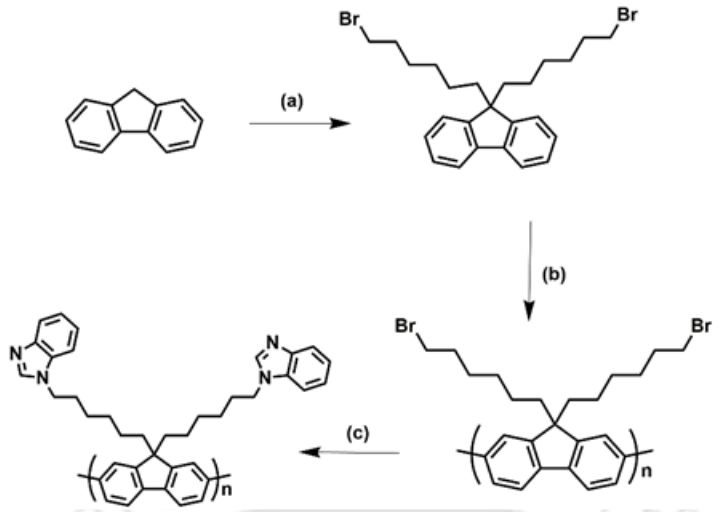

a: 1,6 Dibromohexane, 50% aq. NaOH, TBAI; **b**: $FeCl_3$, nitrobenzene, **c**: Benzimidazole, K_2CO_3, DMF.

Figure C-7: *Synthetic scheme of PFBZ.*

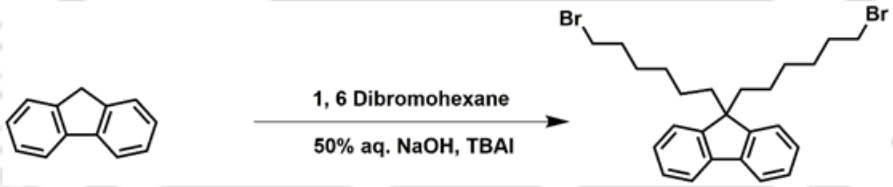

Figure C8: *Synthetic scheme of Fl to Fl-Br.*

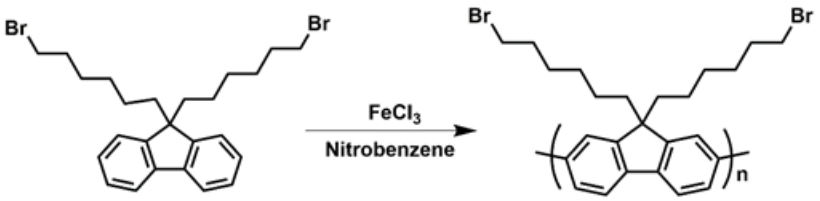

Figure C-9: Synthetic scheme of Fl-Br to PFBr.

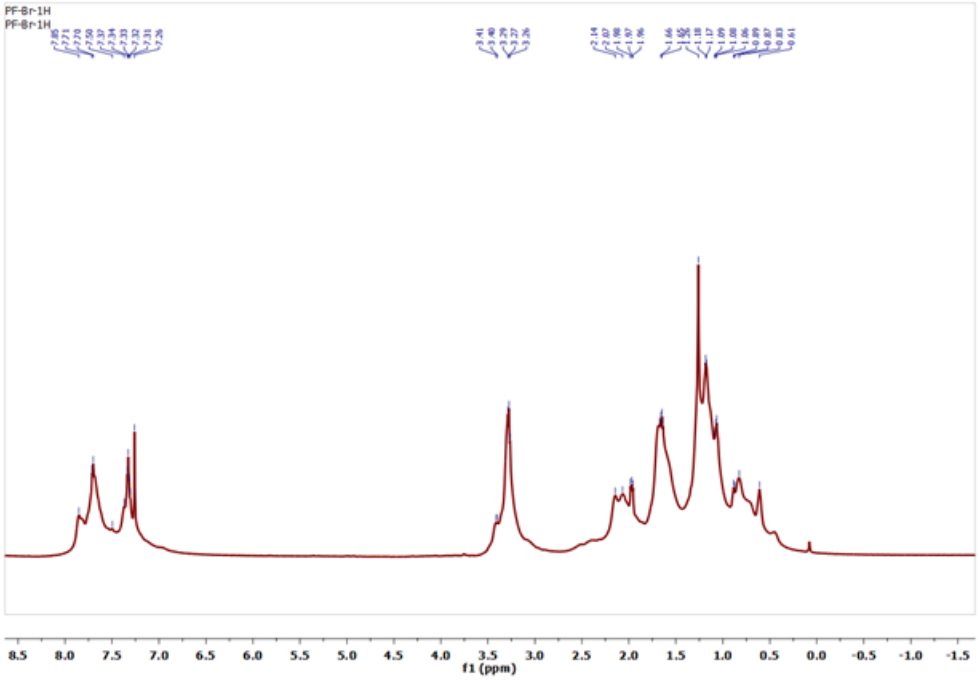

Figure C-10: [1]H NMR spectrum of PFBr.

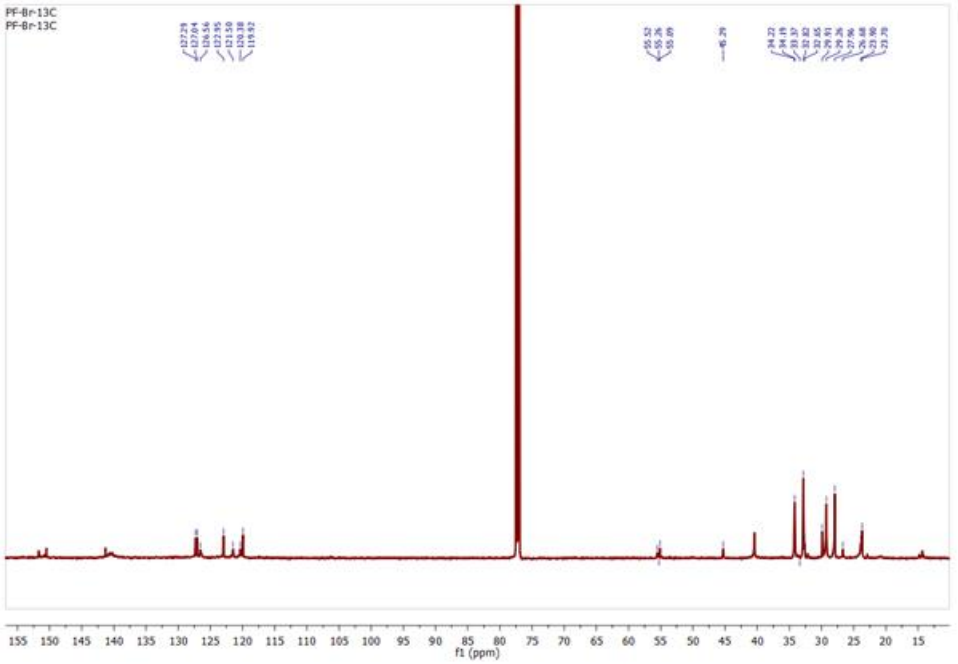

Figure C-11: [13]C NMR spectrum of PFBr

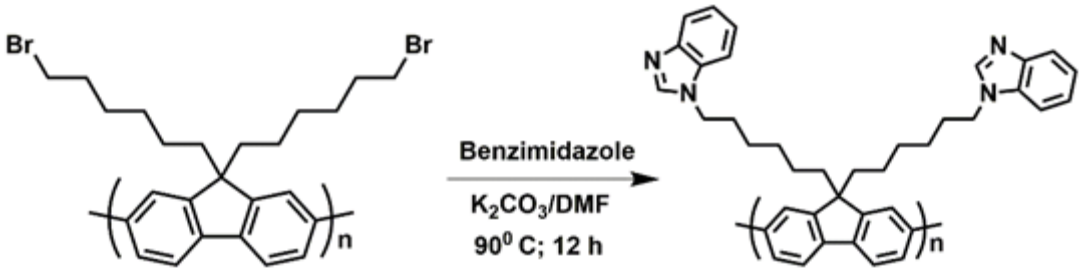

Figure C-12: *Synthetic scheme of PF-Br to PF-BZ.*

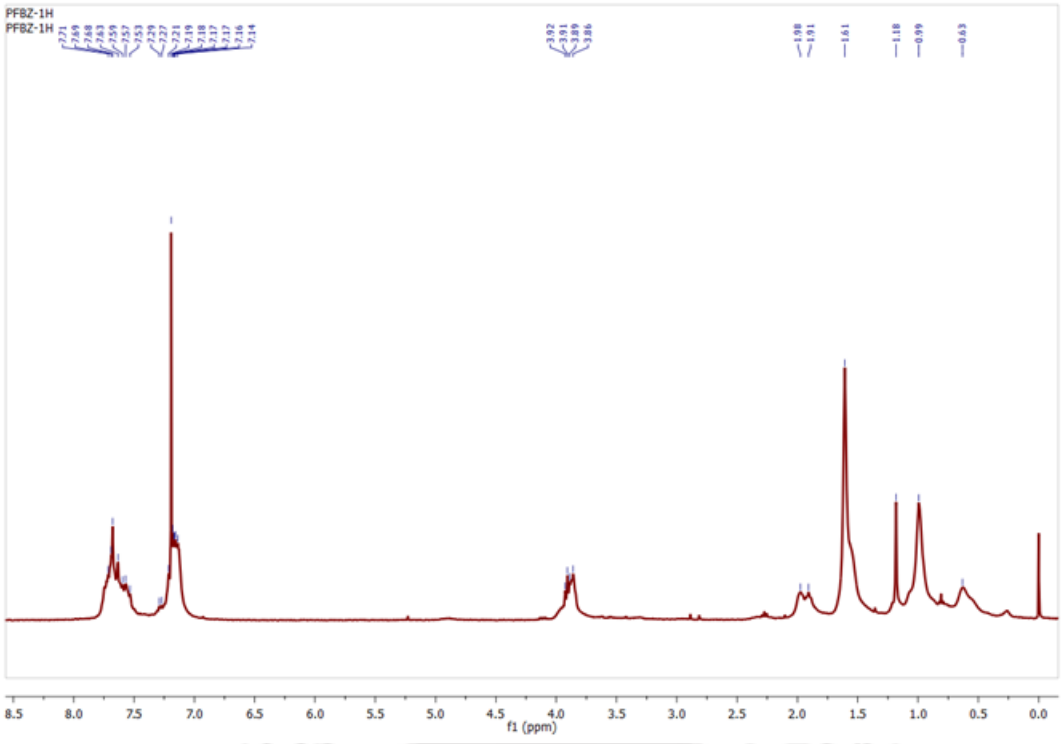

Figure C13: *^{1}H NMR of PFBZ.*

5

Self-Assembly Driven Formation of Functional Ultra-long 'Artificial Fiber' to Mitigate Neuronal Damage Associated with Alzheimer's Disease

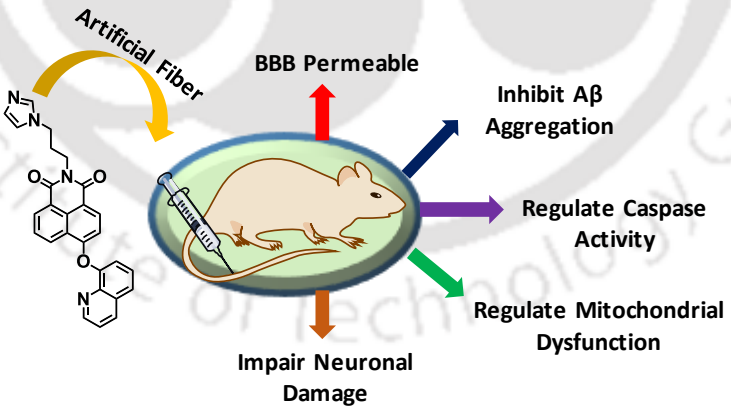

1. **Mondal, S.**; Yoya, V.; Ghosh, P.; Kalita, P.; Kumar, S.; Iyer, P. K.* Self-assembly driven formation of functional ultra-long 'artificial fiber' to mitigate neuronal damage associated with Alzheimer's disease. *(Communicated)*

5

Self-Assembly Driven Formation of Functional Ultra-long 'Artificial Fiber' to Mitigate Neuronal Damage Associated with Alzheimer's Disease

Abstract

Fibrillation of Amyloid beta (Aβ) is the key event in amyloid neurotoxicity process that induces a chain of neurochemical events including oxidative stress, caspase activation, PARP cleavage and mitochondrial dysfunction resulting in neuronal loss and memory decline manifesting clinical dementia in human. Herein, we report the development of a novel drug, INHQ and achieve functional nano-architectures via self-assembly process such that ultra-long fibres are achieved spontaneously. With specifically decorated functional groups on INHQ such as imidazole, hydroxyquinoline, hydrophobic chain and hydroxyquinoline molecules, these ultra-long fibres co-assembled efficiently with toxic Aβ oligomers and mitigated amyloid induced neurotoxicity by blocking the aforementioned biochemical events leading to neuronal damage in mice. These functional ultra-long 'Artificial Fibers' morphologically resemble amyloid fibers and provide higher surface-area of interaction that improve its clearance ability against Aβ aggregates. The efficacy of this novel INHQ molecule was ascertained by its high interaction ability with Aβ. Moreover, this injectable, ultra-long INHQ functional 'artificial fiber' translocates through blood brain barrier and successfully attenuates amyloid triggered neuronal damage and

pyknosis in the cerebral cortex of WT mouse. Utilizing various spectroscopic techniques, morphology analysis, *in vitro, in silico* and *in vivo* studies these ultra-long INHQ fibres hold great promise for treating neurological disorders at all stages with a potential to replace existing medications, reduce complications in the brain and eradicate amyloid triggered neurotoxicity implicated in numerous human disorders through a rare synergistic mechanism.

5.1. Introduction

Alzheimer Disease (AD) is a fatal age dependent neurodegenerative disorder that results in irreversible memory decline and behavioural changes in humans. Post-mortem analysis of AD brain reveals that extracellular Aβ aggregates and neurofibrillary tangles are the major hallmark of AD.[1] According to the amyloid cascade hypothesis, the imbalance between Aβ catabolism and anabolism leads to enhanced amount of Aβ aggregates that initiate a chain of neurochemical events resulting in neuronal death manifesting clinical dementia.[2-3] Recent report reveals that metastable, soluble Aβ oligomers are the most neurotoxic species and play key role in neuronal damage.[4-5] The β enriched oligomers produces high level of oxidative stress resulting in mitochondrial dysfunction.[6] As mitochondria operates a wide range of cellular process like metabolism and energy production, the consequence of mitochondrial dysfunction can be devastating. In addition to this, the defensive mechanism of mitochondria against oxidative stress and protein misfolding could further accelerate the progression of AD.[7] Also role of Poly(ADP-ribose) polymerase (PARP) has been implicated in mitochondrial dysfunction. A recent report reveals that PARP induces mitochondrial apoptosis by releasing apoptosis inducing factor (AIF) to cause depolarization in mitochondrial membrane potential. Several therapeutic materials including peptides, engineered nanoparticles, functionalized polymers and most recently monoclonal antibodies have exhibited appreciable degree of anti-Alzheimer activities.[8-13] However, most of these amyloid targeting therapeutic material has proven to be inefficient and failed in the different phases of clinical trial.[14-15] One plausible reason behind such failure may be the involvement of multidimensional toxicity associated with AD that includes oxidative stress, PARP cleavage, Caspase activation and mitochondrial dysfunction etc. Herein, an amyloid targeting molecule (INHQ) that spontaneously self-assembles into ultra-long fibers and shows striking resemblance with the amyloid morphology has been developed. As fibrillar amyloid aggregate plays key role in amyloid neurotoxicity, targeting fibrillar aggregates using novel drug molecules would be a highly efficient approach. In search of amyloid targeting

novel drug molecules, an 'Artificial Fiber' is highly preferred as it provides higher surface area of interaction. Keeping this vital knowledge in mind, INHQ has been designed by integrating specific functionalities such as imidazole, hydroxyquinoline, hydrocarbon chain of specific length and naphthalimide core that promoted the controlled self-assembly and help INHQ to self- aggregate into fiber like morphology. Newly designed 'artificial fiber' functions to reduce multifaceted toxicity such as Aβ aggregation, PARP fragmentation, caspase activation, and mitochondrial damage involved in AD (Scheme 5.1). Multiple lines of evidences from our in vitro and in vivo studies confirms that INHQ is able to translocate through blood brain barrier (BBB) and protect the neuronal cells

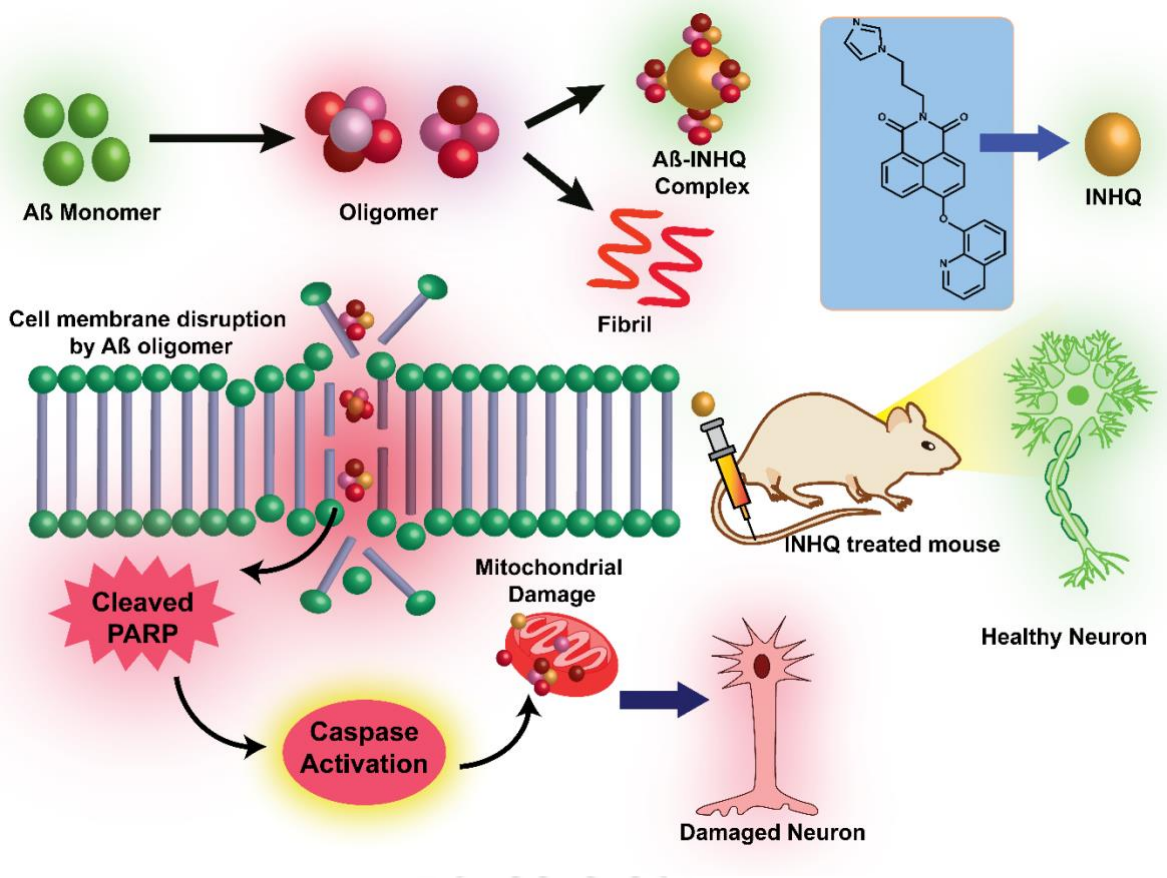

Scheme 5.1: *Schematic presentation of Biochemical pathway associated with Amyloid mediated neuronal damage and neuroprotection by INHQ.*

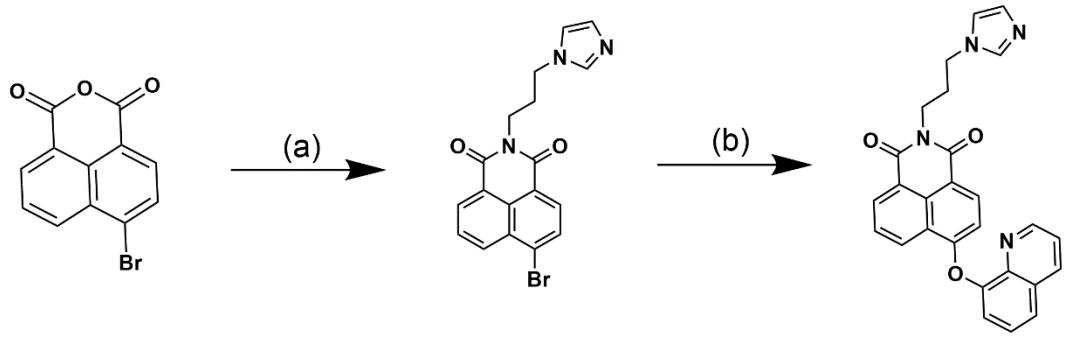

Scheme 5.2: *Synthetic scheme of INHQ. a: 1-(3-Aminopropyl) imidazole, Ethanol, 85 ^{o}C; 12 h b: 8-hydroxyquinoline, K_2CO_3, DMF, 24 h.*

from amyloid induced neurotoxicity in a multifaceted way. Such rapid and efficient co-assembly process of an ultra-long fiber with amyloid peptides at all stages has been observed for the first time and provides a promising lead structure to guide the design of small molecule based anti-Alzheimer drugs.

5.1 Experimental Section

5.1.1 Synthetic Scheme

INHQ was synthesized according to the Scheme-5.2. The precursor INDA (imidazole appended 4-bromo-1,8-naphthalimide) was synthesized through condensation reaction of 4-bromo-1,8-naphthalic anhydride with 1-(3-Aminopropyl) imidazole following a reported protocol (Scheme 5.2).[16] INHQ was synthesized from INDA by a nucleophilic phenoxide substitution reaction with 8-Hydroxyquinoline in presence of a weak base, potassium carbonate (Scheme 5.2). Finally, the crude product was purified using column chromatography. Final pure product was characterised by ^{1}H NMR and ^{13}C NMR spectroscopy (Figure D1 and D2).

5.2 Results:

Aggregation induced emission offers an excellent platform to achieve fine control over morphology of new drug molecules. The design has been motivated from our previous report that explore morphology of some well known Naphthalimide based AIEgens functionalized with butyl (BNQ), hexyl (HNQ), octyl (ONQ), cyclohexyl (CHNQ) and methylcyclohexyl (MCHNQ) pendant chain.[17] Among this, only HNQ offers regular

nanofiber like morphology (Figure D3). INHQ has been designed by integrating an imidazole group over HNQ. INHQ shows aggregation induced emission (AIE) and spontaneously self-assemble to form artificial fiber in aqueous medium (Figure D4). The 'artificial fiber' shows strong affinity towards matured amyloid fiber and block early stages of oligomerisation.

The interaction of INHQ and Aβ40 was primarily anticipated through zeta potential measurement (Figure 5.1a). At pH 7.4 (10 mM PBS, 37 °C), Aβ40 exhibits negative zeta potential (-2.91 mV). In contrast, INHQ possesses a highly positive zeta potential (+7.07 mV), which on interaction with Aβ reduces up to +0.648 mV indicating adsorption of negatively polarized Aβ on positively charged INHQ surface. Owing to the restricted rotation of the photo-excited probe, INHQ (20 μM, 37 °C, pH 7.2, 10 mM PBS buffer) exhibits time dependent fluorescence enhancements on incubation with equivalent amount of Aβ40 (Figure 5.1b). Interestingly, the emission of INHQ reached maxima at 36 hours, and decreased regularly thereafter. The non-linear time dependent variation indicates differential interaction of INHQ with distinct Aβ conformers such as monomers, oligomers and fibrils. Previously, we have reported time dependent variation of zeta potential of Aβ with respect to extent of aggregation.[8] Zeta potential of the Aβ oligomers (negatively charged) decreases up to 24 hours and again increases after passing through a minima. Hence, the interaction with positively charged INHQ and amyloid oligomers also increase with time and again decreases after attaining a maximum value. Considering the strong electrostatic interactions, the impact of INHQ on Aβ fibrillation was studied using ThT assay (Figure 5.1c). The fibrillation kinetics follows a usual amyloid growth model comprised of a lag phase, elongation phase and a plateau (Figure 5.1c). In case of native Aβ (20 μM, 37 °C, pH 7.2, 10 mM PBS buffer), elongation phase appeared at 24 hours, followed by a plateau at 42 hours indicating maximum fibril formation. Aβ monomers possess hydrodynamic diameter of 21 nm which increased up to 4150 nm upon fibrillation (Figure 5.1d). Although DLS measurement does not provide correct size of the monomer, a comparative lower hydrodynamic radius as obtained from DLS indicates the strong inhibition in presence of INHQ. However, in presence of sub-stoichiometric amount (0.01 equivalent) of INHQ fibres, elevation in ThT intensity indicated a sharp dip in aggregation propensity as observed markedly. When 1 equivalent, INHQ was used, no enhancement in ThT intensity was observed which indicates complete inhibition of Aβ fibrillation. The inhibition in fibrillation is mainly due to the electrostatic interaction and efficient receptor ligand interaction that leads to the formation of stable Aβ-INHQ complex with hydrodynamic diameter 459 nm. This was further verified through Native PAGE electrophoresis (Figure 5.1e). Native Aβ undergoes oligomerisation which was

confirmed by the presence of multiple smear at 17-130 kDa. On treatment with of INHQ

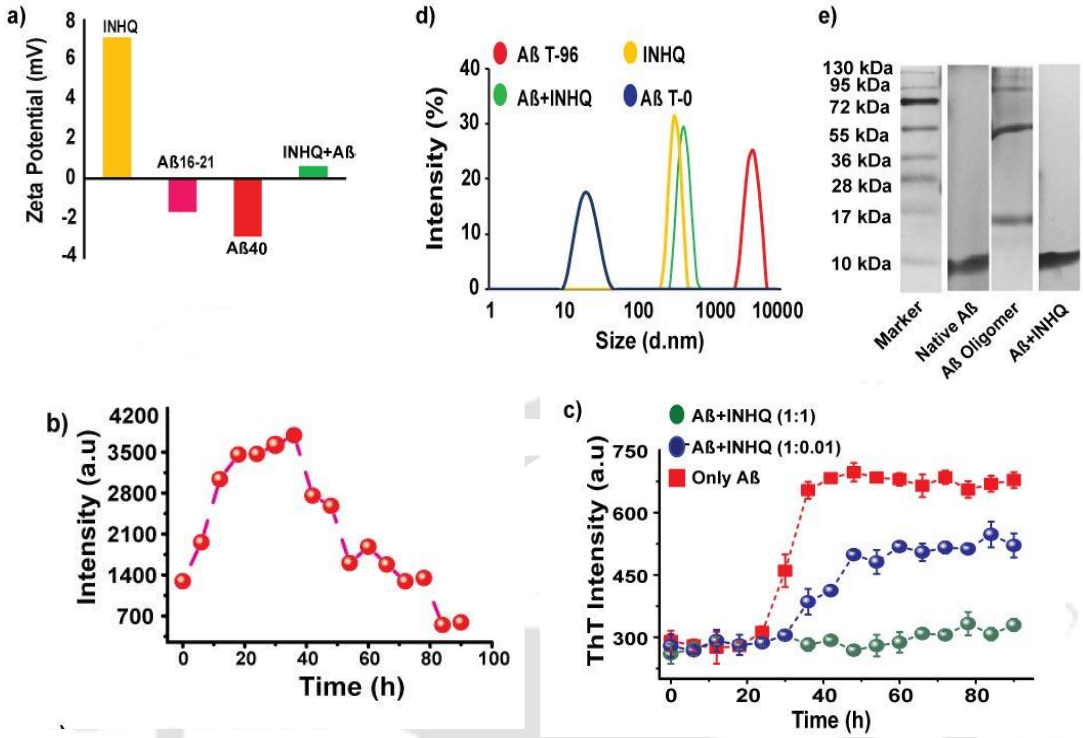

Figure 5.1: *a) Zeta potential of INHQ, INHQ- Aβ40 co-aggregate, Aβ40 and Aβ16-21 at pH 7.0 (10 mM PBS buffer). b) Time dependent Fluorescence spectra of INHQ (10 µM) incubated with Aβ40 (10 µM, wavelength: 365 nm). c) Fibrillation kinetics of Aβ40 (20 µM) in presence and in absence of INHQ in 10 mM phosphate buffered saline for 96 hours in 37 ºC. The fibrillation kinetics of Aβ40 was measured by ThT binding assay. Data has been presented as mean ± S.D, n=3. d) DLS measurement: Hydrodynamic diameter of Aβ40 before and after fibrillation in presence and in absence of INHQ. Aβ40 fibril and Aβ40+INHQ co-aggregate was made by incubating for 96 hours. e) Native-PAGE gel electrophoresis of Aβ40, Aβ40 oligomers and Aβ40+INHQ, f) ^{1}H NMR spectra of INHQ and INHQ+ Aβ40 complex at 298 K.*

fibers, oligomeric bands disappeared and only the band similar to the pre-aggregated (i.e., monomer and dimer) Aβ survived. To obtain further insights into the molecular level interaction among INHQ fibers and Aβ40, molecular docking study was performed using Swissdock which offers numerous clustered docked poses ranked according to CHARMM energies.18 The structure of the INHQ was developed and energy optimized in Gaussian 09 using basis set DFT, B3LYP, 631G (Figure 5.2a). The interactions involved in binding

of INHQ with Aβ fibrils has been illustrated in (Figure 5.2b). Molecular docking studies were carried out using an experimentally resolved structure of Aβ40 fibrils (PDB ID 2LMP).[18] Remarkably, INHQ showed higher binding affinity with Aβ40 fibrils compared to Curcumin, a known binder of Aβ40 fibrils (Figure 5.2c, and Figure D5). Docking studies reveal that INHQ predominantly binds to 35MVGGVV40, the C-terminal hydrophobic domain of Aβ40 (Aβ35-40) with ΔG value -8.48 kcal/mol. INHQ being a conjugated system interact predominantly through its π cloud mainly via π-cation and π-alkyl interactions (Table 5.1). The C-terminal hydrophobic core 35MVGGVV40 plays a vital role in early events of oligomerisation. Hence, potential binding to this region leads to efficient inhibition in fibrillation kinetics (Figure 5.1c).[19] Gly37 is involved in structural conversion of oligomers to fibrils. Gly33 and Met35 plays a vital role in amyloid toxicity. Gly33 of one Aβ molecule is known to be attacked by a sulphur radical of Met35 which leads to the formation of a free radical on Gly33.[20] The free radical formed, accelerates the fibrillation rate and induces oxidative damage in brain.[21] Hence, multiple π-alkyl interaction with the Met35 and strong π-cation interaction with Gly33 leads to the inhibition in fibrillation and potential attenuation in Aβ neurotoxicity. The binding affinity was further compared with Curcumin, a well-known potential sequester of Aβ oligomers (Figure D5 and D6) and was found to be lower than INHQ.[22] Moreover, curcumin yields only 4 interactions while INHQ yields 11 interactions with Aβ.

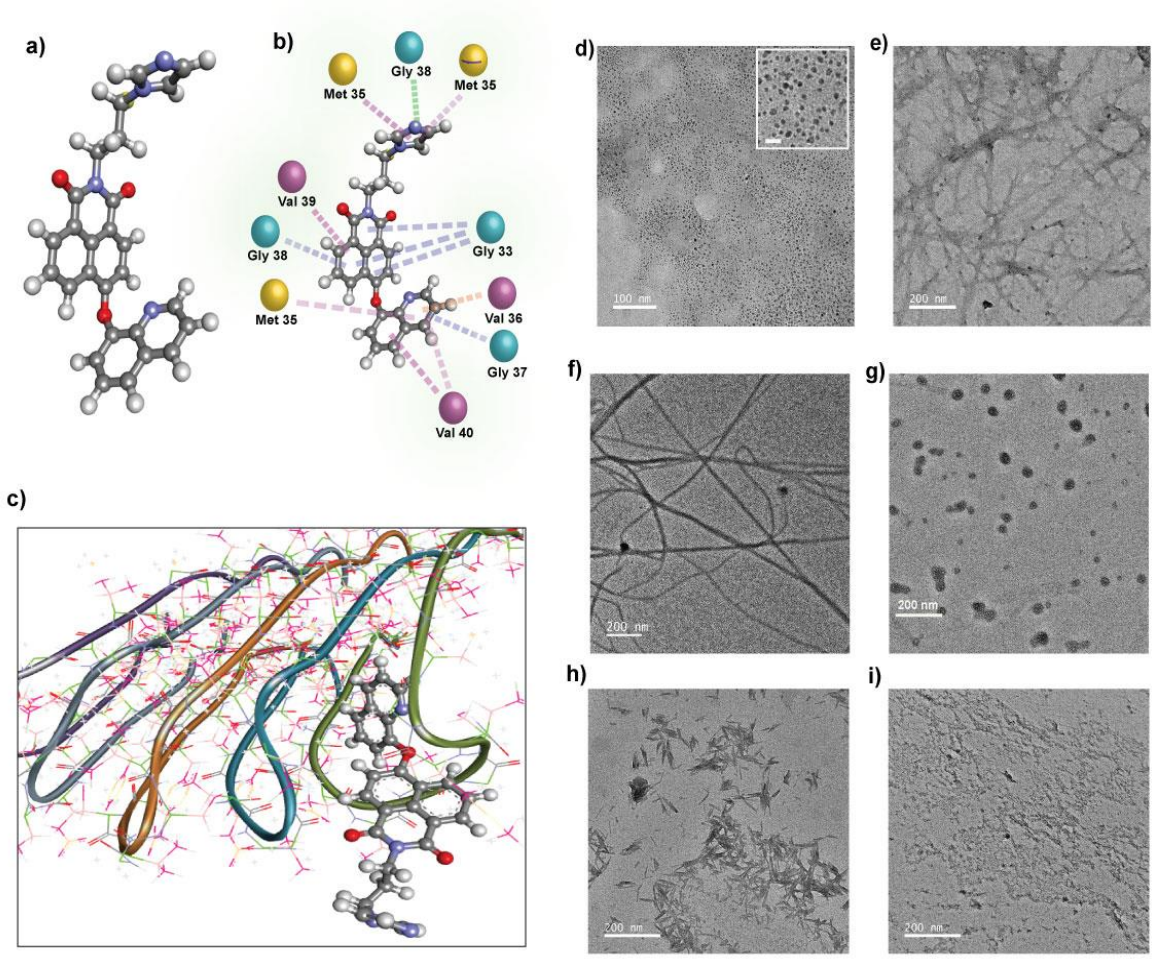

Figure 5.2*: a) Energy optimized structure of INHQ using Gaussian 03 using following parameters: B3LYP method and 6.31G basis set; b) Docking mode of INHQ with fibrillar Aβ40 aggregates. INHQ is shown in the ball & stick mode, the protein in cartoon mode. d-i) TEM image of Aβ40 monomer, fibrillar Aβ40, INHQ in 10 mM PBS buffer, Aβ40+INHQ, matured Aβ40 fibrils incubated with INHQ for 3 days, matured Aβ40 fibrils incubated with INHQ for 7 days respectively.*

The naphthalimide derivatives are well known for their aggregation behaviour.[23] Naphthalimide core attached with 8-hydroxyquinoline predominantly undergoes self-assembly in aqueous media to form 'fiber' like structure.[16] Similarly, INHQ forms ultra-long nano fibrillar morphology (size) to resemble 'amyloid fibre' like surface in physiological conditions mainly via π-interactions (Figure 5.2f). Consequently, INHQ provides higher interaction area resulting in enhanced peptide-ligand interaction. The monomeric Aβ possessing nano-spherical morphology (size) (Figure 5.2d) undergoes self-

Table 5.1: *Summary of molecular interactions involved in between INHQ and curcumin with Aβ40 fibrils through molecular docking.*

Inhibitor	Interacting Amino Acid	Type of Interaction	Bond Distance (°A)	ΔG (kcal/mole)
INHQ	Gly33	π-cation	3.52	-8.48
	Gly33	π-cation	4.26	
	Gly33	π-cation	3.63	
	Met35	π-alkyl	4.99	
	Met35	π-alkyl	5.47	
	Met35	π-alkyl	4.85	
	Val 36	π-amide	4.34	
	Gly37	π-cation	3.97	
	Gly38	hydrogen bond	2.77	
	Val39	π-alkyl	3.95	
	Val40	π-alkyl	4.85	
Curcumin	Ala30	π- π stacking	5.11	-7.79
	Val24	π- π stacking	5.21	
	Ala30	hydrogen bond	2.71	
	Phe20	π-cation	5.00	

aggregation to convert into toxic fibrillar morphology (Figure 5.2e) on incubation for 96 hours in physiological condition. ultra-long INHQ fibers were incubated with fibrillar Aβ40, spherical morphology of Aβ-INHQ was observed rather than fibrillation, owing to the efficient co-assembly process (Figure 5.2g). Thus, the 'artificial fiber' like morphology of INHQ 'exerts higher inhibitory effect towards Aβ at any given stage resulting in mutual inhibition in fibrillation including clearing the preformed mature amyloid fibrils. The preformed mature fibrils were incubated with INHQ for seven days and TEM images were recorded at regular time intervals. After three days of incubation the fibrils were found to be shortened and partly disrupted (Figure 5.2h). On further incubation for seven days, complete disruption of the co-assembly and clearance of the preformed fibrils was achieved (Figure 5.2i).

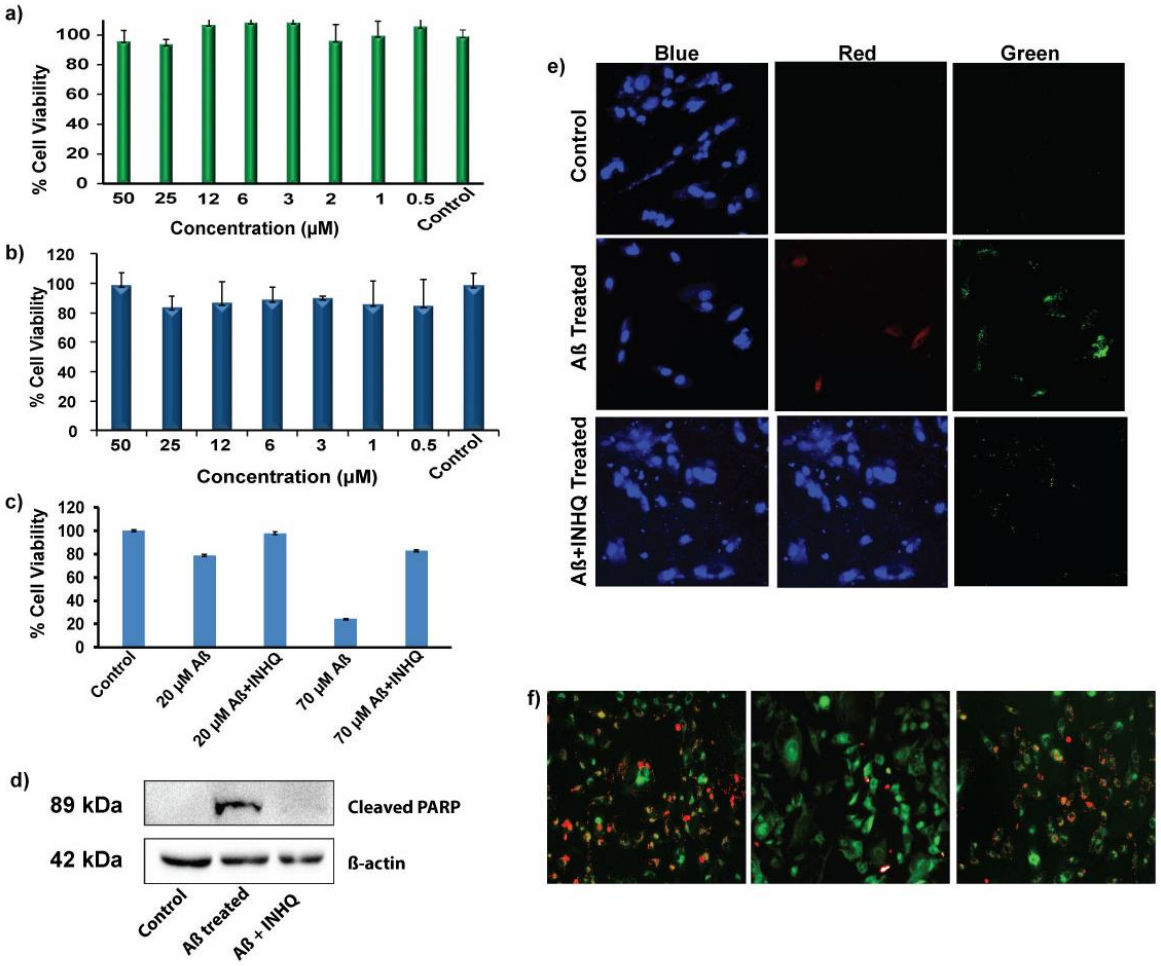

Figure 5.3: *Cell viability of INHQ in (a) SH-SY-5Y cell line and (b) BHK cell line using MTT assay. c) Reduction in Aβ40 neurotoxicity in presence of INHQ. Cell viability was measured by MTT assay and the data were shown as the mean ± SD of replicate groups. d) Western blot analysis of SH-SY-5Y cell lysates using PARP antibody. β-actin was used as loading control. (Primary antibody Catalogue #44-698G (invitrogen), secondary antibody used was anti-rabbit) e) Colorimetric evaluation of caspase-3 activation. g) Monitoring Mitochondrial membrane potential using JC-1 dye.*

5.2.4. Mitigation of Aβ Toxicity *in vitro*:

The cell viability of INHQ in variable concentration ranging from 50 to 0.5 μM was evaluated in both human neuroblastoma (SH-SY-5Y) and fibroblast (BHK) cell lines to show very high cell viability (Figure 5.3a and 5.3b). However, treatment of SH-SY-5Y cells with Aβ oligomers (70 and 20 μM) induced a concentration dependent cell death (24% and 76% respectively) (Figure 5.3c). We propose a biochemical cycle involved in such Aβ

induced cell death that involves poly ADP-ribose polymerase (PARP) and caspase dependent apoptotic pathways followed by mitochondrial damage. Caspase is a class of enzyme that triggers a series of reactions resulting ultimately in cell apoptosis. Hence, caspase activation constitutes an important step in early stage apoptosis.[24] When neuro cells were treated with 20 μM Aβ oligomers for 24 hours, a large number of caspase-3 active cells along with some apoptotic cells were observed (caspase activity can be observed in green channel and dead cells in red channel) (Figure 5.3e). However, caspase activation was completely inhibited by equivalent amount of INHQ and no caspase active cells were found in presence of INHQ. The activated caspase further cleaves PARP which is a general features of cell apoptosis that mainly indicates breakage of DNA strands.[25] To evaluate the extent of PARP cleavage related to neuronal apoptosis SH-SY-5Y cells were treated with 20 μM Aβ oligomers. After 24 hours of incubation a C-terminal fragment (molecular weight: 89 kDa) of PARP was recognized, while full length PARP (molecular weight: 116 kDa) was absent (Figure 5.3d). The cleaved PARP is known as an endogenous mitochondrial toxin that depolarizes mitochondrial membrane potential (MMP) and disrupts membrane integrity.[26] The fluorometric imaging of MMP was performed using JC-1 dye, a dual colour probe that targets live mitochondria in a membrane potential dependent manner. The dye undergoes J-aggregation to emit intense red fluorescence upon entering inside live mitochondria with high membrane potential. However, it does not undergo any aggregation and emit green emission in dying mitochondria with low MMP (Figure 5.3f). In control cells, red fluorescence was dominant but 24-hour treatment with Aβ oligomers reduced the red emission suggesting disruption in mitochondrial membrane. However, the reduction in MMP was markedly inhibited when cells were treated with Aβ in the presence of INHQ. The Aβ oligomers usually interact with the cyclophilin-D and helps to open mitochondrial permeability transition pore (mPTP).[27] The opening of mPTP allows uncontrolled transportation of cytosolic solute that in turn damages the mitochondrial structure and dysfunction including impaired energy production and initiation of neuronal apoptosis.[27] The result is in well accordance with PARP cleavage and Caspase activation assay. INHQ being an amyloid sequester, binds with Aβ to maintain it in its monomeric form and blocks multiple biochemical pathways that leads to toxicity. Consequently, activated caspase and cleaved PARP was not observed when treated with Aβ+INHQ. The inhibition in caspase activation and PARP cleavage highly improves the cell viability.

5.2.5. *In Vivo* Studies:

Swiss albino mice (weight 25-30g) were used as the experimental animal model in the present study. The animal experiments were completed as per the approval of the IAEC, Gauhati University. The mice were caged at usual 12:12 hours light dark cycles with usual diet and water ad libitum. Daily handling of the animals was maintained to reduce the stress. Firstly, the INHQ cytotoxicity was evaluated in RBCs (Figure 5.4a). A lower dose (i.e. upto 6μg/mL) of INHQ treatment shows no significant haemolytic activity. However, at significantly higher concentration (25 and 50 μg/mL) some haemolytic activity was observed. After 90 minutes of incubation, precipitated erythrocytes were stained with Leishmann stain using standard protocol and subjected to microscopic observation. Micro photographic analysis reveal slightly swelled blood cells when treated with high dose of INHQ (Figure D7). However, INHQ treatment in lower dose does not yield any RBC deformation.

For histological analysis, mice were injected with INHQ at the dose of 137 μg /mice through tail vein. After 1 hour of circulation, animals were sacrificed and brain tissues were collected. The sections were stained with DAPI and subjected to confocal microscopy to observe bright yellow fluorescence indicating presence of INHQ which confirms translocation of INHQ through BBB under normal circulation (Figure 5.4b). BBB permeability remained a central challenge as well as prerequisite in CNS drug discovery. Many potential drugs have failed in different stages of clinical trials because of their poor BBB permeability. However, INHQ efficiently permeates through BBB and satisfy such prerequisite. The mice were further administered with FITC conjugated Aβ and INHQ through Intracerebroventricular injection to visualize relative distribution of INHQ and Aβ. The sections were monitored under confocal microscopy to observe colocalization of INHQ and Aβ in the brain (Figure 5.4c). In order to observe, neuronal damage triggered by Aβ40 oligomers, the mice were injected with PBS (control), oligomeric Aβ aggregates, and Aβ-INHQ co-aggregates through Intracerebroven-tricular injection (3 mice per group; Dose: 10 μg PBS/mice, 108.2 μg Aβ/mice, 121.8 μg Aβ-INHQ/mice respectively) for seven days. Histological sections were stained with haematoxylin and eosin (H&E stain) using standard protocols and observed under light microscope (Figure 5.4d).[28] In the brain cell morphometric analysis, plate: A shows features of brain with normal histological architecture. In Aβ induced mice group (Figure 5.4e), mainly the brain parenchymal cells have been largely affected and become vacuolated in some region (black arrow). In parallel to this, several other feature of toxicity including pyknotic nuclei of glial cells have also been observed in the white matter area (yellow arrow). Some Leptomeningeal deformation was also observed (black arrow). Such toxic features can be correlated with very

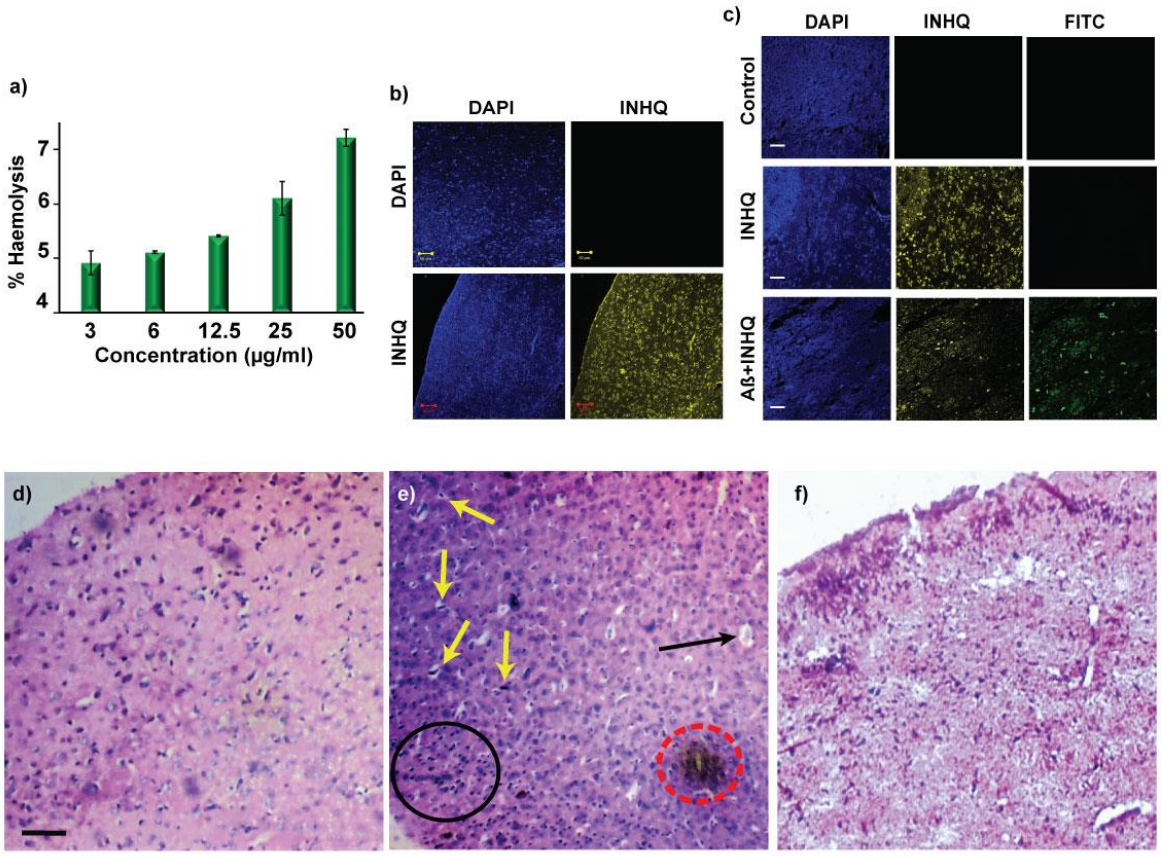

Figure 5.4: *a) a) Concentration dependent Haemolysis induced by INHQ. b) Co-localization of INHQ in WT mouse hippocampus, Images were captured at 20× magnification using confocal microscope. Scale bar: 50 micron colocalization of INHQ and Aβ in mouse hippocampus. Scale bar: 50micron. d-f) Histochemical staining of mouse brain sections with haematoxylin and eosin of (a) control, (b) Aβ treated. Numerous signatures if neuronal damage was observed. Yellow arrow indicates pyknotic cells, black arrow indicates vacuolated cells and black circle indicates neocortex region and red circle indicates region with internal haemor-rhage. (c) Aβ treated in presence of INHQ. Scale bar, 50 µm.*

in vitro toxicity of the amyloid oligomers that exert their toxicity mainly by destroying cell membrane. However, in INHQ treated sample (Figure 5.4f), cells appear with few lesions and tissue damage appears to be minimized. Pyknotic cells and vacuolated region significantly reduced which indicated neuroprotective ability of INHQ from Aβ induced neurotoxicity.

5.3. Discussion

In search of efficient amyloid inhibitors, molecules with amyloidogenic surface motif can be excellent choice because of enhanced surface area of interaction. The advent of aggregation induced emission (AIE) has received significant attention in biomedical research because of its efficacy to tune nanostructure of organic drug molecules in aggregated state. Among the commonly encountered AIEgens, 1,8-napthalimide derivatives are the best choice as it undergoes self-aggregation through π interactions.[29] Suitable functionalization in the Naphthalimide core affects intramolecular π-π stacking and thereby offers a platform to fine tune morphology of such molecules.[17] Our previous re-port reveals that alkylation with different pendant chain like butyl (BNQ), hexyl (HNQ), octyl (ONQ), cyclohexyl (CHNQ) and methylcyclohexyl (MCHNQ) yields distinct nanostructure in their aggregate state.[17] BNQ shows elongated square pyramidal like

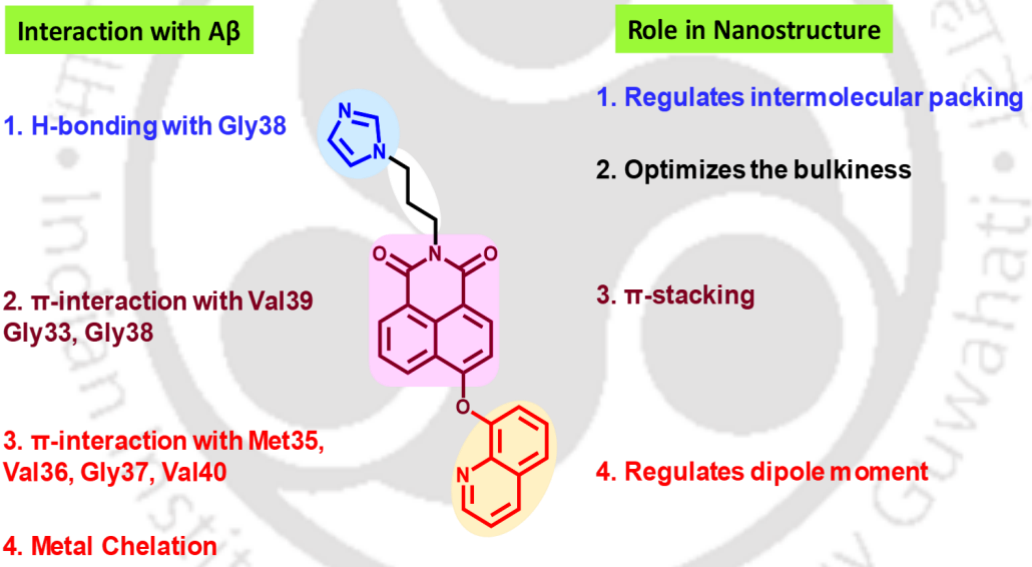

Figure 5.5: *Role of different parts of INHQ in regulating morphology and interaction with Aβ.*

structure, while symmetrical spherical nanostructure was produced by ONQ. Surprisingly, Microfiber and nano-rod like structure was observed in case of CHNQ and MCHNQ respectively. HNQ yields a regular nano-fiber like morphology. Although the congeners have similar electronic environment, a profound morphological disparity observed in their aggregated state which can be attributed to their pendant chain that affects in-termolecular packing in the aggregated state in terms of bulkiness. However, in parallel to the pendant chain, presence of nitrogen atom in quinolone ring functions like a trigger

and plays a crucial role in shaping nanoaggregates. HNN formed discrete nanoparticles but HNQ forms well defined nanofiber like morphologies. The morphological disparity can be attributed to the trigger-ing nature of the nitrogen atom in quinolone ring that affects the dipole moment of the system which in turn regulates molecular packing in aggregated state.

Being motivated from these observation, INHQ has been designed by integrating 8-hydroxyquinoline and imidazole functionality into naphthalimide core to target amyloid aggregation. Although, HNQ Shows amyloidogenic surface motif, it lacks biologically active targeting groups. Presence of an imidazole group in pendant chain enhances biological activities and dipole moment that helps the molecule to undergo J-type aggregation and herald thread like morphology similar to the amyloid fibres in aqueous medium.[16] The amyloid like surface motif provides an extra room to interact with fibrillary aggregates that results in clearance of matured Aβ fibrils. In parallel to this, the N atom in imidazole ring makes H-bonding with Gly38. Also, molecular docking study reveals that aromatic protons of imidazole, naphthalimide core and quinolone ring are involved in binding with Aβ35-40. 35MVGGVV40 (Aβ35-40) is the C-terminal hydrophobic domain of Aβ40 that involved in early stages of oligomerisation. The binding results in inhibition in oligomerisation that further blocks a chain of biochemical events that results in neuronal damage in brain. Hence, a Naphthalimide backbone decorate with imidazole group and hydroxyquinoline ring can be an excellent choice to explore their anti-Alzheimer activities.

5.3. Conclusion

A multi-targeted artificial fiber, INHQ comprised of pendant imidazole group and hydroxyquinoline functionality strapped to Naphthalimide backbone offers an excellent set of anti-alzheimer properties regulating ROS mediated mitochondrial dysfunction. Our *in silico* study reveals that INHQ binds to 35MVGGVV40 region of Aβ1-40 with very high binding affinity and blocks a biochemical cycle including caspase activation, PARP fragmentation and mitochondrial dysfunction which ultimately leads to amyloid toxicity. As a consequence, of such binding a marked elevation in neurotoxicity was observed. Hence, artificial fiber protects neuro cells from amyloid mediated neurotoxicity by blocking multiple events associated with this. The oligomeric Aβ aggregates produces multiple signatures of toxicity including internal haemorrhage, pyknosis etc. in WT

mouse hippocampus. INHQ has been shown to translocate through BBB and recover such amyloid mediated neuronal damage in mouse brain. Hence, INHQ satisfies all the key criterion essential for a potential anti amyloid material and claims it to be a potential lead for the development of anti-alzheimer drugs as an immediate application.

5.4. Materials and Method

5.4.1. Materials

All reagents were procured from Sigma Aldrich and utilized without purification. For experiments HPLC grade solvents and Milli-Q water were used. Amyloid-beta16-21(Aβ16-21) and Amyloid-beta 1-40 peptide fragment (Aβ40) was obtained from G.L Biochem Ltd., Shanghai, China. Borosil microscopy glass slides were used for microscopy study including Atomic Force Microscopy (AFM) and confocal microscopy. TEM grids were obtained of Pacific grid tech and used without any further modifications. Human Cerebrospinal Fluid was collected from Guwahati Neurological Research Centre and Hospital (GNRC), Guwahati, India following all the rules and regulation. A Brief Detail about the purpose of the experiment was described at the time of collection maintaining all the bioethics policy of the hospital. These samples were collected as a part of their routine medication.

5.4.1. Instrumentation:

Fluorescence and UV-Vis spectra were recorded using BioTek SynergyMx microplate reader and Perkin Elmer Lambda-25 spectrometer respectively. Perkin Elmer spectrometer was used for FT-IR spectra acquisition. The zeta potentials and hydrodynamic sizes measurements were performed using Nano-ZS90 Zeta sizer Nano series instrument. TEM images were recorded by JEOL 2100 transmission electron microscope. Atomic force microscopy (AFM) was performed on Bruker Innova SPM model, with the tapping mode. Field Enhanced Scanning Electron Microscopy images were recorded in Zeiss SIGMA 300 instrument. Bruker ASCEND 600 Nuclear magnetic resonance (NMR) instrument was used to record NMR spectra. Agilent mass spectrometer was used for mass acquisition. Fluorescent images were recorded in Nikon ECLIPSE Ts2R-FL fluorescent microscope.

5.4.2. Synthesis and Characterization of INHQ

4-bromo-1,8-naphthalic anhydride (554.2 mg, 2 m.mol) was dissolved in ethanol (20 mL) and 1-(3-Aminopropyl) imidazole (2 m.mol) was added to it at room temperature. The suspension was heated at 85 ºC with stirring for 12h. Then the product was cooled to room temperature and evaporated under reduced pressure. The mixture was extracted with chloroform and washed with water. Then it was dried over anhydrous Na_2SO_4 and concentrated. After that it was finally purified by column over silica gel with 2% ethyl acetate in hexane as eluent which gives pure INDA. INHQ was synthesised from INDA by a nucleophilic phenoxide substitution reaction with 8-Hydroxyquinoline in presence of a weak base, potassium carbonate. Finally, the crude product was purified using column chromatography. Final pure product was characterised by 1H NMR and 13C NMR spectroscopy.

^{1}H NMR (600 MHz, DMSO-d_6), δ (ppm): 8.857 (d, 1H), 8.774 (d, 1H), 8.604 (d, 1H), 8.314 (d, 1H), 8.212 (d, 1H), 7.745 (t, 2H), 7.515 (m, 2H), 7.415 (m, 2H), 6.971 (d, 2H), 6.663 (d, 1H), 4.159 (t, 2H), 4.00 (t, 2H), 2.185 (m, 2H)

^{13}C NMR (600 MHz, DMSO-d_6), δ (ppm): 164.6, 163.9, 160.8, 150.7, 141.1, 137.2, 136.3, 133.0, 132.0, 130.1, 129.7, 129.5, 126.7, 126.5, 125.6, 123.8, 122.2, 120.3, 118.7, 116.1, 111.1, 77.2, 77.0, 76.8, 45.0, 37.5, 29.7

5.4.3. Stock Solution Preparation:

10 mM INHQ was prepared in DMF by dissolving the required amount of solid powdered PFBZ and further diluted in phosphate buffered solution as per requirement. The solution was filtered by 0.22 μM syringe filter.

5.4.4. Preparation of Aβ40 monomer:

Aβ40 monomer was prepared using protocol mentioned in section 2.5.4.

5.4.5. Preparation of Aβ40 oligomer (tetramer):

Aβ40 oligomer(tetramer) was prepared following a protocol mentioned in 3.5.6.

5.4.6. Molecular Docking Study:

We extensively used to Swiss Dock web server to explore the molecular level interaction of Aβ40 fibrils with INHQ and Curcumin. The structure of the target protein (2LMP) was obtained from RSC PDB database. Structure of the ligand (both INHQ and curcumin) was developed in ChemDraw 18.1 and energy minimized in Gaussian 03 software using Basis set: DFT, B3LYP, d, p.

5.4.7. Toxicity Assay

Toxicity assay was performed using a protocol mentioned in section 3.5.9.

5.4.8. Measurement of ROS activities:

The generation of reactive oxygen species (ROS) is expected in healthy cellular entities. ROS production is triggered by photochemical reactions, auto-oxidation, and various enzymes (e.g., mitochondrial respiration, cytochrome P450, NADPH oxidase etc.) and is kept in control by the cell's usual detoxification mechanisms. Oxidative stress comes into play when there is an imbalance between ROS production and the cell's ability to scavenge them. This imbalance can cause transient or permanent oxidative damage in membrane lipids, proteins and nucleic acids. We have extensively used CellRox® green fluorescence to track ROS production *in vitro*. CellROX® Green reagent is a weakly fluorescent, cell-permeant dye that exhibits bright green fluorescence upon reaction with ROS (excitation/emission maxima = 485/520 nm). The presence of ROS can further be quantified by using a flow cytometer.

Cell culture: SH-SY-5Y cells is a neuroblastoma cell line derived from human bone marrow. SH-SY-5Y cells were cultured in complete growth media, Dulbecco's Modified Eagle Medium (DMEM, HiMedia) with 10% fetal bovine serum (Gibco) and antibiotics (Anti-Anti, Gibco) at 37 °C in 5% CO_2 incubator. Cell line used in this study were gifted by National centre for cell science (NCCS), Pune.

SH-SY-5Y cells were seeded in 3 plates at an initial seeding density of 1,00,000 cells/well in 100 µl medium. The cells were treated with PBS (control), toxic Aβ aggregates and Aβ+INHQ for 12 hours in 37 °C in 5% CO2. Then CellROX® Reagent at a final concentration of 5 µM was added to the cells and incubate for 30 minutes at 37°C.

After that, medium was removed and cell were washed with PBS buffer for 3 times. Then, ROS activities was measured in flow cytometer.

5.4.9. PARP Cleavage:

Poly (ADP-ribose) polymerase (PARP) is a family of proteins operates a number of cellular processes such as genomic stability, DNA repair and programmed cell death. PARP can be activated in cells experiencing stress and/or DNA damage.

Activated PARP usually destroys the cell of ATP in a process to repair the damaged DNA. ATP depletion in a cell results in lysis and cell death (necrosis). PARP also has the capability to trigger apoptosis via the production of PAR, which stimulates mitochondria to release apoptosis inducing factor (AIF). This mechanism appears to be caspase-independent. Cleavage of PARP, by enzymes such as caspases or cathepsins, typically inactivates PARP. The size of the cleavage fragments can give insight into which enzyme was responsible for the cleavage and can be useful in gathering information about the pathway of cell death that has been followed.

Cell culture: SH-SY-5Y cells is a neuroblastoma cell line derived from human bone marrow. SH-SY-5Y cells were cultured in complete growth media, Dulbecco's Modified Eagle Medium (DMEM, HiMedia) with 10% fetal bovine serum (Gibco) and antibiotics (Anti-Anti, Gibco) at 37 °C in 5% CO2 incubator. Cell line used in this study were gifted by National centre for cell science (NCCS), Pune.

Cultured SHSY-5Y cells were grown on 6-well plate and treated with 50 μM of Aβ aggregates and Aβ+INHQ. After 24 h, cells were washed with PBS. 100 μl of sodium dodecyl sulfate-polyacrylamide gel electrophoresis (SDS-PAGE) loading buffer was added to each well for immediate cell lysis and increased viscosity of the sample. The extract was transferred to microcentrifuge tube and heated at 95°C for 10 min. Total cell protein was separated by 12% SDS-PAGE and transferred to a nitrocellulose membrane. Membranes were blocked in phosphate-buffered saline 5% dry milk for 2 h and incubated with primary antibody overnight at 4 °C with shaking. The membranes were washed several times with phosphate-buffered saline/Tween-20 and incubated with horseradish peroxidase (HRP)-labeled secondary antibody for 1 h at room temperature with shaking. Band intensity was detected by ECL detection reagent (Biorad) with β-actin as an internal control.

5.4.10. Caspase Activation:

Caspase activation was study was performed using protocol mentioned in 4.8.6.

5.4.11. Mitochondrial Membrane Potential Assay:

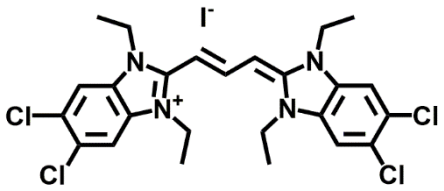

Structure of JC-1 dye

JC-1 is a novel cationic dye which accumulates in mitochondria. The dye exists as a monomer at low concentrations and exhibits green fluorescence, like fluorescein. At higher concentrations, the dye forms J-aggregates to exhibit a broad excitation spectrum and an emission maximum at ~590 nm. These characteristics make JC-1 a sensitive marker for mitochondrial membrane potential.

To monitor mitochondrial membrane potential (MMP), human neuroblastoma cell (SH-SY-5Y) were cultured in DMEM media at at 37 °C in 5% CO2 incubator. The cells were seeded in six well plate. The cell density was 10^6 cells/well containing 10% fetal bovine serum (FBS) in Dulbecco's Modified Eagle Medium (DMEM) and incubated at 37°C in 5% CO_2. After 12 hours, media was discarded and each well was washed with phosphate-buffered saline (PBS) followed by addition of Aβ and Aβ+INHQ to each well at 50 µM concentrations. After 12 hours, 2 µM (final concentration) of JC-1 dye was added in each well and incubated at 37°C, 5% CO_2 for 15-30 min. Cells were then washed with PBS and observed under fluorescence microscope (FLoid Cell Imaging Station, Thermo Fischer Scientific) for progressive loss of red J-aggregate fluorescence and cytoplasmic diffusion of green monomer fluorescence.

5.4.12. Hemolysis Experiments in Mouse Model:

Swiss albino mice (weight 25-30g) were used as the experimental animal model in the present study. The animal experiments were completed as per the approval of the IAEC, Gauhati University. blood samples were collected from the medical laboratory

technician course laboratory of Pub Kamrup College, Assam, India. The blood sample was centrifuged at 900 RPM for 12 min with three repeated washing using 0.9 % saline solution. The settled RBC was suspended in phosphate buffer saline (pH 7.4) and kept in a special buffer composed of a standard amount of protein dissolved in normal saline mimicking the body fluid composition. The suspended RBC treated with various concentrations (0 to 50 µg/mL) of INHQ (dispersed in PBS buffer). As a negative control, the SDS (1 %) was used which is capable of rupturing the red blood cells and PBS is used as positive control. For the assay, 200 µL of the dissolved samples and 800 µL of RBC were added and incubated at 37 ºC for 90 min. After incubation, the samples were centrifuged at 2000 RPM for 10 min and the supernatant was carefully transferred for determining the percentage of hemolysis at absorbance of 540 nm in UV-Vis spectrophotometer. The percentage of hemolysis was calculated as follows:

Percentage of hemolysis (%) = Absorbance of INSQ treated RBC - Absorbance of PBS treated RBC/ Absorbance of SDS treated RBC X 100 - Absorbance of PBS treated RBC.

The reaction mixture was centrifuged at 900 rpm for 5 min. and the cells from pellet were used for RBC morphometric analysis. For RBC morphometric analysis, smeared RBCs were stained with Leishmann stain using standard protocol for further microscopic observation. Excess stain was washed out with distilled water and slides were dried and observed and microphotographs were taken by using a CCD camera attached microscope (Labomed LX300).

5.4.13. BBB permeability Experiment:

Swiss albino mice (weight 25-30g) were used as the experimental animal model in the present study. The animal experiments were completed as per the approval of the IAEC, Gauhati University. The mice were caged at usual 12:12 hours light dark cycles with usual diet and water ad libitum. Daily handling of the animals was maintained to reduce the stress. Animals were divided into two groups (GROUP X and GROUP Y) along with one control group fed with normal saline. Each group contained five mice. Mice were administered at the dose 15 mg/kg per day for one week through teil vein. The drug was allowed to circulate through normal physiological flow. Then the animals were sacrificed and brain tissues were collected. Tissues were fixed in Carnoy's fixative. The fixed tissues were embedded in paraffin wax for histological study. Histological sections were prepared

at 5 μm thickness using the laboratory rotary microtome. Sections were stained with DAPI using standard procedure and observed under confocal microscope.

5.4.14. Neuronal Damage in Mouse Model:

Swiss albino mice (weight 25-30g) were used as the experimental animal model in the present study. The animal experiments were completed as per the approval of the IAEC, Gauhati University. The mice were caged at usual 12:12 hours light dark cycles with usual diet and water ad libitum. Daily handling of the animals was maintained to reduce the stress. Animals were divided into two groups (GROUP X and GROUP Y) along with one control group fed with normal saline. Each group contained five mice. Mice were administered at the dose 15 mg/kg per day for one week through teil vein. After one week of continuous treatment animals were sacrificed and brain and liver tissues were collected. Tissues were fixed in Carnoy's fixative. The fixed tissues were embedded in paraffin wax for histological study. Histological sections were prepared at 5 μm thickness using the laboratory rotary microtome. Sections were stained with haematoxylin and eosin (H&E stain) using standard procedure and observed under microscope.

In the brain cell, morphometric analysis reveals that brain with normal histological architecture. In amyloid beta induced mice group (Figure 5.4e), brain parenchymal cells are seen to be destroyed and become vacuolated resulting in neuronal cell loss. Due to cellular damage edemic cells are observed. Pyknotic nuclei of glial cells are observed in the white matter area of brain. Infiltration of inflammatory cells is seen in a region within neocortex region of cerebral cortex. Hemorrhagic area in the brain is seen. Loss of myelin sheath observed. Leptomeningeal deformation is also found in some area. In protective molecule induced (Figure 5.4f), brain appears with few lesions and tissue damage appears to be minimized. Edematous tissues are lessened to a greater extent. Regeneration of neuronal cells is observed. No haemorrhagic region is seen at all.

5.3. Reference:

(1) Taylor, J. P.; Hardy, J.; Fischbeck, K. H. Toxic proteins in neurodegenerative disease. *Science* **2002**, *296*, 1991.

(2) Hardy, J.; Selkoe, D. J. The Amyloid hypothesis of Alzheimer's disease: progress and problems on the road to therapeutics. *Science 2002*, 297, 353-356.

(3) Karran, E.; Mercken, M.; Strooper, B. D. The amyloid cascade hypothesis for Alzheimer's disease: an appraisal for the development of therapeutics. *Nat. Rev. Drug Discovery* **2011**, *10*, 698-712.

(4) Lesné, S.; Koh, M. T.; Kotilinek, L.; Kayed, R.; Glabe, C. G.; Yang, A.; Gallagher, M.; Ashe, K. H. A specific amyloid-β protein assembly in the brain impairs memory. *Nature* **2006**, *440*, 352-357.

(5) Kayed, R.; Head, E.; Thompson, J. L.; McIntire, T. M.; Milton, S. C.; Cotman, C. W.; Glabe, C. G. Common structure of soluble amyloid oligomers implies common mechanism of pathogenesis. *Science* **2003**, *300*, 486.

(6) LaFerla, F. M.; Green, K. N.; Oddo, S. Intracellular amyloid-β in Alzheimer's disease. *Nat. Rev. Neurosci.* **2007**, *8*, 499-509.

(7) Leuner, K.; Müller, W. E.; Reichert, A. S. From mitochondrial dysfunction to amyloid beta formation: novel insights into the pathogenesis of Alzheimer's disease. *Mol. Neurobiol.* **2012**, *46*, 186-193.

(8) Mondal, S.; Chowdhury, S. R.; Shah, M.; Kumar, V.; Kumar, S.; Iyer, P. K. Nanoparticle assisted regulation of nucleation pathway of amyloid tetramer and inhibition of their fibrillation kinetics. *ACS Appl. Bio Mater.* **2019**, *2*, 2137-2142.

(9) Mondal, S.; Kumar, V.; Chowdhury, S. R.; Shah, M.; Gaur, A.; Kumar, S.; Iyer, P. K. Template mediated detoxification of low-molecular-weight amyloid oligomers and regulation of their nucleation pathway. *ACS Appl. Bio Mater.* **2019**, *2*, 5306-5312.

(10) Sun, H.; Lv, F.; Liu, L.; Wang, S. Reactive conjugated polymers for the modulation of islet amyloid polypeptide assembly. *ACS Appl. Mater. Interfaces* **2019**, *11*, 22973-22978.

(11) Sun, H.; Liu, J.; Li, S.; Zhou, L.; Wang, J.; Liu, L.; Lv, F.; Gu, Q.; Hu, B.; Ma, Y.; Wang, S. Reactive amphiphilic conjugated polymers for inhibiting amyloid β assembly. *Angew. Chem. Int. Ed.* **2019**, *58*, 5988-5993.

(12) Nie, Q.; Du, X.-g.; Geng, M.-y. Small molecule inhibitors of amyloid β peptide aggregation as a potential therapeutic strategy for Alzheimer's disease. *Acta Pharmacol. Sin.* **2011**, *32*, 545-551.

(13) Mondal, S.; Vashi, Y.; Ghosh, P.; Roy, D.; Barthakur, M.; Kumar, S.; Iyer, P. K. Amyloid targeting "artificial chaperone" impairs oligomer mediated neuronal damage and

mitochondrial dysfunction associated with Alzheimer's disease. *ACS Chem. Neuro.* **2020**, *11*, 3277-3287.

(14) Salloway, S.; Sperling, R.; Fox, N. C.; Blennow, K.; Klunk, W.; Raskind, M.; Sabbagh, M.; Honig, L. S.; Porsteinsson, A. P.; Ferris, S.; Reichert, M.; Ketter, N.; Nejadnik, B.; Guenzler, V.; Miloslavsky, M.; Wang, D.; Lu, Y.; Lull, J.; Tudor, I. C.; Liu, E.; Grundman, M.; Yuen, E.; Black, R.; Brashear, H. R. Two phase 3 trials of bapineuzumab in mild-to-moderate Alzheimer's disease. *N. Eng. J. Med.* **2014**, *370*, 322-333.

(15) Doody, R. S.; Raman, R.; Farlow, M.; Iwatsubo, T.; Vellas, B.; Joffe, S.; Kieburtz, K.; He, F.; Sun, X.; Thomas, R. G.; Aisen, P. S.; Siemers, E.; Sethuraman, G.; Mohs, R. A Phase 3 Trial of Semagacestat for Treatment of Alzheimer's Disease. *N. Eng. J. Med.* **2013**, *369*, 341-350.

(16) Meher, N.; Chowdhury, S. R.; Iyer, P. K. Aggregation induced emission enhancement and growth of naphthalimide nanoribbons via J-aggregation: insight into disaggregation induced unfolding and detection of ferritin at the nanomolar level. *J. Mater. Chem. B* **2016**, *4*, 6023-6031.

(17) Meher, N.; Iyer, P. K. Pendant chain engineering to fine tune the nano morphologies and solid state luminescence of naphthalimide AIEEgens: Application to phenolic nitro-explosive detection in water. *Nanoscale* **2017**, *9*, 7674-7685.

(18) Paravastu, A. K.; Leapman, R. D.; Yau, W. M.; Tycko, R. Molecular structural basis for polymorphism in Alzheimer's beta-amyloid fibrils. *Proc. Natl. Acad. Sci. U. S. A.* **2008**, *105*, 18349-54.

(19) Hashemi, M.; Zhang, Y.; Lv, Z.; Lyubchenko, Y. L. Spontaneous self-assembly of amyloid β (1–40) into dimers. *Nanoscale Adv.* **2019**, *1*, 3892-3899.

(20) Kanski, J.; Varadarajan, S.; Aksenova, M.; Butterfield, D. A. Role of glycine-33 and methionine-35 in alzheimer's amyloid β-peptide 1–42-associated oxidative stress and neurotoxicity. *Biochim. Biophys. Acta Mol. Basis. Dis.* **2002**, *1586*, 190-198.

(21) Clementi, M. E.; Marini, S.; Coletta, M.; Orsini, F.; Giardina, B.; Misiti, F. Aβ(31–35) and Aβ(25–35) fragments of amyloid beta-protein induce cellular death through apoptotic signals: Role of the redox state of methionine-35. *FEBS Lett.* **2005**, *579*, 2913-2918.

(22) Yang, F.; Lim, G. P.; Begum, A. N.; Ubeda, O. J.; Simmons, M. R.; Ambegaokar, S. S.; Chen, P. P.; Kayed, R.; Glabe, C. G.; Frautschy, S. A.; Cole, G. M. Curcumin inhibits formation of amyloid beta oligomers and fibrils, binds plaques, and reduces amyloid in vivo. *J. Biol. Chem*. **2005**, *280*, 5892-901.

(23) Gopikrishna, P.; Meher, N.; Iyer, P. K. Functional 1,8-naphthalimide AIE/AIEEgens: recent advances and prospects. *ACS Appl. Mater. Interfaces* **2018**, *10*, 12081-12111.

(24) Yeh, L. K.; Liu, C. Y.; Chien, C. L.; Converse, R. L.; Kao, W. W. Y.; Chen, M. S.; Hu, F. R.; Hsieh, F. J.; Wang, I. J. Molecular analysis and characterization of zebrafish keratocan (zkera) gene. *J. Biol. Chem*. **2008**, *283*, 506-517.

(25) Germain, M.; Affar, E. B.; D'Amours, D.; Dixit, V. M.; Salvesen, G. S.; Poirier, G. G. Cleavage of automodified poly(ADP-ribose) polymerase during apoptosis: Evidence for involvement of caspase-7. *J. Biol. Chem*. **1999**, *274*, 28379-28384.

(26) Baek, S. H.; Bae, O. N.; Kim, E. K.; Yu, S. W. Induction of mitochondrial dysfunction by poly(ADP-ribose) polymer: implication for neuronal cell death. *Mol. Cells* **2013**, *36*, 258-66.

(27) Du, H.; Guo, L.; Fang, F.; Chen, D.; A Sosunov, A.; M McKhann, G.; Yan, Y.; Wang, C.; Zhang, H.; Molkentin, J. D.; Gunn-Moore, F. J.; Vonsattel, J. P.; Arancio, O.; Chen, J. X.; Yan, S. D. Cyclophilin D deficiency attenuates mitochondrial and neuronal perturbation and ameliorates learning and memory in Alzheimer's disease. *Nat. Med*. **2008**, *14*, 1097-1105.

(28) Slaoui, M.; Fiette, L. Histopathology procedures: from tissue sampling to histopathological evaluation. *Methods Mol. Biol*. **2011**, *691*, 69-82.

(29) Banerjee, S.; Kitchen, J. A.; Bright, S. A.; O'Brien, J. E.; Williams, D. C.; Kelly, M. J.; Gunnlaugsson, T. Synthesis, spectroscopic and biological studies of a fluorescent Pt(II) (terpy) based 1,8-naphthalimide conjugate as a DNA targeting agent. *Chem. Commun*. **2013**, *49*, 8522-8524

5.4. Appendix D: Additional Figures for Chapter 5

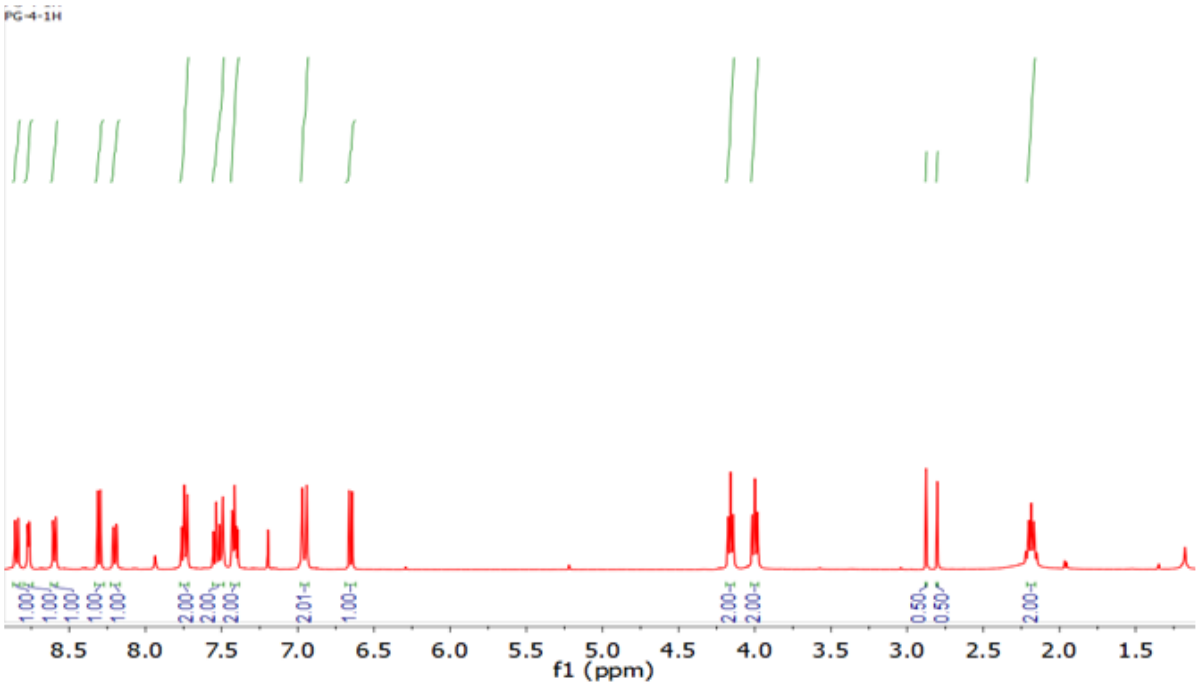

***Figure D-1**: [1]H NMR of INHQ*

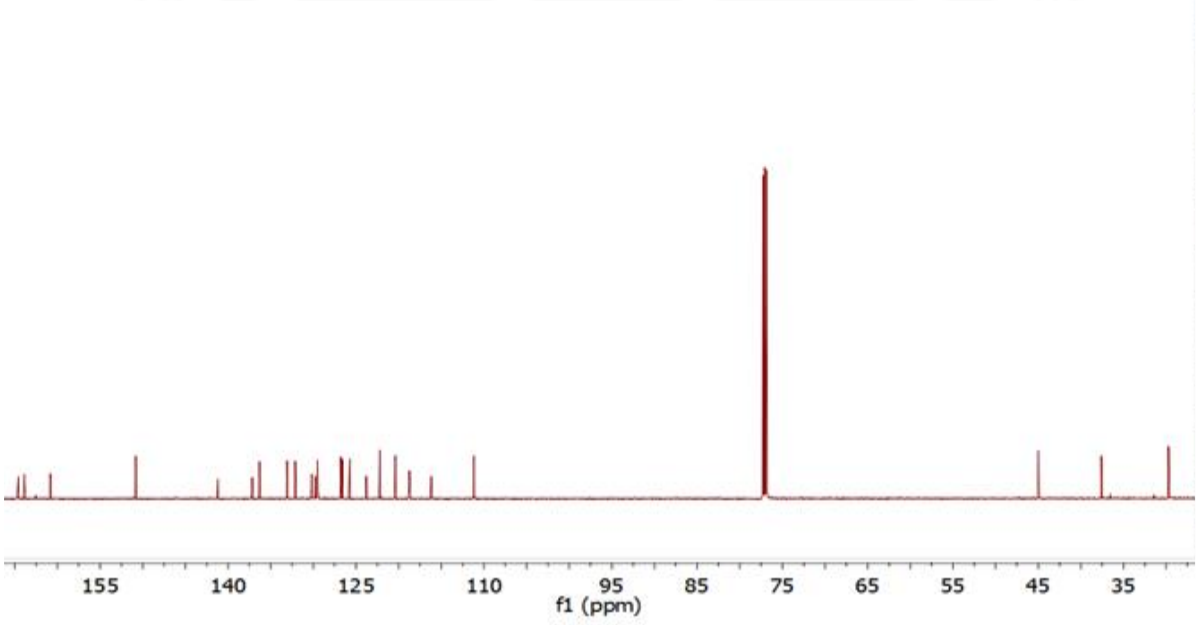

***Figure D-2**: [13]C NMR of INHQ*

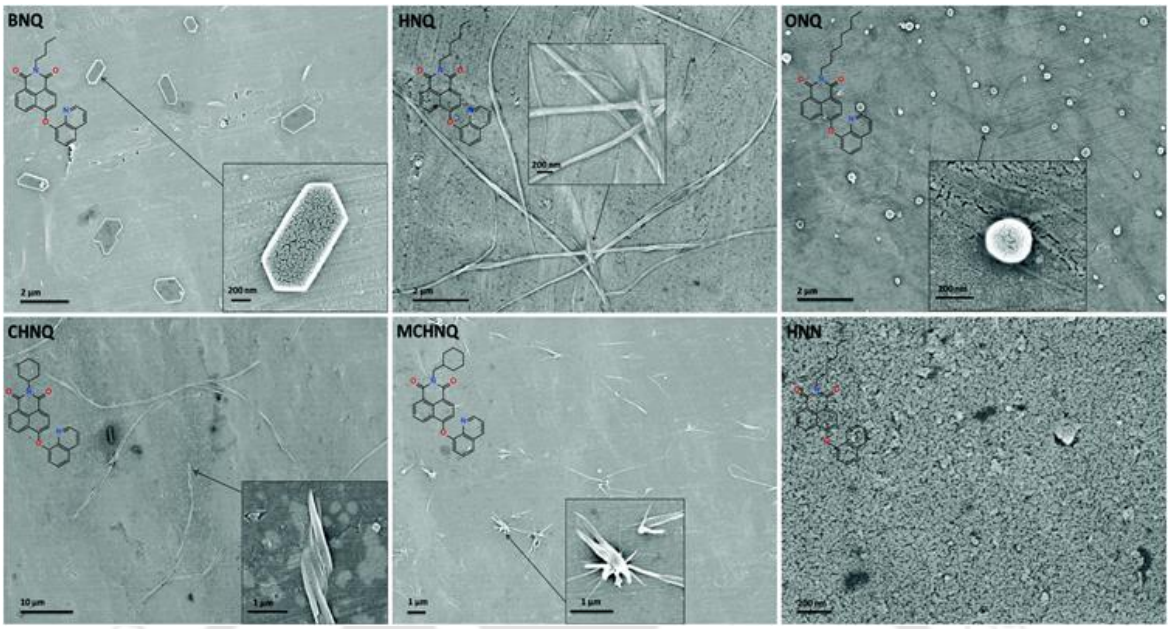

***Figure D-3**: FESEM images of the nano and microstructures of the luminogens formed in 99.9% fw (10 μM) by a simple dropcasting technique. The insets show the corresponding chemical structures (left) and magnified images (right). Reprinted with permission from ref 2. Copyright 2019 Royal Society of Chemistry.*

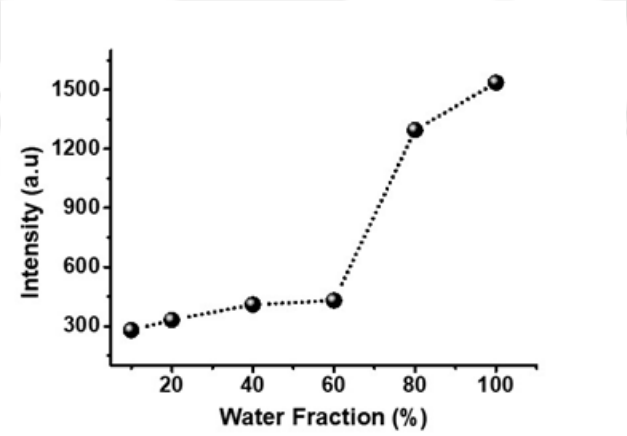

***Figure D-4:** Enhancement INHQ emission with increase in water fraction ($\lambda_{excitation}$=370 nm)*

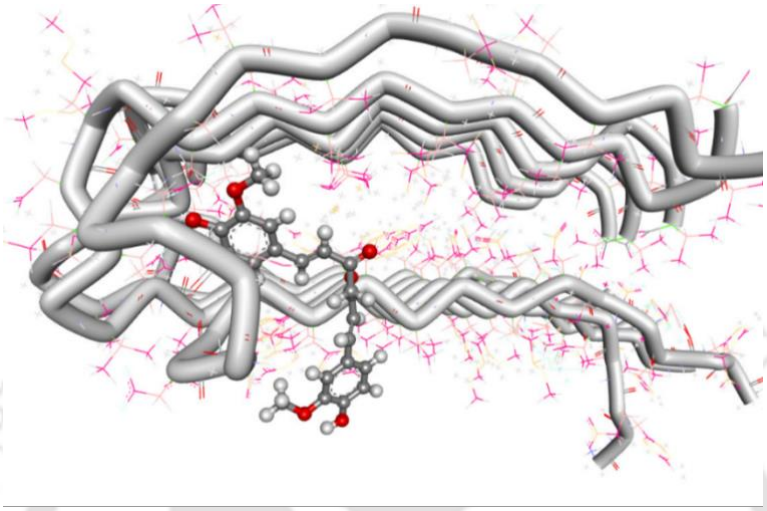

Figure D-5: *Curcumin in complex with Aβ40 fibril*

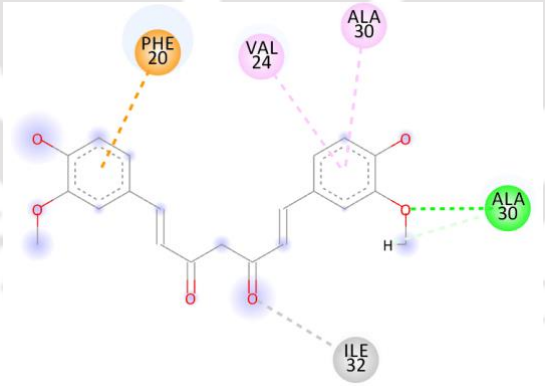

Figure D-6: *The interactions of Curcumin with Aβ40 fibril*

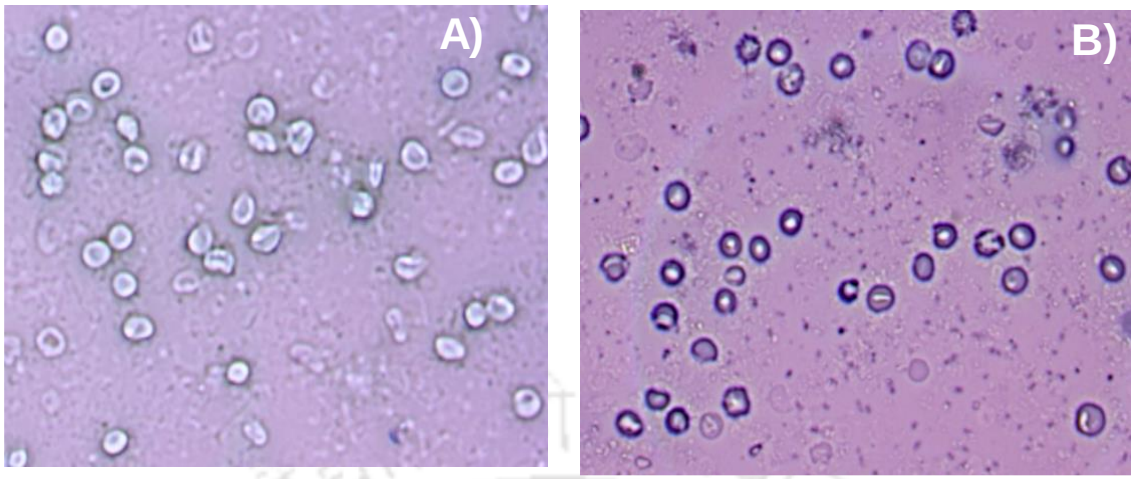

Figure D-7: *Haemolysis in presence of INHQ*

6

Epilogue

6

Epilogue

In the 19th century Esquirol wrote, “A man in a state of dementia is deprived of advantages which he formerly enjoyed; he was a rich man who has become poor”. Due to the unavailability of efficient clinical strategy for AD, and indeed other neurodegenerative disease, this description remains an inevitable truth today. Amyloid toxicity lies at the root of AD, and mitigation of amyloid neurotoxicity is a promising conceptual framework for the development of anti-Alzheimer drugs. However, not only amyloid aggregation but also many other biochemical events including oxidative stress, neuroinflammation, mitochondrial dysfunction has strongly been implicated in Alzheimer etiology. In the past few decades, many therapeutic materials solely targeting Aβ have been developed. However, most of those single targeted drugs have proven to be inadequate and failed during different stages of clinical trials, suggesting a multi-targeted drug approach to address multifactorial toxicity involved in AD to be the best option.

My efforts have been directed into deepening the knowledge about the aggregation kinetics of amyloid beta, their toxic pathways and finally mitigation of such toxicity using novel therapeutic materials. The studies presented in this thesis pioneer manifold avenues that are worthwhile to pursue. It has been strongly demonstrated that efficient designing of materials can successfully inhibit amyloid aggregation and mitigate neurotoxicity associated with it. A wide variety of material starting from engineered nanoparticle to polymer and small molecule based drugs have been tested against amyloid β and their anti-

Alzheimer activity has been evaluated. Although, traditionally Alzheimer research was focused on the amyloid fibers, it has been observed that low molecular weight amyloid oligomers are much more toxic than the fibrillar aggregates. Hence, research activity has been redirected towards oligomeric aggregates. I have isolated a LMW oligomers and their kinetic and physical properties has been explored. A novel gold nanoparticle based anti-aggregation has also been developed and shown to block amyloid oligomerisation. Although, nanoparticles showed appreciable inhibitory activity, their toxicity and BBB permeability remained an unresolved issue. To overcome this, a polymer based 'artificial chaperone' has been developed. In parallel to amyloid inhibition, it could block an essential biochemical cycle that leads to oxidative stress and mitochondrial dysfunction associated with AD. The polymer nano drug was also observed to translocate through BBB in WT mouse model. Overall, the polymer based drug claims to be a potential hit against AD. In last chapter, a small molecule based multipotent drug molecule has been developed and shown to mitigate amyloid induced neuronal damage in WT mouse model. These findings provide a promising lead structure to guide the design of small molecule based anti-Alzheimer drugs.

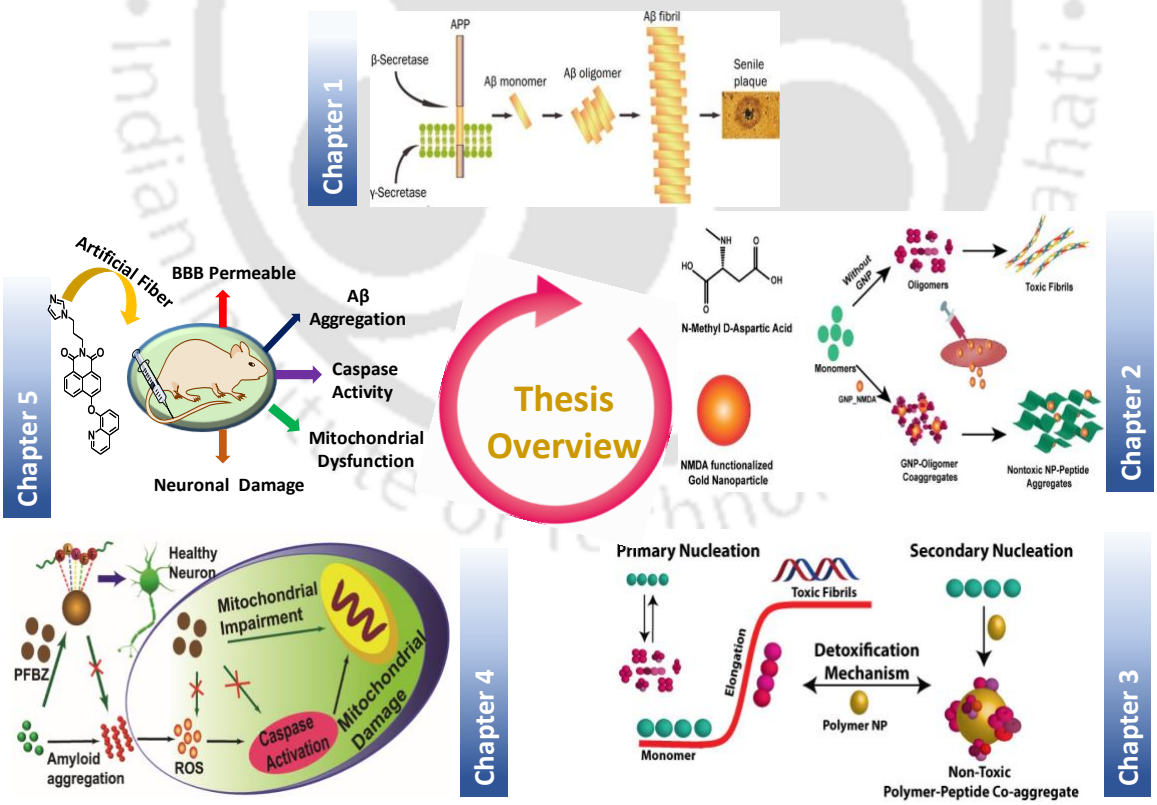

Publications

1. **Mondal, S.;** Chowdhury, S. R.; Shah, M.; Kumar, V.; Kumar, S.; Iyer, P. K.* Nano particle assisted regulation of nucleation pathway of amyloid tetramer and inhibition of their fibrillation kinetics. A*CS Appl. Bio Mater.* **2019***, 2, 5, 2137-2142*.

2. Chowdhury, S. R.; **Mondal, S**.; Iyer, P. K.;* Blocking oligomeric insulin amyloid fibrillation via perylenebisimides containing dipeptide tentacles. *ACS Biomater. Sci. Eng.,* **2018**, *4,* 4076–4083.

3. Chowdhury, S. R.; **Mondal, S.**; Muthuraj, B.; Balaji, S. N.; Trivedi, V.; Iyer, P. K.* Remarkably efficient blood brain barrier crossing polyfluorene–chitosan nanoparticle selectively tweaks amyloid oligomer in cerebrospinal fluid and aβ1–40. *ACS Omega,* **2018**, *3,* 8059-8066.

4. Chowdhury, S. R; Balaji, S. N.; **Mondal, S.**; Meher, N.; Trivedi, V.; Iyer, P. K.* Modulating early stage amyloid aggregates by dipeptide linked perylenebisimides: structure activity relationship, inhibition of fibril formation in human CSF and aβ1-40. *ACS Appl. Bio Mater.,* **2018**, *1*, 403–413.

5. Chakraborty, D. S.; **Mondal, S.**; Satpati, B.; Pal, U.; De, S.; Bhattacharya, M.; Ray, S.; Senapati, D., Wide range morphological transition of silver nanoprism by selective interaction with As (III): tuning-detuning of surface plasmon offers to decode the mechanism. *J. Phys. Chem. C* **2019***, 123, 17, 11044-11054*.

6. Muthuraj, B.; Chowdhury, S. R., **Mondal, S.**; Iyer, P. K. Inhibition of amyloid β fibrillation and modulation effect on preformed aβ fibrils by the influence of aggregation caused red shifted emission from polyfluorene nanoparticle. ***(Communicated)***

7. Mondal, S.; Kumar, V.; Chowdhury, S. R.; Shah, M.; Gaur, A.; Kumar, S.; Iyer, P. K.* template mediated detoxification of amyloid tetramer and regulation of their nucleation pathway. *ACS Appl. Bio Mater.*, **2019**, *2*, 5306-5312.

8. **Mondal, S**.; Vashi, Y.; Ghosh, P.; Roy, D.; Borthakur, M.; Kumar, S.; Iyer, P. K.* Amyloid targeting 'artificial chaperone' impairs oligomer mediated neuronal damage and mitochondrial dysfunction associated with Alzheimer disease. *ACS Chem. Neurosci.* **2020**, *11*, 3277–3287.

9**. Mondal, S.;** Zehra, N.; Choudhury, A.; Iyer, P. K.* Wearable sensing devices for point of care diagnostics. *ACS Appl. Bio Mater.,* (2020) (*Just Accepted)*

10. **Mondal, S.;** Yoya, V.; Ghosh, P.; Kalita, P.; Kumar, S.; Iyer, P. K.* Self-assembly driven formation of functional ultra-long 'artificial fiber' to mitigate neuronal damage associated with Alzheimer's disease. (*Communicated*).

11. Chani, M. A.; **Mondal, S.**; Zehra, N.; Tanwar, A. S.; Iyer, P. K.* Amplified and label-free detection of bilirubin in human blood serum quantitatively using a conjugated polymer as a fluorescent probe. (*submitted*)

Book Chapters

1. Tanwar, A.; Zehra, N.; Adil, L. R.; **Mondal, S**.; Iyer, P. K.* Thin film devices for sensing application. Book Chapter. Copyright © Springer. (*in press*)

2. Mondal, S.; Yathirala, R.; Arunagirinathan, R. N.; Medhi, I.; Iyer, P. K.* Emerging technology for point of care Diagnostics: Recent developments. Copyright © Elsevier. (*submitted*)

Patents

1. **Mondal, S.**; Singh, A,; Das, A,; Iyer, P. K., Development of OFET based Sensing Device for Viral Pathogens. (Communicated)

2. Mondal, S.; Singh, A.; Das, A.; Iyer, P. K. Method for the early stage diagnosis of onset Alzheimer disease. (*Manuscript under preparation*)

Awards

1. Received **BEST POSTER** Presentation award in the 3rd MRS meeting-2019, organized by Material Research Society, **Singapore** in **Nanyang Technological University**.

Conferences

1. Won **Best Poster** Award in **MRS Meeting 2020, Singapore.**

2. Delivered **Oral Presentation** in **ICANN** 2019.

3. Delivered **Oral Presentation** in ***Research Conclave*** 2019.

4. Presented **Poster** in ***FICS 2019*.**

5. Presented **poster** in ***Research Conclave* 2018.**

6. Presented **poster** in ***Reflux* 2018.**

7. Attended ***4th National Workshop on NEMS/MEMS and Theranostic Devices.***

8. Attended ***3rd National Workshop on NEMS/MEMS and Theranostic Devices.***

9. Attended ***workshop*** on ***Summer School on Neuroimaging, IIIT Hyderabad.***

10. Presented **poster** in ***Research Conclave 2017.***

11. Presented **poster** in ***Bioprocessing India 2017 .***

12. Presented **poster** in ***National Workshop on Fluorescence and Raman Spectroscopy 2017.***

13. Presented **poster in *5th International Conference on Advanced Nanomaterials and Nanotechnology 2017.***

14. Attended **workshop *From Basic Invention to Advanced Biomedical Devices .***

15. Attended ***4th International Conference on Advanced Nanomaterials and Nanotechnology 2015 .***

Vitae

Subrata Mondal was born in West Bengal, India. He obtained his Bachelor of Science in Chemistry (Hons.) from Presidency College, Kolkata and completed his Master of Science in from Indian Institute of Technology Guwahati, India in 2013 and 2015 respectively. In 2015, he joined as a PhD student in the Department of Chemistry; Indian Institute of Technology Guwahati under the supervision of Prof. Parameswar K. Iyer. He started his research career on 'Develeopment of New Material Mitigation of Amyloid Neurotoxicity Associated with Alzheimers Disease', which principally deals with development of several therapeutic material to inhibit amyloid aggregation and suppress neurotoxicity associated with the aggregates. Besides, he is interested in working on development of probes for biological imaging, development of sensing devices for biological and theranostic applications.

PhD
Thesis

Development of New Therapeutic Material for Mitigation of Amyloid Neurotoxicity Associated with Alzheimer's Disease

Subrata Mondal

2020